UNIVERSIDAD POLITÉCNICA DE MADRID
Escuela Técnica Superior de Ingeniería y Diseño Industrial

New Solutions in Electrification and Decarbonization of Industrial Energy Model

DOCTORAL THESIS

Submitted for the degree of Doctor by:

Saber Niazi
M.Sc. of Chemical Engineering

Madrid, 2025

UNIVERSIDAD POLITÉCNICA DE MADRID
Escuela Técnica Superior de Ingeniería y Diseño Industrial

Doctoral Degree in Production Engineering and Industrial Design

New Solutions in Electrification and Decarbonization of Industrial Energy Model

DOCTORAL THESIS

Submitted for the degree of Doctor by:

Saber Niazi
M.Sc. of Chemical Engineering

Under the supervision of:
Dr. Antonio Nieto-Márquez Ballesteros
Dr. Carlos Fúnez Guerra

Madrid, 2025

Title: New Solutions in Electrification and Decarbonization of Industrial Energy Model

Author: Saber Niazi

Doctoral Programme: Production Engineering and Industrial Design

Thesis Supervision:

Dr. Antonio Nieto-Márquez Ballesteros

Associate Professor

Escuela Técnica Superior de Ingeniería y Diseño Industrial (ETSIDI)

Universidad Politécnica de Madrid (UPM)

Dr. Carlos Fúnez Guerra

Green Hydrogen Development Manager

Iberdrola, S.A.

External Reviewers:

Ángel Martín Martínez

Alexander Navarrete Muñoz

Sonia Gil Villarino

Thesis Defense Committee:

Thesis Defense Date:

This thesis, as a part of the MSCA COFUND project "SDGine for Healthy People and Cities" has received funding from the European Union's Horizon 2020 research and innovation programme under the Marie Skłodowska-Curie grant agreement No. 945139.

To my beloved wife, my constant light in every storm; this journey would not have been possible without you.
To my parents, who taught me to dream and persevere.
To my siblings, whose love has always warmed my soul.
To Danilo and David, true companions in sound and silence.
And to Antonio and José Antonio whose guidance lit the path, through science and beyond.

Acknowledgement

I would like to express my heartfelt gratitude to my supervisors, Dr. Antonio Nieto-Márquez Ballesteros, Dr. Carlos Fúnez Guerra, as well as to Prof. Laura Torrente Murciano and Dr. José Antonio Díaz López, for their continuous support, insightful guidance, and invaluable feedback throughout the development of this thesis.

I am also sincerely grateful to our research group, especially Evangelina Atanes Sánchez, Fernando Gutiérrez Martín, Francisco Fernández Martínez, Ángel Caravaca Huertas, Antonio Juan Dos Santos García, María José Martín de Vidales Calvo, and David García Casillas, whose expertise, encouragement, and support have been instrumental throughout the course of my PhD.

I would like to thank the SDGine project management team at EID and OPI of UPM, particularly Estela Hernández, for their unwavering support and dedication during my doctoral journey.

I am also deeply thankful to my friends and colleagues, especially Hernan Danilo Jara Echeverría, Shuqin Geng, and Charilaos Dragoidis, whose friendship and support have made this journey not only possible, but also truly meaningful.

Scientific Achievements

Journal Publications:

1- S. Niazi, J. A. Díaz-López, A. Nieto-Márquez, C. Fúnez Guerra, F. Gutiérrez Martín. "Design and optimization of an integrated solar PV–electrolyzer system using modelling tools." (Under preparation).
2- S. Niazi, J. A. Díaz-López, A. Nieto-Márquez. "Heat integration and process improvement of a batch distillation unit using a gradual feeding strategy: A case study on MIBK-water separation." Separation and Purification Technology (2025): 131956.
3- S. Niazi, J. A. Díaz-López, A. Nieto-Márquez. Improvement of energy efficiency and production performance in a heteroazeotropic batch distillation unit: A study on decanter control and feeding strategy. Separation and Purification Technology 357 (2025): 130132.
4- S. Niazi, J. A. Díaz-López, A. Nieto-Márquez. Process design and simulation of Methyl Isobutyl Ketone (MIBK) dehydration by batch distillation: A study on unit configuration and operational policies. Separation and Purification Technology (2024): 127942.

International Conferences:

1- S. Niazi, J. A. Díaz-López, A. Nieto-Márquez. Feeding strategy: an efficient key to enhance energy efficiency in batch distillation units. Annual Meeting of Process Engineering and Materials Technology, 2024, Frankfurt, Germany. (Oral Presentation)
2- S. Niazi, J. A. Díaz-López, A. Nieto-Márquez. CO2 Capture Using Potassium Carbonate Solution. 5th Ibero-American Congress on Biorefineries (CIAB), 2024, Jaén, Spain. (Oral Presentation)
3- S. Niazi, M.I. Parma-García, J.A. Díaz-López, A. Nieto-Márquez, Batch Distillation of Water/MIBK Heteroazeotropic Mixture; Evaluation and Optimization of Process, 15th Mediterranean Congress of Chemical Engineering, 2023, Barcelona, Spain.

National Conferences:

1- S. Niazi, J. A. Díaz-López, A. Nieto-Márquez. Energy optimization of a batch distillation unit in separation of a self-entrained heteroazeotropic mixture. II Jornadas de Investigación de la ETSIDI, 2024, ETSIDI-UPM, Madrid, Spain. (Oral Presentation)
2- S. Niazi, J. A. Díaz-López, A. Nieto-Márquez. New solutions in the decarbonization of the industrial energy model: Application to industrial distillation. I Jornada de Investigación de la ETSIDI, 2022, ETSIDI-UPM, Madrid, Spain. (Oral Presentation)

Abstract

Energy efficiency and green hydrogen are strategic pathways toward industrial electrification and decarbonization. This PhD thesis presents two technological approaches for industrial decarbonization: (1) improving energy efficiency in a batch distillation unit (BDU) employed in a solvent recovery process and (2) enhancing green PEM electrolyzer performance for application under variable energy sources.

In the first part of this study, a heteroazeotropic BDU is employed for dehydration of methyl isobutyl ketone (MIBK) as a solvent recovery process. The BatchSep module of the commercial package Aspen Plus is employed for simulations. Three configurations, namely a conventional BDU (Mode I), a BDU with a decanter (Mode II), and a simple refluxless BDU (Mode III), are compared in a wide range of operating conditions. According to the results, a perfect decanter offers an almost complete MIBK recovery. Mode III offers the fastest process but provides the lowest recovery. The aqueous phase return fraction lower than 0.5 does not significantly impact MIBK recovery. Applying a decanter (Mode II) with a return fraction above 0.5 for the MIBK-rich phase and below 0.55 for the aqueous phase yields superior performance over Mode I. A perfect decanter in Mode II improves production rate and energy efficiency by 8% over Mode I. Also, Mode III is preferred over Mode I with a total return fraction over 0.7.

In the second part, the impacts of feed quantity, decanter design/control policy, decanter holdup volume, and subsequent phase separation quality on the unit performance are evaluated. Feed quantity is recognized as a key factor influencing unit performance. The decanter holdup volume is subject to optimization, showing that a more effective decanter lies on a larger aqueous phase holdup, and a smaller organic design can improve the unit recovery by up to 6% and the production rate (and energy cost) by up to 7% compared to a conventional BDU. Furthermore, an inverted BDU with a gradual feeding policy is applied as an alternative and compared to other operation policies. The results reveal that an inverted distillation unit equipped with a well-designed decanter provides up to 17% improvement in energy and production rate, 7% higher recovery, and 9% shorter process time compared to a conventional BDU.

The third part of this study is aimed at further improvement of the distillation operation. Gradual feeding is found to be an efficient approach to upgrading the unit operation. Top feeding (inverted BDU) and decreasing feed flow rate proved

to be the most efficient feeding, resulting in a 10% improvement in production rate and energy cost over a conventional BDU equipped with a decanter. Also, based on the gradual feeding strategy, feed preheating is proposed as a feasible heat integration technique in the batch distillation process. This strategy is found to be effective in process intensification, leading to a maximum of 47% improvement in energy efficiency and production rate compared to a conventional BDU equipped with a decanter.

In the fourth part of this thesis, a proton exchange membrane electrolyzer (PEMEL) model adaptable to variable power sources is developed. Aspen Plus is employed for unit modelling, and the PEM stack model is developed in Aspen Custom Modeler (ACM) based on empirical and semi-empirical correlations. The results show that the model is in close agreement with the experimental findings. In accordance with empirical results, the model shows that lower operating pressure improves the electrolyzer performance and increasing the temperature from 40 to 80 °C results in about 13.7% lower cell voltage at a current density of 2 A/cm² (from 2.24 to 1.93). Accordingly, two different operation scenarios of (1) fixed circulating water flow rate and (2) fixed operating temperature are proposed for operation of a PEMEL unit, and the model is adapted to enable both options in simulation. The provided PEMEL model and the proposed scenario are potentially adaptable to variable input power profiles.

Resumen

La eficiencia energética y el hidrógeno verde son vías estratégicas hacia la electrificación y descarbonización industrial. Esta tesis doctoral presenta dos enfoques tecnológicos para la descarbonización industrial: (1) la mejora de la eficiencia energética en una unidad de destilación discontinua (UDD) empleada en un proceso de recuperación de disolventes y (2) la optimización del rendimiento de un electrolizador PEM verde para su aplicación bajo fuentes de energía variables.

En la primera parte de este estudio, se emplea una UDD heteroazeotrópica para la deshidratación de metil isobutil cetona (MIBK) como proceso de recuperación de disolventes. Para las simulaciones se utiliza el módulo BatchSep del paquete comercial Aspen Plus. Se comparan tres configuraciones: una UDD convencional (Modo I), una UDD con decantador (Modo II) y una UDD simple sin reflujo (Modo III), bajo un amplio rango de condiciones operativas. Según los resultados, un decantador perfecto permite una recuperación casi completa de la MIBK. El Modo III ofrece el proceso más rápido, pero con la menor recuperación. Un coeficiente de retorno de la fase acuosa inferior a 0,5 no afecta significativamente la recuperación del MIBK. La aplicación de un decantador (Modo II) con un coeficiente de retorno superior a 0,5 para la fase rica en MIBK y menor a 0,55 para la fase acuosa ofrece un rendimiento superior al Modo I. Un decantador perfecto en el Modo II mejora la tasa de producción y la eficiencia energética en un 8% respecto al Modo I. Además, el Modo III es preferible al Modo I cuando el coeficiente de retorno total supera 0,7.

En la segunda parte, se evalúan los efectos de la cantidad de alimentación, el diseño/control del decantador, el volumen de retención del decantador y la calidad de separación de fases sobre el rendimiento de la unidad. La cantidad de alimentación se identifica como un factor clave que influye en el rendimiento. El volumen de retención del decantador está sujeto a optimización, demostrando que un decantador más eficaz presenta una mayor retención en la fase acuosa y un diseño más pequeño para la fase orgánica. Esta configuración puede mejorar la recuperación de la unidad hasta un 6% y aumentar la tasa de producción (y reducir el coste energético) hasta un 7% en comparación con una UDD convencional. Además, se aplica como alternativa una UDD invertida con una política de alimentación gradual, comparándose con otras políticas operativas. Los resultados muestran que una unidad de destilación invertida equipada con un decantador bien diseñado proporciona hasta un 17% de mejora en eficiencia energética y tasa

de producción, un 7% más de recuperación y un 9% menos de tiempo de proceso respecto a una UDD convencional.

La tercera parte de este estudio se orienta a una mejora adicional de la operación de destilación. La alimentación gradual se identifica como un enfoque eficiente para optimizar la operación de la unidad. La alimentación superior (UDD invertida) junto con un caudal decreciente demostraron ser las estrategias de alimentación más eficientes, logrando una mejora del 10% en la tasa de producción y coste energético respecto a una UDD convencional con decantador. Asimismo, basándose en la estrategia de alimentación gradual, se propone el precalentamiento del alimento como una técnica viable de integración térmica en el proceso de destilación discontinua. Esta estrategia se demuestra eficaz en la intensificación del proceso, alcanzando una mejora máxima del 47% en eficiencia energética y tasa de producción respecto a una UDD convencional equipada con decantador.

En la cuarta parte de esta tesis, se desarrolla un modelo de electrolizador de membrana de intercambio protónico (PEMEL) adaptable a fuentes de energía variables. Aspen Plus se emplea para la modelización de la unidad, y el modelo del stack PEM se desarrolla en Aspen Custom Modeler (ACM) a partir de correlaciones empíricas y semiempíricas. Los resultados muestran una estrecha concordancia entre el modelo y los datos experimentales. De acuerdo con los resultados empíricos, el modelo indica que una presión operativa más baja mejora el rendimiento del electrolizador y que un aumento de temperatura de 40 a 80 °C reduce el voltaje de celda en aproximadamente un 13,7% a una densidad de corriente de 2 A/cm² (de 2,24 a 1,93 V). En consecuencia, se proponen dos escenarios operativos diferentes para una unidad PEMEL: (1) caudal de agua circulante fijo y (2) temperatura operativa fija, y el modelo se adapta para habilitar ambas opciones en simulación. El modelo de PEMEL propuesto y el escenario operativo planteado son potencialmente adaptables a perfiles de entrada de energía variables.

Table of Contents

List of Figures

List of Tables

Abbreviations and Acronyms

AC	Alternating Current
ACM	Aspen Custom Modeler
AEL	Alkaline Electrolysis
BD	Batch Distillation
BDU	Batch Distillation Unit
BECCS	Bioenergy With Carbon Capture And Storage
BP	Bipolar Plate
BoP	Balance Of Plant
CAPEX	Capital Expenditures
CCS/U	Carbon Capture and Storage/Utilization
CO_2e	Carbon Dioxide Equivalents
DC	Direct Current
ED	Extractive Distillation
EL	Electrolyzer
GDL	Gas Diffusion Layer
GHG	Greenhouse Gas
Gt	Gigatons
HABDU	Heteroazeotropic Batch Distillation Unit
HAD	Heterogeneous Azeotropic Distillation
HER	Hydrogen Evolution Reaction
HETP	Height Equivalent to Theoretical Plate
HHV	Higher Heating Value
HTO	Hydrogen-To-Oxygen
IEA	International Energy Agency
IRENA	International Renewable Energy Agency
LCOH	Levelized Cost Of Hydrogen
LHV	Lower Heating Value
MEA	Membrane Electrode Assembly

MEK	Methyl Ethyl Ketone
MIBK	Methyl Isobutyl Ketone
NIST	National Institute of Standards and Technology
NZE	Net-Zero Emission
OER	Oxygen Evolution Reaction
OPEX	Operational Expenditures
PEM	Proton Exchange Membrane
PEMEL	Proton Exchange Membrane Electrolyzer
PP	Porous Transport Layer
PSD	Pressure-Swing Distillation
PTL	Porous Transport Layer
PV	Photovoltaic
Persp.	Perspective
RD	Reactive Distillation
RF	Return Fraction
RR	Reflux Ratio
SDGs	Sustainable Development Goals
SEC	Specific Energy Cost
SOEL	Solid Oxide Electrolyzer
SPE	Solid Polymer Electrolyte
SPF	Specific Product Flow
SSO	Single-Step Operation
TDE	Thermo Data Engine
TSO	Two-Step Operation
UN	United Nations
VLL	Vapor-Liquid-Liquid
VRC	Vapor Recompression
VRE	Variable Renewable Energy
WMO	World Meteorological Organization

1. Introduction

In 2023, the global average temperature reached 1.45°C above pre-industrial levels (1850–1900). This unprecedented warming is accompanied by a series of extreme climate events, including intense heatwaves, floods, droughts, and wildfires, highlighting the accelerating impacts of climate change. The World Meteorological Organization (WMO) has characterized this situation as a "Red Alert," underscoring the urgent need for comprehensive and prompt action to reduce greenhouse gas emissions and transition to sustainable energy systems [1,2]. In response, the concept of a net-zero emission (NZE) strategy has emerged as a guiding framework, seeking to balance the greenhouse gas emissions with an equivalent quantity removed from the atmosphere, ultimately halting the global warming trend [3]. Figure 1-1 shows the global annual greenhouse gas (GHG) emission from 1990 to 2023, categorized by sector. According to this figure, global GHG emissions, measured in carbon dioxide equivalents (CO_2e) unit, have exhibited a significant increase from 38.0 gigatons (Gt) CO_2e in 1990 to around 51.8 Gt CO_2e in 2023, marking a rise of about 36% during this period. This increase reflects the persistent challenges in reducing emissions alongside economic development and population growth. Carbon dioxide (CO_2) emissions, predominantly resulting from fossil fuel combustion and industrial processes, constitute the largest share of GHG emissions. The CO_2 emission of about 22.7 Gt in 1990 had risen to about 37.4 Gt by 2023, representing an increase of roughly 65%. Industrial activities, from manufacturing chemicals and materials to refining fuels, significantly contribute to greenhouse gas emissions. They consume a substantial quantity of energy (majorly from fossil fuels) and emit carbon both directly (via combustion and processes) and indirectly (via electricity use). Consequently, without significant emissions reductions across all sectors, the objective of global warming control and restricting it to 1.5 °C is at risk [4].

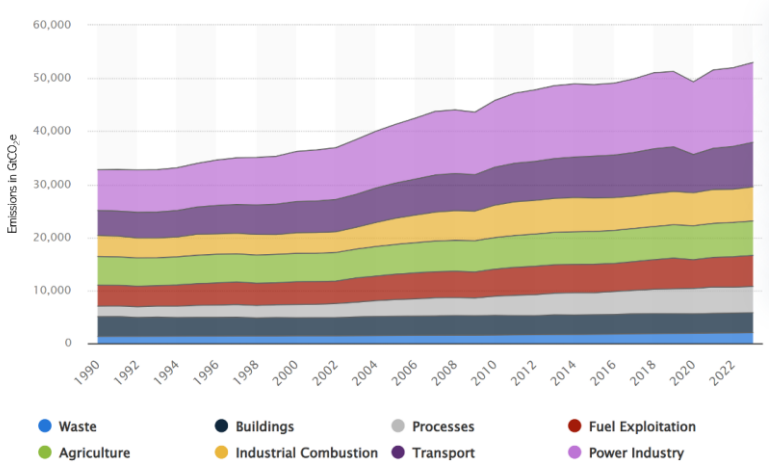

Figure 1-1. Global greenhouse gas emissions by sector from 1990 to 2023 [5].

Global efforts to address climate change and transform energy systems in recent years have prioritized decarbonization and electrification in industrial innovation. In addition to the challenges posed by climate change, high fossil fuel prices and energy security issues in recent years have highlighted the necessity to expedite the transition to sustainable and clean energy systems.

The necessity of the energy transition is emphasized by international accords and targets, from the United Nations Sustainable Development Goals (SDGs) [6] to climate conventions like the Paris Agreement [7]. In particular, SDG 7 (Affordable and Clean Energy) mandates a doubling of the global rate of energy efficiency improvement by 2030, acknowledging that the enhanced energy efficiency is as vital as switching to clean sources [8,9]. Similarly, SDG 13 (Climate Action) underscores the necessity of immediate action to reduce greenhouse gas emissions, noting that global emissions must be reduced to about half by 2030 to avert catastrophic warming [10]. In addition, the European Union (EU), as a global leader in climate action, is dedicated to achieving climate neutrality by 2050 along with stringent interim targets. Under the European Climate Law [10], which serves as a cornerstone of the European Green Deal, the EU has legally committed to reducing its net greenhouse gas emissions by at least 55% by 2030 compared to 1990 levels, as proposed in the "Fit for 55" legislative package [11,12]. Achieving these cuts will effectively require a complete transformation of the industrial energy model in Europe over the next few decades.

In order to achieve NZE by mid-century, industry and other challenging sectors must undergo a major transformation in the next few decades [13]. Various pathways and frameworks have been proposed by different organizations for policymakers aiming at a fundamental reform of the current energy system. Figure 1-2 illustrates the global CO_2 emission trajectories to the end of the century under different scenarios as listed below:

1- 1.5°C-aligned scenario (proposed by the International Renewable Energy Agency, IRENA): To keep global warming below 1.5°C, a significant and sustained reduction in greenhouse gas emissions is essential.
2- Pledges and commitments: Should countries fulfil their stated emission reduction promises, the projected rise in global average temperature could be limited to about 2.1 to 2.4°C by 2100.
3- Current policy trajectory: If only the existing climate measures are maintained, global temperatures are expected to increase by around 2.5 to 3° C by 2100.

4- No policy scenario (pre-Paris Agreement): In the absence of climate action, global temperatures are projected to rise by approximately 4.1°C to 4.8°C by the end of the century.

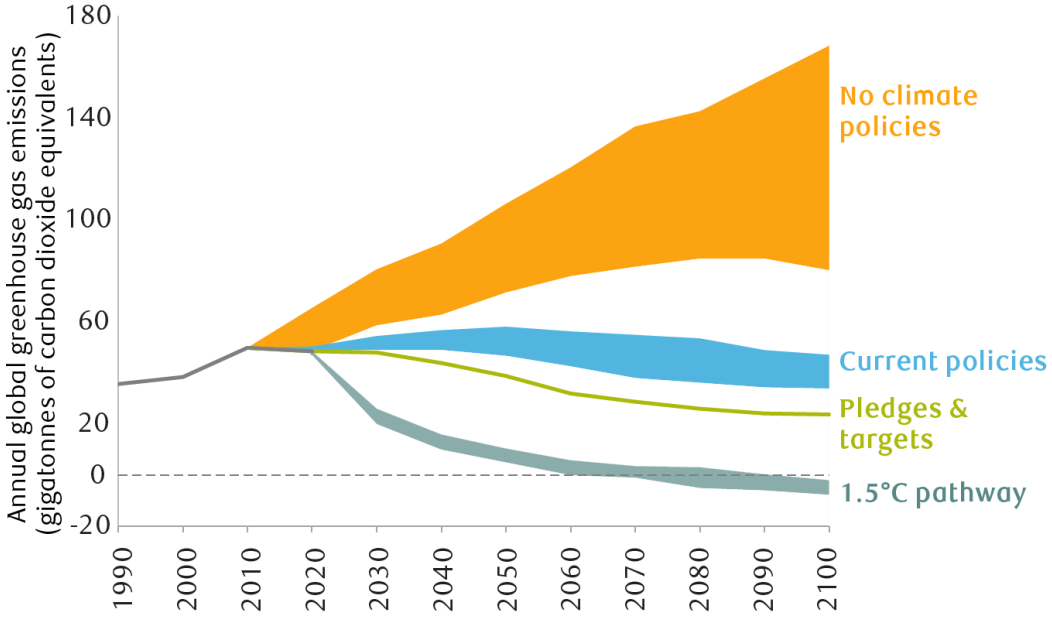

Figure 1-2. Global CO_2 emission trajectories under different scenarios [14].

There are also estimations stating that each sector should receive a particular value of investment, implicitly indicating the importance of each sector in energy transition plans. Figure 1-3 illustrates the contribution of various technology sectors according to the 1.5°C scenario, developed by IRENA [15]. As this figure shows, the targeted CO_2 emission reductions would be achievable through six principal technological transformations: (1) expanding the renewable energy generation capacity with a 25% contribution; (2) improvements in energy efficiency with a 25% contribution; (3) widespread electrification across end-use sectors with a 19% contribution; (4) development of hydrogen-oriented technology and using clean hydrogen (and its derivatives, including synthetic fuels and feedstocks) with a 12% contribution; (5) application of bioenergy in conjunction with carbon capture and storage (BECCS) with an 11% contribution; and (6) carbon capture and storage/utilization with an 8% contribution. Accordingly, achieving these objectives requires fundamental alterations in industries' energy consumption and implementation of new technologies to mitigate emissions.

BECCS = bioenergy with carbon capture and storage; CCS/U = carbon capture and storage/utilization.

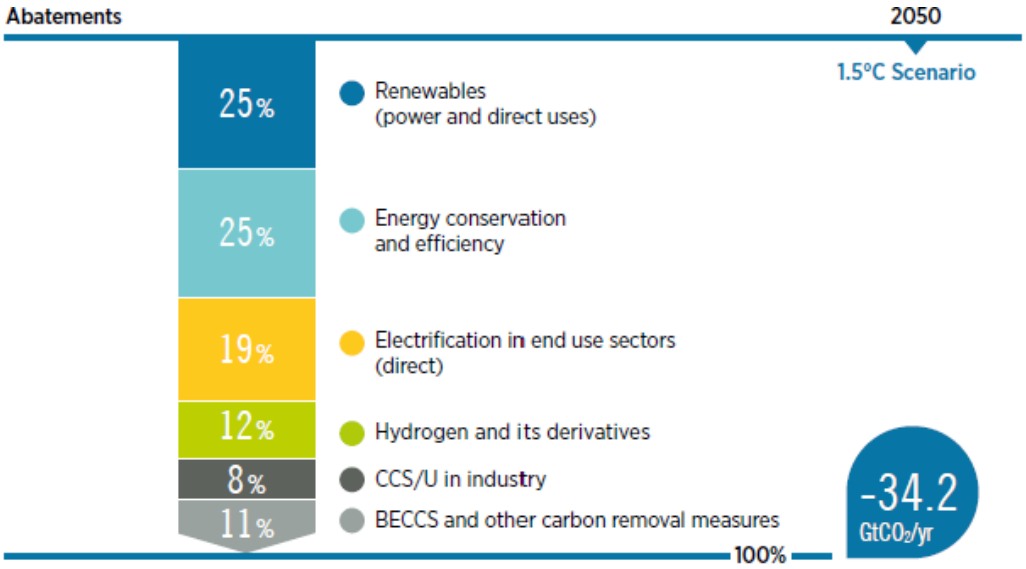

Figure 1-3. The six essential technological pathways and contribution of each to mitigate emissions by 2050 [15].

Various energy transition frameworks identify energy efficiency and clean energy vectors like hydrogen as pillars of decarbonization plan. Energy efficiency is the most sustainable and economical form of energy saving because each amount of energy saved directly reduces emissions, lowers operational costs, and supports renewable integration. In addition, hydrogen is recognized as a key factor in decarbonization. Green hydrogen, produced via electrolysis, offers a practical way to decarbonize industry by electrifying energy use where direct application of renewable electricity is not feasible.

Together, energy efficiency and clean energy vectors like hydrogen form the backbone of the global decarbonization strategy. Sustainable Development Goal 7 (SDG 7) explicitly calls for a doubling of the global rate of improvement in energy efficiency by 2030, highlighting its major role in NZE pathways [9]. Also, the European Union has recognized efficiency as a strategic priority. The EU's revised Energy Efficiency Directive (2023) mandates at least an 11.7% reduction in final energy consumption by 2030 compared to previous expectations. The "energy efficiency first" principle applies to the entire energy chain, from generation to end use, and it aims to lower energy costs, reduce emissions, and reduce dependency on imported fossil fuels [16,17].

In parallel, hydrogen is seen as a strategic solution for industrial decarbonization and the long-term energy system transformation. According to the European Hydrogen Strategy (2020) and the REPowerEU initiative (2022), the EU aims to install 40 GW of electrolysis plants by 2030 and produce 10 million tons of green hydrogen and import 10 million tons. Over the longer term, hydrogen is estimated to supply up to 23% of the total energy in Europe by 2050 [8,18].

To achieve the aforementioned objectives, a group of integrated policy packages (including the European Green Deal, the Fit for 55 legislations, and the UN SDGs) are developed to promote energy efficiency and hydrogen deployment through rules, financial mechanisms, and innovation programs. However, policy alone is insufficient to meet decarbonization targets. Without scalable technological solutions, such as high-efficiency energy-intensive unit operations and advanced electrolysis processes, these goals remain out of reach. This underscores the need for focused research and innovation, particularly in two high-impact areas: (1) improving energy efficiency in industrial systems and (2) developing high-performance and cost-effective hydrogen production technologies.

Regarding the hydrogen transition, rapid policy-driven expansion has accelerated academic and industrial development at the same time. Ongoing research aims to enhance electrolyzer performance via various approaches such as developing alternative catalysts, durable membranes, integrated thermal management, and novel process designs, ultimately reducing both capital and operating costs.

Also, energy efficiency as a critical concern across industrial sectors involves various fields such as upgrading equipment, optimizing process parameters, recovering waste heat, and revamping systems to minimize consumption. The thermal separation processes, such as distillation, are among the most energy-intensive industrial operations. Distillation, as a process relying on boiling and condensation, accounts for about 40% of the total energy consumption in chemical industries [19,20]. Distillation units, mainly working in high-grade heat levels, suffer from low energy efficiency and lose much of the energy as low-grade heat. Hence, despite the long history of distillation units, improving their energy efficiency remains vital.

Ultimately, technological innovation is the key to connect the policy to practice, whether in updating relatively mature technologies like distillation or advancing relatively new technologies like PEM electrolysis.

Advances in modelling and simulation enable optimization of reflux ratios, heat integration, and batch operation strategies in distillation. Similarly, electrochemical and thermal modelling enable us to conduct detailed analysis of electrolyzer behavior under different conditions and help next-generation designs for better efficiency and durability. In both areas, modelling is not just theoretical but a strategic tool of innovation. It enables scenario analysis, system integration, and performance optimization, helping reduce experimental costs and accelerate development procedure.

This PhD thesis, titled "New Solutions in Decarbonization and Electrification of the Industrial Energy Model," presents two technological approaches for industrial decarbonization: (1) improving energy efficiency in the solvent recovery process, exemplified by the dehydration of methyl isobutyl ketone (MIBK) through batch distillation, and (2) enhancing green hydrogen production via proton-exchange membrane (PEM) electrolyzers. The research focuses on solvent recovery and PEM electrolysis as illustrative challenges, intending to produce insights relevant to more extensive industrial systems. The ultimate goal can be defined as creating an energy model that uses less energy for each quantity of product and is fed by clean and renewable energy sources. This will help with SDG 13 (climate action), SDG 7 (clean energy access), and growth through innovation and energy security.

Structure of the thesis

In the chapters listed below, we delve deeper into these themes and present the research undertaken to contribute new insights and solutions:

- Chapter 2 - State of the art and literature review: This chapter surveys the state-of-the-art in industrial energy efficiency techniques, with emphasis on distillation improvements and hydrogen production technologies. Research opportunities are identified, particularly in modelling approaches for batch distillation and PEM electrolyzers.
- Chapter 3 - Process design and simulation of methyl isobutyl ketone (MIBK) dehydration by batch distillation: A study on unit configuration and operational policies: In this chapter, the design and simulation of a batch distillation process for the dehydration of methyl isobutyl ketone (MIBK) from a water-containing heteroazeotropic mixture is presented. Using Aspen Plus and its dynamic BatchSep module, various unit configurations and operational strategies are evaluated to optimize product purity, recovery, and energy

efficiency. Three configurations, including a conventional batch column, a column with a decanter, and a simple unit without reflux, are compared under different operating conditions. The study shows that integrating a decanter notably improves MIBK recovery and reduces energy consumption, while non-reflux operation accelerates processing time at the cost of lower recovery. The chapter concludes with recommendations on optimal reflux ratios and configurations for balancing energy use and product yield.

- Chapter 4 - Improvement of energy efficiency and production performance in a heteroazeotropic batch distillation unit: a study on decanter control and feeding strategy: In this chapter, strategies to enhance energy efficiency and production performance in the heteroazeotropic batch distillation of methyl isobutyl ketone (MIBK) are explored through process simulation. The role of decanter design and control, along with feed quantity and separation quality, is critically analysed. Key findings highlight that while increasing feed quantity improves productivity and reduces specific energy consumption, its benefits plateau beyond an optimal point. The study also reveals that decanter holdup volume and phase separation efficiency significantly impact recovery and operational losses. Moreover, an inverted batch distillation configuration with a controlled feeding strategy is introduced and shown to further improve recovery (up to 7%) and production efficiency (up to 17%) over conventional setups. The chapter provides practical insights into optimizing decanter and feeding policies for improved batch distillation performance.
- Chapter 5 - Heat Integration and Process Improvement of a Batch Distillation Unit Using a Gradual Feeding Strategy; A Case Study on MIBK-Water Separation: In this chapter, the energy efficiency and production capacity of a batch distillation unit for methyl isobutyl ketone (MIBK) dehydration are improved through a gradual feeding strategy and heat integration. Using the MIBK–water heteroazeotropic system as a case study, the effects of batch size, feed rate profiles, and feed locations (top vs. bottom) are systematically analysed. Results show that gradual feeding, especially top feeding with a decreasing flow rate, enhances energy and production performance compared to conventional setups. Additionally, a novel heat integration approach tailored to the gradual feeding policy is proposed, demonstrating up to 47% improvement in combined energy efficiency and production rate.
- Chapter 6 - Aspen Plus model of PEM electrolysis system for hydrogen production: In this chapter, a semi-dynamic model of a proton exchange membrane (PEM) electrolysis unit is developed using Aspen Plus, employing a

custom-built stack model integrated from Aspen Custom Modeler (ACM). The model incorporates thermodynamic and electrochemical formulations to simulate voltage behavior, overpotentials, and Faraday efficiency as a function of current density. System components such as separators and heat exchangers are modelled using standard Aspen Plus tools. The model is validated against literature data and used to evaluate the effects of temperature and pressure on performance. Two operational control scenarios, fixed water flow rate and fixed operating temperature, are compared, offering insights into voltage efficiency, system stress, and thermal control strategies. The model is adaptable to fluctuating renewable energy inputs and can support techno-economic assessments or integration with downstream processes like green ammonia or methanol synthesis.

- Chapter 7 - Conclusions and outlook: This chapter summarizes the key findings from both studies on energy efficiency and hydrogen studies. The contributions to knowledge and the practical implications are discussed. This chapter also outlines recommendations for future research, such as pilot-scale testing of the distillation scheme in a real unit, providing a custom-model for simulation of batch distillation as well as further improving the PEM model to account for degradation, lifetime, utility consumption details, etc. The reflections on how these solutions help driving the industries in a more sustainable pathway is also discussed in order to link this study to the decarbonization goals.

Through this structure, the thesis systematically addresses how new solutions in energy efficiency and electrification (via hydrogen) can contribute to the industrial energy model.

References

[1] Climate change indicators reached record levels in 2023: WMO, (n.d.). https://wmo.int/news/media-centre/climate-change-indicators-reached-record-levels-2023-wmo (accessed June 7, 2025).

[2] UN sounds “Red Alert” as world smashes heat records in 2023 | Reuters, (n.d.). https://www.reuters.com/business/environment/un-sounds-red-alert-world-smashes-heat-records-2023-2024-03-19/ (accessed June 7, 2025).

[3] What does net zero emissions mean? | Explainer | Climate Council, (n.d.). https://www.climatecouncil.org.au/resources/what-does-net-zero-emissions-mean/ (accessed June 7, 2025).

[4] Take urgent action to combat climate change and its impacts, Https://Sdgs.Un.Org/Goals/Goal13 (n.d.).

[5] Global GHG emissions by sector 1990-2023| Statista, Https://Www.Statista.Com/Statistics/1423179/Global-Ghg-Emissions-by-Sector-Annual/ (n.d.).

[6] THE 17 GOALS | Sustainable Development, (n.d.). https://sdgs.un.org/goals (accessed June 7, 2025).

[7] U. Nations, The Paris Agreement | United Nations, (n.d.). https://www.un.org/en/climatechange/paris-agreement (accessed June 7, 2025).

[8] Energy efficiency targets, (n.d.). https://energy.ec.europa.eu/topics/energy-efficiency/energy-efficiency-targets-directive-and-rules/energy-efficiency-targets_en (accessed June 7, 2025).

[9] Goal 7 | Department of Economic and Social Affairs, (n.d.). https://sdgs.un.org/goals/goal7 (accessed June 7, 2025).

[10] European Climate Law - European Commission, (n.d.). https://climate.ec.europa.eu/eu-action/european-climate-law_en (accessed June 7, 2025).

[11] 2030 climate targets - European Commission, (n.d.). https://climate.ec.europa.eu/eu-action/climate-strategies-targets/2030-climate-targets_en (accessed June 7, 2025).

[12] Delivering the European Green Deal - European Commission, (n.d.). https://commission.europa.eu/strategy-and-policy/priorities-2019-2024/european-green-deal/delivering-european-green-deal_en (accessed June 7, 2025).

[13] Executive summary – World Energy Outlook 2022 – Analysis - IEA, Https://Www.Iea.Org/Reports/World-Energy-Outlook-2022/Executive-Summary (n.d.).

[14] Net zero: What will life be like in 2050? - RBC Wealth Management, (n.d.). https://www.rbcwealthmanagement.com/en-us/insights/net-zero-what-will-life-be-like-in-2050 (accessed June 7, 2025).

[15] World energy transitions outlook 2023：1.5°C pathway, International Renewable Energy Agency IRENA, 2023.

[16] European Union energy efficiency & Trends policies | European Union profile | ODYSSEE-MURE, (n.d.). https://www.odyssee-mure.eu/publications/efficiency-trends-policies-profiles/european-union.html (accessed June 7, 2025).

[17] Recast Energy Efficiency Directive (EU) 2023/1791 | Climate Policy Database, (n.d.). https://climatepolicydatabase.org/policies/recast-energy-efficiency-directive-eu-20231791 (accessed June 7, 2025).

[18] EU Hydrogen Strategy under the EU Green Deal | European Hydrogen Observatory, (n.d.). https://observatory.clean-hydrogen.europa.eu/eu-policy/eu-hydrogen-strategy-under-eu-green-deal (accessed June 7, 2025).

[19] R.E. Fitzmorris, R.S.H. Mah, Improving distillation column design using thermodynamic availability analysis, AIChE Journal 26 (1980) 265–273. https://doi.org/10.1002/AIC.690260209;WEBSITE:WEBSITE:AICHE;WGROUP:STRING:PUBLICATION.

[20] J. Fang, X. Cheng, Z. Li, H. Li, C. Li, A review of internally heat integrated distillation column, Chin J Chem Eng 27 (2019) 1272–1281. https://doi.org/10.1016/j.cjche.2018.08.021.

2. State of the art and literature review

2.1. Energy efficient solvent recovery via batch distillation

2.1.1. Distillation

The globally growing trend of energy consumption and environmental protection policies justify the necessity of optimization in energy-intensive industries to improve energy efficiency [1]. Distillation is one of the most popular separation methods, contributing to about 40% of the energy consumption of the chemical industries [2]. Separation processes alternative to distillation, like separating molecules according to their chemical properties or size, are still underdeveloped or expensive to scale up [3].

Despite the high energy intensity and high cost of capital and operation, the energy efficiency of distillation units is often too low [4]. Accordingly, despite the long history of distillation units in industries, and numerous studies and developments, distillation columns are still attractive cases for energy and separation efficiency improvement and development works in academic and industrial categories [5,6]. Batch distillation (BD) is preferred over continuous distillation in plants that do not operate in continuous or that work at small or medium scale [7,8]. BD is extensively used for product purification or solvent recovery in pharmaceuticals, polymers, fine and high-value market chemicals, and biochemical industries [9,10]. While batch distillation developments and applications are limited compared to its continuous counterpart, its popularity is growing due to its interesting features as listed below [5,6]:

1- Applicability on small scales, especially for high-value market products.
2- Low capital cost
3- Flexibility to handle variable feed composition.
4- Allowing small-volume production
5- Providing a wide range of product separation using a single column
6- Possibility to operate in different configurations.

Accordingly, batch distillation can potentially be applied in a wider variety of separation processes, but there is still an array of challenges regarding selecting proper operation policy, configuration, and design parameters in different steps from design to operation [10,11]. The recent advances in computer-aided engineering and modelling and process simulation tools have facilitated the simulation, optimisation and development of complex operations with dynamic

nature [26,30]. Hence, a growing number of studies are being conducted on batch operations to provide deeper insights into its complex and dynamic operation.

2.1.2. Heteroazeotropic distillation

Separation of a heteroazeotropic mixture, involving a liquid-liquid-vapor three-phase equilibrium, is always associated with complexity and requires specialized measures and techniques. While distillation is one of the most popular separation processes, conventional distillation techniques are not applicable for separation of azeotropic or close-boiling mixtures. Hence, distillation units are developed in a broad spectrum of unit configuration and operation to handle the azeotropic and complex systems, including extractive distillation (ED) [12,13], pressure-swing distillation (PSD)[14–18], reactive distillation (RD) [19,20], heterogeneous azeotropic distillation (HAD) [21–26], or a combination of them [27,28]. These approaches are generally limited to distinct cases and conditions; the PSD method does not need any new component in the feed mixture, but it is only applicable for pressure-sensitive mixtures. Also, the ED and HAD methods are associated with introducing an additional agent called "entrainer" which offers different possibilities for separation: in the ED, which is a homogeneous azeotropic distillation technique, the entrainer is used to form a miscible homogenous mixture with a more favourable equilibrium condition and modified relative volatility of the original mixture and is fed continuously to the column. Alternatively, in HAD, an entrainer is added to the feed in order to form a heteroazeotropic system with an immiscible mixture (including rich and lean) in the reflux drum/decanter, enabling the operator to split the feed components mechanically to a specific extent [29,30]. One of the main issues in such techniques is the entrainer selection, and due to the necessity of a second separation process for entrainer removal/recovery, the distillation is not regarded as an independent unit, but it must be studied as a part of the unit. Subsequently, any optimization approach for HAD and ED operations shall cover the cost, time, and energy required for the entire separation steps. These techniques are also applicable to the batch distillation process of azeotropic systems. The HAD can be an efficient approach to improve production rate and energy efficiency of a BDU through integrating a mechanical liquid-liquid separator into the unit, transforming it to a heteroazeotropic batch distillation unit (HABDU). Zhang et al. [21] proposed using a HABDU for phenol dehydration as an alternative to direct distillation, providing higher product quality and

approximately 20–25% energy savings. In the last two decades, around 40 works related to heteroazeotropic batch distillation have been published in reputed journals. These works cover aspects of batch heteroazeotropic distillation such as entrainer selection [25,31], distillation regions, strategies and feasibility [26,32,33], novel configurations [34–36] or practical applications [22,23,37].

Given the complexity of the system, including a batch rectifier and a liquid-liquid decanter both with dynamic operation, control strategies are of particular interest. Skouras, Kiva and Skogestad have reported a comprehensive study on the analysis and control of this operation. They described an indirect temperature control scheme, by controlling the temperature in the middle of the column. This temperature is related to the reflux flow and subsequently, with the entrainer-rich phase holdup in the decanter. This scheme was preferred to the direct holdup control in the decanter vessel [38].

A particularly interesting case of heteroazeotropic distillation is where the heteroazeotrope appears with the components of the original feed without adding a new component as entrainer to the system. Such systems are known as "auto-entrained" or self-entrained" systems and their intrinsic phase immiscibility can be used to enhance the separation. A well-known and widely studied example of such systems is the water-tert-butanol (2-methyl-2-propanol) binary mixture [5].

2.1.3. Heat integration and novel configurations of batch distillation units

The energy saving and efficiency improvement methods have been widely applied for continuous distillation, but the BD operation have not experienced the same development and still needs to be addressed [39]. There are different approaches developed for heat integration and process intensification of a batch distillation unit (BDU), among which heat pumps have gained more attention recently. As representative examples, Nair and Raykar [40] used a two-stage vapor recompression (VRC) heat pump to enhance the separation of a ternary mixture of hexanol, octanol, and decanol, observing a 52% energy saving and a 12.2% total annual cost reduction. Radhika et al. [41] incorporated a double-stage VRC heat pump into a BDU to integrate heat and separate the ternary mixture. Their proposed integrated configurations resulted in a 41.7% lower energy consumption compared with a conventional BDU. Gandu et al. [42] proposed a heat pump-assisted batch distillation unit for separation of a ternary mixture aiming for

reduced cost and carbon emissions. A multi-stage VRC algorithm is introduced as an alternative for the single-stage VRC approach due to its challenges with high vapor compression ratio (>3.5). They found that the feed composition determines each approach's cost-effectiveness, with the highest reported total annual cost reduction in their work being about 10%. Kazemi et al. [43] proposed using the bottom flashing heat pumps as an alternative to VRC heat pumps. They reported a total annual cost saving of 19%, using a flashing heat pump and lower annual costs in the range of 4.2-10.9% compared to the equivalent process with vapor recompression heat pumps. Modla and Lang [44] conducted a study on integrating different heat pump systems in batch distillation units, concerning the economic feasibility of heat integration and payback periods. According to their evaluation, direct application of VRC was not economically feasible, as the minimum payback period was over 10 years, while they managed to reduce it to about seven years by adding a heat exchanger. A conclusion extracted from these studies is that, while heat pumps for heat integration in a BDU offer significant improvements in energy efficiency, they face key challenges, including high capital costs, long payback periods, and complexity in design, control, and operation [44–46]. Alternatively, external energy integration by feed stream heating/flashing stands as a simple and practical approach in continuous distillation [47,48]; however, since the feed in batch distillation units is conventionally charged in the pot before starting the operation, there is no feed stream in the unit configuration, making this approach infeasible in batch distillation. To this end, gradual feeding to the unit seems to be a potential solution to unlock the heat integration possibility within the batch distillation units.

On the other hand, there is also a less popular arrangement of BDU called inverted batch distillation or batch stripper with feed charged into the reflux drum at the top, and the products are usually withdrawn as bottom product [6,49,50]. This configuration has been proven to enhance the operation time for separation of mixtures in which the light components present in a small fraction [51]. Moreover, it is suggested for the mixtures with a minimum boiling azeotrope [52], the cases with a small fraction of light component and some cases in which the regular configuration (batch rectifier) is not feasible for that separation [11]. This configuration is not a recently emerged batch column configuration, but it has not received sufficient attention and has been rarely applied in practice. Here, we have modified an inverted batch distillation by adding a decanter, aiming to utilize it in separation of a heteroazeotropic mixture.

2.1.4. Solven recovery (MIBK dehydration)

Solvents are widely used in industry, existing different families and applications. These applications usually take place in the chemical industry, where they are used as separation agent for solid or liquid extraction processes, or as an auxiliary or intermediate in manufacturing of paints or polymers, by decreasing their viscosity. An important family of solvents are the ketones, characterized by the functional group C=O connected to two alkyl groups, which include a large list of molecules with excellent properties as solvents, finding applications in adhesive and coating industries and other uses that need to dissolve organic substances. Methyl isobutyl ketone, ethyl amyl ketone, methyl ethyl ketone, diisobutyl ketone, acetone or hexanone belong to this family [53]. Particularly, MIBK is used in pharmaceutical industry [39], as well as in paint industries as solvent/carrier of organic dyes. The high toxicity of many of these solvents, together with their rising prices, originated by the low availability and high cost of feedstocks for their synthesis [54], make it of great importance to develop separation techniques in order to purify and recover them for further use. Solvent recovery must be an effective approach to purify the solvent to the desired level for further use.

Depending on the specific application of the solvent, different recovery scenarios can be employed, i.e., separation of solvents from heavy residues, polymers, or inorganic salts; separation of solvent mixtures into their individual components; or separation of water (dehydration/drying) from organic solvents. Among these approaches, water removal is one of the most common separation processes employed for solvent recovery, and various alternatives have been proposed for this purpose, including adsorption, liquid–liquid extraction, membrane separation, and distillation [3]. Despite the relatively high capital cost and being an energy-intensive process, distillation still stands out as one of the first alternative when selecting a solvent recovery process.

Methyl Iso-Butyl Ketone (MIBK) is a versatile solvent with a broad range of industrial applications. Its outstanding dissolution capabilities, biodegradability, and limited water solubility it is utilized in numerous chemical processes and in the industrial production of pharmaceuticals, paints, rubber, pesticides, cleaning solvents, etc. [55,56]. Specifically, it is used as a solvent in the paint industry, where it ends up mixed with water after use. MIBK, used as a solvent, is frequently found polluted by a small fraction of water. On the other hand, due to the high toxicity, limited availability, and high cost of fresh MIBK, a reliable approach for

solvent recovery/dehydration is demanded to meet the sustainable production goals in the economic and environmental protection aspects of the process [39,54].

The low solubility of water in MIBK (around 2% by weight at room temperature and atmospheric pressure) cause forming a heterogenous two-phase mixture, which allows mechanical removal of the main fraction of water, by decanting the two-phase mixture. After the initial decanting, the remaining MIBK–water mixture forms a self-entrained heteroazeotropic system. Since HABDU is studied in numerous research works on separation of self-entrained mixtures [34,57], it seems to be a suitable candidate for separation of this mixture, especially in small production capacities and low budget for initial investment. Despite the large number of industrial operations in which MIBK gets polluted by water after use, the only work reported on the dehydration of MIBK for solvent recovery is a previous study of our team [58]. In that study a batch distillation unit equipped with a decanter was employed and evaluated for MIBK dehydration showing its superior performance over a conventional batch distillation. There are other studies addressing MIBK separation from different mixtures such as the purification of MIBK-toluene mixtures by heteroazeotropic distillation, using methanol as entrainer [59], the removal of MIBK from aqueous solutions by vacuum membrane distillation, where MIBK is the pollutant (minority compound) in residual water streams [60], or the purification of MIBK after synthesis by an extractive distillation column followed by a solvent recovery column [61].

In the HABDU employed for MIBK-dehydration, the aqueous phase in the decanter can be discharged, and the organic phase (MIBK-rich phase), as the desired liquid phase, can be refluxed for further purification. Here, the study continues to address the subject in more detail, provide deeper insight into the process, and prepare perceptible guidelines for operators. Wider ranges of operation, non-ideal operation of the column and decanter, and various configurations including gradually feeding and inverted batch distillation are considered in this study. The primary objectives of this study are summarized below:

- To apply, evaluate, and compare different configurations and operation policies for separation of heteroazeotropic systems in terms of recovery, process duration, and production rate.
- To evaluate different configurations and operation scenarios in terms of energy cost.

- To introduce an effective approach for distillation of heteroazeotropic mixtures and specify the optimum operation ranges.
- To improve the process in terms of separation efficiency and energy demand at the same time.

2.2. PEM electrolyzer system for green hydrogen production

2.2.1. Green hydrogen

As the global population continues to grow and living standards improve, energy demand is steadily rising. The estimations shows that global energy demand may double by 2050 and potentially triple by the end of the century [62]. The majority of energy production still relies on the combustion of fossil fuels, contributing to serious environmental challenges and climate change. These challenges underscore the urgency of transitioning to cleaner and more sustainable energy sources. In this context, hydrogen is gaining attention as one of the most promising clean and sustainable energy carriers. It produces only water when used as a fuel, without emitting carbon, and offers an impressive energy density of around 140 MJ/kg, which is more than double that of typical solid fuels like coal or biomass [63,64]. In addition, hydrogen plays a vital role as feedstock in key products such as fertilizers, petroleum refining, and petrochemicals. Hydrogen can be produced through different approaches, from fossil-based methods like methane steam reforming and coal gasification to more sustainable ones such as biomass conversion and water electrolysis, etc. [65]. The various hydrogen production methods are provided in Figure 2-1. Currently, about 96% of hydrogen worldwide is produced from non-renewable fossil sources, with methane steam reforming being the predominant method [66,67]. Hydrogen produced from fossil fuels results in significant greenhouse gas (GHG) emissions, which undermines its potential benefits in supporting energy transition efforts. The true value of hydrogen in the energy transition lies in producing it from renewable clean sources. Water electrolysis, defined as splitting the water molecule under the action of electricity, represents the most prominent electrochemical route for producing molecular hydrogen, and it is expected to grow substantially in parallel with the expansion of renewable energy sources [68]. The hydrogen produced from water electrolysis using renewable electrical power is commonly known as green hydrogen [69]. Green hydrogen plays a key role in energy transition pathways, not only as an

energy vector for storing and transferring renewable power, but also in the production of valuable chemicals, especially when combined with essential reactants such as carbon dioxide or nitrogen [70]. It is also anticipated to serve as a pivotal energy carrier in developing markets, particularly within the transportation sector and the integration of renewable energy sources [71].

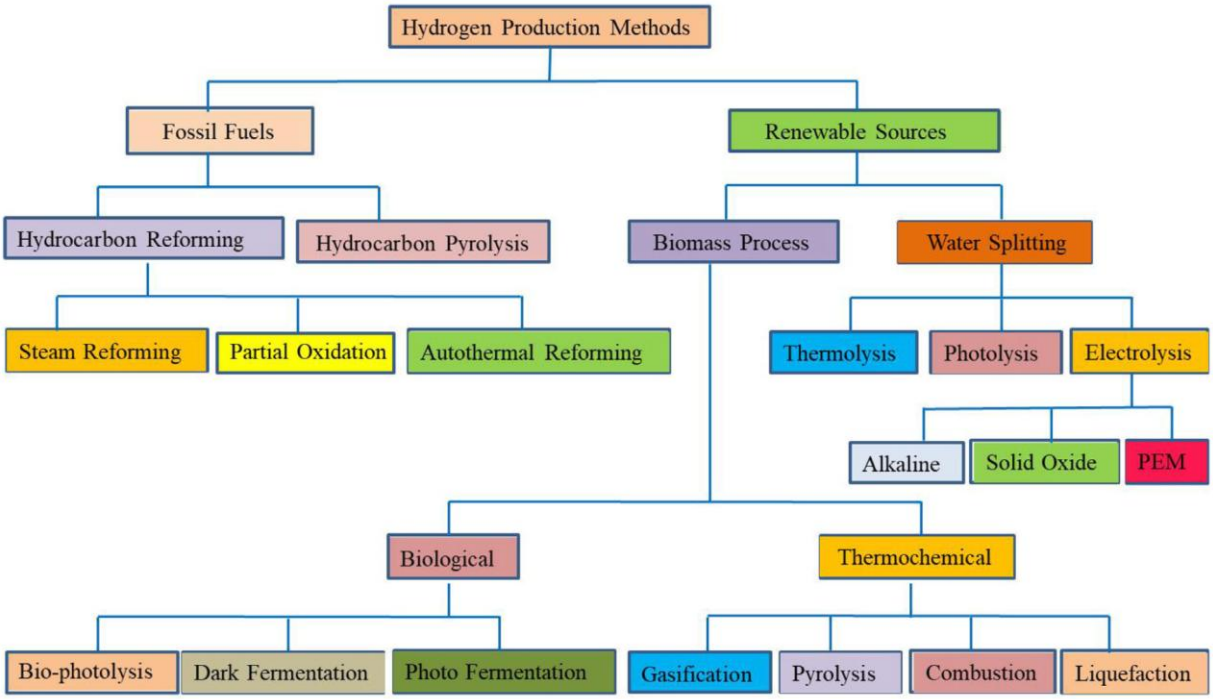

Figure 2-1. Various Hydrogen production approaches [65].

The hydrogen produced from water electrolysis using renewable power sources offers a carbon-neutral pathway in which it can be applied in transportation, agricultural, industrial, and residential sectors. Figure 2-2 shows a representative value chain for green hydrogen, highlighting its production through renewable-powered electrolysis and its diverse applications across multiple sectors. This figure describes how electricity generated from renewable sources is used to produce green hydrogen via electrolysis and the hydrogen which can be stored during periods of low energy demand or to be transported and converted into liquid energy carriers such as ammonia or methanol [72]. The produced hydrogen also supports various end-uses, such as agriculture, fuel for transportation or industrial processes, and residential applications for power generation and heating.

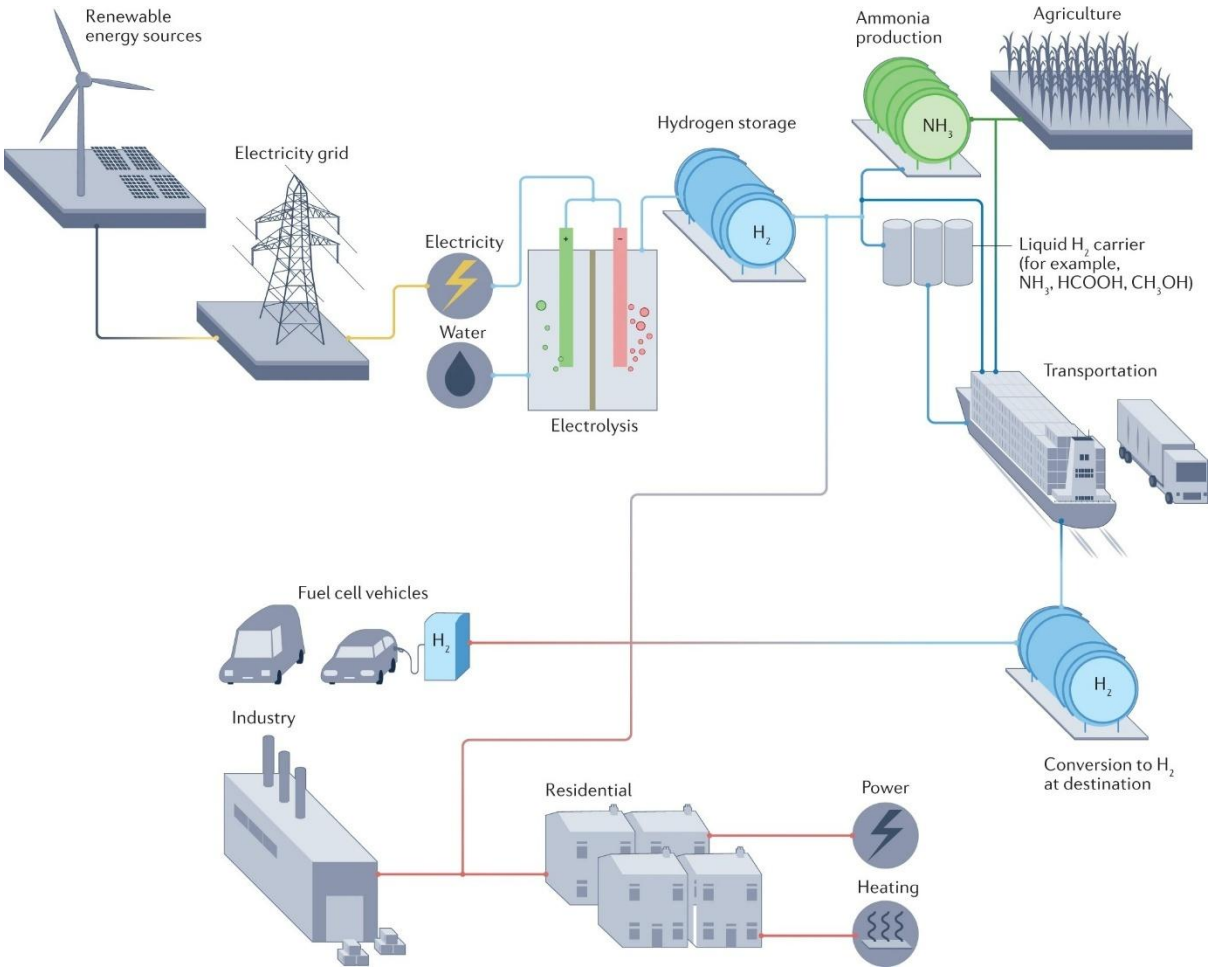

Figure 2-2. Overview of green hydrogen production and its application in different sectors including industries, transportation, agriculture, and residential use [73].

2.2.2. Water electrolysis

Water electrolysis is an electrochemical technique applied for decomposition of water into hydrogen and oxygen gases through the application of an electric current. The electrolysis process is fundamentally driven by redox (reduction–oxidation) reactions. Generally, the electrons are released at the anode (oxidation) and are received at the cathode (reduction) implying that the oxygen is produced in the anodic compartment and hydrogen is produced in the cathodic compartment. The electrochemical reactions occurring at each electrode depends on the electrolyte type (acidic or alkaline) [74]. The electrode-specific reactions, known as oxygen evolution reaction (OER) and hydrogen evolution reaction (HER) are presented in Table 2-1. The general electrolysis process in an electrolysis cell including an anode, a cathode, and an electrolyte is illustrated in Figure 2-3. The notations "(g)" and "(l)" indicates that the substances are in the gaseous and liquid phases, respectively.

Table 2-1. Electrode reactions for different electrolyte types.

Electrolyte	Electrode	Reaction
Alkaline	Cathode (HER)	$2H_2O(l) + 2e^- \rightarrow H_2(g) + 2OH^-$
	Anode (OER)	$4OH^- \rightarrow 2H_2O(l) + O_2(g) + 4e^-$
Acidic	Cathode (HER)	$2H^+ + 2e^- \rightarrow H_2(g)$
	Anode (OER)	$2H_2O(l) \rightarrow 4H^+ + O_2(g) + 4e^-$

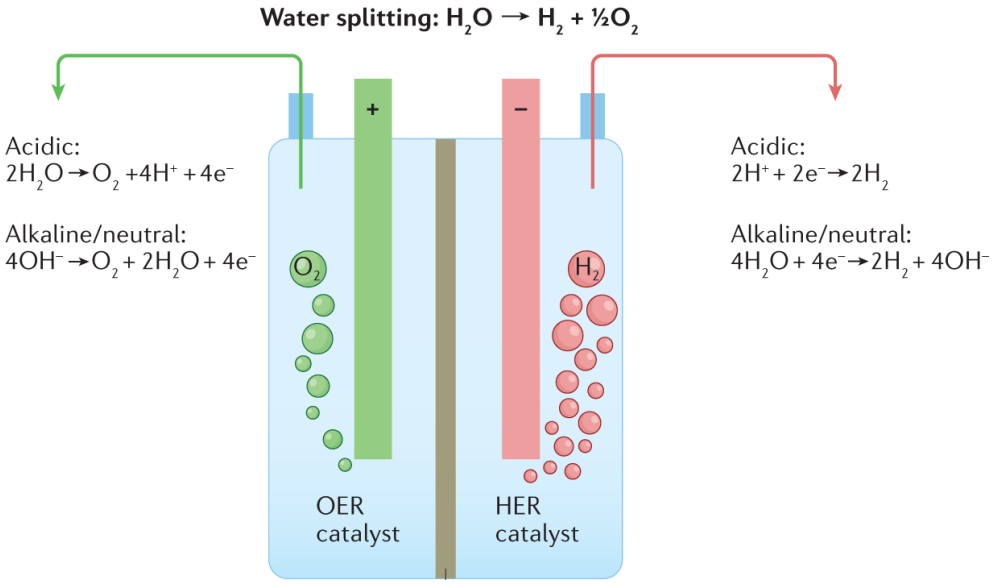

Figure 2-3. Overview of a typical electrolysis cell and the associated reactions [73].

Regardless of the electrolyte composition, the overall chemical equation of water electrolysis is the same [75]:

$$2H_2O(l) + 2e^- \rightarrow H_2(g) + 2OH^- \quad (1)$$

According to this equation, for 2 moles of water that undergo electrolysis, an equivalent quantity of hydrogen moles and half of that quantity of oxygen are generated. Water electrolysis is not a spontaneous reaction at temperatures below approximately 2250 °C [76], and therefore requires an external thermal and electrical energy input. The enthalpy changes per mole of water (ΔH, in kJ/mol) is given as follows [76]:

$$\Delta H = \Delta G + T\Delta S \quad (2)$$

These enthalpies representing the enthalpy difference between the reactants and products, known as reaction enthalpy, reflects the total energy change required to drive the reaction. It includes two terms of reversible and irreversible. The term

$T\Delta S$ represents the irreversible portion of the energy change in system. Since the gaseous products, hydrogen and oxygen, possess greater entropy than the liquid-phase reactants, the overall entropy change $\Delta S > 0$. The term ΔG reflects the reversible portion of the energy change in the system. Since electrolysis is inherently non-spontaneous and requires external energy input, the Gibbs free energy is positive ($\Delta G > 0$)[76]. Under standard conditions (P=1 atm. and T=25 °C), the Gibbs free energy is $\Delta G^0 = -237.2 kJ/mol$. This energy quantity can be supplied by applying a voltage of $E^0 = \Delta G^0/2F \approx 1.229\, V$, known as reversible voltage or open circuit voltage, which is a function of operating temperature and pressure. Depending on the supplied input power, the operating voltage of the electrolysis cells may exceed the standard reversible cell voltage, E^0, thereby enabling hydrogen and oxygen production while also reflecting the presence of irreversibility terms such as activation, ohmic, and concentration overpotentials.

2.2.3. Water electrolysis technologies

There are several electrolysis technologies, but alkaline electrolysis (AEL) and proton exchange membrane electrolysis (PEMEL) are the most widely adopted and commercially mature low temperature electrolyzers and solid oxide electrolyzer (SOEL) is the relatively mature high temperature electrolysis technique [77,78]. A schematic of these three major categories of electrolyzers is shown in Figure 2-4. Another emerging technology is anion exchange membrane (AEM) electrolysis, which is a promising alternative in the near future [79]. More details of the electrolyzers is provided in the following sections.

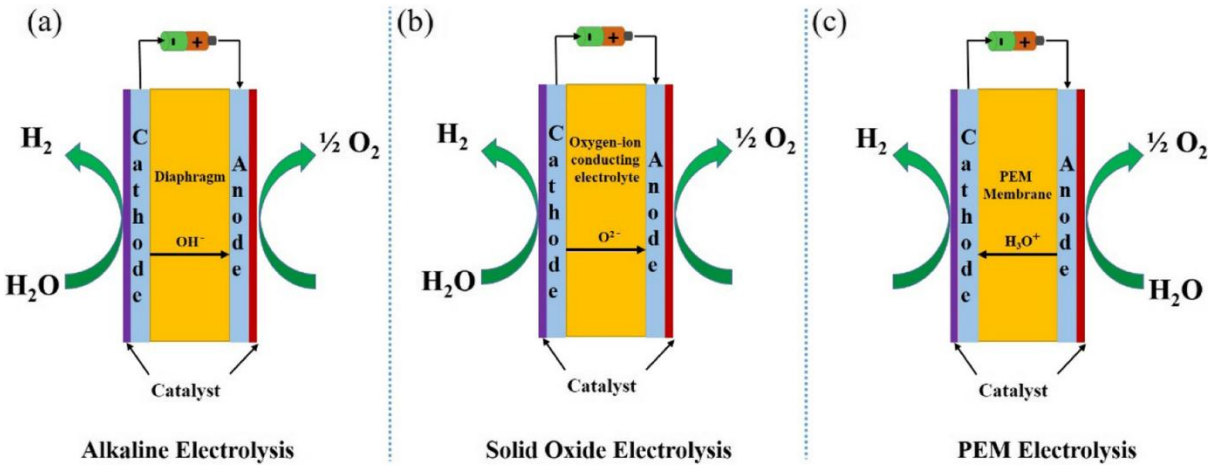

Figure 2-4. Schematic illustration of (a) alkaline water electrolysis, (b) solid oxide electrolysis, and (c) proton exchange membrane water electrolysis [80].

2.2.3.1. Alkaline Electrolysis (AEL)

Alkaline electrolyzer (AEL) is the oldest and most widely utilized water electrolysis technique [81]. However, it typically operates with lower efficiencies compared to two other technologies (PEMEL and SOEL), ranging between 59% and 70% [82]. An AEL cell typically consists of two metallic electrodes submerged in an alkaline solution as electrolyte. The anodic and cathodic compartments are separated by a porous diaphragm. The AEL benefits from relatively simple configuration, high stability, durability, and a well-established manufacturing process which contributes to its lower production costs [83]. However, the AEL requires high chemically resistant materials due to the corrosive nature of the electrolyte, it works in low current density which, causes large footprint, and it suffers from limited dynamic response to variable power load [68,81].

2.2.3.2. Proton Exchange Membrane Electrolyzer (PEMEL)

Proton Exchange Membrane Electrolysis (PEMEL) employs a membrane as the electrolyte located between anode and cathode. The water mainly introduced to the anode compartment splits into oxygen molecule and hydrogen proton (H^+). The proton will be conducted to the cathodic compartment through a membrane. The membrane also prevents the mixing of the hydrogen and oxygen gases. This technology offers several benefits, including a quick dynamic response, high gas purity, high current density and a compact system [84]. The operating temperature in this technology maintains in the range of 50 to 80 °C [85] and the PEMEL efficiency is typically in range 62 to 80% [78]. Nonetheless, due to the highly acidic nature of the membrane, it requires employing precious metal-based catalysts (typically iridium for the anode and platinum for the cathode) resulting in substantially high capital costs [68].

2.2.3.3. Solid Oxide Electrolyzer (SOEL)

Solid oxide electrolyzers operate based on solid oxide materials as electrolytes. In this technology steam fed to the cathode compartment undergoes reduction, generating hydrogen molecules and oxygen anions (O^-). At elevated temperatures, typically ranging from 500 to 1000 °C, these anions then migrate through the solid oxide membrane to the anode, where they are oxidized [86]. The elevated operating temperatures significantly lower the electrical energy requirements in comparison to low-temperature electrolysis technologies [85]. In theory, solid oxide electrolyzers can offer efficiencies approaching 100%. The high-temperature

process of SOEL is well-suited for applications involving substantial waste heat recovery. While the thermally activated electrochemical reactions in SOEL systems results in high efficiency and reversible operation, challenges associated with thermal and mechanical degradation have limited their broader commercial deployment [87].

2.2.4. Electrolysis Technology selection

A comparative overview of different types of electrolyzers is provided in Table 2-2. According to these table, the maturity of AEL and PEMEL technologies and low temperature operation in both makes them suitable candidates for commercial use. On the other hand, PEMEL offers higher purity of hydrogen, higher current density and faster dynamic response compared to AEL technology.

Table 2-2. Comparative summary of three major electrolysis technologies [77,88,89].

Parameter	PEMEL	AEL	SOEL
Efficiency [%]	65–82	59–70	80–100
Current density [A/cm²]	1–2.2	0.2–0.8	0.3–2
Cell voltage [V]	1.4–2.5	1.4–3	1–1.5
Initial cost [€/kW]	1400–2400	800–1600	>2000-2500
Operating temperature [°C]	50–80	70–90	500–1000
Operating pressure [bar]	<70	1–30	1–5
Cold start duration	~15 min	~50 min	Several hours
Commercial usage	Used	Widely used	Academic, pilot projects
Durability [h]	10,000–50,000	>100,000	500–2000
Specific energy consumption [kWh/kg H_2]	45–62	45–65	—
Hydrogen Purity [%]	99.9999	>99.5	>99.9
Key advantages	- High-purity H_2 - Fast cold start - Fast dynamic	- Mature Tech. - Low CAPEX - Long lifespan	- High efficiency - Suitable for co-electrolysis (syngas)- High temperature operation
Key disadvantages	- High CAPEX - Use precious metal catalysts	- Slow cold start - Lower gas purity	- High CAPEX - Degradation - Immature technology
Main challenges	- Catalyst material sourcing	- Safety - Response time - Corrosion	- Thermal stability of electrodes - Commercialization

Since the performance of an electrolyzer is closely linked to the input power level, a meaningful comparison should be conducted across the entire operating range

rather than at a single operating point. Figure 2-5 presents a comparative analysis of the three electrolysis technologies in terms of electrolyzer efficiency (based on the lower heating value, LHV), operational costs, capital investment, and specific hydrogen production per unit cell area, evaluated within their respective current density ranges. According to this figure, PEM electrolyzers can work with higher current densities and higher efficiency compared to AEL. The SOEL, as a high temperature electrolyzer, operates in endothermic mode, which means that the electrolyzers stack require external heat source and application of this type is not common yet. It should be noted that stack efficiency in this figure is calculated assuming an ideal Faraday efficiency (100%), while Faraday efficiency decreases drastically in low current density ranges. A more detailed discussion on electrolyzer efficiency including the effect of Faraday efficiency at low current density levels is provided in chapter 6.

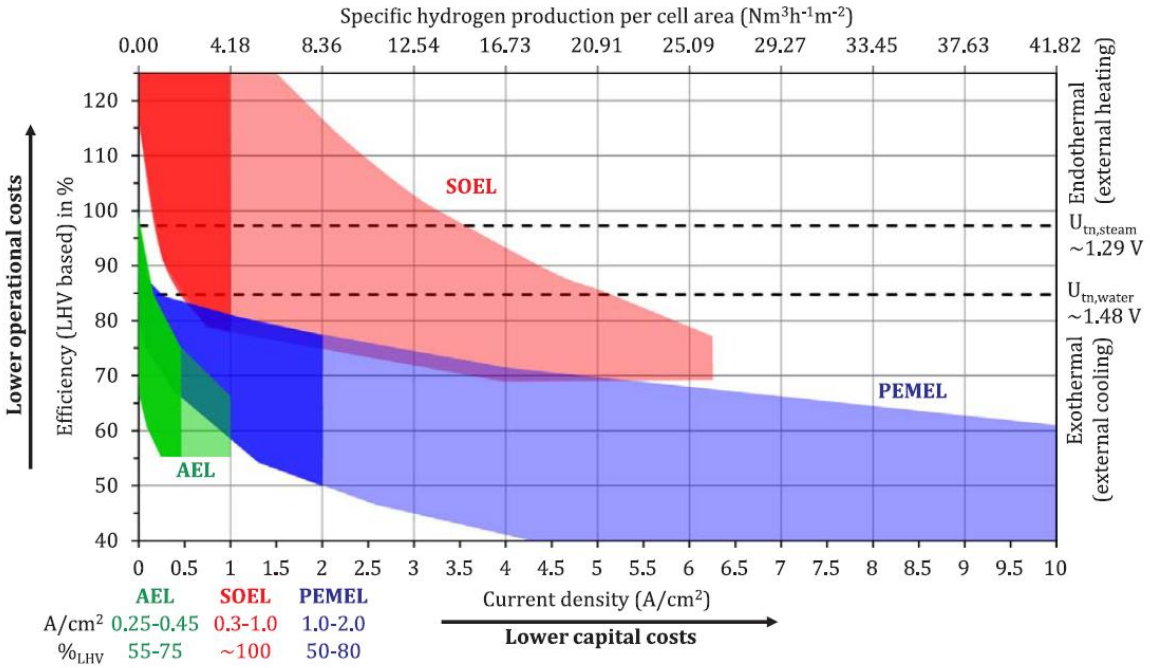

Figure 2-5. Comparison of different electrolysis technologies in terms of efficiency and specific energy consumption in their respective operational current density range

In recent years, significant efforts have been dedicated to advancing low-temperature electrolysis technologies, particularly PEMEL and AEL, with the aim of enhancing their technical performance and reducing hydrogen production costs. Table 2-3 summarizes the evolution of key techno-economic indicators for PEMEL and AEL systems between 2017 and 2025. Modern PEMEL systems exhibit notable advantages in terms of dynamic response and operational flexibility

compared to AEL. Due to the broader operating range and fast response to the power variation, PEMEL is well-suited for integration with variable electricity supply conditions.

Table 2-3. Techno-economic features of PEMEL and AEL between 2017 and 2025 [88].

Feature	PEMEL 2017	PEMEL 2025	AEL 2017	AEL 2025
Efficiency (kWh per kg of hydrogen)	58	52	51	49
Lifespan stack (working hours)	40,000	50,000	80,000	90,000
Low Heating Value Efficiency (%)	57	64	65	68
OPEX (Initial CAPEX % per year)	2	2	2	2
CAPEX – overall cost (EUR per kW)	1200	700	750	480
Lifespan of the system (years)	20	20	20	20
Output pressure (Bar)	30	60	Atmospheric	15
CAPEX – replacement of stack (EUR per kW)	420	210	340	215

2.2.5. Dynamic electrolysis operation

Flexibility of the electrolysis operation can significantly improve its integration of renewable electricity. Such adaptation also reduces the need for large-scale storage infrastructure or auxiliary systems, making the system more cost-efficient [90]. The AEL have generally been used at constant load to meet industrial purposes since it was not initially intended to be flexible. However recent efforts have been made to adapt the AEL systems with renewable power grid-connected services [84,91]. Nevertheless, the AEL system still has lower flexibility and slower dynamics compared to the PEMEL technology. The dynamic operation features of different electrolysis technologies are presented in Table 2-4 [88]. According to this table, PEMEL exhibits significantly shorter response times compared to both alkaline (AEL) and solid oxide (SOEL) electrolysis technologies. This superior dynamic operation enables PEMEL systems to more effectively accommodate the variability of electricity supply, positioning them as a more suitable option for dynamic integration with variable renewable energy (VRE) sources [92]. PEM electrolysis is selected as the subject of this study due to its superior dynamic characteristics compared to other electrolysis technologies.

Table 2-4. Summary of the dynamic operation features of different electrolyzer technologies [90,93].

Function	PEMEL	AEL	SOEL
Load flexibility	0 to 160%	15 to100%	–100 to +100%
Warm start-up	<1 min	1–10 min	15 min
Cold start-up	5–10 min	1–2 h	hours
Ramp up/down Rate	10-100% per second	0.2%–20% per second	-
Shut down	<1 min	1–10 min	-

2.2.6. PEM electrolyzer

The PEMEL was initially developed in the early 1950s, aiming to overcome the limitations associated with alkaline water electrolysis [65,94].

In a PEM water electrolyzer, water is supplied to the anode side, where it undergoes electrochemical splitting into protons (H^+), oxygen (O_2), and electrons (e^-). The protons then migrate through a solid polymer electrolyte (SPE) membrane toward the cathode. Simultaneously, the generated oxygen, along with any unreacted water, is expelled from the anode compartment. The electrons travel through an external circuit to reach the cathode, where they recombine with the protons to form hydrogen gas [95].

A schematic of a single-cell PEMEL structure, its key components and a single PEMEL cell assembly is shown in Figure 2-6. A PEMEL cell is comprised of two electrodes and a membrane in between, commonly called Membrane Electrode Assembly (MEA). Each electrode is composed of a (I) flow field plate or bipolar plate (BP) made from conductive materials (e.g., coated titanium on the anode side, stainless steel or carbon-based for the cathode), (II) flow channels embedded in the BP to distribute water and remove gases, (III) gas diffusion layer (GDL) also known as Porous Transport Layer (PTL) placed between the flow field plate and the catalyst layer, commonly made of porous titanium (for anode), carbon paper or cloth (for cathode) which facilitate the gas and liquid transport, uniform contact of catalyst, electron conduction and water management, and (IV) catalyst layer coated directly in the membrane or applied separately as distinct later.

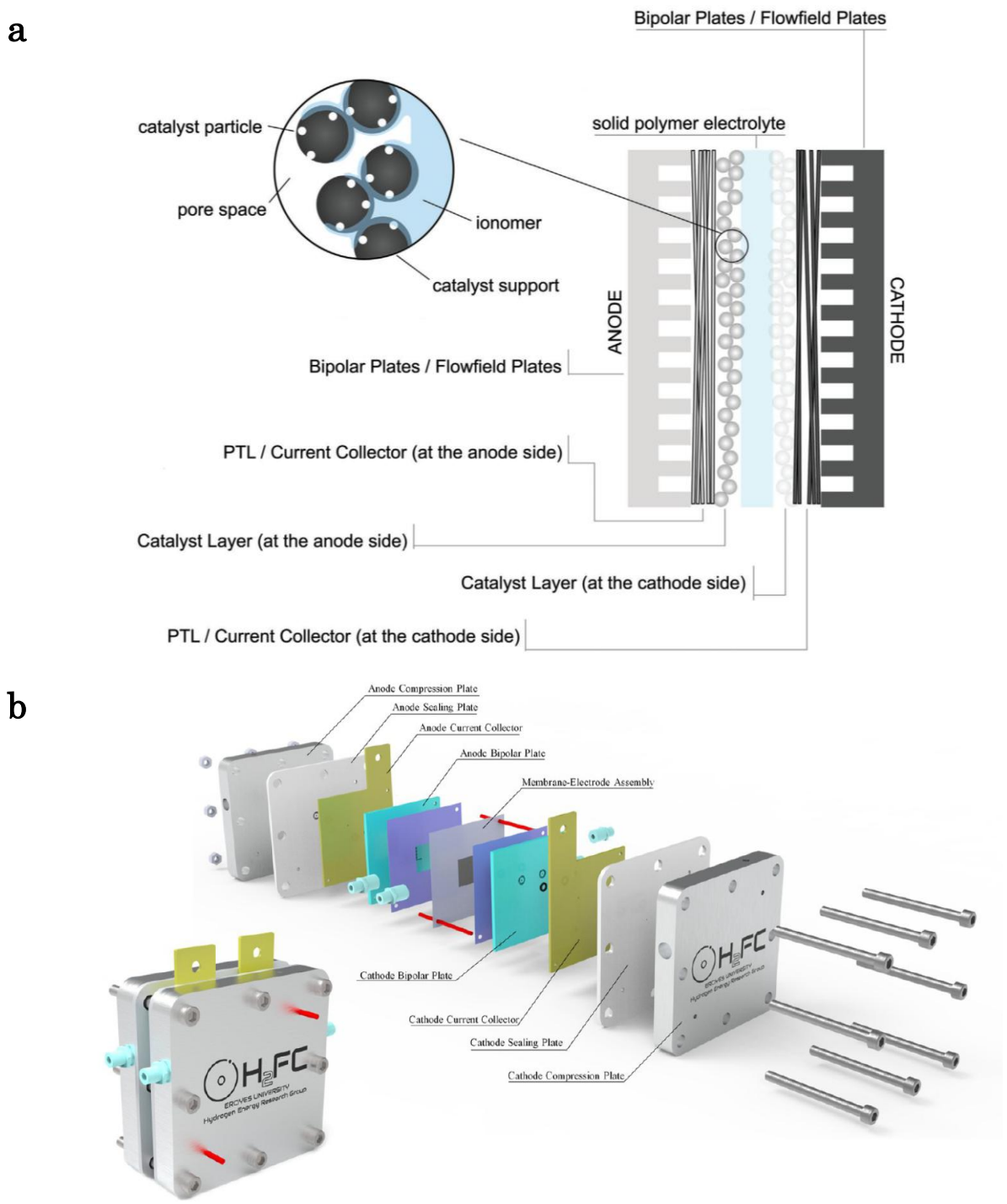

Figure 2-6. A schematic view of (a) cross-sectional illustration depicting the key structural elements of a PEMEL cell, and (b) a single-cell PEMEL assembly [96,97].

PEMEL system configuration

Each electrolyzer system typically includes multiple electrolysis cells, along with components for gas drying, purification, and heat removal. To meet product quality standards, the generated hydrogen and oxygen gases may need to be purified, cooled, and dried before they can be stored or supplied to end users. Also depending

on the demanded pressure, compressors may exist in the unit [69]. Figure 2-7 shows two general configurations of a PEMEL stack. According to this figure, the electrolysis systems may operate with separate water cycles for the anodic and the cathodic compartments while many electrolyzers operate with water supplied only for the anodic compartment [98]. Supplying water exclusively to the cathode is also technically possible and tends to be more suitable for systems with thinner membranes, although its application is restricted to the lower power densities compared to anodic water feed systems [99].

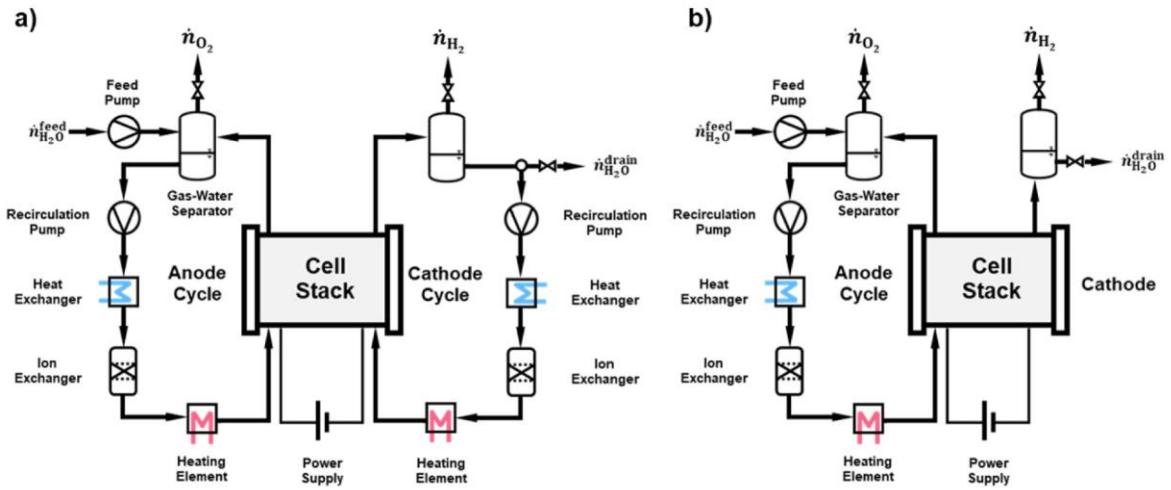

Figure 2-7. Schemes of PEM water electrolyzer configurations with (a) water circulation on both the anode and cathode sides; (b) incorporating water circulation only on the anode side [100].

2.2.6.1. PEMEL role in green hydrogen pathway

Due to the energy transition policies and urgent need to meet climate objectives, academic and industrial research on electrolysis and related factors such as renewable electricity pricing is progressing rapidly in parallel. These developments are occurring within short time intervals, particularly in the context of emerging technologies and the advancement of methods for their practical implementation.

As mentioned earlier, among the various electrolysis technologies, the PEM water electrolyzer appears to be the most suitable for operating under the intermittency inherent to renewable power sources, owing to its rapid dynamic response [101]. Moreover, PEMEL possesses unique features that make it stand out as a practical tool in the energy transition and hydrogen pathways. These include high efficiency, high-purity hydrogen production, low gas crossover, moderate operating

temperature, compact design, relatively high current density, and compatibility with high-pressure operation [102].

The ongoing and expanding research and development on PEMEL aim to enhance the efficiency of the electrolysis process and reduce the overall cost of green hydrogen production. These efforts target both capital (CAPEX) and operational (OPEX) expenditures through various approaches, such as optimization of unit operations [103] or enhancing the durability and efficiency of structural materials in the membrane and electrodes [65].

The research works on the performance of PEMEL systems can be categorized as (I) improvements in cell chemistry and membrane quality [104–106], (II) optimization of cell and stack design [97], (III) deeper insight into key degradation mechanisms [107], and (IV) refinement of operational conditions and optimization of unit operation [103,108]. Other novelties are also being applied to develop PEM electrolyzers, such as applying vapor-fed PEM electrolyzer [109], or elevated-temperature PEM electrolyzer [96]. It is worth mentioning that the research on water electrolysis continues not only to enhance existing technologies but also to explore novel approaches in operation and control of the units.

There are different metrics and methods to evaluate the effectiveness of hydrogen production technologies, among which the Levelized Cost of Hydrogen (LCOH) is the most popular. The LCOH is a standardized metric used to measure the cost-effectiveness of hydrogen production technologies over their lifetime, and it represents the average cost per kilogram of hydrogen produced, accounting for all capital and operational costs and financial factors. The LCOH value can be calculated by dividing the total cost of building and operating a hydrogen production system, discounted over its lifetime, by the total amount of hydrogen produced, also discounted over the same period:

$$LCOH = \frac{\sum_{t=0}^{n} \frac{I_t + O_t + F_t}{(1 + r)^t}}{\sum_{t=0}^{n} \frac{H_t}{(1 + r)^t}} \quad (1)$$

where:

I_t : Investment and capital expenditure in year t

O_t : Operating and maintenance costs in year t

F_t : Fuel or electricity cost in year t

H_t : Amount of hydrogen produced in year t (kg/year)

r : Discount rate

n : Project lifetime (years)

Based on the LCOH definition, a lower LCOH can be achieved through various strategies, including lowering electricity price (power generation technology and management), extending the operating hours of the PEMEL system (planning, durability, and lifetime), reducing capital and operational expenditures (CAPEX and OPEX), and enhancing overall system efficiency [110,111]. Hence, LCOH is considered as a key indicator to assess both the technical and economic aspects of hydrogen production and allows for fair comparison across different hydrogen production routes. This parameter can be also used to measure and evaluate the potentials of a scientific research work on improving a PEMEL system.

Figure 2-8 shows the LCOH of green hydrogen at different locations globally. According to this figure, the solar and wind resource availability significantly influences both hydrogen production potential and associated costs, leading to different LCOH values at different geographical locations; in areas with high-capacity factors of renewable power sources, electricity generation is more cost-effective, thereby lower LCOH is achievable.

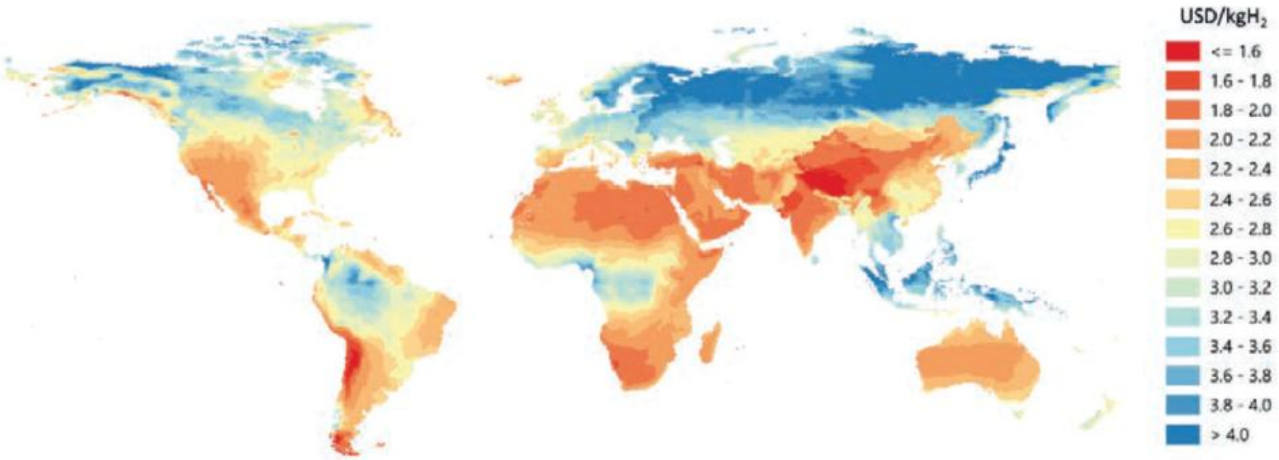

Figure 2-8. Simulated hydrogen production costs based on electricity supplied from solar PV or wind energy sources [68,112].

The impact of key factors on both current and projected LCOH values, including electrolyzer CAPEX and electricity price, is illustrated in Figure 2-9. As shown, access to lower electricity prices or reductions in electrolyzer capital costs can significantly reduce hydrogen production costs, potentially bringing them into a range that is competitive with fossil fuel-based alternatives.

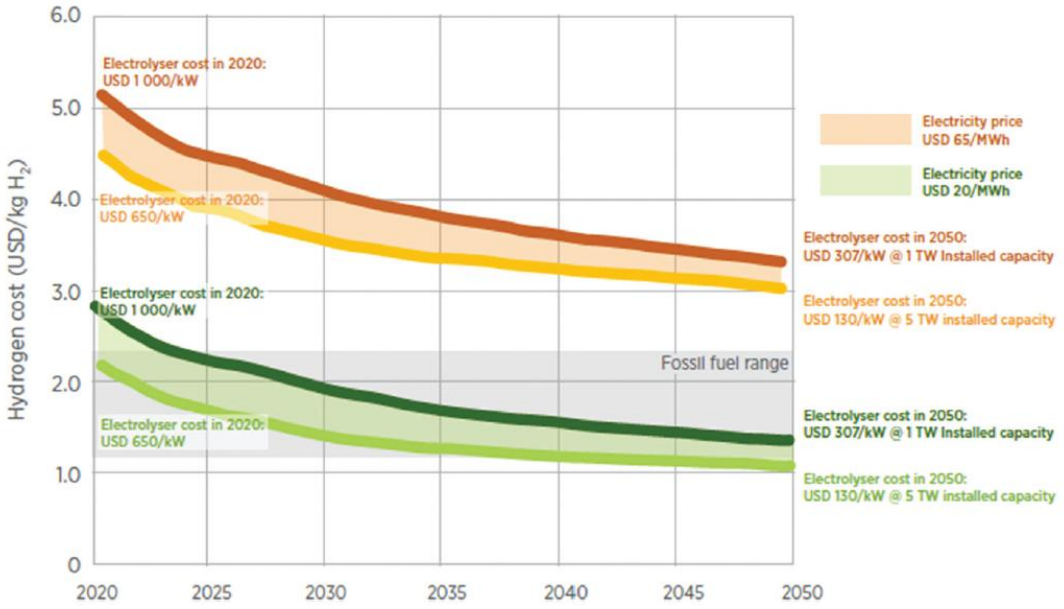

Figure 2-9. Projected costs for green hydrogen production over time as a function of electrolyzer capital expenditure and electricity prices [68,111].

2.2.6.2. PEMEL Modelling

Modelling and simulation serve as essential tools for design engineers and researchers, enabling deeper insight, performance prediction, and the advancement of hydrogen technologies [113]. A wide range of modelling approaches has been proposed in the scientific literature to characterize the performance and operational behavior of PEM electrolyzers [114]. The modelling may be conducted in a broad spectrum of approaches in cell scale [115–117], system scale [118], or integrated multi-systems scale [119–121]. Each model presents specific advantages and constraints, and its applicability is typically limited to assumptions and operating conditions. Depending on the modelling objectives, the model may cover different aspects of PEMEL performance, including thermodynamic, electrochemical, energy balance, mass transfer, fluidic, and physical aspects of an electrolysis process [114]. The modelling approach must be appropriately aligned with the intended objectives to ensure a suitable balance between computational accuracy and cost.

In this study, a model of the PEM electrolyzer unit is developed in Aspen Plus, incorporating a subroutine constructed in Aspen Custom Modeler (ACM). The model is aimed to be applied under variable renewable energy (VRE) sources for long-term system or multi-system scale. The prepared model framework established on reasonable assumptions and simplifications allows for flexible adaptation of the PEMEL unit to a wide range of power profiles, offering flexibility

toward variations in input parameters while minimizing the need for frequent adjustment under high-frequency input fluctuations.

2.3. References

[1] I. López, J. Andreu, S. Ceballos, I. Martínez De Alegría, I. Kortabarria, Review of wave energy technologies and the necessary power-equipment, Renewable and Sustainable Energy Reviews 27 (2013) 413–434. https://doi.org/10.1016/j.rser.2013.07.009.

[2] J. Fang, X. Cheng, Z. Li, H. Li, C. Li, A review of internally heat integrated distillation column, Chin J Chem Eng 27 (2019) 1272–1281. https://doi.org/10.1016/j.cjche.2018.08.021.

[3] Ian M. Smallwood, Solvent Recovery Handbook, 2nd ed, 2002.

[4] A.A. Kiss, Rethinking energy use for a sustainable chemical industry, Chem Eng Trans 76 (2019) 13–18. https://doi.org/10.3303/CET1976003.

[5] U. Diwekar, Batch Distillation: Simulation, Optimal Design, and Control, Second Edition, CRC Press, 2011. https://books.google.es/books?id=jH06DwAAQBAJ.

[6] E. Sorensen, Chapter 5 - Design and Operation of Batch Distillation, in: A. Górak, E. Sorensen (Eds.), Distillation, Academic Press, Boston, 2014: pp. 187–224. https://doi.org/https://doi.org/10.1016/B978-0-12-386547-2.00005-3.

[7] T.M.M. Barakat, E. Sørensen, Simultaneous optimal synthesis, design and operation of batch and continuous hybrid separation processes, Chemical Engineering Research and Design 86 (2008) 279–298. https://doi.org/10.1016/J.CHERD.2007.12.004.

[8] T.M.M. Barakat, E.S. Fraga, E. Sørensen, Multi-objective optimisation of batch separation processes, Chemical Engineering and Processing: Process Intensification 47 (2008) 2303–2314. https://doi.org/10.1016/j.cep.2008.01.005.

[9] H. Yu, Q. Ye, H. Xu, X. Dai, X. Suo, R. Li, Comparison of alternative distillation processes for the maximum-boiling ethylenediamine dehydration system, Chemical Engineering and Processing: Process Intensification 97 (2015) 84–105. https://doi.org/10.1016/j.cep.2015.09.008.

[10] B. Nemeth, L. Hegely, P. Lang, Investigating the processing capacity of batch distillation by applying a second, smaller column, Sep Purif Technol 280 (2022). https://doi.org/10.1016/j.seppur.2021.119883.

[11] K.-J. Kim, U. Diwekar, Batch distillation, in: Batch Processes, CRC Press, 2005: pp. 119–162.

[12] S.S. Parhi, G.P. Rangaiah, A.K. Jana, A novel vapor recompressed batch extractive distillation: Design and retrofitting, Sep Purif Technol 260 (2021). https://doi.org/10.1016/j.seppur.2020.118225.

[13] H. Zhang, S. Wang, J. Tang, N. Li, Y. Li, P. Cui, Y. Wang, S. Zheng, Z. Zhu, Y. Ma, Multi-objective optimization and control strategy for extractive distillation with dividing-wall column/pervaporation for separation of ternary azeotropes based on mechanism analysis, Energy 229 (2021). https://doi.org/10.1016/j.energy.2021.120774.

[14] A. Yu, Q. Ye, J. Li, Y. Wang, Q. Rui, Energy-saving improvement of heat integration and heat pump for separating multi-azeotropes mixture via novel pressure swing distillation, Chem Eng Sci 282 (2023). https://doi.org/10.1016/j.ces.2023.119239.

[15] M. Ferchichi, L. Hegely, P. Lang, Economic and environmental evaluation of heat pump-assisted pressure-swing distillation of maximum-boiling azeotropic mixture water-ethylenediamine, Energy 239 (2022). https://doi.org/10.1016/j.energy.2021.122608.

[16] Z. Zhang, Y. Wang, M. Zhang, C. Guang, M. Li, J. Gao, Energy-saving investigation of pressure-swing distillation strengthening configurations for benzene/isobutanol binary azeotrope, Sep Purif Technol 296 (2022). https://doi.org/10.1016/j.seppur.2022.121381.

[17] L. Hegely, P. Lang, Optimisation of the higher pressure of pressure-swing distillation of a maximum azeotropic mixture, Energy 271 (2023). https://doi.org/10.1016/j.energy.2023.126939.

[18] G. Miao, K. Zhuo, G. Li, J. Xiao, An advanced optimization strategy for enhancing the performance of a hybrid pressure-swing distillation process in effective binary-azeotrope separation, Sep Purif Technol 282 (2022). https://doi.org/10.1016/j.seppur.2021.120130.

[19] D.Y. Aqar, I.M. Mujtaba, Economic feasibility of an integrated semi-batch reactive distillation operation for the production of methyl decanoate, Sep Purif Technol 257 (2021). https://doi.org/10.1016/j.seppur.2020.117871.

[20] D.Y. Aqar, A.S. Abbas, R. Patel, I.M. Mujtaba, Optimisation of semi-batch reactive distillation column for the synthesis of methyl palmitate, Sep Purif Technol 270 (2021). https://doi.org/10.1016/j.seppur.2021.118776.

[21] C. Zhang, Y. Liu, Z. Gao, L. Huang, J. Xiong, Process design, simulation and experimental studies of heteroazeotropic batch distillation for phenol dehydration, Chemical Engineering Research and Design 195 (2023) 682–690. https://doi.org/10.1016/j.cherd.2023.05.062.

[22] T. Ooms, S. Vreysen, G. Van Baelen, V. Gerbaud, I. Rodriguez-Donis, Separation of ethyl acetate–isooctane mixture by heteroazeotropic batch distillation, Chemical Engineering Research and Design 92 (2014) 995–1004. https://doi.org/https://doi.org/10.1016/j.cherd.2013.10.010.

[23] H. Gao, F. Zhao, L. Zhu, F. Yang, Y. Wang, D. Li, Dehydration of a Dilute Acetic Acid-Water Mixture via Batch Heteroazeotropic Distillation, Chem Eng Technol 44 (2021) 477–487. https://doi.org/10.1002/ceat.202000367.

[24] G. De Guido, C. Monticelli, E. Spatolisano, L.A. Pellegrini, Separation of the Mixture 2-Propanol + Water by Heterogeneous Azeotropic Distillation with Isooctane as an Entrainer, Energies (Basel) 14 (2021). https://doi.org/10.3390/en14175471.

[25] S. Skouras, V. Kiva, S. Skogestad, Feasible separations and entrainer selection rules for heteroazeotropic batch distillation, Chem Eng Sci 60 (2005) 2895–2909. https://doi.org/10.1016/j.ces.2004.11.056.

[26] P. Lang, G. Modla, Generalised method for the determination of heterogeneous batch distillation regions, Chem Eng Sci 61 (2006) 4262–4270. https://doi.org/https://doi.org/10.1016/j.ces.2006.02.004.

[27] A. Yang, Z.Y. Kong, J. Sunarso, Design and optimisation of novel hybrid side-stream reactive-extractive distillation for recovery of isopropyl alcohol and ethyl acetate from wastewater, Chemical Engineering Journal 451 (2023) 138563. https://doi.org/https://doi.org/10.1016/j.cej.2022.138563.

[28] K. Jayant, C. Gupta, S. Seethamraju, S.M. Mahajani, Entrainer assisted production of high purity 2-phenyl ethyl acetate by reactive distillation, Sep Purif

Technol 331 (2024) 125650. https://doi.org/https://doi.org/10.1016/j.seppur.2023.125650.

[29] E.-K. Hilmen, Separation of azeotropic mixtures : tools for analysis and studies on batch distillation operation, 288 (2000). https://ntnuopen.ntnu.no/ntnu-xmlui/handle/11250/248113 (accessed June 6, 2025).

[30] B. Nemeth, L. Hegely, P. Lang, Comparison of batch heteroazeotropic distillation operational strategies for the dehydration of isopropanol, Chemical Engineering Research and Design 146 (2019) 486–498. https://doi.org/10.1016/j.cherd.2019.04.033.

[31] H.J. Huang, I.-L. Chien, Choice of suitable entrainer in heteroazeotropic batch distillation system for acetic acid dehydration, Journal of the Chinese Institute of Chemical Engineers 39 (2008) 503–517. https://doi.org/https://doi.org/10.1016/j.jcice.2008.04.002.

[32] L. Hegely, P. Lang, Optimization of Batch Heteroazeotropic Distillation Operational Strategies with Entrainer Recycle, in: Computer Aided Chemical Engineering, Elsevier B.V., 2018: pp. 1505–1511. https://doi.org/10.1016/B978-0-444-64235-6.50262-X.

[33] L. Hegely, V. Gerbaud, P. Lang, Batch heteroazeotropic distillation with variable decanter hold-up: Feasibility studies, in: I.D.L. Bogle, M. Fairweather (Eds.), 22nd European Symposium on Computer Aided Process Engineering, Elsevier, 2012: pp. 527–531. https://doi.org/https://doi.org/10.1016/B978-0-444-59519-5.50106-4.

[34] F. Denes, P. Lang, G. Modla, X. Joulia, New double column system for heteroazeotropic batch distillation, Comput Chem Eng 33 (2009) 1631–1643. https://doi.org/https://doi.org/10.1016/j.compchemeng.2009.01.011.

[35] P. Lang, F. Denes, X. Joulia, New configuration for hetero-azeotropic batch distillation: I. Feasibility studies, Computer Aided Chemical Engineering 25 (2008) 115–120. https://doi.org/10.1016/S1570-7946(08)80024-7.

[36] S. Skouras, S. Skogestad, Separation of ternary heteroazeotropic mixtures in a closed multivessel batch distillation–decanter hybrid, Chemical Engineering and Processing: Process Intensification 43 (2004) 291–304. https://doi.org/https://doi.org/10.1016/S0255-2701(03)00126-0.

[37] I. Rodriguez-Donis, J. Acosta-Esquijarosa, V. Gerbaud, E. Pardillo-Fondevila, X. Joulia, Separation of n-hexane–ethyl acetate mixtures by azeotropic

batch distillation with heterogeneous entrainers, Chemical Engineering and Processing: Process Intensification 44 (2005) 131–137. https://doi.org/10.1016/J.CEP.2004.05.006.

[38] S. Skouras, S. Skogestad, V. Kiva, Analysis and control of heteroazeotropic batch distillation, AIChE Journal 51 (2005) 1144–1157. https://doi.org/10.1002/aic.10376.

[39] D.B. Kaymak, Design and control of an alternative intensified process configuration for separation of butanol-butyl acetate-methyl isobutyl ketone system, Chemical Engineering and Processing - Process Intensification 159 (2021) 108233. https://doi.org/https://doi.org/10.1016/j.cep.2020.108233.

[40] R.R. Nair, A. Raykar, Performance investigation of vapour recompressed batch distillation for separating ternary wide boiling constituents, Resource-Efficient Technologies 3 (2017) 452–458.

[41] G. Radhika, A.K. Burolia, P.K. Raghu Raja, S.R. Ambati, D.S. Patle, U.B.B. Gara, Energy saving in batch distillation for separation of ternary zeotropic mixture integrated with vapor recompression scheme: dynamics and control, Chemical Product and Process Modeling 16 (2021) 101–115.

[42] R. Gandu, A.K. Burolia, S.R. Ambati, U.B.B. Gara, Reducing total annual cost and CO2 emissions in batch distillation for separating ternary wide boiling mixtures using vapor recompression heat pump, Chemical Product and Process Modeling 18 (2023) 177–194.

[43] A. Kazemi, A. Mehrabani-Zeinabad, M. Beheshti, Novel heat pump assisted distillation configurations for energy and economic savings and their application on propylene/propane and I-butane/N-butane separation systems, Chem Eng Sci 295 (2024) 120139.

[44] G. Modla, P. Lang, Heat pump systems with mechanical compression for batch distillation, Energy 62 (2013) 403–417.

[45] M.M. Vibhute, S.S. Jogwar, Optimal operation and tracking control of vapor-recompressed batch distillation, AIChE Journal 66 (2020). https://doi.org/10.1002/aic.17049.

[46] A.A. Kiss, C.A.I. Ferreira, Heat pumps in chemical process industry, CRC Press, 2016.

[47] H.A. Kooijman, E. Sorensen, Recent advances and future perspectives on more sustainable and energy efficient distillation processes, Chemical Engineering Research and Design 188 (2022) 473–482. https://doi.org/10.1016/j.cherd.2022.10.005.

[48] M. Ledezma-Martínez, M. Jobson, R. Smith, Simulation–optimization-based design of crude oil distillation systems with preflash units, Ind Eng Chem Res 57 (2018) 9821–9830.

[49] H.Z. Kister, J.R. Haas, D.R. Hart, D.R. Gill, Distillation design, McGraw-Hill New York, 1992.

[50] C.S. Robinson, E.R. Gilliland, Find distillation stages graphically, Chem. Eng 65 (1985) 129.

[51] E. Sørensen, S. Skogestad, Comparison of regular and inverted batch distillation, Chem Eng Sci 22 (1996) 4949–4962.

[52] C. Bernot, M.F. Doherty, M.F. Malone, Feasibility and separation sequencing in multicomponent batch distillation, Chem Eng Sci 46 (1991) 1311–1326.

[53] N.P. Cheremisinoff, Industrial Solvents Handbook, Revised And Expanded, Industrial Solvents Handbook, Revised And Expanded (2003). https://doi.org/10.1201/9780203911334.

[54] C. Barker, European MIBK spot prices continue to rise on feedstocks, Tightness, (2017). https://www.icis.com/explore/resources/news/2017/02/14/10078953/e uropean-mibk-spot-prices-continue-to-rise-on-feedstocks-tightness/ (accessed February 6, 2024).

[55] S.E. Gad, Methyl Isobutyl Ketone, in: P. Wexler (Ed.), Encyclopedia of Toxicology (Second Edition), Second Edition, Elsevier, New York, 2005: pp. 79–81. https://doi.org/https://doi.org/10.1016/B0-12-369400-0/00615-3.

[56] S.D. Jackson, A.S. Canning, E. Mcleod, G.M. Parker, 89 - Strong Base Catalysts for Fine Chemical Synthesis: Relating Reaction Energetics to Base Strength, in: K. Eguchi, M. Machida, I. Yamanaka (Eds.), Science and Technology in Catalysis 2006, Elsevier, 2007: pp. 401–404. https://doi.org/https://doi.org/10.1016/B978-0-444-53202-2.50089-0.

[57] W.L. Luyben, Control of the Heterogeneous Azeotropic n-Butanol/Water Distillation System, Energy & Fuels 22 (2008) 4249–4258. https://doi.org/10.1021/ef8004064.

[58] M.I. Parma-García, J.A. Díaz-López, A. Nieto-Márquez, Separation of a water/MIBK mixture by batch heteroazeotropic distillation: A self-entrained case, Chemical Engineering and Processing - Process Intensification 171 (2022). https://doi.org/10.1016/j.cep.2021.108761.

[59] Distillation process for recovery of methyl isobutyl ketone, (1978).

[60] J.J. Tang, K.G. Zhou, Q.X. Zhang, Q.G. Li, Study on the removal of MIBK from aqueous solution by vacuum membrane distillation, Journal of Central South University of Technology (English Edition) 7 (2000) 178–181. https://doi.org/10.1007/S11771-000-0048-2/METRICS.

[61] Z. Lei, J. Li, C. Li, B. Chen, Improvement of separation process of synthesizing MIBK by the isopropanol one-step method, Korean Journal of Chemical Engineering 23 (2006) 264–270. https://doi.org/10.1007/BF02705725/METRICS.

[62] World Energy Outlook 2024 – Analysis - IEA, (n.d.). https://www.iea.org/reports/world-energy-outlook-2024 (accessed June 6, 2025).

[63] A. Kazim, T.N. Veziroglu, Utilization of solar–hydrogen energy in the UAE to maintain its share in the world energy market for the 21st century, Renew Energy 24 (2001) 259–274. https://doi.org/10.1016/S0960-1481(00)00199-3.

[64] J. Chi, H. Yu, Water electrolysis based on renewable energy for hydrogen production, Chinese Journal of Catalysis 39 (2018) 390–394. https://doi.org/10.1016/S1872-2067(17)62949-8.

[65] S. Shiva Kumar, V. Himabindu, Hydrogen production by PEM water electrolysis – A review, Mater Sci Energy Technol 2 (2019) 442–454. https://doi.org/10.1016/j.mset.2019.03.002.

[66] A. Borgschulte, The hydrogen grand challenge, Front Energy Res 4 (2016). https://doi.org/10.3389/fenrg.2016.00011.

[67] B. Lee, J. Heo, S. Kim, C. Sung, C. Moon, S. Moon, H. Lim, Economic feasibility studies of high pressure PEM water electrolysis for distributed H2 refueling stations, Energy Convers Manag 162 (2018) 139–144. https://doi.org/10.1016/J.ENCONMAN.2018.02.041.

[68] M. Chatenet, B.G. Pollet, D.R. Dekel, F. Dionigi, J. Deseure, P. Millet, R.D. Braatz, M.Z. Bazant, M. Eikerling, I. Staffell, P. Balcombe, Y. Shao-Horn, H. Schäfer, Water electrolysis: from textbook knowledge to the latest scientific strategies and industrial developments, Chem Soc Rev 51 (2022) 4583–4762. https://doi.org/10.1039/d0cs01079k.

[69] J. Chi, H. Yu, Water electrolysis based on renewable energy for hydrogen production, Chinese Journal of Catalysis 39 (2018) 390. https://doi.org/10.1016/S1872-2067(17)62949-8.

[70] E.R. Morgan, J.F. Manwell, J.G. McGowan, Sustainable Ammonia Production from U.S. Offshore Wind Farms: A Techno-Economic Review, ACS Sustain Chem Eng 5 (2017) 9554–9567. https://doi.org/10.1021/ACSSUSCHEMENG.7B02070/ASSET/IMAGES/MEDIUM/SC-2017-02070Q_0007.GIF.

[71] Z. Abdin, A. Zafaranloo, A. Rafiee, W. Mérida, W. Lipiński, K.R. Khalilpour, Hydrogen as an energy vector, Renewable and Sustainable Energy Reviews 120 (2020) 109620. https://doi.org/10.1016/J.RSER.2019.109620.

[72] G.W. Crabtree, M.S. Dresselhaus, M. V. Buchanan, The Hydrogen Economy, Phys Today 57 (2004) 39–44. https://doi.org/10.1063/1.1878333.

[73] A.J. Shih, M.C.O. Monteiro, F. Dattila, D. Pavesi, M. Philips, A.H.M. da Silva, R.E. Vos, K. Ojha, S. Park, O. van der Heijden, G. Marcandalli, A. Goyal, M. Villalba, X. Chen, G.T.K.K. Gunasooriya, I. McCrum, R. Mom, N. López, M.T.M. Koper, Water electrolysis, Nature Reviews Methods Primers 2 (2022). https://doi.org/10.1038/s43586-022-00164-0.

[74] Encyclopedia of Applied Electrochemistry, Encyclopedia of Applied Electrochemistry (2014). https://doi.org/10.1007/978-1-4419-6996-5.

[75] M.-C. Péra, Electrochemical components, (2013) 324.

[76] M. Sankir, N.D. Sankir, eds., Hydrogen Production Technologies, (2017). https://doi.org/10.1002/9781119283676.

[77] T. Paulec, J. Tvarožek, P. Resutík, P. Špánik, M. Praženica, Review of the dynamic response of water electrolyzer, Electrical Engineering (2025). https://doi.org/10.1007/s00202-025-03042-6.

[78] M. Yue, H. Lambert, E. Pahon, R. Roche, S. Jemei, D. Hissel, Hydrogen energy systems: A critical review of technologies, applications, trends and

challenges, Renewable and Sustainable Energy Reviews 146 (2021) 111180. https://doi.org/10.1016/J.RSER.2021.111180.

[79] A.W. Tricker, J.K. Lee, J.R. Shin, N. Danilovic, A.Z. Weber, X. Peng, Design and operating principles for high-performing anion exchange membrane water electrolyzers, J Power Sources 567 (2023). https://doi.org/10.1016/j.jpowsour.2023.232967.

[80] T. Wang, X. Cao, L. Jiao, PEM water electrolysis for hydrogen production: fundamentals, advances, and prospects, Carbon Neutrality 1 (2022). https://doi.org/10.1007/s43979-022-00022-8.

[81] I. Vincent, D. Bessarabov, Low cost hydrogen production by anion exchange membrane electrolysis: A review, Renewable and Sustainable Energy Reviews 81 (2018) 1690–1704. https://doi.org/10.1016/J.RSER.2017.05.258.

[82] M. El-Shafie, Hydrogen production by water electrolysis technologies: A review, Results in Engineering 20 (2023) 101426. https://doi.org/10.1016/J.RINENG.2023.101426.

[83] M.S.Y. Ebaid, M. Hammad, T. Alghamdi, THERMO economic analysis OF PV and hydrogen gas turbine hybrid power plant of 100 MW power output, Int J Hydrogen Energy 40 (2015) 12120–12143. https://doi.org/10.1016/J.IJHYDENE.2015.07.077.

[84] T. Wang, X. Cao, L. Jiao, PEM water electrolysis for hydrogen production: fundamentals, advances, and prospects, Carbon Neutrality 2022 1:1 1 (2022) 1–19. https://doi.org/10.1007/S43979-022-00022-8.

[85] O. Schmidt, A. Gambhir, I. Staffell, A. Hawkes, J. Nelson, S. Few, Future cost and performance of water electrolysis: An expert elicitation study, Int J Hydrogen Energy 42 (2017) 30470–30492. https://doi.org/10.1016/J.IJHYDENE.2017.10.045.

[86] B. Mohamed Jan, M. Bin Dahari, M. Abro, R. Ikram, Exploration of waste-generated nanocomposites as energy-driven systems for various methods of hydrogen production; A review, Int J Hydrogen Energy 47 (2022) 16398–16423. https://doi.org/10.1016/J.IJHYDENE.2022.03.137.

[87] A. Pandiyan, A. Uthayakumar, R. Subrayan, S.W. Cha, S.B.K. Moorthy, Review of solid oxide electrolysis cells: A clean energy strategy for hydrogen generation, Nanomaterials and Energy 8 (2019).

https://doi.org/10.1680/JNAEN.18.00009;WEBSITE:WEBSITE:ICEP-SITE;PAGE:STRING:ARTICLE/CHAPTER.

[88] S.G. Nnabuife, A.K. Hamzat, J. Whidborne, B. Kuang, K.W. Jenkins, Integration of renewable energy sources in tandem with electrolysis: A technology review for green hydrogen production, Int J Hydrogen Energy (2024). https://doi.org/10.1016/j.ijhydene.2024.06.342.

[89] X. Li, Y. Yao, Y. Tian, J. Jia, W. Ma, X. Yan, J. Liang, Recent advances in key components of proton exchange membrane water electrolysers, Mater Chem Front 8 (2024) 2493–2510. https://doi.org/10.1039/d4qm00086b.

[90] S. Mucci, A. Mitsos, D. Bongartz, Power-to-X processes based on PEM water electrolyzers: A review of process integration and flexible operation, Comput Chem Eng 175 (2023). https://doi.org/10.1016/j.compchemeng.2023.108260.

[91] F. Allebrod, C. Chatzichristodoulou, M.B. Mogensen, Alkaline electrolysis cell at high temperature and pressure of 250 °C and 42 bar, J Power Sources 229 (2013) 22–31. https://doi.org/10.1016/J.JPOWSOUR.2012.11.105.

[92] M. Nasser, T.F. Megahed, S. Ookawara, H. Hassan, Performance evaluation of PV panels/wind turbines hybrid system for green hydrogen generation and storage: Energy, exergy, economic, and enviroeconomic, Energy Convers Manag 267 (2022). https://doi.org/10.1016/j.enconman.2022.115870.

[93] H. Sayed-Ahmed, I. Toldy, A. Santasalo-Aarnio, Dynamic operation of proton exchange membrane electrolyzers—Critical review, Renewable and Sustainable Energy Reviews 189 (2024). https://doi.org/10.1016/j.rser.2023.113883.

[94] W.T. Grubb, Batteries with Solid Ion Exchange Electrolytes, J Electrochem Soc 106 (1959) 275. https://doi.org/10.1149/1.2427329/XML.

[95] D. Bessarabov, H. Wang, H. Li, N. Zhao, PEM electrolysis for hydrogen production: Principles and applications, PEM Electrolysis for Hydrogen Production: Principles and Applications (2016) 1–382. https://doi.org/10.1201/B19096/PEM-ELECTROLYSIS-HYDROGEN-PRODUCTION-HUI-LI-HAIJIANG-WANG-DMITRI-BESSARABOV-NANA-ZHAO/RIGHTS-AND-PERMISSIONS.

[96] M. Bonanno, K. Müller, B. Bensmann, R. Hanke-Rauschenbach, D. Aili, T. Franken, A. Chromik, R. Peach, A.T.S. Freiberg, S. Thiele, Review and Prospects

of PEM Water Electrolysis at Elevated Temperature Operation, Adv Mater Technol 9 (2024). https://doi.org/10.1002/admt.202300281.

[97] M. Kıstı, B. Hüner, A. Albadwi, E. Özdoğan, İ.N. Uzgören, S. Uysal, M. Conağası, Y.O. Süzen, N. Demir, M.F. Kaya, Recent Advances in Polymer Electrolyte Membrane Water Electrolyzer Stack Development Studies: A Review, ACS Omega 10 (2025) 9824–9853. https://doi.org/10.1021/acsomega.4c10147.

[98] M. Maier, K. Smith, J. Dodwell, G. Hinds, P.R. Shearing, D.J.L. Brett, Mass transport in PEM water electrolysers: A review, Int J Hydrogen Energy 47 (2022) 30–56. https://doi.org/10.1016/J.IJHYDENE.2021.10.013.

[99] M. Müller, M. Carmo, A. Glüsen, M. Hehemann, S. Saba, W. Zwaygardt, D. Stolten, Water management in membrane electrolysis and options for advanced plants, Int J Hydrogen Energy 44 (2019) 10147–10155. https://doi.org/10.1016/J.IJHYDENE.2019.02.139.

[100] E. Rauls, M. Hehemann, F. Scheepers, M. Müller, R. Peters, D. Stolten, System dynamics of polymer electrolyte membrane water electrolyzers and impact of renewable energy sources on systems design, Int J Hydrogen Energy 65 (2024) 83–94. https://doi.org/10.1016/j.ijhydene.2024.03.302.

[101] M.J. Ginsberg, M. Venkatraman, D. V. Esposito, V.M. Fthenakis, Minimizing the cost of hydrogen production through dynamic polymer electrolyte membrane electrolyzer operation, Cell Rep Phys Sci 3 (2022). https://doi.org/10.1016/j.xcrp.2022.100935.

[102] R. Hancke, T. Holm, Ø. Ulleberg, The case for high-pressure PEM water electrolysis, Energy Convers Manag 261 (2022). https://doi.org/10.1016/j.enconman.2022.115642.

[103] L. Bornemann, J. Lange, M. Kaltschmitt, Optimizing temperature and pressure in PEM electrolyzers: A model-based approach to enhanced efficiency in integrated energy systems, (2025). https://doi.org/10.5281/zenodo.1.

[104] R. Vinodh, T. Palanivel, S.S. Kalanur, B.G. Pollet, Recent advancements in catalyst coated membranes for water electrolysis: a critical review, Energy Advances 3 (2024) 1144–1166. https://doi.org/10.1039/d4ya00143e.

[105] M. Suermann, T.J. Schmidt, F.N. Büchi, Comparing the kinetic activation energy of the oxygen evolution and reduction reactions, Electrochim Acta 281 (2018) 466–471. https://doi.org/10.1016/J.ELECTACTA.2018.05.150.

[106] N. Snir, M. Caspary Toroker, Kinetic Properties of Oxygen Evolution Reaction Catalysis in Hematite, Adv Theory Simul 6 (2023) 2300182. https://doi.org/10.1002/ADTS.202300182;CSUBTYPE:STRING:SPECIAL;PAGE:STRING:ARTICLE/CHAPTER.

[107] B. Xu, W. Ma, W. Wu, Y. Wang, Y. Yang, J. Li, X. Zhu, Q. Liao, Degradation prediction of PEM water electrolyzer under constant and start-stop loads based on CNN-LSTM, Energy and AI 18 (2024). https://doi.org/10.1016/j.egyai.2024.100420.

[108] G. Zwaschka, L. Thiel, R. Leskau, Temperature optimization of PEM water electrolyzers for minimum hydrogen prices, Int J Hydrogen Energy 138 (2025) 58–63. https://doi.org/10.1016/j.ijhydene.2025.05.146.

[109] M.A. Ebbert, S. Litster, Experimental assessment and analysis of mass transport limiting current density in water vapor-fed polymer electrolyte membrane electrolyzers, Sci Rep 14 (2024) 1–10. https://doi.org/10.1038/S41598-024-79935-6;SUBJMETA=299,301,4073,4077,639;KWRD=ENERGY+INFRASTRUCTURE,MATERIALS+FOR+ENERGY+AND+CATALYSIS.

[110] Making renewable hydrogen cost-competitive (Study), (n.d.). https://www.agora-energiewende.org/publications/making-renewable-hydrogen-cost-competitive-study (accessed June 6, 2025).

[111] GREEN HYDROGEN COST REDUCTION SCALING UP ELECTROLYSERS TO MEET THE 1.5°C CLIMATE GOAL H 2 O 2, 2020. www.irena.org/publications.

[112] The Future of Hydrogen – Analysis - IEA, (n.d.). https://www.iea.org/reports/the-future-of-hydrogen (accessed June 6, 2025).

[113] F. Gutiérrez-Martín, J.A. Díaz-López, A. Caravaca, A.J. Dos Santos-García, Modeling and simulation of integrated solar PV - hydrogen systems, Int J Hydrogen Energy 52 (2024) 995–1006. https://doi.org/10.1016/j.ijhydene.2023.05.179.

[114] A. Benmehel, S. Chabab, A.L. Do Nascimento Rocha, M. Chepy, T. Kousksou, PEM water electrolyzer modeling: Issues and reflections, Energy Conversion and Management: X 24 (2024). https://doi.org/10.1016/j.ecmx.2024.100738.

[115] E.T. Ojong, J.T.H. Kwan, A. Nouri-Khorasani, A. Bonakdarpour, D.P. Wilkinson, T. Smolinka, Development of an experimentally validated semi-

empirical fully-coupled performance model of a PEM electrolysis cell with a 3-D structured porous transport layer, Int J Hydrogen Energy 42 (2017) 25831–25847. https://doi.org/10.1016/J.IJHYDENE.2017.08.183.

[116] J.A. Wrubel, Z. Kang, L. Witteman, F.-Y. Zhang, Z. Ma, G. Bender, Mathematical Modeling of Novel Porous Transport Layer Architectures for Proton Exchange Membrane Electrolysis Cells, 2021. https://www.elsevier.com/open-access/userlicense/1.0/.

[117] J. Zheng, Z. Kang, B. Han, J. Mo, Three-Dimensional Numerical Simulation of the Performance and Transport Phenomena of Oxygen Evolution Reactions in a Proton Exchange Membrane Water Electrolyzer, Materials 2023, Vol. 16, Page 1310 16 (2023) 1310. https://doi.org/10.3390/MA16031310.

[118] R. Dufo-López, J.M. Lujano-Rojas, J.L. Bernal-Agustín, Optimisation of size and control strategy in utility-scale green hydrogen production systems, Int J Hydrogen Energy 50 (2024) 292–309. https://doi.org/10.1016/j.ijhydene.2023.08.273.

[119] R. Dufo-López, J.L. Bernal-Agustín, Multi-objective design of PV-wind-diesel-hydrogen-battery systems, Renew Energy 33 (2008) 2559–2572. https://doi.org/10.1016/j.renene.2008.02.027.

[120] P. Lykas, E. Bellos, A. Kitsopoulou, C. Sammoutos, C. Tzivanidis, Electricity and hydrogen cogeneration: A case study simulation via the Aspen plus tool, Energy 294 (2024). https://doi.org/10.1016/j.energy.2024.130903.

[121] F. Gutiérrez-Martín, L. Amodio, M. Pagano, Hydrogen production by water electrolysis and off-grid solar PV, Int J Hydrogen Energy 46 (2021) 29038–29048. https://doi.org/10.1016/j.ijhydene.2020.09.098.

3. Process design and simulation of methyl isobutyl ketone (MIBK) dehydration by batch distillation: A study on unit configuration and operational policies

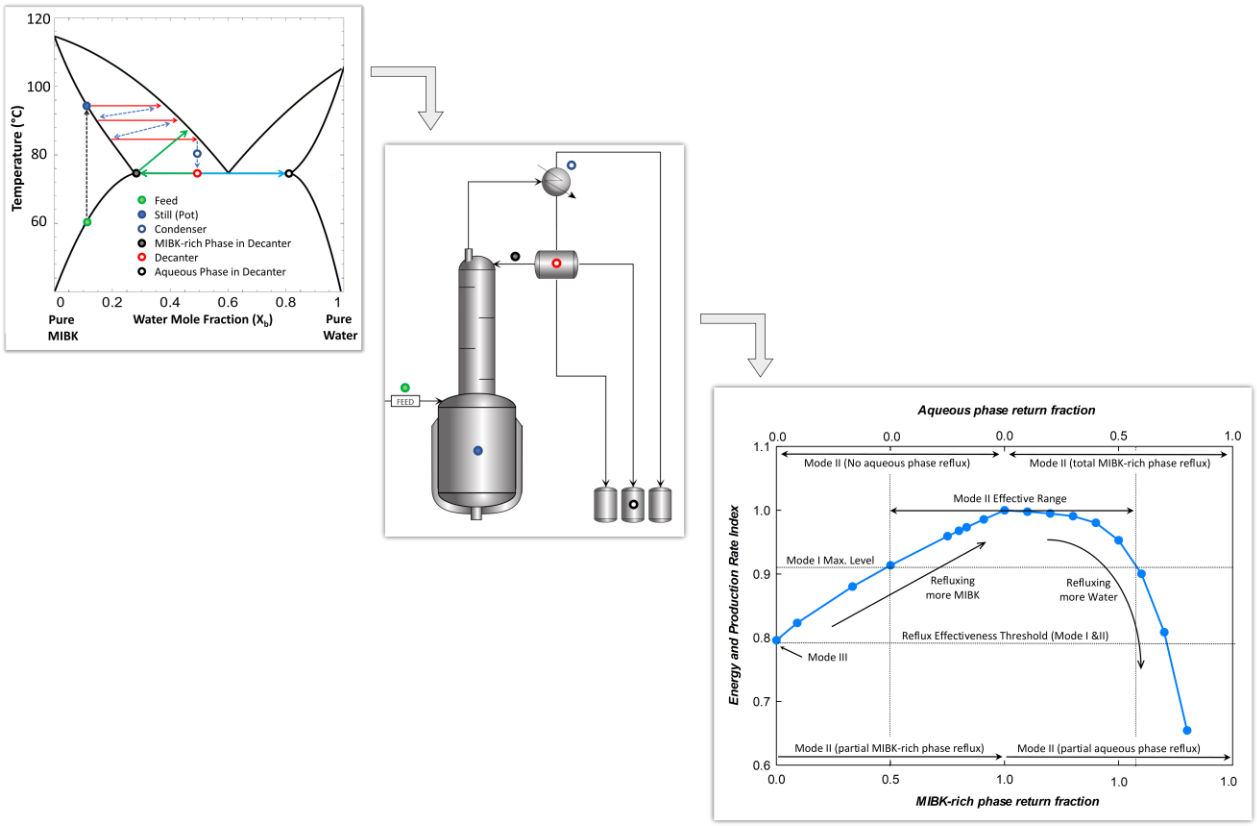

Abstract

Heteroazeotropic batch distillation of methyl isobutyl ketone-water binary mixture is investigated, seeking a reliable operation for dehydration of methyl isobutyl ketone (MIBK). The dynamic batch distillation module (BatchSep) of the commercial package Aspen Plus V.12.1® is applied for simulations. An initially fed unit at atmospheric pressure is simulated from the heating-up step until it reaches the desired MIBK purity of 99.8 wt.%. Three configurations, namely conventional batch distillation unit (Mode I), batch distillation unit with decanter (Mode II), and a simple distillation unit (Mode III), are compared in a wide range of operating conditions. The effects of condenser temperature and the number of theoretical stages are also examined. According to the results, applying a decanter (Mode II) with a return fraction of over 0.75 for the MIBK-rich phase and below 0.4 for the aqueous phase provides higher MIBK recovery than the maximum achievable value in a conventional unit (Mode I), with almost no increase in process time. A perfect decanter offers an almost complete MIBK recovery, which is about 5% over the maximum value by conventional units (Mode I). Moreover, cutting the reflux (Mode III) offers the fastest way to the desired product but provides the lowest MIBK recovery value. The aqueous phase return fraction does not significantly impact MIBK recovery, but if it exceeds 0.5, it remarkably affects the process time/energy cost. When maximum MIBK recovery rate/minimum energy cost is desired, applying a decanter (Mode II) with a return fraction above 0.5 for the MIBK-rich phase and below 0.55 for the aqueous phase yields a higher production rate and a lower energy cost per unit quantity of product compared to the best achievable values for a conventional unit (Mode I). A perfect decanter improves production rate and energy efficiency by 8 % over the best case in a conventional unit (Mode I). Also, operation without reflux (Mode III) is preferred over a conventional operation (Mode I) with a total return fraction over 0.7 due to its superior energy efficiency and production rate.

Keywords: MIBK-water, Heteroazeotropic Distillation, Batch Distillation, Aspen Plus

3.1. Introduction

The globally growing trend of energy consumption and environmental protection policies justify the necessity of optimization in energy-intensive industries to improve energy efficiency [1]. Distillation is one of the most popular separation methods in chemical and associated industries. Despite the high energy intensity and high cost of capital and operation, the energy efficiency of distillation units is often too low [2]. Accordingly, despite the long history of distillation units in industries, distillation columns are still attractive cases for energy and separation efficiency improvement.

The energy saving and efficiency improvement methods have been widely applied for continuous distillation, but the batch distillation (BD) operation still needs to be addressed due to the growing popularity of batch distillations [3]. With the recent advances in computer modelling and process simulation tools for dynamic operations, a growing number of studies are being conducted on batch operations, and to provide a deeper insight into its complex and dynamic operation. The advantages of batch distillation that make it an attractive option, particularly in the pharmaceutical, food, and fine chemical industries include [4]:

7- Applicability on small scales, especially for high-value market products.
8- Low capital cost
9- Flexibility to handle variable feed composition.
10- Allowing small-volume production
11- Providing a wide range of product separation using a single column
12- Possibility to operate in different configurations.

Conventional distillation methods are not practical for separation of azeotropic or close-boiling mixtures. Depending on the mixture features, some special techniques such as extractive distillation (ED) [5,6], pressure-swing distillation (PSD) [7–12], reactive distillation (RD) [13–15], heterogeneous azeotropic distillation (HAD) [16–21], or a combination of them [22,23] can be applied.

The PSD method does not need any new component in the feed mixture, but it is only applicable for pressure-sensitive mixtures. On the other hand, ED and HAD methods are associated with introducing an additional agent called “entrainer”. The principle of adding an entrainer in ED is to form a miscible homogenous mixture with a more favourable equilibrium condition for distillation, while in HAD, it leads to forming a heteroazeotrope so that the condensed stream appears as an immiscible mixture in the reflux drum/decanter, enabling the operator to

split the feed components mechanically to a specific extent [24]. One of the main issues in such techniques is the entrainer selection, and due to the necessity of a second separation process for entrainer removal/recovery, the distillation is not regarded as an independent unit, but it must be studied as a part of the unit. Subsequently, any optimization approach for HAD and ED operations shall cover the cost, time, and energy required for the entire separation steps.

There is also an interesting category of distillation processes where the heteroazeotrope appears by adding no new component to the mixture. The butanol-water mixture is a well-known instance of this category known as “auto-entrained” or “self-entrained” systems [25,26].

Methyl isobutyl ketone (MIBK), a well-known aliphatic ketone, is widely used as an industrial solvent in paint industries as well as a basic raw material of organic synthesis in the pharmaceutical industry [27]. There are many examples in which MIBK is polluted with a small fraction of water, especially when applied as a solvent. On the other hand, due to the high toxicity, limited availability, and high cost of fresh MIBK, a reliable approach for solvent recovery/dehydration is demanded to meet the sustainability criteria in the economic and environmental protection aspects of the process [28]. The solvent recovery must be an effective approach to purify the solvent to the desired level for further use. Despite the high energy intensity and capital costs, distillation is still a popular operation for solvent recovery. To the best of the authors' knowledge, despite the large number of operations in which MIBK utilized as a solvent gets polluted by water, the only work reported on the dehydration of MIBK for solvent recovery is our previous study [29], where a batch distillation unit equipped with a decanter was introduced in response to an inquiry from a paint production factory. Here, the study continues to address the subject in more detail, provide deeper insight into the process, and prepare perceptible guidelines for operators. Wider ranges of operation, considering the most likely non-ideal cases in column and decanter operation, are studied. After studying some of the most likely reasons for separation failures, some easy-to-apply debottlenecking solutions for practical applications are proposed. The primary objectives of this study are summarized below:

- To apply, evaluate, and compare different configurations and operation policies for separation of heteroazeotropic systems in terms of recovery, process duration, and production rate.

- To evaluate different configurations and operation scenarios in terms of energy cost.
- To introduce an effective approach for distillation of heteroazeotropic mixtures and specify the optimum operation ranges.
- To improve the process in terms of separation efficiency and energy demand at the same time.

3.2. Methodology and study plan

3.2.1. Simulation Procedure

The commercial chemical process simulator Aspen Plus V12.1® was used for this study. The UNIQUAC model was applied to model the phase equilibrium of the MIBK-water mixture. The relevant phase diagram of the mixture according to the UNIQUAC model and experimental values is presented in Figure 3-1a. The experimental data points are obtained from the NIST Thermo Data Engine (TDE) database [30] and the binary interaction parameters are obtained from APV100 VLE-IG database, accessed through Aspen Properties V.12.1®. This figure shows two immiscible liquid phases in equilibrium with the vapor due to the MIBK-water heterogeneous azeotrope formation. This batch distillation process, engaged with water removal as volatile component, would have a relatively large energy cost due to heat capacity and latent heat of water. Having an azeotropic mixture complicates the situation, and accordingly, the energy consumption is relatively high for removing a specific amount of water from the studied mixture.

Specifically, this study aims to assess the batch-mode separation of a binary MIBK-water mixture with 98 wt.% of MIBK as a typical waste stream in the paint industry. This composition (water concentration of 2 *wt*.%) corresponds to the solubility of water in MIBK at room temperature after decanting the main water fraction. Further purification up to 99.8 *wt*.% is demanded as a standard criterion for solvent reuse; thus, it becomes the scope of separation in the present study. The initial temperature of the feed is 25 ℃, which represents the room temperature, and the total initial feed charge is 15 kg.

Generally, a batch distillation/rectifying unit comprises three main elements: (1) a still (or pot) that contains the initial mixture batch charge (feed) and provides the heating facilities via an external heat source or embedding a heater within; (2) a

column consisting of the mass transfer internals such as trays or packings; and (3) a condenser that condenses the vapor leaving the column, partially or totally. The unit might also include some accessories, such as distillate collection tanks, reflux drums, control systems, etc. The basic distillation unit studied in this project presented schematically in Figure 3-1b, comprises a packed column filled with Raschig rings of size 1/2 inch, a still of 25 *L* volume, and a total condenser that provides a constant temperature outlet stream.

The necessary technical data to define the basic batch distillation model are listed in Table 3-1. This table presents the feed properties, process objectives, column internals, unit accessories, heater (reboiler), and condenser characteristics applied in the simulation model. The contents of Table 3-1 are applied in almost all the simulations unless otherwise specified in a particular case.

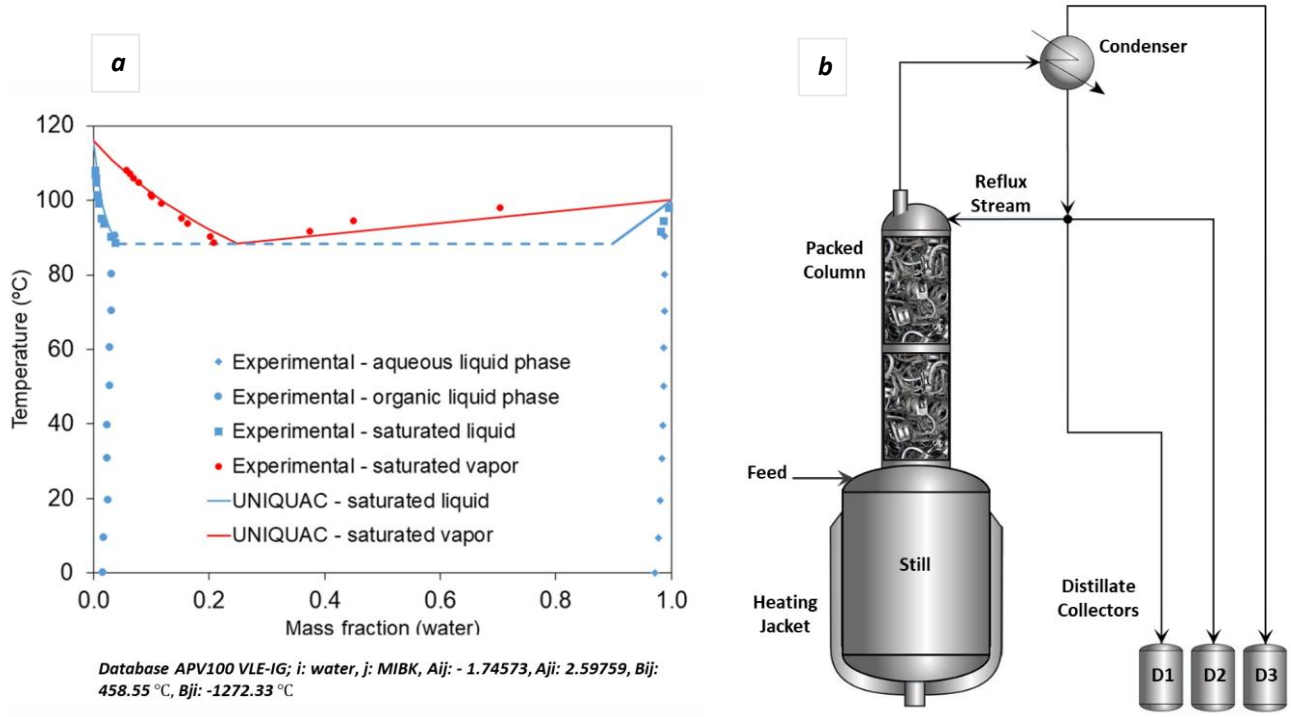

Figure 3-1. (a) Phase equilibrium diagram of MIBK-water system at 1 atm. and temperature range: 0 - 116 ℃ [29,30].

Table 3-1. General operating conditions and technical features applied in the batch distillation unit simulation.

Parameter	Symbol	Value	Units
Initial charge (Batch size)	r_0	*15*	$[kg]$
Operating pressure (Condenser pressure)	$P = P_c$	*1*	$[atm.]$
Initial MIBK mass fraction	x_{r0}	*0.98*	$[-]$
Final MIBK mass fraction	x_r	*0.998*	$[-]$
Valid phases	$-$	*VLL*	$[-]$
Still diameter	ϕ_s	*0.3*	$[m]$
Still volume	V_s	*25*	$[l]$
Reboiler duty	W	*5040*	$[kJ/h]$
Reboiler type	$-$	*Jacket Heating*	$[-]$
Condenser type (Total/Partial) *	$-$	*Total*	$[-]$
Diameter of condenser inlet	ϕ_c	*0.1*	$[m]$
No. of collectors	$-$	*3*	$[-]$
Column diameter	ϕ_t	*0.1*	$[m]$
Packing type	$-$	*Metal Raschig ring*	$[-]$
Packing size	ϕ_p	*13 (1/2")*	$[mm]$
Assumed height of the equivalent theoretical plate	*HETP*	*1*	$[m]$
Packing Bed Height	H_p	*2*	$[m]$
Dry packing factor	F_p	*984*	$[m^{-1}]$
Packing porosity	ε	*0.85*	$[-]$
Specific area of packing	α	*400*	$[m^2/m^3]$
Foaming factor	f_f	*1*	$[-]$

* It is a total condenser regarding MIBK and water components (section 3.2.2.1)

Regarding the column internal calculations, the simulator performs the flooding and pressure drop calculations via the Eckert model [31]. Since the mixture has a low foaming tendency, the system factor applied is equal to 1. A random packing bed of 2 m height is introduced to the model, as described in Table 3-1. The simulation approach is based on the equilibrium stages, and the *HETP* is set to 1 m. Accordingly, the packing bed defined in the model is equal to two equilibrium stages. Subsequently, considering the still/reboiler as another equilibrium stage, the batch distillation unit comprises three equilibrium stages. Since the heterogeneous liquid phases are supposed to be simulated, the model is adjusted to recognize three phases: an organic liquid phase (MIBK-rich), an aqueous liquid phase (MIBK-lean), and a vapor phase.

Jacket heating with a constant rate of 5040 kJ/h is continuously applied on the still for the entire process duration, and the condenser provides a fixed-

temperature condition for the outlet stream, which subsequently divides into the reflux and top outlet (distillate) streams.

The main operation scenario in this study is the "constant reflux ratio" [3], and the operation continues until the MIBK purity of the mixture within the unit reaches the desired value of 99.8 $wt.\%$. The total amount of liquid and vapor in the column and the still are considered for stop criteria recognition. In this order, the final condition is set to recycle the holdup mixture to the still, and no amount of the mixture will be discharged to the distillate receivers after the operation stop time. The desired product (high-purity MIBK) will be collected in the still, and the top product, mainly composed of the volatile component (water), is generally identified as effluent or, in some cases, as an unrefined mixture (section 3.3). In all simulations, the top product (distillate) is divided into three phases, and each phase is collected in a particular distillate receiver for accurate phase and component tracking and a better understanding of observations. The collectors D1, D2, and D3 (Figure 3-1b) receive the aqueous phase, the MIBK-rich phase, and the vapor product (section 3.2.2.1), respectively.

The state variables used to evaluate the unit performance and the necessary parameters to specify them are presented in Table 3-2. These variables enable us to analyse the batch distillation unit performance in different terms. This way, the optimum operation approach can be recognized in terms of process time, energy consumption, production quantity, or production rate. The ultimate goal in this unit is to recover the maximum amount of MIBK with the desired purity of 99.8 $wt.\%$ at the shortest possible time which, in turn, implies the maximum production rate and minimum energy consumption, for a case with constant reboiler duty. On the other hand, production rate and, in some batch operations, energy consumption have varying values during the batch distillation operation, which requires a proper way to be quantified. Accordingly, in addition to process duration (t) and recovered mass (r), three other parameters, namely fractional recovery (η), specific product flow (SPF), and specific energy cost (SEC) are introduced as follows [29,32]:

$$SPF = \left[\frac{r.x_r}{t}\right] = \left[\frac{kg_{MIBK\ obtained}}{h_{operation}}\right] \quad (1)$$

$$\eta = \left[\frac{r.x_r}{r_0.x_{r0}}\right] = \left[\frac{kg_{MIBK\ obtained}}{kg_{MIBK\ fed}}\right] \quad (2)$$

$$SEC = \left[\frac{W}{SPF}\right] = \left[\frac{kJ/h_{operation}}{kg_{MIBK\ obtained/h_{operation}}}\right] = \left[\frac{kJ}{kg_{MIBK\ obtained}}\right] \quad (3)$$

Where η presents the fraction of MIBK recovered in one time running the unit, SPF expresses the average rate of recovery in the batch distillation process, and SEC determines the amount of energy required to recover a unit amount of MIBK, which enables one to evaluate (and compare) the effectiveness of different strategies in terms of energy cost, regardless of the feed quantity or scale of the unit. Table 3-3 presents the studied operational parameters and their associated range of variation in this project. The (external) reflux ratio, RR, refers to the ratio of reflux to distillate for each liquid phase received in the condenser/decanter. It can be calculated as follows:

$$RR = \frac{R}{D} \quad (4)$$

Where R and D are the mass flow rate of reflux and distillate streams, respectively. The return fraction, RF, refers to the fraction of each liquid phase received in the condenser/decanter, that returns to the column along with the reflux stream. This definition is identical to internal reflux ratio (L/V) for the top stage in the column but applied to each liquid phase. This term and its relationship with reflux ratio is as follows:

$$RF = \frac{R}{D+R} = \frac{RR}{1+RR} = \frac{L}{V} \quad (5)$$

Where L is the mass flow rate of the liquid refluxed to the column and V is the mass flow rate of the vapor leaving the top stage of the column. In this work, RF_1 refers to the MIBK-rich phase return fraction and RF_2 refers to the aqueous phase return fraction.

Table 3-2. State variables for batch distillation unit assessments.

Parameter	Symbol	Units
Process Duration	t	$[h]$
Recovered Mass	r	$[kg]$
Fractional Recovery	η	$[-]$
Specific Product Flow	SPF	$[kg.h^{-1}]$
Specific Energy Cost	SEC	$[kJ.h^{-1}]$

Table 3-3. Variable operating parameters and the range of study.

Parameter	Symbol	Range of Study	Units
Number of theoretical stages in column	N_e	*0-5*	[–]
Reflux ratio	RR	*0.1~20*	[–]
Reflux ratio of MIBK-rich phase (Rich)	RR_1	*0.1~20*	[–]
Reflux ratio of Aqueous phase (Lean)	RR_2	*0.1~20*	[–]
Return fraction of MIBK-rich phase (Rich)	RF_1	*0~1*	[–]
Return fraction of Aqueous phase (Lean)	RF_2	*0~0.95*	[–]
Condenser temperature	T_c	*25~85*	[℃]

3.2.2. Unit configurations and operation policies

Employing a suitable operation policy while using an efficient configuration offers desirable production and simple operation at a reasonable energy and time cost. Based on the previously developed knowledge on MIBK-water distillation [29] and potential strategies in heteroazeotropic batch distillation [21,33], three main batch distillation configurations are studied under different operation strategies. Figure 3-2 shows the three configurations entitled Mode I, Mode II, and Mode III. Mode I represents a conventional batch distillation unit according to the basic unit description in section 3.2.1, Mode II refers to a batch distillation unit equipped with a reflux drum on the condenser outlet stream, which enables the operator to remove (or return) an intended phase after decanting, and Mode III is an extreme case of Mode I (or II) in which the external reflux stream is cut and no part of the vapor leaving the column returns back to it. Mode III turns the complex distillation unit into a very simple unit. Each mode/configuration is studied in a range of operating conditions under different operation policies. The results are discussed in detail to characterize the operation sensitivity and its dependency upon the operating parameters presented in Table 3-3. As mentioned before, the scope of the process for all cases in this study is to recover MIBK at 99.8 *wt*.% in the still at the end of operation. Table 3-4 briefly presents the study plan, including the different sections of this study, classified based on the concerned variable parameter and the studied range of each parameter.

Partial reflux, in this table, refers to the condition where a fraction of a liquid phase received in the condenser/decanter returns to the column along with the reflux stream (0<RF<1). Total reflux refers to the condition where the liquid phase

entirely returns to the column (RF=1) and Reflux of 0 refers to the condition where the liquid phase totally discharges as top product (distillate). Simulation of all three configurations is conducted using BatchSep module provided in Aspen Plus V12.1®, and the relevant flowsheet is presented in Figure 3-3.

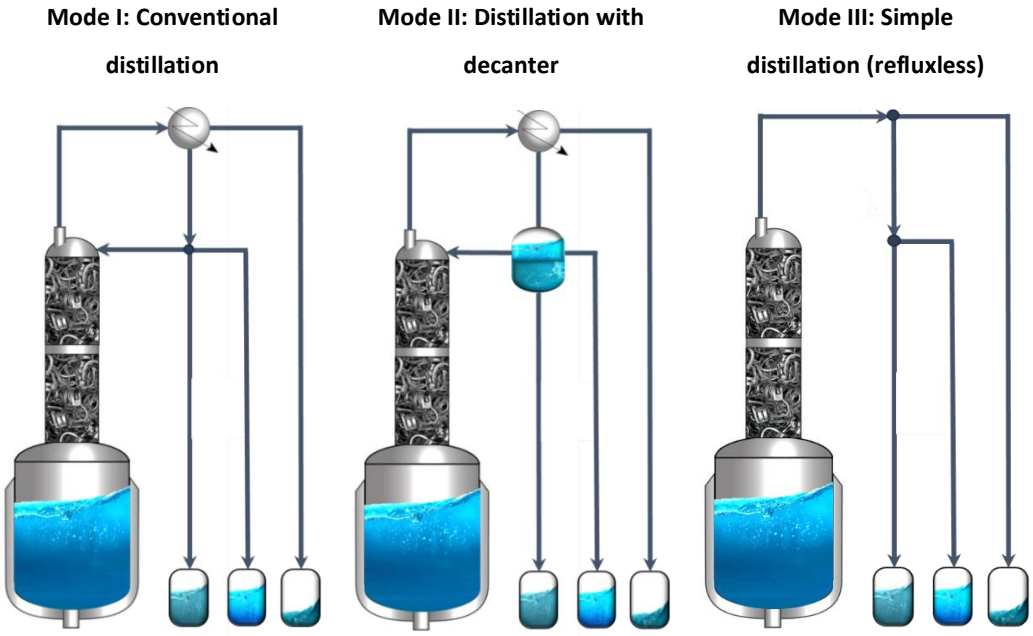

Figure 3-2. Three different batch distillation configurations studied in the present investigation.

Table 3-4. Operation policies for different batch distillation configurations

Case no.	Description	Config.	Total reflux as start-up	MIBK-rich phase reflux	Aqueous phase reflux	N_e	T_c (℃)
1	Conventional distillation	Mode I	Yes	Partial	Partial	2	85
2	Start-up procedure assessment	Mode I	No	Partial	Partial	2	85
3	Batch distillation with decanter	Mode II	No	Total	0	2	85
4	Deficient water removal	Mode II	No	Total	Partial	2	85
5	Deficient MIBK reflux	Mode II	No	Partial	0	2	85
6	Simple distillation (Refluxless)	Mode III	No	0	0	2	NA.
7	Effect of condenser temperature	Modes I-II	No	Partial	Partial	2	25~85
8	Effect of no. of theoretical stages	Mode II	No	Total	0	0~5	25~85
9	Troubleshooting approaches	Mode II-III	No	Total	0	0&2	25&85

3.2.2.1. Conventional distillation (two-step operation)- Mode I

Before addressing the variety of configurations, modes, and strategies applied for separation unit assessment, it is necessary to define the basic unit model. Conventionally, the first step to run a distillation unit is to start the process in total reflux mode until reaching the steady state condition, known as the "start-up" (or heating) step. Once the steady state is achieved, a finite reflux ratio (known as the "production step") is set based on the overall unit objectives and desired product specifications. Since there is no production during the start-up step, it might be ignored in energy efficiency evaluation. The start-up step energy consumption might be significant compared to the total energy consumption in a batch distillation process so it should be included in the operation assessment. In addition, the largest amount of mixture within a batch distillation unit corresponds to the start-up step. Consequently, the energy consumption at the beginning seems to be significant due to covering both temperature rise and evaporation for a large quantity of mixture. Accordingly, the start-up step is considered in the energy and production rate evaluation of all studied cases in the present work. For this purpose, “Initial charge” option is applied as initial condition of BatchSep Model. While utilizing the "initial charge" option, a pad gas must be introduced to fill the empty space within the column/containers. Hence, nitrogen gas is assigned as "pad gas", which matches the industrial cases where nitrogen is purged in the non-operating equipment for equipment protection, and it is also the main air component in a normal case with no purge gas. On the other hand, since using a total condenser is not compatible with the pad gas presence, a partial condenser with a fixed temperature of 85 ℃ is employed with no reflux drum. This temperature is slightly lower than the azeotrope temperature of the water-MIBK mixture at atmospheric pressure (88.38℃), and it ensures condensing the MIBK and water content at the highest possible temperature that provides a saturated liquid outlet with no sub-cooling in the condenser. Regarding the Aspen Plus instructions, the distillation unit comprises four theoretical stages, including a still/reboiler, two theoretical stages in the column, and a partial condenser. On the other hand, since the condenser is a total condenser with respect to the feed components (MIBK-water mixture), the model should be literally identified as a three-stage distillation unit based on the fundamental knowledge of unit operations.

In simulations conducted by BatchSep module, unsteady-state heat and mass balance equations and phase equilibrium relationships are applied by Aspen Plus

to simulate the process with details in each element of the unit. The implicit Euler integration method is employed for calculations. The initial and minimum time step sizes are 10^{-5} h and the maximum time step is 0.01 h. The absolute and relative integration tolerances were set to 10^{-4}. The maximum number of iterations for the non-linear solver is set to 100. No convergence issue was raised by applying the described solver configuration, calculation methods and adjusted parameters.

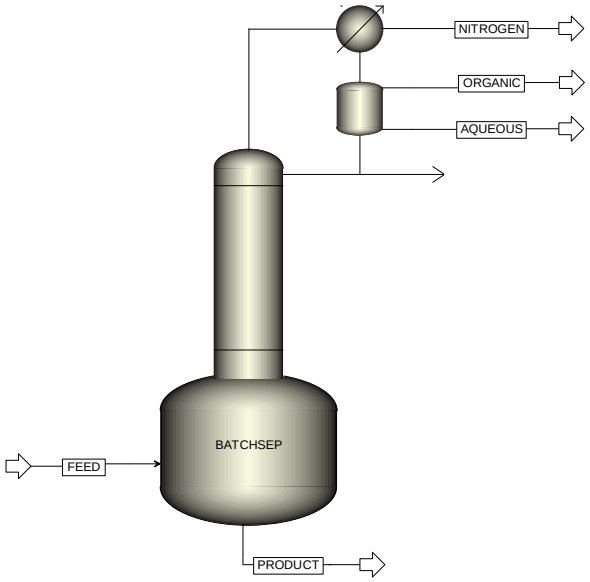

Figure 3-3. Process flow sheet of distillation unit by BatchSep Module

3.2.2.2. Start-up procedure assessment (single-step operation)-Mode I

Generally, conducting a batch distillation operation takes a relatively short time and consists of two (or more) steps. In addition to the significant contribution of heating/start-up step in total energy consumption, the operator might have a delay in recognition of the steady state condition to turn the operating mode "total reflux" to "finite reflux" in order to start production [34,35]. Any delay in steady state recognition causes an extra energy cost and a longer process time. In addition, the total reflux operation mode is fundamentally a crucial stage for a continuous distillation unit start-up to reach a steady state condition and fulfil the desired product specification from the beginning of production. Hereupon, an assessment is conducted in this study to see if this operator-oriented start-up instruction must be necessarily followed for a batch distillation unit or if it can be replaced by an alternative approach. Accordingly, the simulation described in "conventional

distillation" is repeated, skipping the first operation step, "total reflux", to assess the necessity of this strategy. The results for both cases are compared at varied reflux ratios in the range of 0.1–20 to see the probable advantages of each scenario at different reflux levels.

3.2.2.3. Batch distillation with decanter (perfect decanter) – Mode II

As explained before, the MIBK-water mixture is a self-entrained binary system, which means the heteroazeotrope appears with the original components of the mixture with no need to introduce a third component as an entrainer. The liquid-phase immiscibility in the MIBK-water binary system can be used to leverage the distillation unit by installing a decanter downstream of the condenser. This can be interpreted as implementing a mechanical separation process to assist the distillation process. The distillation using a decanter, refluxing the total amount of MIBK-rich phase, and discharging the aqueous phase has already been studied and proved to be an effective way for process improvement in terms of production, process time, and energy consumption [29]. On this basis, a reflux drum is added to the unit to separate the MIBK-rich liquid (organic) and the MIBK-lean liquid (aqueous) and also to control the reflux and distillate stream content. The ideal case is to consider a perfect phase separation, immediately returning the entire MIBK-rich phase to the column as a reflux stream and discharging the entire aqueous phase to the distillate collector tank. The column for Mode II is modelled with the same adjustments as in the basic distillation unit (Mode I). The reflux ratio of 0 for the aqueous phase and total reflux for the MIBK-rich phase are set to simulate the perfect decanter.

3.2.2.4. Batch distillation with decanter (deficient water removal) – Mode II

Applying a decanter in a heteroazeotropic continuous distillation and achieving a perfect phase separation is relatively easy due to the steady-state condition and constant stream rates. On the other hand, in a batch distillation unit with dynamic behaviour and relatively short time operation, achieving a perfect liquid-liquid separation is challenging. In addition, the small scale of the unit and its low capital cost are crucial factors for a batch distillation unit. Accordingly, employing a small number of control elements is generally preferred. Hence, it is important to know if a sophisticated control system for decanter is necessary or an imperfect (partial) decanter can sufficiently fulfil the process requirements.

On this basis, deficient decanting with two scenarios of "deficient water removal" and "deficient MIBK reflux" are studied to assess how decanter accuracy may affect the unit operation performance. To simulate the deficient water removal, a specific fraction of the aqueous phase received in the decanter is returned to the tower along with the entire MIBK-rich phase. Since this part of the study concerns the decanter separation performance (not the distillation column), decanting quality can be quantified and presented by "return fraction," which is defined as the fraction of each decanted liquid phase that returns to the column along with the reflux stream (Eq. 5). Various aqueous phase return fractions (RF_2) in the range of 0 to 0.95 are studied (corresponding to RR_2 range of 0 to 19), along with the total reflux of the MIBK-rich phase ($RF_1 = 1$) to characterize the impact of deficient water removal in the decanter. No need to mention, the case with $RF_2 = 0$ is obviously replicating the perfect decanting, and the case with ($RF_2 = 1$) implies no water removal that is not compatible with the unit objectives, so the maximum studied value is $RF_2 = 0.95$.

3.2.2.5. Batch distillation with decanter (deficient MIBK reflux) – Mode II

The second scenario to simulate an imperfect decanter is to consider the MIBK-rich phase's partial discharge to the distillate receiver along with the aqueous phase, which might be identified as "MIBK loss". This scenario is studied, assuming perfect aqueous phase removal by decanter. Various MIBK-rich phase return fractions (RF_1) in the range of 0 to 1 are studied. The case with ($RF_2 = 0, RF_1 = 1$) is obviously replicating the perfect decanter case, and the case with no reflux ($RF_1 = RF_2 = 0$) turns the unit into a simple distillation (Mode III). Accordingly, the effects of missing some of the MIBK content in the top product could be identified.

3.2.2.6. Simple distillation as an alternative - Mode III

As mentioned in section 3.2.2.5, by extending the study range, the user faces an extreme case with no reflux stream ($RF_1 = RF_2 = 0$). It turned out that due to the small amount of water, it can be removed by vaporizing the mixture with no reflux stream at the cost of discharging a large fraction of the MIBK content into the top product. This operation scenario is supposed to assess the feasibility range for a unit with no column (packing bed), decanter, reflux stream, etc., and ultimately downscale a complex distillation unit (Mode II) into a simple distillation unit (Mode III).

3.2.2.7. Effect of condenser temperature - Modes I-II

Condenser temperature is known as an important parameter to control in a distillation unit. A distillation unit condenser is an attractive element for thermal integration and energy recovery, so a lower temperature in the condenser might be of interest in order to recover more energy. On the other hand, the effects of temperature on distillation performance must be carefully characterized. Sometimes these impacts can be complicated and hard to predict, particularly once a new operation policy is applied. Knowing the fact that subcooling in a condenser leads to repelling more water from the MIBK-rich phase, it is basically expected to improve the process but still needs to be evaluated in detail. Accordingly, the simulations of Mode I and Mode II (with a perfect decanter) are repeated, varying the condenser temperature in the range of 25 to 85 °C in order to specify the effects of subcooling on the performance indicators. This temperature range is expanded from normal ambient temperature and available coolers (25 °C) up to approximately the maximum temperature for total condensing (85 °C).

3.2.2.8. Effects of no. of theoretical stages - Mode II-III

The number of mass transfer stages in column, specifically is one of the major factors to be specified and optimized during the distillation unit design procedure since it directly affects the internal hydraulic condition and, consequently, the separation performance. Due to the dynamically changing loads of liquid and vapor in a batch distillation column, the mass transfer internals are expected to work out of the satisfying hydraulic range, in which they function efficiently. Even a precise hydraulic calculation on packing beds is based on a perfect liquid and gas distribution assumption, so the HETP value depends directly on the hydraulic condition within the bed [36]. This means that for an inherently dynamic batch distillation unit, specifying the HETP is probably not an accurate approach so that a batch distillation column shall be necessarily characterized in a wide range of operations with different amounts of packings. Accordingly, the simulation of Mode II with a perfect decanter is repeated for different sizes of mass transfer sections from 0 to 5 theoretical stages. The case $N_e = 0$ represents a distillation column with an inefficient packing bed or when the unit comprises an evaporation pot and a condenser. This case is also supposed to be compared with Mode III, where neither a functional mass transfer internal nor the condenser are employed. In addition, the case with no packing bed is repeated at a lower condenser temperature (subcooling at 25 °C). These cases are simulated to assess the extreme operation

scenarios and the possibilities of adapting and upgrading an existing, poorly designed unit by manipulating the operating variables such as reflux stream or condenser temperature.

3.3. Results and discussion

Before discussing the results for the batch distillation unit, it must be clarified that identifying an operation as "efficient" or "inefficient" strongly depends on the user's point of view. A unit might be exploited once with no repeat, such as in the case of a rental batch unit, or when repeating the process is not of interest. In such cases, the production quantity and time for every single batch matters. In case the heavy component is the product of interest, any part of it leaving as top product would be identified as “loss” and the top product would be identified as “effluent”. Another approach is to run a batch unit repeatedly to purify the continuously receiving feed batches. This approach is more common, and since it implies a semi-continuous trend, it can be analogized to a continuous operation for performance evaluation. On the other hand, the single-batch process shall be evaluated independently with no further steps. Figure 3-4 presents these two approaches. Accordingly, in order to evaluate the batch distillation unit in this study, two perspectives have been applied:

(1) Perspective I (Persp. I): When repeating the process is not of interest, for instance in case of exploiting a rental batch unit. It considers a *single batch* operation and evaluates the unit performance in terms of batch recovery (η), recovered mass (r) process duration (t), production rate (SPF), and energy consumption (SEC), and finally select the best operation range in a trade-off procedure among the principal factors and priorities. For instance, purity or the amount of recovered mass (or fraction) might override energy efficiency, and the user might prefer to obtain the maximum possible product. In this perspective, the amount of MIBK leaving the unit along with the top product is considered as "lost" along with the effluent (as shown in Figure 3-4a). There is no subsequent recovery for the lost MIBK, so the recovered mass (or fraction) can be a decisive factor for the user in this approach.

(2) Perspective II (Persp. II): It Considers *sequential batches*, which implies repeating the batch distillation and reprocessing the distillate by a subsequent batch. This practice is more common, and since it implies a semicontinuous trend, it can be analysed as continuous operation for performance evaluation. Using this perspective, the overall performance of

the process over time shall be evaluated instead of a single batch performance. On this basis, the rate of production (SPF) and the energy consumption per unit quantity of product (SEC) will be suitable criteria to evaluate the operation. In this case, fractional recovery (η) or a single batch time duration (t) are not good indicators for process performance. According to this point of view, discharging some MIBK along with the top outlet stream is not necessarily an adverse issue, and that quantity of MIBK will not be considered as "loss". The top product can be collected and decanted at room temperature, and the MIBK-rich phase will be added to the feed charge in the subsequent batch operations (Figure 3-4b). It has to be noted that the batch distillation columns shown in this figure are the same unit operating at different times to refine a new batch of feed.

The results for different parts of this study, presented in the following sections, cover the required data for both perspectives but with more focus on Persp. II due to an industrial inquiry, in which the end user is supposed to run the unit frequently during the time, what matches the concept of Persp. II.

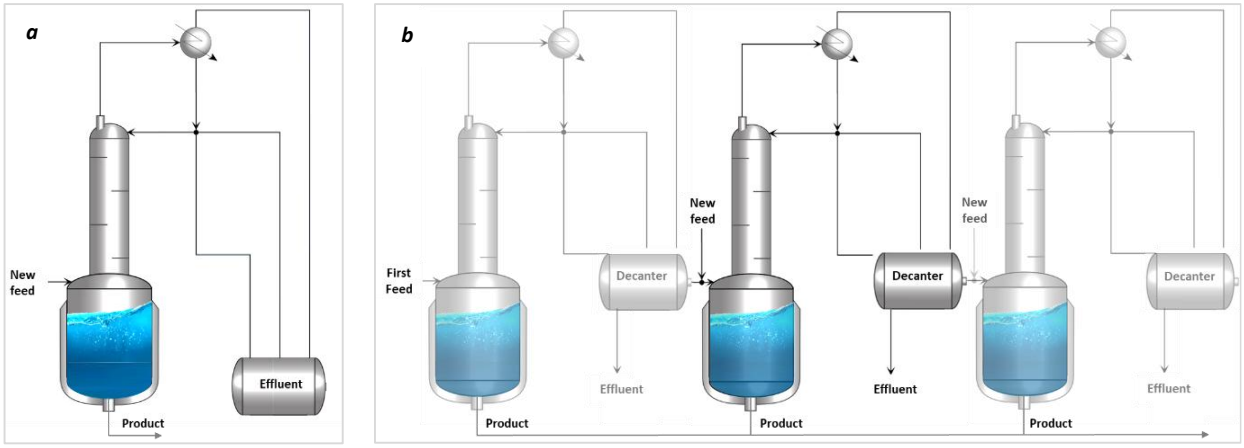

Figure 3-4. Commonly applied perspectives for evaluation of a batch distillation unit (a) single batch (Persp. I) and (b) sequential batches (Persp. II).

3.3.1. Conventional distillation (two-step operation) - Mode I

As explained in section 3.2.2.1, to establish a steady-state condition in the column before starting production, a total reflux condition is set within the unit which implies a “two-step operation (TSO)”. Steady state recognition was achieved through monitoring the vapor and liquid loads on the top column stage. A constant liquid load within the column represents a fully developed reflux stream and the steady state condition in the column. To be confident that the criteria for steady state recognition are adequate, the thermal and component profiles of the entire

system were also monitored simultaneously in total reflux mode. No further change in composition, temperature, or fluid loads was observed after 2500 s. Accordingly, the simulations for the start-up step (total reflux) in the conventional distillation process continued for 2500 s, then the operation turned to the production step (finite reflux ratio). Nine different reflux ratio levels in the range of 0.1 to 20 are studied to see the impact of reflux ratio on unit performance. The duration of the total reflux operation step is constant in all cases.

Variation of fractional recovery (η) and process duration (t) with reflux ratio for single-step operation is presented in Figure 3-5a. According to this figure, the fractional recovery (η) increases by increasing the reflux ratio, which was expected due to holding more MIBK in the unit by means of a high reflux quantity. In other words, with a lower reflux ratio, a larger fraction of MIBK leaves the column before achieving the desired purity. On the other hand, the process duration increases with increasing the reflux ratio, which can be explained by retaining a larger fraction of water in the system, which needs a longer time to be removed as a top product. The results also show that the start-up step duration corresponds to about 63% of the total operation time for the case RR=0.1 and it is about 16% of the total time for the case RR=20. Accordingly, the initial heating step is a significant part of batch distillation, particularly in short-time operations.

Taking a more precise look at the graph, it can be observed that increasing the reflux ratio leads to a slight increase in process duration in the range below RR = 5, and with further increases in the reflux ratio, the process time increases drastically. On the other hand, the fractional recovery (η) is sharply increased by increasing the reflux ratio in range RR<3 and beyond this point, the recovered mass is almost constant (about 13.9 kg). These observations indicate that for a high recovery value, the reflux ratio should be increased to a specific value (RR=3) which has a slight time/energy cost but increasing the reflux ratio over this point causes a higher time/energy cost and no significant improvement in recovery.

In all studied cases, a trace of MIBK leaves the column along with the aqueous phase as well as the nitrogen gas leaving the column at the beginning of operation.

Based on Persp. I, a minimum reflux ratio of 3 is necessary to recover the MIBK almost completely, and since the recovery will not improve with further increases in the reflux ratio, operation with RR=3 is the optimum point.

To evaluate the process based on Persp. II, it is necessary to analyse the SEC and SPF values. SEC and SPF values for a single-step operation are presented in

Figure 3-5b. It can be observed that the minimum SEC value and maximum SPF value are obtained at RR=1. This can be explained by the relatively high recovery of MIBK compared to the cases with lower return fraction besides the negligible increase in time with increasing the return fraction up to 1. On the other hand, however, further increase of reflux ratio still increases recovery but the time also increases sharply so that the SEC and SPF change adversely. Accordingly, in order to recover a particular amount of MIBK, conducting the operation with RR=1 minimizes the energy consumption and maximizes the recovery rate. Based on Persp. II, however, the recovered MIBK at the point RR=1 is not as high as it could potentially be in a single batch operation, but this point is the optimum condition since it leads to a smaller energy cost and a larger production rate for a specific amount of MIBK recovered. Regarding Eq. 5, the point RR=1 corresponds to an operation in which 50% of the MIBK-rich liquid and 50% of the aqueous liquid received in the condenser are returned to the column as reflux stream. It is worth mentioning that to recycle the MIBK content discharged from top and to recover it in the next batch operations, based on Persp. II, the top product would be located in the two-liquid region of the equilibrium phase diagram (Figure 3-1a). Accordingly, after a primary liquid-liquid phase separation, the decanted MIBK-rich phase would have a composition in the range of 0.96-0.98 wt.% MIBK, depending on the temperature. In case of cooling the mixture to 25 °C (room temperature, identical to the feed condition), the composition is expected to be identical to the feed composition (~0.98 wt.% MIBK) since it is determined by solubility of water in MIBK.

It should be noted that SEC and SPF are also applicable to evaluate a single-batch operation (Persp. I) but are not sufficient to describe the performance since a low SEC value does not necessarily indicate a desirable performance because it might be due to a low fractional recovery (η) which means the short operation time and lower energy cost are due to the loss of valuable components. Hence, one must consider the recovery indicators (η or r) besides the SEC and SPF, to provide a valid evaluation based on Persp. I. For instance, based on Persp. I, the case with the RR=1 is not an ideal case because that leads to a considerable loss of MIBK (about 0.5 kg) compared to the case $RR \geq 3$ so that it can be evaluated only by recovery indicators (η or r).

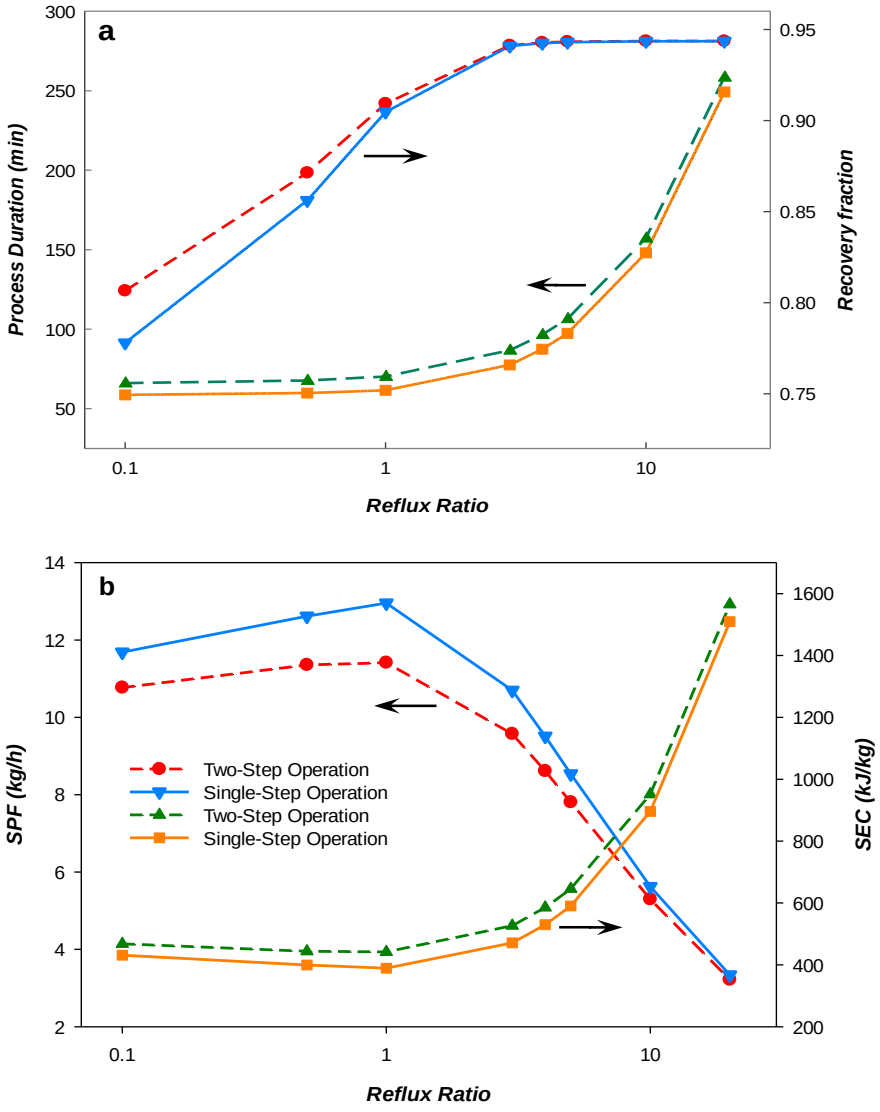

Figure 3-5. Effect of reflux ratio on single-step operation and two-step operation in terms of (a) recovery and process duration time and (b) SPF and SEC

3.3.2. Start-up procedure assessment (single-step operation) - Mode I

As explained in section 3.2.2.2, the simulation cases of conventional distillation unit are repeated, skipping the start-up step. The values of fractional recovery (η) and process duration time (t) in both scenarios of "single-step operation" (SSO) and "two-step operation" (TSO) can be observed in Figure 3-5a. As this figure indicates, operation in single-step results in a shorter process time in the range of 3.5% (for RR=20) up to 11.1% (for RR=0.1). On the other hand, a single-step operation results in a lower MIBK recovery, especially in cases with a low reflux ratio. This can be explained by the amount of MIBK discharges at the beginning of the process in a single-step operation that could be retained by means of a total reflux start-

up approach. Accordingly, based on Persp. I, applying the single-step operation scenario with low reflux values may have an adverse impact on fractional recovery and is not recommended. It must be noted that the recovery at RR=3, which is the optimum point of operation based on Persp. I, is the same for both scenarios, and the process time is still less than the two-step operation (with start-up). Accordingly, regarding Persp. I, using a single-step operation is advantageous if the unit is running at a proper reflux level.

The SEC and SPF values for single-step operation are presented in Figure 3-5b, along with those for two-step operation. As it can be observed, the single-step operation scenario results in lower SEC and higher SPF in all cases, which means skipping the total reflux start-up step not only offers an easier operation and a shorter operating time but is also beneficial in terms of energy cost and production rate. Accordingly, regarding Persp. II, the single-step operation is preferred over a two-step operation, and the rest of the study is conducted with the same operation scenario, using a constant reflux ratio from the beginning of the operation.

3.3.3. Batch distillation with decanter (Perfect decanter) – Mode II

Based on section 3.2.2.3, and since the main objective of the studied process is to remove water from the MIBK-water mixture, employing a decanter to separate the aqueous phase and reflux the MIBK-rich phase is investigated in detail. Based on a previous study [29], the decanter holdup time is neglected in this mode, and a perfect phase separation is assumed for the simulation model. Accordingly, the entire MIBK-rich phase is immediately returned to the column, and the water is completely discharged to the collector tanks. Figure 3-6 presents a comparison of all state indicators for a unit equipped with a perfect decanter and the conventional distillation unit with no decanter.

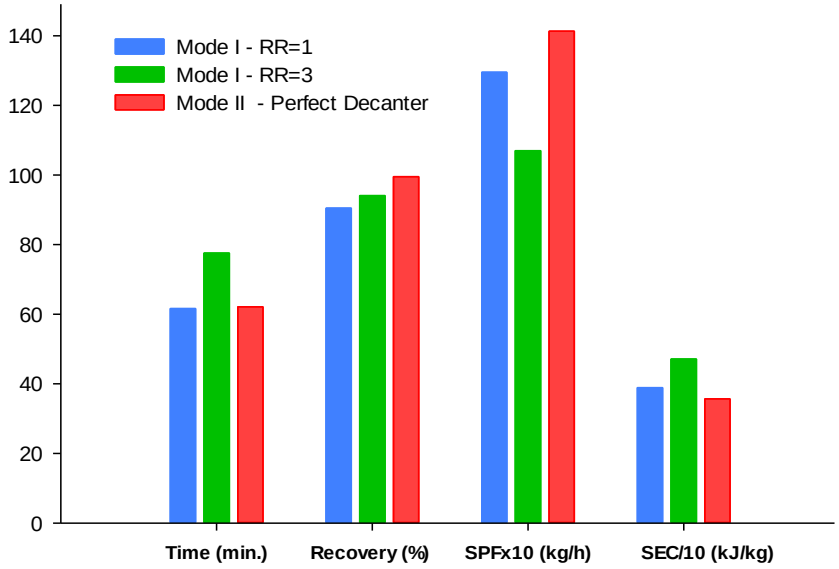

Figure 3-6. Comparison of state indicators in Mode II with a perfect decanter and Mode I at RR=1 and RR=3

The Mode I - RR=1 case, as the optimum point in Persp. II, and the Mode I - RR = 3 case, as the optimum point in Persp. I, are compared to the unit equipped with a perfect decanter. According to this figure and based on Persp. I, using a perfect decanter enhances the recovery and decreases the process time. Also, applying Persp. II for unit evaluation, Mode II with a perfect decanter offers a lower SEC and a higher SPF compared to Mode I. This can be explained by locating the reflux and distillate composition in the phase equilibrium diagram (Figure 3-1). By applying a perfect decanter, the reflux stream is a saturated MIBK-rich liquid with low content of water that keeps the MIBK within the unit, and on the other hand, the top product (distillate) is a diluted aqueous phase that takes out a small amount of MIBK outside the unit.

The perfect decanter is theoretically an ideal case. In practice, there are some deviations from this ideal case, such as delay in reflux, insufficient decanter size to provide effective separation, slow dynamics of the control system, etc. These facts probably cause a deficient phase separation. Accordingly, and as explained in sections 3.2.2.4 and 3.2.2.5, operation under partial return fraction of aqueous and organic phases are investigated.

3.3.4. Data processing

It was probably not a surprising conclusion that employing a perfect decanter to remove the aqueous phase improves the unit performance in all aspects and offers the lowest SEC and highest SPF values. Accordingly, a unit equipped with a perfect decanter, identified as an ideal case of operation, is a suitable benchmark to measure different aspects of other situations and operation scenarios. The partial return/reflux of the aqueous phase and the MIBK-rich phase are supposed to resemble the possible circumstances in which the unit deviates from the theoretically ideal case (Mode II with a perfect decanter). These cases are compared to the ideal case to identify their potential for separation on a reasonable scale. In this order, the state indexes, including the time index (t_i), recovery index (η_i), Production rate index (P_i), and energy index (E_i) are defined as below:

$$t_i = \left[\frac{t_d}{t}\right] \tag{6}$$

$$\eta_i = \left[\frac{\eta}{\eta_d}\right] \tag{7}$$

$$P_i = \left[\frac{SPF}{SPF_d}\right] \tag{8}$$

$$E_i = \left[\frac{SEC_d}{SEC}\right] \tag{9}$$

The subscript "d" represents the case with a perfect decanter that offers perfect aqueous phase removal and total MIBK-rich phase reflux. Normally, the magnitude of these indexes is between 0 and 1, unless the separation is more effective in all or one of these aspects compared to the perfect decanter case. The closer the index is to 1, the closer that aspect of the process is to the perfect decanter case. The state indexes show how far an operation is from the ideal case. The use of these variables facilitates the feasibility evaluation and helps in the trade-off or compromising procedure for unit design and operating planning. For instance, these indexes enable the user to know how accurately the decanter must operate to provide an efficient distillation. In addition, due to the relationship between SEC and SPF (SEC × SPF = W = Constant), the energy index and production rate index are identical, so using one index presents the quality for both factors. Moreover, in cases with the same recovery, the time index will also be equal to the energy and production rate indexes.

3.3.5. Batch distillation with decanter (deficient aqueous phase removal) – Mode II

In order to provide a realistic evaluation, deficient decanting is studied by varying the aqueous phase return fraction. Figure 3-7a indicates the process duration and fractional recovery for various aqueous return fractions from 0 to 0.95. Figure 3-7b presents the SEC and SPF values at different aqueous phase return fractions.

As explained in section 3.3.4 for better illustration of the results, all state indicators are combined in Figure 3-7c on a common scale. The noticeable point in this graph is that the plots of time, production rate, and energy indexes have the same trend with changing aqueous phase return fractions. The energy and production rate indexes are expected to have the same value, but the time index matches those two due to the constant recovery in this part of the study.

Another important point of this figure is that returning less than 50 % of the water does not change the recovery significantly, which means that even if the decanter is not capable of perfect water removal and only removes 50 % of the aqueous phase, it is still offering a high level of performance, which is very close to the case with perfect decanting. On the other hand, process time, energy, and production rate change slightly by increasing the aqueous phase return fraction from 0 to about 0.5, but further increases in the aqueous phase return fraction accelerate the changes. Accordingly, if $RF_2 \leq 0.5$ the energy, production rate, and time indexes are still over 0.95, which means a 50 % deficiency in water removal leads to only a 5% decrease in the state indexes.

According to these observations, there is no need for a sophisticated control system or a large decanting drum to provide perfect aqueous-phase decanting, but a minimum of 50 % aqueous-phase return fraction is necessary for an efficient operation. Regarding the operation scenarios/perspectives, the following can be generally stated:

- Based on Persp. I, using a decanter with partial water removal and total MIBK-return fraction will ensure a high MIBK recovery, but the process time needs to be considered carefully to avoid long process duration and, consequently, high energy costs. A minimum of 50 % water removal in the decanter ensures a time index of over 0.95.
- Based on Persp. II, the less water returned, the better the operation in terms of time, energy cost, and production rate. A minimum of 50 % water removal

in the decanter is necessary to ensure production rates and energy indexes of over 0.95.

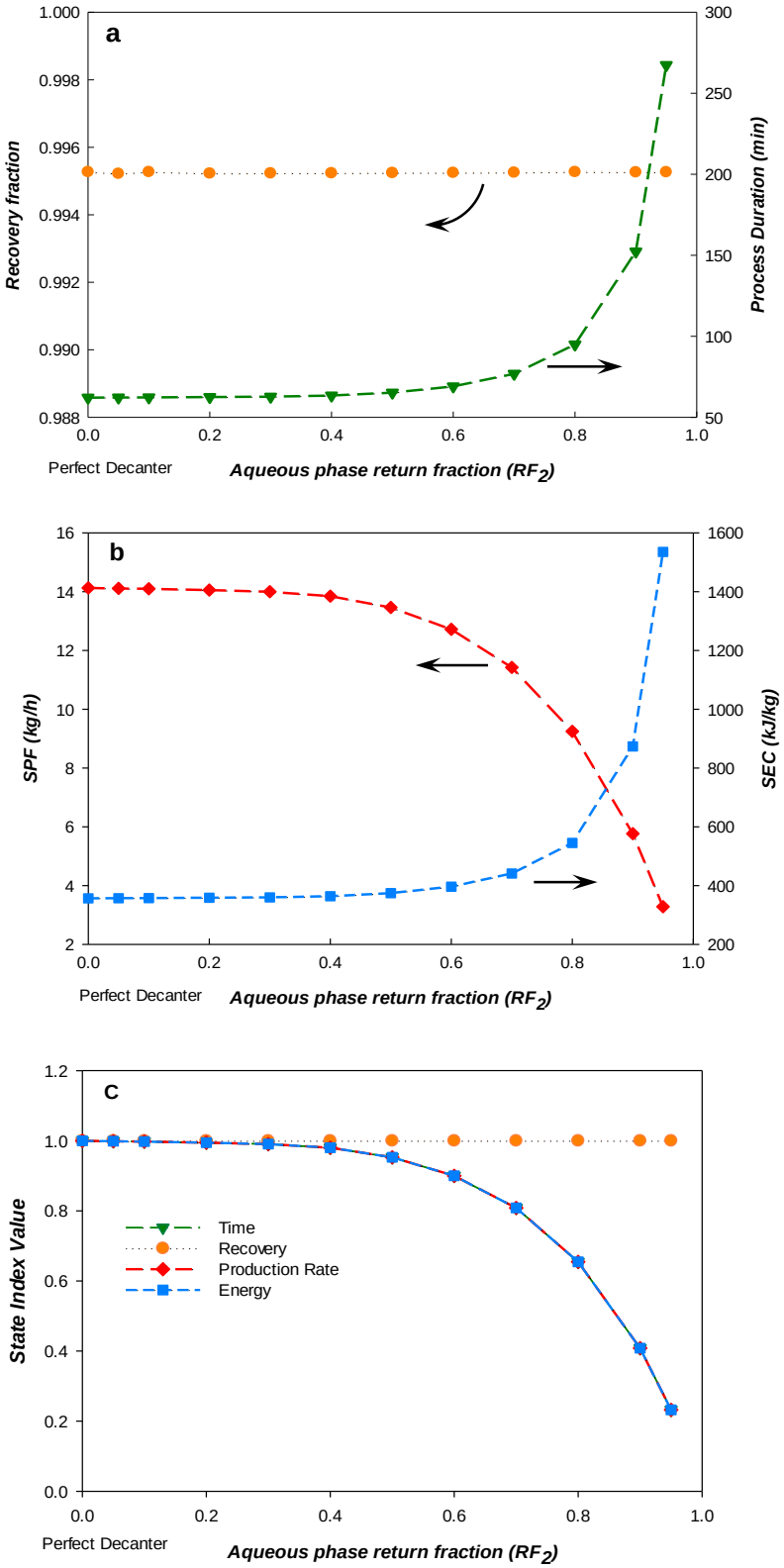

Figure 3-7. Effects of aqueous phase return fraction on (a) recovery and process time (b) SEC and SPF (c) state indexes

3.3.6. Batch distillation with decanter (deficient MIBK-rich phase reflux) – Modes II & III

To assess the distillation performance in case of missing some MIBK content along with the top product, some simulations are conducted with partial reflux of MIBK-rich phase. According to section 3.3.5, the unit is not sensitive to aqueous phase removal at a moderate level. Hence, simulations for this part of the study are conducted assuming perfect aqueous phase removal. Figure 3-8 presents the state indexes for different MIBK-rich phase return fractions (RF_1) in range of 0 to 1. The time index is over 1 for the entire range of study, which implies a shorter time of operation compared to the perfect decanting case. This can be attributed to the lower quantity of mixtures to be purified when a larger amount of that is discharged as the top product. On this basis, it can be clearly perceived that a shorter time is not necessarily associated with better operation. Process time also increases linearly by increasing the MIBK-rich phase return fraction. On the other hand, the energy, production rate, and recovery indexes improved by increasing the MIBK-rich phase return fraction. It can be stated that, despite the high tolerance of operation toward aqueous phase removal accuracy, it is sensitive to MIBK-rich phase preservation/removal in the unit. According to both Persp. I and Persp. II, the MIBK-rich phase shall be retained in the unit, and because of the linear dependency of all indexes upon RF_1, the more MIBK returns to the column, the better the operation performs.

There are two extreme cases at two ends of the graph; one is the perfect decanter with the total reflux of the MIBK-rich phase ($\mathrm{RF}_1 = 1$ and $\mathrm{RF}_2 = 0$) and the other one is where the MIBK-rich phase is totally discharged along with the top product ($\mathrm{RF}_1 = 0$ and $\mathrm{RF}_2 = 0$) so that the reflux stream is cut. The latter is identified as "Mode III" in the present study which can be considered as an evaporation unit or a distillation unit without reflux. Achieving the desired purity at this condition reveals that Mode III is a practical approach to recover MIBK at the shortest possible time with no need for condenser, decanter, or even the column packing section. This option can be considered by one who is seeking a simple approach with a low capital cost and refuses to deal with any complications in start-up or operation control.

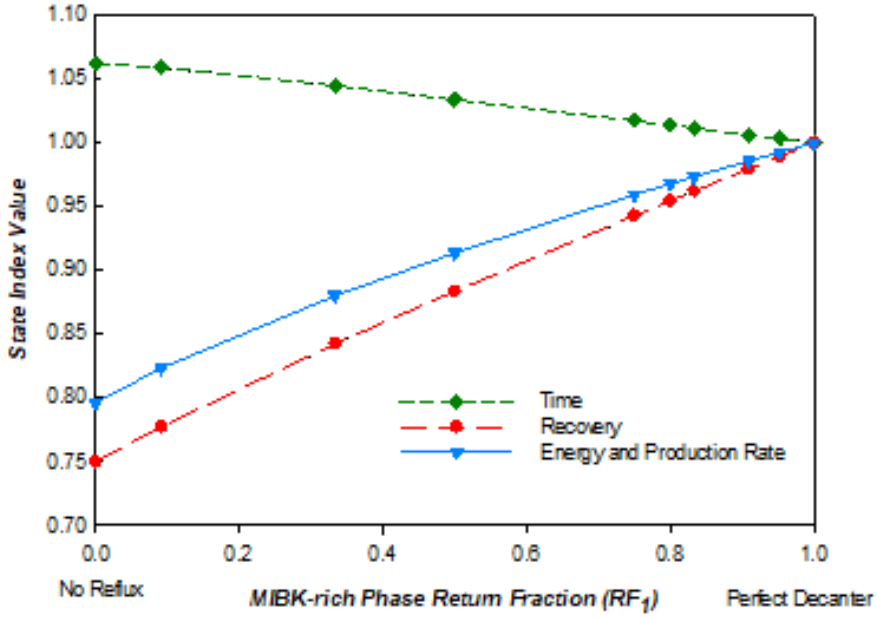

Figure 3-8. Effects of MIBK-rich phase return fraction on state indexes.

3.3.7. Effect of condenser temperature (Modes I-II)

To evaluate the effect of condenser temperature on distillation performance, the case RR=4 in Mode I is simulated with different condenser temperatures from 25 to 85°C. The results for all evaluation terms are presented in Figure 3-9a. As this figure indicates, decreasing the condenser temperature adversely affects the operation in terms of time, production rate, and energy, but very slightly enhances the recovery, so that the recovery index increases from 0.9470 to 0.9482 by decreasing the condenser temperature from 85 to 25°C. The longer operation time at low condenser temperatures can be attributed to the low-temperature refluxed liquid that needs to be heated up by reboiler. This slight recovery improvement at lower condenser temperature can be attributed to the larger liquid load across the tower as well as the smaller amount of MIBK leaving the column along with the pad gas at the beginning. Applying Persp. I in Mode I, a low condenser temperature can improve the recovery very slightly, but one must be careful with its energy and time cost and probably there is no justification to apply a lower temperature in condenser but if it is to recover the energy. Based on Persp. II, a low condenser temperature is not recommended since it increases the energy cost and decreases the production rate.

Since temperature affects the amount of water repelled from a liquid mixture of MIBK-water, it is also expected to affect the performance of a distillation unit equipped with a decanter. The simulation of Mode II with a perfect decanter (RF_1 =

1 *and* $RF_2 = 0$) is repeated at various condenser temperatures. The outcomes are presented in Figure 3-9b. This figure reveals that a lower condenser temperature leads to a slight enhancement in all aspects of unit performance. This is due to repelling more water in decanter based on phase equilibrium diagram (Figure 3-1) which leads to higher purity of MIBK in reflux stream and larger amount of water discharge at a specific operation time. The positive impacts of low condenser temperature are so slight that applying any change in condenser temperature in a functioning unit is not justifiable unless it is for troubleshooting in a defective unit. The remarkable point to be noted is that the condenser temperature causes different impacts on a unit equipped with a decanter (Mode II) and a conventional unit (Mode I).

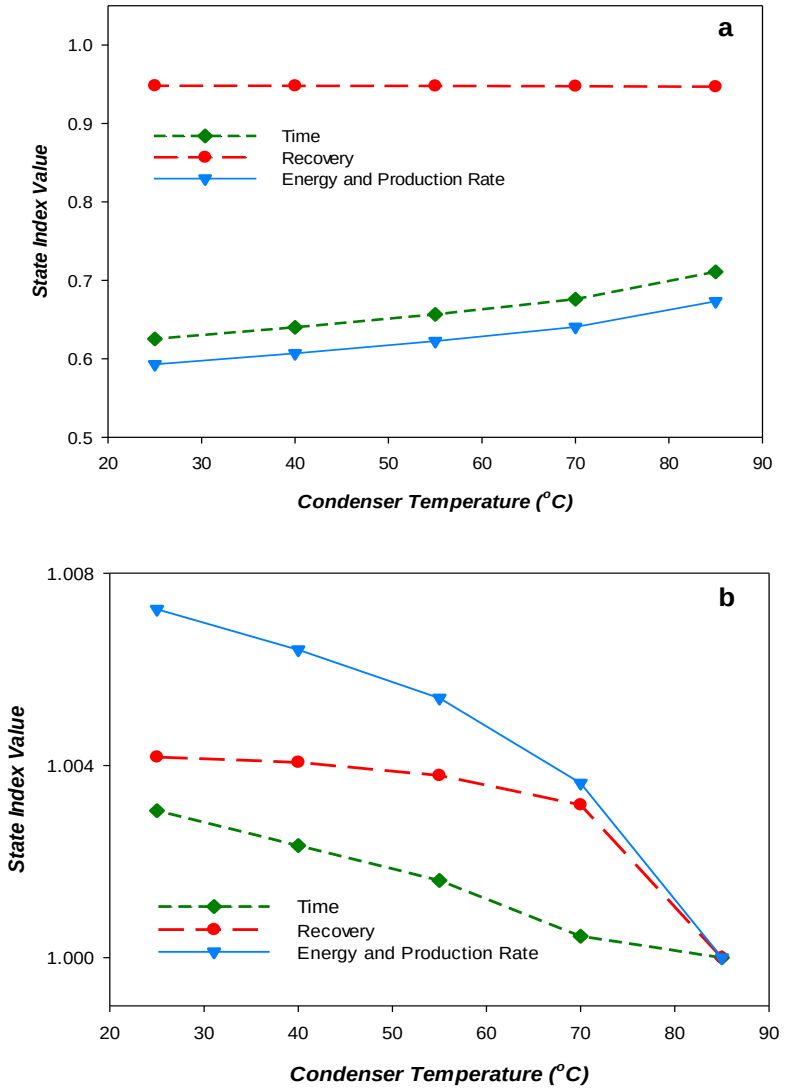

Figure 3-9. Effect of Condenser Temperature on distillation process in (a) Mode I at RR=4 (b) Mode II with a perfect decanter

3.3.8. Effects of number of theoretical stages

Figure 3-10a presents the state indexes for different numbers of theoretical stages in the column of Mode II with a perfect decanter. As this figure shows, the time index increases with increasing the number of stages which implies on decreasing the process time. This change is sharp between 1 to 2 stages, but it is less intense by increasing the number of stages over 2. The recovery is slightly decreased by increasing the number of stages, and generally, its variation is slight. The production rate and energy index increase with increasing the number of stages from 1 to 2, but applying more stages results in a less efficient operation in terms of SEC and SPF. Since the change in recovery is very slight, the variation trend for SEC & SPF indexes follows the trend of process time variation.

The simulation with no theoretical stage did not converge in 24 hours because the process specification was not achieved and the MIBK purity stopped at 99.55% with no further change. This reveals that even using an efficient decanter, in case of an inefficient column, the distillation would possibly fail.

Based on Persp.I, it can be stated that there is a minimum column part quality/quantity below which fulfilling the process objectives is not possible (at least in a reasonable time), and there is also a point over which increasing the column size/contact quality does not improve the recovery significantly, however the operation time/energy cost would still improve.

Based on Persp. II, there is an optimum point for column part quality/quantity to meet the process objectives beyond which employing a more efficient mass transfer media or extending the number of beds needs to be justified carefully in technical and commercial terms since the improvement in energy cost and production rate is not significant.

Assuming an inefficient mass transfer media (packing or tray) in column, there should be some instructions to improve the operation and meet the unit specifications. In this order, two troubleshooting approaches are studied. From previous parts of the study, it was concluded that the unit can provide the desired purity with no need for a reflux stream, condenser, or column (mode III). Also, a lower condenser temperature can offer a slight improvement in recovery, which seems adequate to cover the encountered deficiency. Accordingly, simulation with no column (no theoretical stage) is repeated with a condenser temperature of 25 °C in one case and no reflux condition (Mode III) in another case. Both approaches helped the operation to meet the desired purity and the results for both approaches

are presented in Figure 3-10b. Accordingly, shutting off the reflux or decreasing the condenser temperature can be considered as two practical troubleshooting approaches for an existing unit with an inefficient column. This figure also includes the state variables for the case with perfect decanter, two theoretical stages and condenser temperature of 85 °C in Mode II. Figure 3-10b compares the state variables for a unit with an efficient packing section (Mode II, Ne=2, Tc=85 °C) to a unit with an inefficient packing section, upgraded by a low-temperature condenser (Mode II , Ne=0, Tc=25 °C) or cutting the reflux stream (Mode III, Ne=0). This comparison shows the importance of the packing section and the suitability of the two proposed solutions for the deficient packing section can be measured. According to this figure, even if there is no efficient packing section, an equal (or even higher) recovery can be achieved by decreasing the condenser temperature but in a longer process time. The SPF and SEC also show undesirable conditions for the case with no theoretical stage and low condenser temperature compared to the case with two theoretical stages. On the other hand, shutting off the reflux (Mode III) to upgrade the case with no theoretical stage section offers the shortest possible process time and a reasonable SEC and SPF level but provides a low fractional recovery.

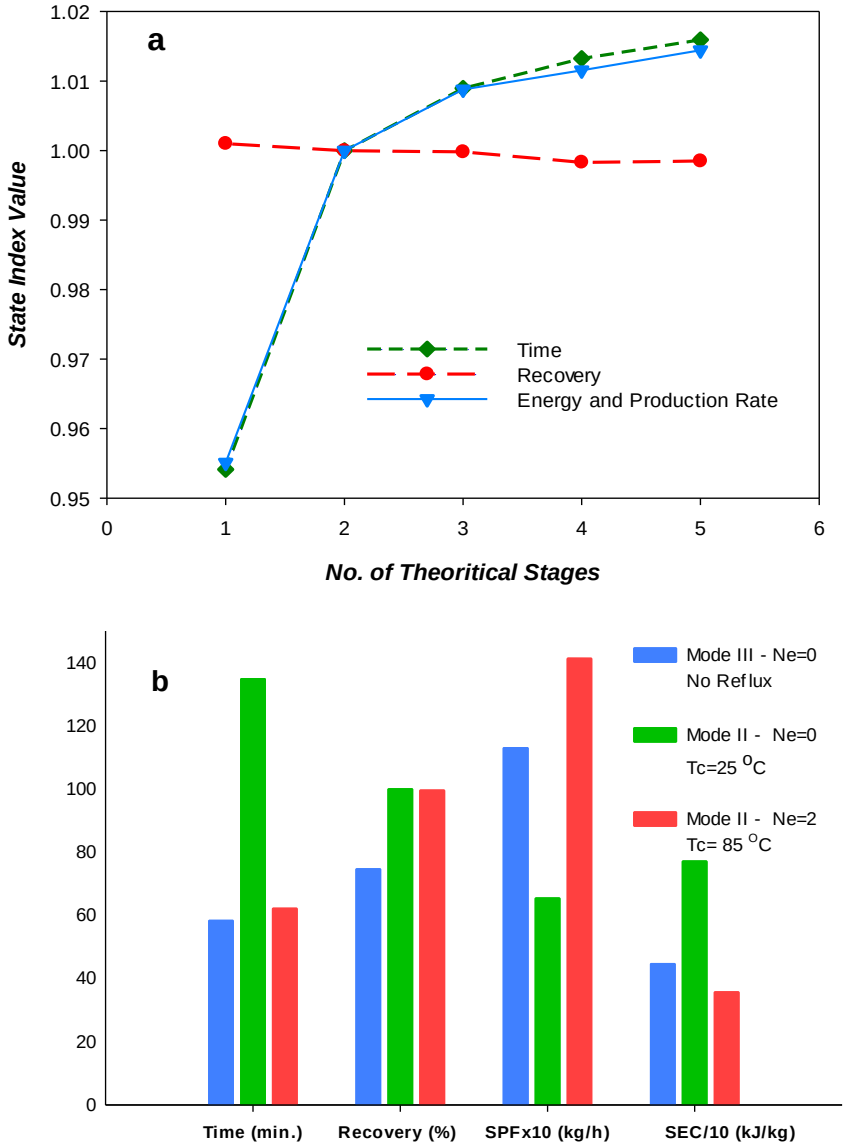

Figure 3-10. performance of a unit at (a) different no. of theoretical stages(b) alternatives for a non-effective column

3.3.9. Comparison of results in the three Modes

Since the main part of this study concerns different operation scenarios with and without decanter, setting a comparison is necessary to clearly show the effective range of each scenario and to provide comprehendible guidelines for operators based on Persp. I and II.

Figure 3-11a presents the recovery index for Modes I and II at different return fraction values, as well as for Mode III. According to this figure and as expected, Mode III offers the minimum recovery value, since the evaporated MIBK is not refluxed to the column. The recovery index for Mode II when no MIBK-rich phase

is leaving the unit (partial aqueous phase reflux) is almost constant around one. On the other hand, with no decanter or with partial MIBK-rich phase reflux, increasing the return fraction improves the recovery index.

For Mode II with over 25 % MIBK-rich phase slip ($RF_1 \leq 0.75$), recovery is lower than that of Mode I with the same return fraction (which corresponds to RR=3 in section 3.3.1). In other words, applying Mode II offers an enhanced recovery level only if the return fraction of the MIBK-rich phase is over 0.75. Another interesting point about $RF_1 = 0.75$ is that increasing the return fraction beyond this point results in no further enhancement for Mode I while employing a decanter with $RF_1 \geq 0.75$ recovery level will exceed this limit. This feature is noticeable when evaluating a single-batch process (Persp. I). It is worth noting that RF = 0.75 corresponds to RR = 3, which was the optimum point for Mode I based on Presp. I, as discussed in section 3.3.1.

Based on these observations, the following can be stated as conclusions:

- To see a noticeable positive impact of a decanter on recovery performance, aqueous phase reflux can be at any level ($RF_2 < 1$) but the MIBK-rich phase shall be refluxed by $RF_1 \geq 0.75$. This range is specified as "Decanter Effective Range" in Figure 3-11a.
- The recovery index for Mode III is about 0.75, indicating that the amount of product for one-time operation is 25 % less than that of Mode II with a perfect decanter. In other words, four times operation in Mode III provides the same quantity of product as if conducting three times operation in Mode II with a perfect decanter. Also, the recovery index for Mode III is about 16 % less than Mode I at RR = 1, and about 20 % less than Mode I maximum achievable recovery ($RR \geq 3$).
- Adding a perfect decanter to the unit offers over 9 % improvement in recovery compared to Mode I at RR = 1 and over 5 % compared to the maximum achievable recovery in Mode I ($RR \geq 3$).

Figure 3-11b presents the time index for Modes I, II, and III. It can be generally observed that the operation time for Mode II with partial MIBK-rich phase discharge (and perfect water removal) is less than the cases with perfect MIBK recovery. It can be stated that the process time is shorter when more MIBK discharges along with the top product. Accordingly, however, Mode III is not a good option to recover a large fraction of MIBK, but it is the shortest way to achieve the product with the desired purity. This is a clear reason why process duration is not a suitable indicator of process quality.

Operation time for a conventional unit (Mode I) working in a low return fraction tends to the case with partial MIBK-rich phase reflux, and it is close to the case with partial aqueous phase reflux at higher return fractions. Overall, the time for conventional unit operation (Mode I) is limited by two bounds of Mode II with partial water and MIBK reflux.

Another main point in this graph is that a longer residence time of both water and MIBK (by means of a larger reflux ratio) leads to a longer process duration. The effect of the MIBK-rich phase return fraction is moderate and in a linear trend, whereas the effect of water residence/return fraction is negligible in the range ($RF_2 \leq 0.5$) but its impact grows exponentially with a further increase in aqueous phase return fraction.

The points on two sides of the graph connected by a dotted line (perfect decanter line) in Figure 3-11b represent the same case (Mode II, perfect decanter) and correspond to the time index of 1.

Based on the observations, the following can be stated as conclusions:

- To obtain a noticeable positive effect of a decanter on process time, the aqueous phase shall be removed completely, and the MIBK-rich phase needs to be refluxed by $RF_1 \geq 0.5$. This range is specified as "Decanter Effective Range" in Figure 3-11b. Also, in case of perfect MIBK-rich phase reflux, returning the aqueous phase by $RF_2 \leq 0.4$ would not significantly deteriorate the operation in terms of process time. This range is specified as "Acceptable Decanting Range".
- According to this figure, employing Mode III for processing the same amount of feed, offers around 6 % shorter time in comparison with a perfect decanter (Mode II optimum point) and the case with RR=1 in Mode I. Also, it offers about 10 % shorter time compared to the case with RR=3 in Mode I.
- Refluxing any amount of MIBK or water in either of configurations, Mode I or Mode II, results in a longer operation time for processing a particular quantity of feed.
- Adding a decanter to the unit with MIBK-rich phase total reflux and a relatively high removal fraction of aqueous phase offers the same process time with Mode I at RR=1 and about 4 % shorter time than the RR=3.

Figure 3-11c presents the energy and production rate indexes for the three studied configurations. As this figure shows, three plots intersect approximately at RF=0.55. The plots of Mode II align with that of Mode I before and after the

intersection point. It can be generally stated that in the ranges where the results of Mode II correspond to those of Mode I, employing a decanter (Mode II) offers no significant advantage over a conventional distillation unit (Mode I). Accordingly, in Figure 3-11c, operation above the intersection (vertical axis) is recommended, which corresponds to a MIBK-rich phase return fraction over 0.55 and an aqueous phase return fraction below 0.55. Moreover, the aqueous phase return fraction in the range $RF_2 \leq 0.4$ seems to be an ineffective factor on energy and production rate indexes, so that an imperfect water removal by decanter can be tolerated with no significant adverse effect on energy and production efficiency of the distillation unit.

An important point of this figure is that conducting the separation via Mode III is still more efficient than some cases in Mode I or Mode II. In case of refluxing over 70 % of the condensed stream in Mode I or refluxing over 70 % of the aqueous phase in Mode II, employing a distillation unit has no technical or economic feasibility, even if the MIBK-rich phase is perfectly returned to the column. The horizontal dashed line crossing the point of Mode III indicates the maximum reasonable energy cost and minimum acceptable production rate of a distillation unit with a reflux stream for MIBK-water separation.

Two points connected by a dotted line (the perfect decanter line) in Figure 3-11c represent the same operation case (total aqueous phase removal and total MIBK-rich phase reflux), corresponding to the energy and production index of 1.

Based on the observations, the following can be stated as conclusions:

- The production rate and energy index of Mode III are 0.8, which means that compared to the perfect decanter case (Mode II optimum point), it takes 20 % more energy and time to provide the same product quantity.
- The energy and production rate index of Mode III is about 12 % lower than the maximum achievable value in Mode I (RR = 1). This means it takes about 12 % more energy/longer time to provide the same amount of product.
- Adding a decanter to the unit with total MIBK-rich phase reflux and a relatively high removal of the aqueous phase improves the energy and production rate index by about 11 % compared to the case RR = 3 in Mode I and over 8 % compared to the case RR = 1 as the maximum achievable value in Mode I.

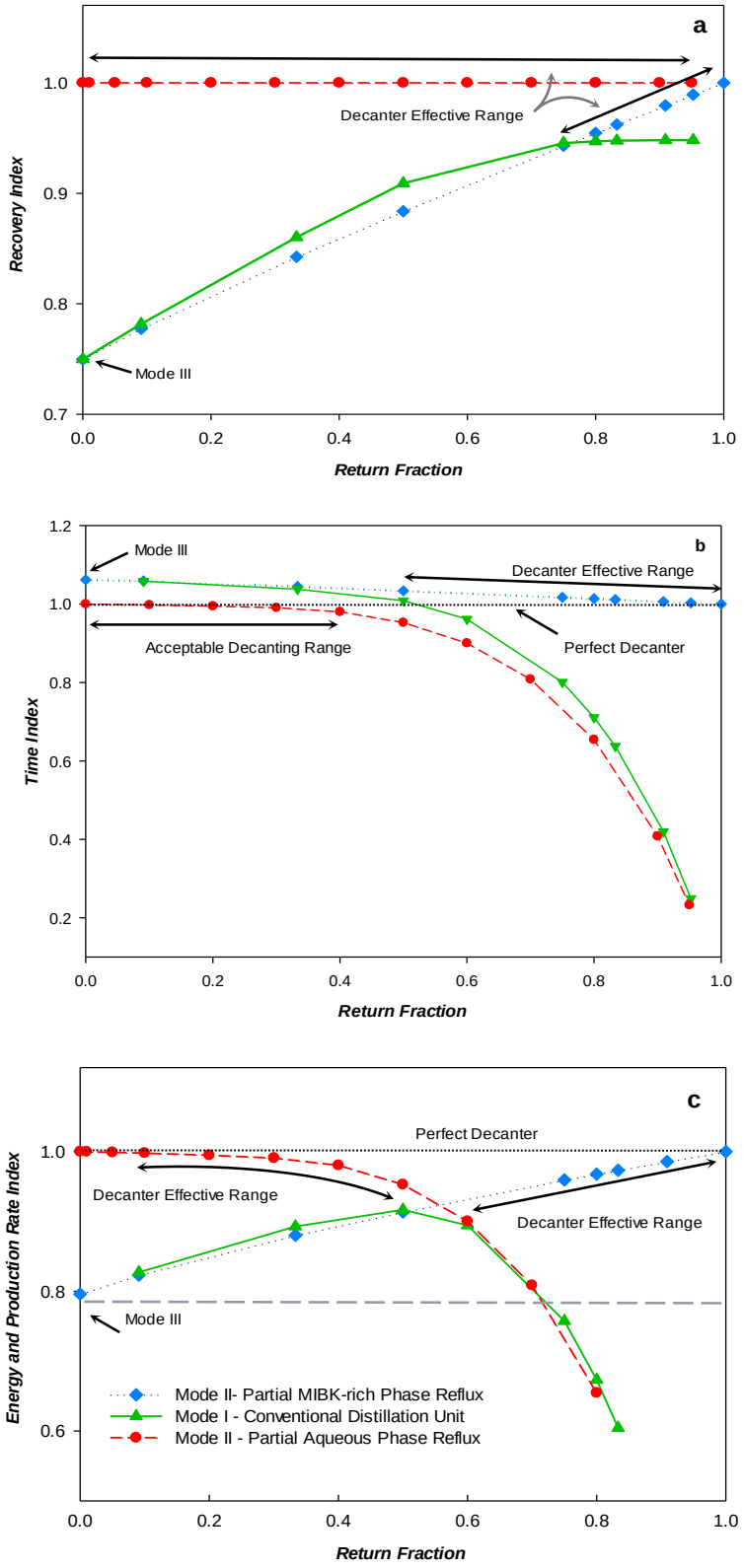

Figure 3-11. Comparison of Modes I, II and III in terms of (a) Recovery, (b) process time, and (c) production rate and energy consumption

To present the results in a practical form based on Persp. I. (single batch operation), the process features are outlined below:

1- In terms of MIBK recovery, Mode III provides the minimum recovery value, and refluxing the MIBK-rich phase offers an improvement in recovery. Since recovery is a term defined by MIBK content, returning any amount of water due to an imperfect decanter makes no change in recovery. On the other hand, Mode II is advantageous only at high MIBK-rich phase return fractions (over 75%), and below this limit, a conventional distillation unit (Mode I) is preferred. Accordingly, to obtain a high recovery value, the decanter control system shall be focused on returning the MIBK-rich phase in the unit rather than perfect removal of the aqueous phase.
2- In terms of process time duration, Mode III has the shortest process duration, and refluxing any amount of MIBK or water extends the process time. A decanter is only advantageous at high MIBK-rich phase return fractions (over 50 %). Also, a limited aqueous phase return fraction (below 40 %) can be tolerated with no significant adverse effect on process duration. Refluxing over 50 % of the aqueous phase shall be strictly avoided while using a decanter, otherwise, a conventional distillation unit (Mode I) is preferred since it offers a shorter process time.

To present the results in a practical form based on Persp. II, the graphs of energy and production rate indexes for three configurations (Modes I, II, and III) are integrated into one, shown in Figure 3-12. The point corresponding to Mode III can be seen on the left side of the graph with an energy index of 0.8. Once the MIBK-rich phase reflux is established and increases gradually, the state index increases up to 1 for the perfect decanter case. Beyond this point, by refluxing any part of the aqueous to the column, the energy and production rate will be adversely affected. The aqueous phase return fraction below 40 % does not significantly affect the operation quality, but over this value, the state indexes decrease sharply, so by returning over 70 % of the aqueous phase, there is no advantage in applying a reflux stream due to the higher energy (operating) cost, lower production rate, and obviously the larger capital costs. As explained before, a trade-off procedure is required for designing an efficient unit, in which the capital and operating costs are considered besides safety, ease of operation, and maintenance issues.

The horizontal line at the state index of 0.913 specifies the maximum achievable energy and production rate index for operation in Mode I. Regarding Persp. II for unit evaluation, operation in Mode II is efficient only when the operation index is

above this line. The associated operating range is specified as "Mode II Effective Range".

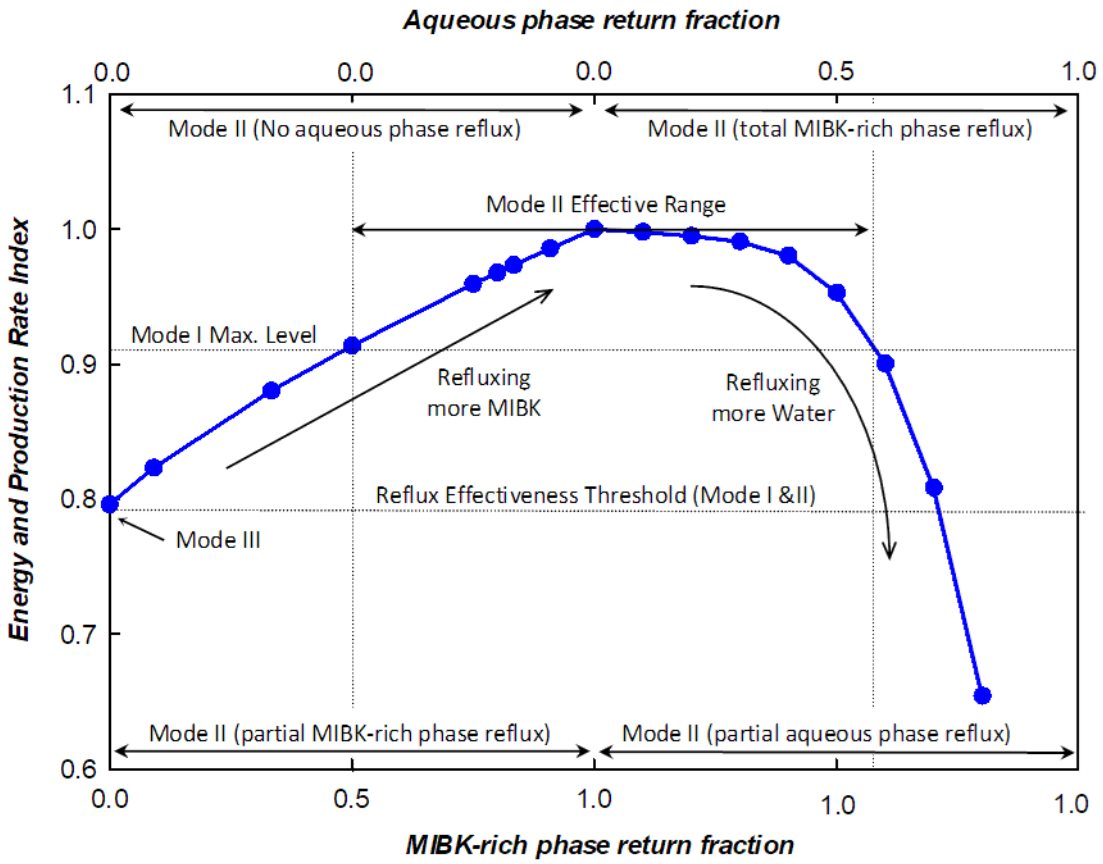

Figure 3-12. Integrated energy and production rate indexes for three configurations (Modes I, II, and III).

Since energy and production rate indexes are sufficient terms to evaluate a distillation unit based on Persp. II, the interpretations in Figures 3-11c and 3-12 can be directly applied to controlling the operation under the *sequential batches* scenario.

3.4. Conclusion:

Three general batch separation unit configurations titled Mode I, Mode II, and Mode III are compared in terms of recovery level, operation time, production rate, and energy cost. These configurations represent, respectively, a conventional distillation unit, a batch distillation unit with a decanter, and a simple distillation unit (refluxless).

The simulations of MIBK-water separation using a conventional batch distillation approach (Mode I), resulted in the following conclusions:

- According to Persp. I, the case with RR = 3 in a conventional batch distillation is the optimum point due to the maximum achievable recovery in the shortest possible time, while based on Persp. II, the case with RR = 1 is recognized as the optimum point due to the maximum SPF and minimum SEC in the studied range.
- A single-step operation, skipping the start-up step in "total-reflux" mode, generally results in a shorter operation time and a smaller SEC. Despite the lower recovery achieved by skipping the start-up step for low reflux cases, it still offers a higher production rate due to the shorter time. Both scenarios yield in the same recovery value in a high reflux ratio.

Applying a perfect decanter (the most efficient case in Mode II) results in the maximum recovery level ($\eta \approx 0.995$) and this case is used as a benchmark to measure the performance of other studied cases. Mode II with a perfect decanter offers:

- Over 9 % recovery improvement compared to the case $RR = 1$ and over 5 % compared to the maximum achievable recovery ($RR \geq 3$) in Mode I.
- A slightly longer time compared to Mode I at RR = 1 (below 0.1% and about 4% less time compared to the case $RR = 3$).
- About 11 % improvement of energy and production rate index compared to Mode I at $RR = 3$ and over 8 % improvement compared to the maximum achievable value in Mode I ($RR = 1$)

Mode III offers the minimum operation time while yields the minimum recovery. In details, Mode III offers:

- About 25 % less recovery compared to Mode II with a perfect decanter case. It also provides about 16 % less recovery compared to Mode I at $RR = 1$ and about 20% less than Mode I maximum achievable recovery ($RR \geq 3$).
- About 6% shorter time compared to Mode II with a perfect decanter case. It also offers about 6% shorter time compared to Mode I at $RR = 1$ and about 10% shorter time than Mode I with $RR = 3$.

Mode II with a deficient decanter performance, can tolerate refluxing below 40 % of the aqueous phase since it does not affect the operation time or recovery. Any further increase in aqueous return fraction adversely affects the operation time, energy cost, and production rate. On the other hand, slipping any amount of MIBK-

rich phase into the top outlet stream linearly affects the recovery level, time, energy cost, and production rate. It can be stated that the decanter control/design must be more concerned about refluxing the MIBK-rich phase, even if that costs in a partial aqueous phase reflux to the column. Not considering the capital costs of employing a piece of additional equipment in the unit, the followings are concluded for Mode II:

- According to Persp. I, Mode II is recommended in the range of $RF_1 \geq 0.75$ and $RF_2 \leq 0.4$ to provide a higher recovery in a reasonable time compared to Mode I. On the other hand, Mode III is not recommended according to Persp. I due to the lowest recovery value, but it can be justified by one who demands a shorter operation time regardless of the fractional recovery.
- According to Persp. II, Mode II is recommended in the range $RF_1 \geq 0.5$ and $RF_2 \leq 0.55$ to provide a higher production rate and lower energy cost compared to Mode I. Mode III is also preferred over Mode I, working with $RF \geq 0.7$.

The impact of condenser temperature on Mode I and Mode II is very slight but is not in the same trend; decreasing the condenser temperature in Mode I adversely affects the SEC, SPF, and time besides a slight enhancement in recovery. On the other hand, it slightly improves all state variables in Mode II.

The number of stages (or effectiveness of the contact media) in the column is a significant factor below a particular value (below 2 theoretical stages) while there would be less benefit in applying further a bigger (or more efficient) column. In case of employing no equilibrium stage within the column, the desired purification is not achievable but by decreasing the condenser temperature or cutting off the reflux stream (Mode III).

3.5. References

[1] I. López, J. Andreu, S. Ceballos, I. Martínez De Alegría, I. Kortabarria, Review of wave energy technologies and the necessary power-equipment, Renewable and Sustainable Energy Reviews 27 (2013) 413–434. https://doi.org/10.1016/j.rser.2013.07.009.

[2] A.A. Kiss, Rethinking energy use for a sustainable chemical industry, Chem Eng Trans 76 (2019) 13–18. https://doi.org/10.3303/CET1976003.

[3] E. Sorensen, Chapter 5 - Design and Operation of Batch Distillation, in: A. Górak, E. Sorensen (Eds.), Distillation, Academic Press, Boston, 2014: pp. 187–224. https://doi.org/https://doi.org/10.1016/B978-0-12-386547-2.00005-3.

[4] M. Zhu, Y. Hou, N. Yu, M. Chen, Z. Ma, L. Sun, Design and control of a middle-vessel batch distillation for separating DMC–EMC–DEC mixture, Chin J Chem Eng 26 (2018) 1837–1844. https://doi.org/https://doi.org/10.1016/j.cjche.2017.11.014.

[5] S.S. Parhi, G.P. Rangaiah, A.K. Jana, A novel vapor recompressed batch extractive distillation: Design and retrofitting, Sep Purif Technol 260 (2021). https://doi.org/10.1016/j.seppur.2020.118225.

[6] H. Zhang, S. Wang, J. Tang, N. Li, Y. Li, P. Cui, Y. Wang, S. Zheng, Z. Zhu, Y. Ma, Multi-objective optimization and control strategy for extractive distillation with dividing-wall column/pervaporation for separation of ternary azeotropes based on mechanism analysis, Energy 229 (2021). https://doi.org/10.1016/j.energy.2021.120774.

[7] F. Zhao, Z. Xu, J. Zhao, J. Wang, M. Hu, X. Li, Z. Zhu, P. Cui, Y. Wang, Y. Ma, Process design and multi-objective optimization for separation of ternary mixtures with double azeotropes via integrated quasi-continuous pressure-swing batch distillation, Sep Purif Technol 276 (2021). https://doi.org/10.1016/j.seppur.2021.119288.

[8] G. Miao, K. Zhuo, G. Li, J. Xiao, An advanced optimization strategy for enhancing the performance of a hybrid pressure-swing distillation process in effective binary-azeotrope separation, Sep Purif Technol 282 (2022). https://doi.org/10.1016/j.seppur.2021.120130.

[9] L. Hegely, P. Lang, Optimisation of the higher pressure of pressure-swing distillation of a maximum azeotropic mixture, Energy 271 (2023). https://doi.org/10.1016/j.energy.2023.126939.

[10] Z. Zhang, Y. Wang, M. Zhang, C. Guang, M. Li, J. Gao, Energy-saving investigation of pressure-swing distillation strengthening configurations for benzene/isobutanol binary azeotrope, Sep Purif Technol 296 (2022). https://doi.org/10.1016/j.seppur.2022.121381.

[11] M. Ferchichi, L. Hegely, P. Lang, Economic and environmental evaluation of heat pump-assisted pressure-swing distillation of maximum-boiling azeotropic

mixture water-ethylenediamine, Energy 239 (2022). https://doi.org/10.1016/j.energy.2021.122608.

[12] A. Yu, Q. Ye, J. Li, Y. Wang, Q. Rui, Energy-saving improvement of heat integration and heat pump for separating multi-azeotropes mixture via novel pressure swing distillation, Chem Eng Sci 282 (2023). https://doi.org/10.1016/j.ces.2023.119239.

[13] D.Y. Aqar, I.M. Mujtaba, Economic feasibility of an integrated semi-batch reactive distillation operation for the production of methyl decanoate, Sep Purif Technol 257 (2021). https://doi.org/10.1016/j.seppur.2020.117871.

[14] D.Y. Aqar, A.S. Abbas, R. Patel, I.M. Mujtaba, Optimisation of semi-batch reactive distillation column for the synthesis of methyl palmitate, Sep Purif Technol 270 (2021). https://doi.org/10.1016/j.seppur.2021.118776.

[15] K. Jayant, C. Gupta, S. Seethamraju, S.M. Mahajani, Entrainer assisted production of high purity 2-phenyl ethyl acetate by reactive distillation, Sep Purif Technol 331 (2024). https://doi.org/10.1016/j.seppur.2023.125650.

[16] C. Zhang, Y. Liu, Z. Gao, L. Huang, J. Xiong, Process design, simulation and experimental studies of heteroazeotropic batch distillation for phenol dehydration, Chemical Engineering Research and Design 195 (2023) 682–690. https://doi.org/10.1016/j.cherd.2023.05.062.

[17] T. Ooms, S. Vreysen, G. Van Baelen, V. Gerbaud, I. Rodriguez-Donis, Separation of ethyl acetate–isooctane mixture by heteroazeotropic batch distillation, Chemical Engineering Research and Design 92 (2014) 995–1004. https://doi.org/https://doi.org/10.1016/j.cherd.2013.10.010.

[18] H. Gao, F. Zhao, L. Zhu, F. Yang, Y. Wang, D. Li, Dehydration of a Dilute Acetic Acid-Water Mixture via Batch Heteroazeotropic Distillation, Chem Eng Technol 44 (2021) 477–487. https://doi.org/10.1002/ceat.202000367.

[19] G. De Guido, C. Monticelli, E. Spatolisano, L.A. Pellegrini, Separation of the Mixture 2-Propanol + Water by Heterogeneous Azeotropic Distillation with Isooctane as an Entrainer, Energies (Basel) 14 (2021). https://doi.org/10.3390/en14175471.

[20] S. Skouras, V. Kiva, S. Skogestad, Feasible separations and entrainer selection rules for heteroazeotropic batch distillation, Chem Eng Sci 60 (2005) 2895–2909. https://doi.org/https://doi.org/10.1016/j.ces.2004.11.056.

[21] P. Lang, G. Modla, Generalised method for the determination of heterogeneous batch distillation regions, Chem Eng Sci 61 (2006) 4262–4270. https://doi.org/https://doi.org/10.1016/j.ces.2006.02.004.

[22] A. Yang, Z.Y. Kong, J. Sunarso, Design and optimisation of novel hybrid side-stream reactive-extractive distillation for recovery of isopropyl alcohol and ethyl acetate from wastewater, Chemical Engineering Journal 451 (2023) 138563. https://doi.org/https://doi.org/10.1016/j.cej.2022.138563.

[23] K. Jayant, C. Gupta, S. Seethamraju, S.M. Mahajani, Entrainer assisted production of high purity 2-phenyl ethyl acetate by reactive distillation, Sep Purif Technol 331 (2024) 125650. https://doi.org/https://doi.org/10.1016/j.seppur.2023.125650.

[24] H. Yu, Q. Ye, H. Xu, X. Dai, X. Suo, R. Li, Comparison of alternative distillation processes for the maximum-boiling ethylenediamine dehydration system, Chemical Engineering and Processing: Process Intensification 97 (2015) 84–105. https://doi.org/10.1016/j.cep.2015.09.008.

[25] F. Denes, P. Lang, G. Modla, X. Joulia, New double column system for heteroazeotropic batch distillation, Comput Chem Eng 33 (2009) 1631–1643. https://doi.org/https://doi.org/10.1016/j.compchemeng.2009.01.011.

[26] W.L. Luyben, Control of the Heterogeneous Azeotropic n-Butanol/Water Distillation System, Energy & Fuels 22 (2008) 4249–4258. https://doi.org/10.1021/ef8004064.

[27] D.B. Kaymak, Design and control of an alternative intensified process configuration for separation of butanol-butyl acetate-methyl isobutyl ketone system, Chemical Engineering and Processing - Process Intensification 159 (2021) 108233. https://doi.org/https://doi.org/10.1016/j.cep.2020.108233.

[28] C. Barker, European MIBK spot prices continue to rise on feedstocks, Tightness, (2017). https://www.icis.com/explore/resources/news/2017/02/14/10078953/e uropean-mibk-spot-prices-continue-to-rise-on-feedstocks-tightness/ (accessed February 6, 2024).

[29] M.I. Parma-García, J.A. Díaz-López, A. Nieto-Márquez, Separation of a water/MIBK mixture by batch heteroazeotropic distillation: A self-entrained case, Chemical Engineering and Processing - Process Intensification 171 (2022). https://doi.org/10.1016/j.cep.2021.108761.

[30] V. Diky, R.D. Chirico, A.F. Kazakov, C.D. Muzny, M. Frenkel, ThermoData Engine (TDE): software implementation of the dynamic data evaluation concept. 3. Binary mixtures, J Chem Inf Model 49 (2009) 503–517. https://doi.org/10.1021/ci800345e.

[31] J. Stichlmair, J.L. Bravo, J.R. Fair, General model for prediction of pressure drop and capacity of countercurrent gas/liquid packed columns, 1989.

[32] B. Nemeth, L. Hegely, P. Lang, Comparison of batch heteroazeotropic distillation operational strategies for the dehydration of isopropanol, Chemical Engineering Research and Design 146 (2019) 486–498. https://doi.org/10.1016/j.cherd.2019.04.033.

[33] L. Hegely, P. Lang, Optimization of Batch Heteroazeotropic Distillation Operational Strategies with Entrainer Recycle, in: Computer Aided Chemical Engineering, Elsevier B.V., 2018: pp. 1505–1511. https://doi.org/10.1016/B978-0-444-64235-6.50262-X.

[34] D.Y. Aqar, N. Rahmanian, I.M. Mujtaba, A novel split-reflux policy in batch reactive distillation for the optimum synthesis of a number of methyl esters, Sep Purif Technol 221 (2019) 363–377. https://doi.org/https://doi.org/10.1016/j.seppur.2019.03.071.

[35] B. Kotai, P. Lang, G. Modla, Batch extractive distillation as a hybrid process: separation of minimum boiling azeotropes, Chem Eng Sci 62 (2007) 6816–6826. https://doi.org/https://doi.org/10.1016/j.ces.2006.10.002.

[36] H.Z. Kister, P.M. Mathias, D.E. Steinmeyer, W.R. Penney, B.B. Crocker, J.R. Fair, Equipment for distillation, gas absorption, phase dispersion, and phase separation, McGraw-Hill, 2008.

4. Improvement of energy efficiency and production performance in a heteroazeotropic batch distillation unit: a study on decanter control and feeding strategy

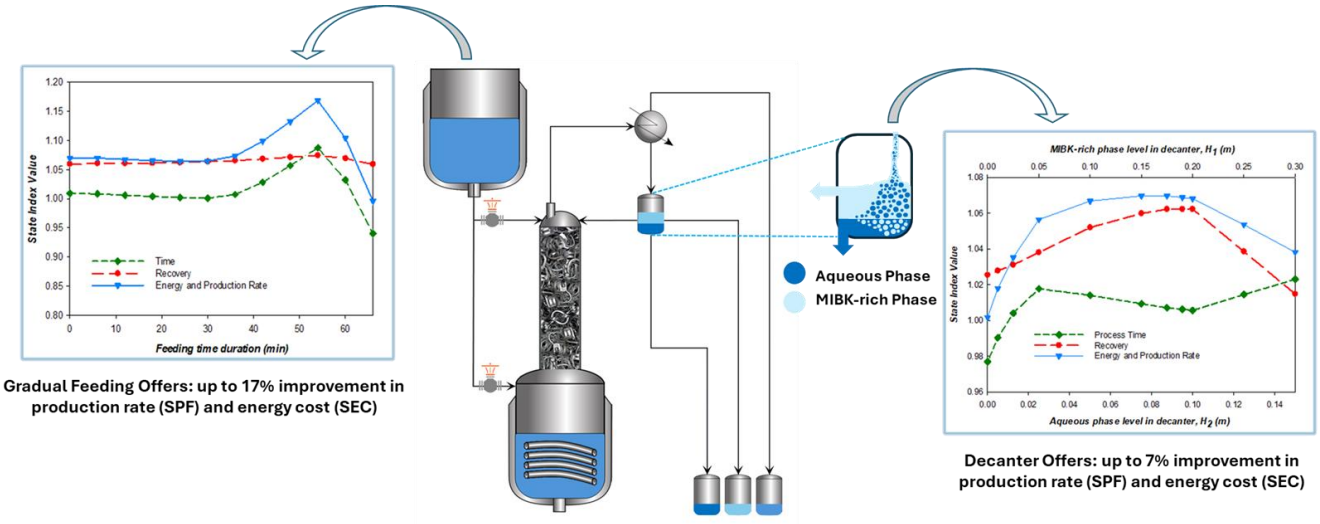

Gradual Feeding Offers: up to 17% improvement in production rate (SPF) and energy cost (SEC)

Decanter Offers: up to 7% improvement in production rate (SPF) and energy cost (SEC)

Abstract

Dehydration of methyl isobutyl ketone (MIBK) using a batch distillation unit has been investigated through process simulation. Applying a decanter for upgrading the heteroazeotropic distillation is analysed in different aspects. The unit performance dependency on the feed quantity, decanter design/control policy, decanter holdup volume, and subsequent phase separation quality are evaluated in detail. Feed quantity is recognized as a key factor influencing unit performance. Although increasing the feed quantity leads to a higher production rate (SPF) and lower specific energy cost (SEC), the optimal feed quantity is identified as the point beyond which further improvements in these variables become negligible. Also, reflux initiating time, liquid-liquid separation grade, loss of the desired component along with the effluent stream, and holdup loss at the end of the process are recognized as functions of decanter holdup quantity. Accordingly, a perfect decanter with a large holdup volume is not necessarily the best option. The evaluation indicates that an effective decanter lies on a larger aqueous phase holdup and smaller organic phase holdup, as long as it is capable of efficiently separating the liquid phases (over 75% separation efficiency for each phase). It is found that applying a well-designed and properly controlled decanter for the mixture separation (MIBK-water) can improve the unit recovery by up to 6% and the production rate (and energy cost) by up to 7% compared to a conventional batch distillation unit. Furthermore, an inverted batch distillation configuration with a gradual feeding policy is applied as an alternative and compared to other operation policies. The feeding schedule is found to be the key factor in this mode. The results reveal that an inverted distillation unit equipped with a properly designed and controlled decanter provides up to 17% improvement in energy and production rate as well as 7% in recovery for a 9% shorter process time compared to a conventional batch distillation unit.

Keywords: MIBK-water, Heteroazeotropic Distillation, Batch Distillation, Batch stripper, Inverted Batch Distillation, Energy Efficiency

4.1. Introduction

Methyl isobutyl ketone (MIBK, 4-methylpentan-2-one) is a versatile solvent with a wide range of applications. Due to its excellent dissolution capabilities, biodegradability, and low solubility in water, it is used in various chemical processes and industrial production of pharmaceuticals, paint and rubber, pesticides, cleaning solvents, etc. [1,2]. MIBK, used as a solvent, is frequently found in contact with and mixed with water in many operations and needs to be recovered and reused due to its relatively high price, high toxicity, and limited availability [3,4]. Accordingly, an efficient solvent recovery operation is necessary to close the production circle and meet the sustainable production criteria. Since the MIBK-water mixture forms a heterogenous two-phase mixture at room temperature and atmospheric pressure, the main fraction of water can be easily separated by decanting the two-phase mixture. The phase split in MIBK-water system is spontaneous, not needing an additional component as "entrainer," and it is categorized as an "auto-entrained" or "self-entrained" heteroazeotropic mixture, similar to the well-known butanol-water mixture [5,6]. The small quantity of water that remains in the mixture after decanting needs to be removed by a second separation process.

Separation of a heteroazeotropic mixture, involving a liquid-liquid-vapor three-phase equilibrium, is always associated with complexity and requires specialized measures and techniques. Distillation, as one of the most popular separation processes, has shown a robust performance for complicated separation processes. Distillation units are developed in a broad spectrum, including extractive distillation (ED) [7,8], pressure-swing distillation (PSD) [9–14], reactive distillation (RD) [15,16], heterogeneous azeotropic distillation (HAD) [17–22], or a combination of them [23,24]. While distillation is a widely studied and well-developed unit operation, it is still an interesting field for research and development in academic and industrial categories, especially in batch mode [25,26]. The popularity of batch distillation is growing due to its interesting features such as low capital cost, flexibility to process different feed compositions, providing a wide range of products using a single column, possibility to operate in various configurations, applicability on small scales or preference of small-scale operation for high-value market products [27]. Accordingly, batch distillation can potentially be applied in a wide variety of separation processes, but there is still an array of challenges regarding selecting proper operation policy, configuration, and design parameters in different steps from design to operation [28,29]. The

advances in computer-aided engineering and optimization methods during the last decades have facilitated the simulation and design of batch distillation units for handling complex operations such as separation of a heteroazeotropic mixture associated with liquid-liquid-vapor equilibrium phases [26,30].

In our previous research works, separation of MIBK-water mixture using a batch distillation has been analysed, and adding a decanter to a batch distillation unit has been proven as an efficient, easy-to-apply, and reliable solution to upgrade the unit performance in separation of self-entrained heteroazeotropic mixtures [31,32]. A decanter, as a mechanical phase separator, located in a suitable location in the unit can improve the distillation by removing the undesired liquid phase and retaining the desired liquid phase within the unit. In the MIBK-water separation process, two liquid phases form downstream of the condenser. Considering the process objective, which is water removal, the aqueous phase can be discharged, and the organic phase, as the desired liquid phase, can be refluxed for further purification. Many details still need to be assessed in order to achieve a comprehensive understanding and be able to develop a sound methodology for the study, design, and optimization of self-entrained heteroazeotropic batch distillation (HABD) units. In this work, the effect of reflux drum/decanter capacity on a batch distillation unit is assessed. Decanter performance is optimized with respect to the batch distillation process objectives. Also, gradual feeding is introduced and studied as an effective way to upgrade a batch distillation unit. Different batch distillation configurations, including the conventional batch distillation unit, batch distillation unit equipped with a decanter, and inverted batch distillation unit, are studied and compared in terms of separation efficiency, operation time, production rate, and energy performance.

4.2. Methodology and study plan

4.2.1. Simulation procedure

The commercial package Aspen Plus V.14® is applied for process simulations. The phase equilibrium is modelled using UNIQUAC, and the batch distillation unit is modelled by applying the BatchSep module. The water-MIBK mixture phase diagram calculated using UNIQUAC is presented along with experimental data in Figure 4-1a. The empirical data points are found in the Aspen Plus V.14® properties, provided by NIST Thermo Data Engine (TDE) database [33]. Further

details regarding the mixture and the simulation are available in our previous studies on the same mixture [31,32].

The scope of this distillation is to dehydrate a mixture of 98 wt.% MIBK-water, obtained as a residual stream in the paint industry, up to 99.8 wt.%. Dehydration serves as a solvent recovery process, enabling the paint industries to recycle and reuse the MIBK in their processes. The mixture was fed at room temperature (25 ℃) in batches of 15 kg. This amount can be divided into smaller volumes to be processed in multiple batch operations or to be collected and processed in a single operation.

Figure 4-1b shows the basic batch distillation unit applied in this study. The unit is comprised of three main parts: (1) the still (or pot) that holds the feed and accommodates the heating facilities/reboiler, (2) the column equipped with trays or packings, and (3) the condenser and reflux drum. Some other elements might be employed, such as distillate collection tanks. The general characteristics of this unit and its operation are given in Table 4-1.

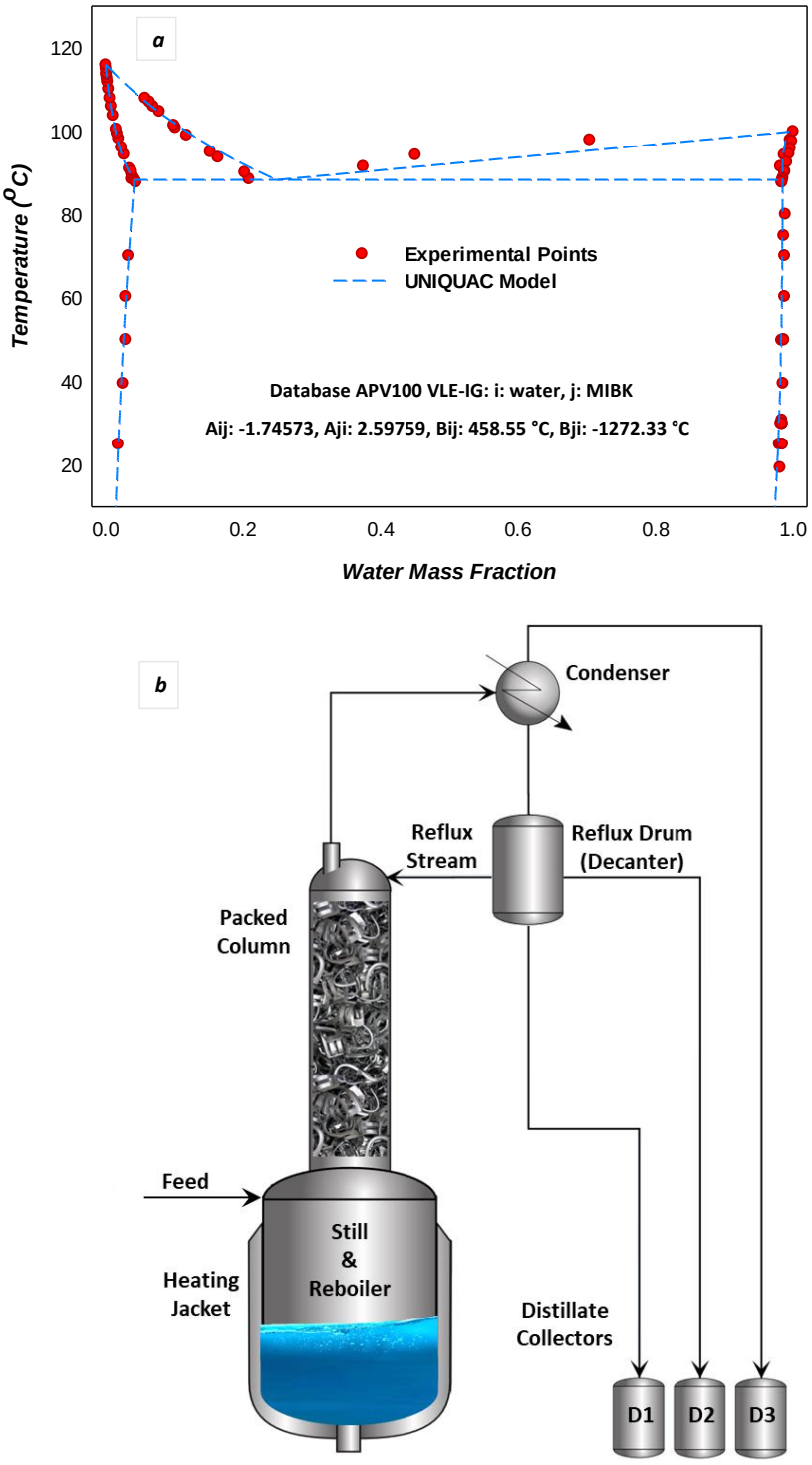

Figure 4-1. (a) Phase equilibrium diagram of MIBK-water system at 1 atm. and temperature range: 0 - 116 ℃ [33] (b) Schematic view of the batch distillation unit.

Table 4-1. General operating conditions and technical features applied in the batch distillation unit simulation.

Parameter	Symbol	Value	Units
Feed quantity	r_0	*15*	$[kg]$
Product quantity (recovered mass)	r	-	$[kg]$
Operating pressure (Condenser pressure)	$P = P_c$	*1*	$[atm]$
Initial MIBK mass fraction	x_{r0}	*0.98*	$[-]$
Final MIBK mass fraction	x_r	*0.998*	$[-]$
Equilibrium phases	$-$	*VLL*	$[-]$
Still volume	V_s	*40*	$[l]$
Reboiler duty	W	*5040*	$[kJ/h]$
Reboiler type	$-$	*Heating Jacket*	$[-]$
Condenser type	$-$	*Total*	$[-]$
Condenser outlet temperature	T_c	*85*	[℃]
Diameter at condenser inlet	ϕ_c	*0.1*	$[m]$
No. of collectors	$-$	*3*	$[-]$
Column diameter	ϕ_s	*0.1*	$[m]$
Packing type	$-$	*Metal Raschig ring*	$[-]$
Packing size	ϕ_p	*1/2*	$[inch]$
Height of the equivalent theoretical plate (Specified)	*HETP*	*1*	$[m]$
Packing Bed Height	H_p	*2*	$[m]$
Dry Packing factor	F_p	*984*	$[m^{-1}]$
Packing porosity	ε	*0.85*	$[-]$
Specific area of packing	α	*400*	$[m^2/m^3]$
Foaming (system) factor	f_f	*1*	$[-]$

* Characteristic data for metal Raschig ring 1/2" can be found in [34].

The column internals are included in the simulation to calculate the gas and liquid holdups, pressure drop, and, generally, the hydraulics within the column. The remarkable volume of holdups, compared to the feed quantity, makes them necessary for an accurate simulation.

The column simulation is done applying the equilibrium-based approach. The Eckert model [35] is employed for flooding and pressure drop calculations. Three equilibrium phases, liquid-liquid-vapor (LLV), are included in the simulation, as per the phase equilibrium diagram modelled by UNIQUAC.

The operation strategy "constant reflux ratio" is applied for all cases in this study [26], and simulations cover the "heat-up" and "production" stages until reaching

the desired purity of 99.8 *wt*.%. The desired product is collected in the pot, and water, as the volatile component, leaves the unit as the top product. The final condition in the simulation is set to discharge the holdup mixture content into the distillate collectors. The top product consists of three phases: (1) MIBK-rich phase liquid, (2) aqueous (liquid) phase, and (3) vapor outlet phase. Each phase is collected in a separate collector (D1, D2, and D3, respectively) to track the mixture components accurately. It must be noted that due to assigning a non-condensable pad gas (nitrogen), a partial condenser is applied in the simulation model, but since it operates as a total condenser regarding the condensable component (Water and MIBK), it is commonly referred to as a total condenser.

The state variables, including process time (t), fractional recovery (η), specific product flow (SPF), and specific energy cost (SEC), are used to measure different aspects of the unit operation. The relationships to calculate these parameters are as follows [31,36]:

$$\eta = \left[\frac{r.x_r}{r_0.x_{r0}}\right] = \left[\frac{kg_{MIBK\ obtained}}{kg_{MIBK\ fed}}\right] \quad (1)$$

$$SPF = \left[\frac{r.x_r}{t}\right] = \left[\frac{kg_{MIBK\ obtained}}{h_{operation}}\right] \quad (2)$$

$$SEC = \left[\frac{W}{SPF}\right] = \left[\frac{kJ/h_{operation}}{kg_{MIBK\ obtained}/h_{operation}}\right] = \left[\frac{kJ}{kg_{MIBK\ obtained}}\right] \quad (3)$$

4.2.2. Unit configurations and operation policies

According to our previous study on batch distillation of MIBK-water, the unit configuration and operation policy play key roles in operation efficiency [32]. The three main configurations studied in the present work are indicated in Figure 4-2. The first configuration, hereinafter referred to as Mode I, is a conventional batch distillation unit with a reflux drum. This configuration has been applied for decades as a basic separation unit operation [25,26]. The second, Mode II, is a unit equipped with a decanter which has been proven as an efficient configuration to upgrade the heteroazeotropic batch distillation [37–39]. The third, Mode III, is a unit with a feed tank at the top, which gradually feeds the unit. This configuration, commonly known as inverted batch distillation or batch stripper [25,26], is modified by adding a decanter to facilitate the separation of a heteroazeotropic mixture. More detail on this configuration is presented in section 4.2.6. It is worth

mentioning that besides the unit configuration, the mixture properties and the operation policy are two main factors that affect the results and need careful consideration. In fact, the optimal operation is a function of these three main factors. More details on each configuration can be found in the following sections.

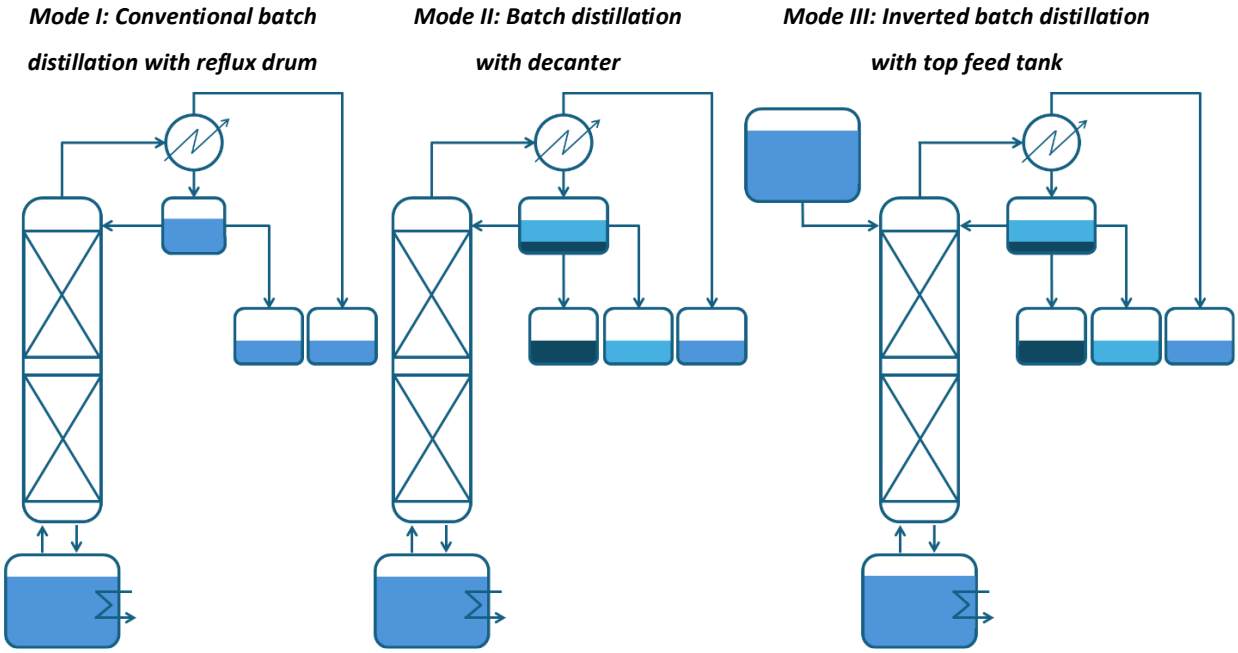

Figure 4-2. Batch distillation configurations evaluated in the study

Table 4-2 briefly presents the manipulated/controlled operational parameters and the studied range for each one in this work. The details for each part are given in the following sections. The widely used term "reflux ratio", RR, is defined as the ratio of the reflux mass flow rate to the distillate mass flow rate, and the term "return fraction", RF, is defined as the mass fraction of the liquid phase received in the reflux drum that returns to the column along with the reflux stream. These two parameters can be calculated as follows:

$$RR = \frac{R}{D} \tag{4}$$

$$RF = \frac{R}{D+R} = \frac{RR}{1+RR} \tag{5}$$

Where R and D are the mass flow rates of reflux and distillate streams, respectively. The return fraction and reflux ratio apply to both individual liquid phases and the entire liquid mixture.

Although both return fraction and reflux ratio convey the same concept and present the magnitude of the reflux stream, return fraction is a bounded value in the range 0-1, which can also be translated as fractional separation for each phase. Hence, the return fraction parameter enables us to clearly express the decanter separation performance by indicating the fraction of each phase returned to the column. Accordingly, return fraction is preferred over reflux ratio to present the results in this study.

Table 4-2. Variable parameters and the studied ranges in the present investigation

Parameter	Unit Configuration	Symbol	Range of Study	Units
Return fraction	Mode I	RF	*0-0.95*	$[-]$
Feed quantity	Mode I	r_0	*5-30*	$[kg]$
MIBK-rich phase level in decanter (Fig. 4-3)	Mode II	H_1	*0-0.3*	$[m]$
Aqueous phase level in decanter (Fig. 4-3)	Mode II	H_2	*0-0.15*	$[m]$
Return fraction of MIBK-rich phase (Rich)	Mode II	RF_1	*0-1*	$[-]$
Return fraction of Aqueous phase (Lean)	Mode II	RF_2	*0-0.95*	$[-]$
Feeding time	Mode III	t_f	*0-66*	$[min]$

4.2.3. Effect of reflux ratio/return fraction - Mode I

Reflux ratio is known as a key factor in the batch distillation operation, and it needs to be specified carefully. Since the condensed liquid is usually collected in a reflux drum before splitting into distillate and reflux streams, a delay in receiving the reflux stream to the column is expected. Also, due to the relatively small feed quantity, short operation time, and dynamic behaviour of the process, reflux drum holdup volume (and subsequent retention time) is identified as an important factor that might affect the unit performance. Accordingly, a reflux drum with a diameter of 0.1 m and liquid volume of 1 L is considered in Mode I. The simulations are conducted in two scenarios [32]:

1- Two-step operation (TSO): in which the operation starts under total-reflux condition (known as “start-up step”) until it reaches a steady-state condition

within the unit, and then a finite reflux ratio (known as the "production step") is set based on the overall unit objectives and desired product specifications.

2- Single-step operation (SSO): in which the “start-up step” under total-reflux condition is skipped, and the top outlets are open from the beginning of the operation.

Both approaches are studied in the range of $0 < RF < 0.95$, and the results are presented in section 4.3.1.

4.2.4. Effect of feed quantity – Mode I

As explained in section 4.2.2, different feed quantities can be processed depending on the user's time schedule and unit capacity (pot size). Processing a small amount of feed, which implies a higher frequency of operation for processing a specific amount of production, is expected to cause excess energy costs and a larger amount of MIBK loss. This is due to the approximately constant quantity of “holdup loss” at each time of operation, regardless of the feed quantity. Hence, it is logically expected to have less MIBK loss with a larger batch size (less frequent operation) compared to a smaller batch size (frequent operation). The feed quantity of 5 to 30 kg is studied to assess the unit performance in processing different amounts of feed. The results are presented in section 4.3.2.

4.2.5. Distillation with Decanter - Mode II

The positive effect of adding a decanter on distillation performance has been reported in previous works [31,32]. A reflux drum of proper size can turn into a decanter, providing sufficient residence time for separating the organic and aqueous phases. Presuming that a decanter with a perfect separation performance would be the best scenario in terms of operation efficiency, the deviations from this condition are analysed, in order to validate or redefine such presumption. Figure 4-3 indicates the general arrangement of a decanter containing the organic and aqueous phases. This part of the study specifically addresses the decanter design considerations, priorities in control, and available options to provide a simple and efficient decanter.

Setting constant reflux ratios for two liquid phases in dynamic operations such as batch distillation columns is challenging and requires a sophisticated control system. On the other hand, setting constant liquid levels within the decanter, refluxing the organic phase by an overflow pipe, and draining the aqueous phase

from the bottom enables the user to reflux the desired phase (organic) and remove the undesired phase (aqueous). Hence, the vessel volume, liquid levels, and the location of the outlet nozzles are the design factors to be considered.

From a different point of view, the liquid level in the decanter determines its residence time (holdup) within the decanter, which in turn determines the liquid-liquid separation quality. Accordingly, the separation quality of a decanter can be controlled by controlling the liquid levels, and a perfect phase separation requires a certain liquid residence time within the decanter. As depicted in Figure 4-3, reducing the height of the organic phase (H_1), which is the desired phase to be refluxed, might cause carrying some of the aqueous phase to the reflux stream. Also, setting an insufficient aqueous phase level (H_2) might cause some organic phase to be carried out of the unit.

Although a certain liquid level is necessary for a perfect separation, an excess aqueous phase level elevates the liquid-liquid interphase location and consequently restricts the space of the organic phase. Also, an excess holdup quantity/time of the MIBK-rich phase in the decanter, aimed to reflux a higher purity stream, would result in a large "holdup loss" since it would be dumped to the distillate collectors at the end of the operation. Hence, assuming a perfect decanter, with liquid levels equal to H_{1P} and H_{2P}, may not offer the optimum operation for a distillation unit.

Accordingly, monitoring and controlling the liquid levels within the decanter can be identified as the key to control the reflux set-on time, the phase separation efficiency, and the quantity and quality (composition) of the reflux stream.

Due to the varying quantity and composition of the decanter inlet and outlet streams, it is not easy to predict the effects of the liquid level in the decanter on distillation unit performance. The first step for determining the effects of decanting performance on distillation unit behaviour is to design a decanter considering the following guidelines [40,41]:

1- A minimum holdup volume of the liquid is required to provide sufficient time for the controller (or operator) to intervene in the process (typically, equal to 100 mm or 2-4 minutes, as a minimum for each control level).
2- A minimum of liquid volume (height, vessel length, etc.) is required for each phase to damp the turbulence imposed by inlet stream. Laminar flow is necessary for liquid-liquid separation.

3- For decanters dealing with interdispersed liquids, the priorities between settling or rising (or both) shall be identified.
4- Once all guidelines are observed to provide a suitable condition for separation, liquid-liquid separation relies on the stability of dispersion and droplet size distribution. For dispersions with low to moderate stability, for which decanters are applicable, settling (or rising) of a specific drop size determines the required liquid residence time and, subsequently, the decanter dimensions. Generally, the dispersions with interfacial tension (IFT) over 0.01 N/m and density difference over 10% do not form a stable dispersion unless containing stabilizer agents. In cases with a volume fraction of the minority phase below 10 to 20 %, the dispersion may contain a wide droplet size distribution, including a long tail in small droplet diameters, which needs very careful consideration and taking conservative measures for separation.

It should be noted that the droplet size distribution of dispersions is a complex function of turbulence level, interfacial properties of two phases, volume fraction of the dispersed phase, operating temperature and pressure, and presence of a third component/phase. Accordingly, an accurate design of a decanter is normally associated with elaborate experimental work [42], which falls out of the scope of this study.

In the studied mixture (MIBK-water), the IFT is over 0.01 N/m, the density difference of liquid phases is over 10%, and there is no stabilizer agent in the mixture. Hence, it is not expected to have very fine droplets or stable dispersion. Nevertheless, since the dispersed phase volume fraction is below 10%, the turbulence must be carefully controlled, and the separation of dispersed drops from both phases should be considered.

Considering the features of the studied mixture, some assumptions and simplifications are made to avoid complicated calculations on decanter design, as follows:

1- A vertical decanter is applied due to simpler liquid level control and the low flow rate of the condensed mixture.
2- A minimum liquid level of 0.1 m is required to suppress the turbulence induced by the inlet stream
3- A minimum residence time of 10 minutes (based on the liquid flow rates in total-reflux condition) to achieve sufficient settling/rising as well as providing sufficient residence time for control system intervention.

4- The maximum liquid height obtained from criteria 1 and 2 provides perfect separation in the decanter. Lower liquid levels result in imperfect separation and fractional separation varies linearly proportional to the liquid level. Obviously, a higher liquid level is also expected to provide perfect decanting.

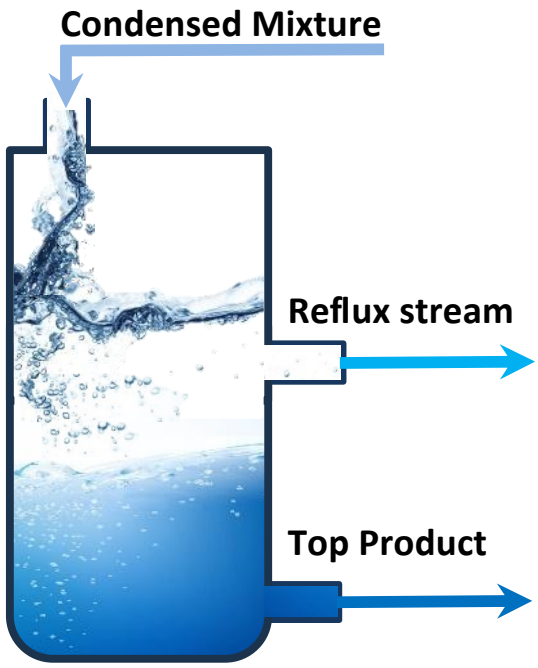

Figure 4-3. General arrangement of a decanter containing an organic phase (H_1) and an aqueous phase (H_2)

4.2.6. Inverted batch distillation (Mode III)

The feed in batch distillation units is conventionally charged before starting the operation, in a pot at the bottom of the column, where heating and boiling take place. The products can be extracted from top or bottom of the column. There is also a less popular arrangement called inverted batch distillation with feed charged into the reflux drum at the top, and the products are usually withdrawn as bottom product [26,43,44]. This configuration has been proven to enhance the operation time for separation of mixtures in which the light components present in a small fraction [45]. Moreover, it is suggested for the mixtures with a minimum boiling azeotrope [46], the cases with a small fraction of light component and some cases in which the regular configuration (batch rectifier) is not feasible for that separation [29]. This configuration is not a recently emerged batch column configuration, but it has not received sufficient attention and has been rarely

applied in practice [29]. Here, we have modified an inverted batch distillation by adding a decanter, aiming to utilize it in separation of a heteroazeotropic mixture.

In the MIBK-water system, a small quantity of water, as the volatile and minority component, needs to be removed from MIBK (the component of interest) as the main component of the bottom product. Accordingly, an Inverted batch distillation configuration modified by adding a decanter, called Mode III, is applied to assess its potential in heteroazeotropic distillation processes. Since the reflux drum in this study is utilized as a decanter, another storage tank is assigned to charge the feed into the unit. The feed tank is assumed to be located above the column, and its content enters the column from the top stage. To simulate the process in Mode III, feeding starts simultaneously with heating. The feed stream enters the column, over the top packing bed. Feeding rate can be specified according to the feed driver (gravity or a pump). This step, called "feeding step", stops when the feed content is entirely charged into the column, and the feed tank is empty. Different feeding times from 0 to 66 minutes, under gravity feeding scenario (varying feed flow rate) are studied to find the optimum feeding flow rate. The gravity feeding scenario is applied to keep the unit as simple as possible without adding an extra element for driving the feed stream. The initial feed inlet flow rate for operation under the gravity feeding scenario is specified as:

$$F_0 = 2 \times \left[\frac{r_0}{t_f}\right] \tag{6}$$

Where t_f is the specified feeding time, r_0 is the feed quantity, and F_0 is the initial feed stream flow rate corresponding to the time of opening the valve between the feed tank and the column. The feed flow rate is adjusted to ramp down linearly during the feeding step. In all simulated cases, a very small amount of mixture (0.001 kg) is initially charged into the bottom pot to be compatible with the module protocols.

4.3. Results and Discussion

As reported in a previous study, the operation can be analysed under two different perspectives: Persp. I in which there is a single batch operation/run, and the outcome of a single batch represents the final product, and Persp. II, in which the operation is repeated, recycling the product of the previous one. In the former, the production quantity and time of a single batch determines the operation

performance, while in the latter, the rate of production and specific energy consumption (SPF and SEC) have higher priority than the single batch production amount or batch operation time. The fractional recovery and process time are considered and presented, but this study is mainly oriented to evaluate the unit performance based on the "sequential batches" perspective (Persp. II) in which the criteria to recognize the optimum condition are the SEC and SPF parameters [32].

Two main categories of MIBK loss are identified in analysing the results in batch distillation: one is due to discharging the MIBK from top during the production step, called "operation loss" and the other one is due to discharging the holdup content in column, condenser, and reflux drum/decanter after achieving the desired purity level in the pot (stop criteria) called "holdup loss". Accordingly, the "overall loss" is considered in analysing the batch distillation operation under different operation policies.

4.3.1. Effect of return fraction - Mode I

As described in section 4.2.3, two different operational approaches, two-step-operation (TSO) and single-step-operation (SSO), are simulated in the range of $0 < RF < 0.95$. The results for fractional recovery and process time are given in Figure 4-4a, and the results for SEC and SPF are presented in Figure 4-4b. According to Figure 4-4a, there is a slight difference between the fractional recovery of two approaches at high return fraction while the differences become wider at low return fraction. For both approaches, as expected, fractional recovery improves by increasing the return fraction but beyond a specific point (about $RF \approx 0.75$) this improvement is not noticeable. The fraction recovery improvement for SSO is sharper than that of TSO. Accordingly, despite the significantly lower recovery of SSO than TSO at a low return fraction, it exceeds the recovery of TSO at return fractions over $RF \approx 0.65$. Lower fractional recovery of SSO at low return fraction can be attributed to the considerable amount of MIBK discharged along with the water and nitrogen at the first minutes of operation, while it does not happen in the TSO approach. At relatively higher return fractions, the top product stream is restricted so that the total MIBK loss at the start-up and production stages is lowered significantly, and the start-up approach is no longer a significant factor.

On the other hand, the operation time for both approaches increases slightly with increasing the return fraction up to about $RF \approx 0.75$, but it increases drastically by a further increase in return fraction. The difference between the two approaches

is more significant at higher return fractions due to the larger amount of mixture in SSO compared to TSO, which in turn takes a longer time to process. This small difference in recovery amplifies the difference between the two approaches in terms of process time. This is due to the high return fraction, which slows down the water discharge from the top. It should be noted that while the ultimate goals of the operation are to retain MIBK within the unit and discharge water, a trade-off between these two objectives is necessary since a high return fraction of MIBK could result in retaining too much water, leading to prolonged operation times and, conversely, a low return fraction may effectively discharge water but at the cost of losing a significant amount of MIBK, thereby reducing the overall recovery efficiency.

Based on these observations, it can be concisely stated that a high return fraction is not desirable due to significantly high operation time, which causes a high energy cost and a low production rate for both TSO and SSO approaches (it is discussed on Figure 4-4b). Also, a low return fraction is not desirable as it causes more MIBK loss in both approaches which leads to low fractional recovery. Accordingly, a suitable range of return fraction must be in the range 0.4-0.8, in which both approaches lead to very close results.

Figure 4-4b reveals that the SEC and SPF for both approaches are in good agreement, especially in lower return fractions. Considering Perspective II, referred to as “sequential batches”, SPF and SEC are the touchstones of process efficiency, and an operation with maximum SPF and minimum SEC determines the optimal operation point. According to Figure 4-4b, RF=0.5 provides the maximum SPF and the minimum SEC values in both approaches, making it the optimal point of operation. Another considerable point on RF=0.5 is that all four state variables of process time, fractional recovery, SEC, and SPF are almost equal for both approaches of SSO and TSO. According to these observations, employing a two-step operation offers no advantage, so it is skipped for the rest of this study and the return fraction of RF=0.5 is the optimal operating condition while utilizing Mode II for MIBK-water separation.

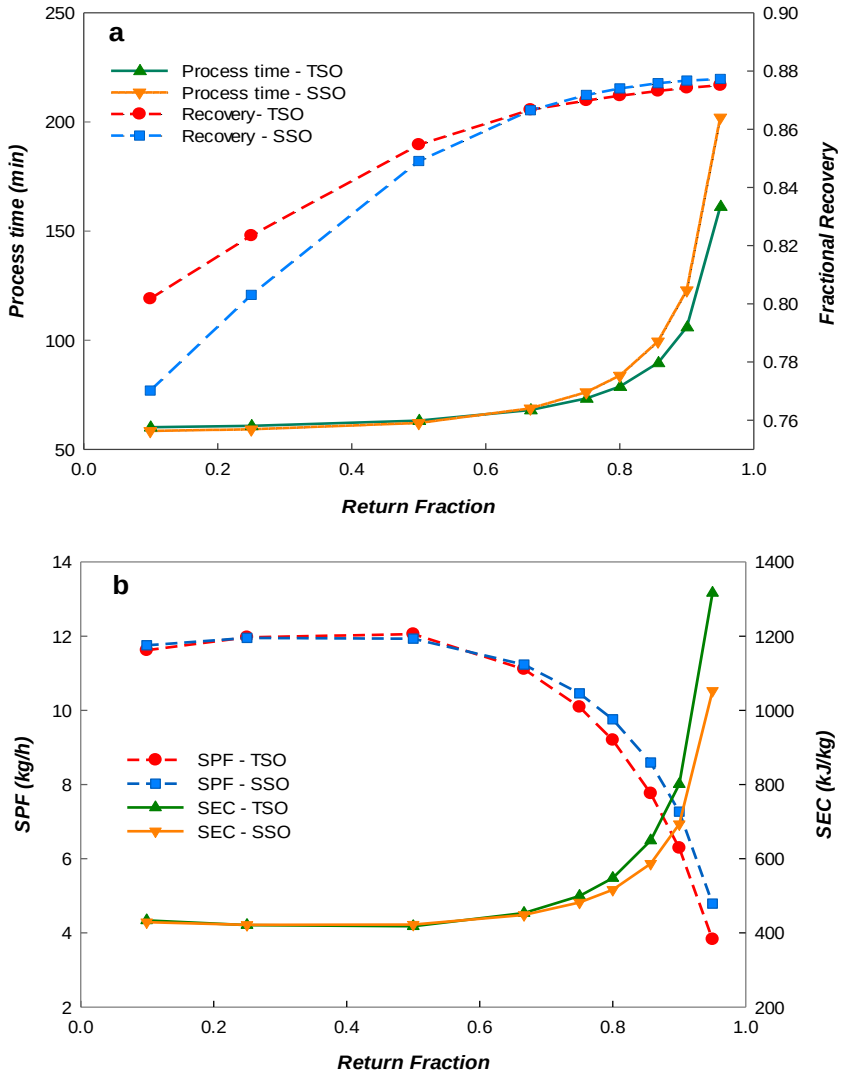

Figure 4-4. Effect of return fraction on single-step operation (SSO) and two-step operation (TSO) in terms of (a) recovery and process time (b) SPF and SEC

4.3.2. Effects of feed quantity – Mode I

As explained in section 4.2.4. different feed quantities are studied in the range of 5 to 30 kg.

Instead of using the state variables $(t, \eta,\ SPF\ and\ SEC)$ the results of this study are presented using the state indexes, including the time index (t_i), recovery index (η_i), production rate index (P_i), and energy index (E_i) as defined below [32]:

$$t_i = \left[\frac{t_d}{t}\right] \tag{7}$$

$$\eta_i = \left[\frac{\eta}{\eta_d}\right] \tag{8}$$

$$P_i = \left[\frac{SPF}{SPF_d}\right] \tag{9}$$

$$E_i = \left[\frac{SEC_d}{SEC}\right] \tag{10}$$

The subscript "d" represents the reference case which is the optimum case of the conventional distillation unit (Mode I) that corresponds to $RF = 0.5$. The larger the index is, the more efficient the process results in terms of that variable. All four indexes for the case $RF = 0.5$ in Mode I are equal to 1. Accordingly, if an operation results in indexes larger than 1, it indicates superior performance over the case with a 15 kg feed quantity and $RF = 0.5$ in Mode I, whereas the indexes below 1 indicate a less efficient operation. Applying these dimensionless indexes enables us to provide the results of different aspects on the same scale using a single graph. Also, using the relative scale provides a clear and intuitive way to understand the variation of each state variable compared to a reference case.

Figure 4-5 presents the state indexes at different feed quantities. Since the amount of feed directly affects the process time, comparing the process time does not provide a meaningful conclusion. It should be noted that regarding the relationship between SEC and SPF ($SEC \times SPF = W = Const.$) the energy and production rate indexes (Eq. 9 & 10) are identical, so reporting one value for both is sufficient. According to this figure, the state indexes improve sharply by increasing the feed quantity from 5 to 15 kg but further increases in feed quantity result in slight improvement in the indexes. According to this graph, a larger feed quantity results in a higher production rate, less energy consumption, and higher fractional recovery. The enhanced fractional recovery is due to the relatively small amount of decanter and column holdups (relative to the total feed mass), which are discharged to distillate collectors at the end of the process.

Since the *sequential batches* perspective (Persp. II) is applied for process evaluation, a feed quantity of 15 kg is considered a suitable feed quantity, and it is applied for the rest of this study since it leads to a reasonable SEC and SPF level.

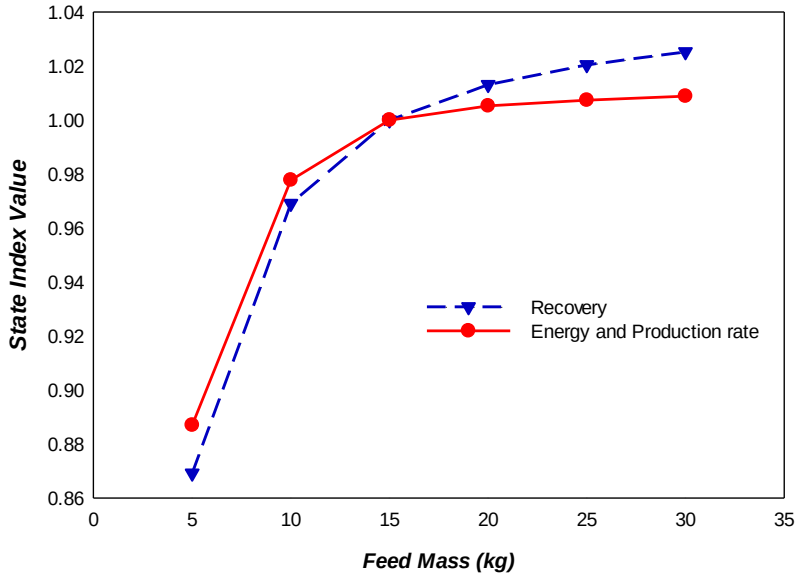

Figure 4-5. Effects of feed quantity on state indexes

4.3.3. Distillation with Decanter (Mode II)

As discussed in section 4.2.5, fractional phase separation and, subsequently, the return fraction for each phase can be related to the liquid levels in the decanter. The maximum liquid flow rate entering the reflux drum during the operation in Mode I at RF=1 is applied to design the decanter, which is about 9 kg/h aqueous phase and 0.6 kg/h organic phase. Conducting a primary decanter sizing, the reflux drum diameter ($0.1\ m$) is assessed to check its applicability to handle the condensed liquids as a decanter. Since this diameter offers a relatively low vertical velocity (about 1.5 m/h in total reflux condition), it seems to be applicable as a decanter. Although the proper vertical velocity depends on many factors, such as settling/rising droplet size, the velocities lower than 10-15 m/h are known as generally proper values to design a decanter [40]. A smaller diameter decanter can probably be employed, but due to some fundamental limits in fabrication, internal space accessibility, required space for instrument installation, and reusing the reflux drum as decanter, a diameter of $0.1\ m$ is finally selected. According to the assumptions and simplifications mentioned in section 4.2.5, the required liquid volume in the decanter (for each liquid phase) that provides a perfect phase separation is estimated as the maximum of two criteria: 10 minutes liquid holdup time at total reflux condition or $0.1\ m$ of liquid level [40,47]. Accordingly, the organic phase liquid level and aqueous phase liquid level corresponding to perfect decanting condition are respectively specified as $H_{1P} = 0.2\ m$ and $H_{2P} = 0.1\ m$.

As explained in section 4.2.5, fractional phase separation for liquid levels larger than $H_{1P}\ and\ H_{2P}$ is equal to 1, while it decreases for smaller liquid levels proportional to the liquid level down to the level of 0. Hence, fractional phase separation at ($H_2 = H_1 = 0$) would be equal to 0, which implies no decanting, as it is in Mode I. On the other hand, since the value $RF = 0.5$ is found to be the optimum condition in Mode I (explained in section 4.3.1), the return fraction value for this case in Mode II is set to $RF = RF_2 = RF_1 = 0.5$. Accordingly, the return fraction of MIBK-rich phase (RF_1) and aqueous phase (RF_2) are related to the liquid level in decanter by following correlations:

$$RF_1 = 0.5 + \left(\frac{0.5}{0.1}\right) H_2 \qquad \text{for} \quad 0 < H_2 < 0.1 \text{ m} \tag{11}$$

$$RF_1 = 1 \qquad \text{for} \quad H_2 \geq 0.1 \text{ m} \tag{12}$$

$$RF_2 = 0.5 - \left(\frac{0.5}{0.2}\right) H_1 \qquad \text{for} \quad 0 < H_1 < 0.2 \text{ m} \tag{13}$$

$$RF_2 = 0 \qquad \text{for} \quad H_1 \geq 0.2 \text{ m} \tag{14}$$

Based on these assumptions, there is no need for a complex analysis or monitoring system, and decanting quality can be controlled by liquid phase level control.

According to these relationships, the return fraction for the aqueous phase is equal to 0 (perfect decanter) for an organic phase liquid level of ($H_1 = H_{1P} = 0.2\ m$), and it is equal to 0.5 for the case with no phase separation ($H_1 = 0$). Analogously, the return fraction for the organic phase is equal to 1 (perfect decanter) for an aqueous phase liquid level of ($H_2 = H_{2P} = 0.1\ m$) and it is equal to 0.5 for ($H_1 = 0$), at which there is no phase separation.

Organic liquid levels in a range of ($0 \leq H_1 \leq 0.3\ m$) and aqueous liquid levels in a range of ($0 \leq H_2 \leq 0.15\ m$) are studied, and the results are presented in Figure 4-6. This figure indicates the state indexes obtained for different aqueous and organic phase levels in the decanter. The levels of both liquid phases are varied simultaneously and in the same proportion.

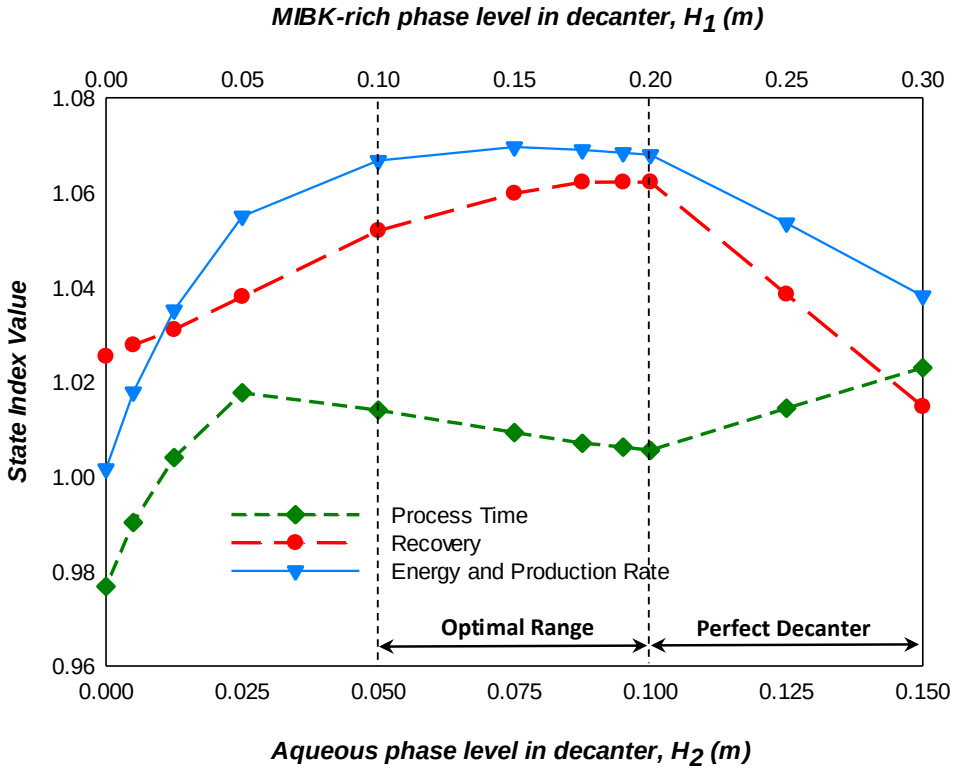

Figure 4-6. Variation of state indexes with liquid level in decanter

As mentioned, the minimum index values in the graph correspond to the point with no phase separation ($H_1 = H_2 = 0$). This case represents an operation with no liquid holdup in the reflux drum/decanter, where the condensed stream splits immediately and equally into reflux and distillate streams ($RF = RF_1 = RF_2 = 0.5$). Initially, it might be expected to achieve the same results as Mode I at $RF = 0.5$, in which all state indexes are equal to 1, but as this figure shows, the case ($H_1 = H_2 = 0$) in Mode II leads to different results. The differences can be explained by no-holdup in the reflux drum and, subsequently, the lower "holdup loss", as well as earlier reflux initiating in the unit in this case compared to Mode I. On the other hand, higher fractional recovery and lower "holdup loss" imply a larger quantity of mixture to be purified, which in turn results in a longer process time compared to Mode I at $RF = 0.5$.

Increasing the liquid level in the decanter, up to $H_1 = 0.05\,m, H_2 = 0.025\,m$, improves the operation in all aspects. Accordingly, the indexes of fractional recovery, process time, production rate, and energy cost are respectively increased to 1.038, 1.018, and 1.056. Based on these observations, it can be concluded that while a larger decanter holdup may result in greater "holdup loss", it also enhances

decanting efficiency and reduces "operation loss". Ultimately, this balance improves the overall performance of the distillation process.

With further increase in liquid levels, up to $H_1 = 0.2\,m, H_2 = 0.1\,m$, the recovery index improves up to $\eta_i = 1.062$ while the time index declines down to $t_i = 1.0006$. The improvement in recovery can be attributed to a reduction in "operation loss", resulting from more efficient decanting, while the extended operation time is due to the enhanced distillation process, where more MIBK remains in the unit and requires additional time for complete processing. Overall, the improvement in recovery indicates that with the liquid levels below $(H_1 = 0.2\,m, H_2 = 0.1\,m)$, the reduction in "operation loss" achieved by extending the liquid level outweighs the resulting increment of "holdup loss".

On the other hand, by increasing the liquid levels up to $H_1 = 0.15\,m, H_2 = 0.075\,m$ the SPF and SEC index reaches a maximum value of $(P_i = E_i = 1.07)$ and is flattened (with a slight decline) with further increasing the liquid levels to $H_1 = 0.2\,m, H_2 = 0.1\,m$. Despite achieving the maximum recovery at $(H_1 = 0.2\,m, H_2 = 0.1\,m)$, due to the relatively longer operation time at this point, the maximum energy and production rate index is achieved at the point $(H_1 = 0.15\,m, H_2 = 0.075\,m)$, making it the optimum operation point based on the "sequential batches" perspective. It is worth mentioning that this point corresponds to return fractions of $RF_1 = 0.875$ and $RF_2 = 0.125$. Similarly, the range where the energy and production rate index level off at a high value represents the optimal operating range. Accordingly, the range from $(H_1 = 0.1\,m, H_2 = 0.05\,m)$ to $(H_1 = 0.2\,m, H_2 = 0.1\,m)$, are specified as "optimal range" in Figure 4-6. This range corresponds to the return fraction range from $(RF_1 = 0.75\,m, RF_2 = 0.25\,m)$ to $(RF_1 = 1\,m, RF_2 = 0\,m)$. Extending the liquid levels beyond this range adversely affects the recovery, production rate, and energy cost. This can be attributed to the increase in "holdup loss" with larger decanter holdup while the "operation loss" as a function of decanter performance is almost equal for all cases in this range. On the other hand, process time decreases with extending the liquid level beyond $(H_1 = 0.2\,m, H_2 = 0.1\,m)$. This can be explained by lower fractional recovery induced by larger "holdup loss" that implies on a smaller quantity of mixture to be purified and consequently needs a shorter process time.

Two extra points are also tested to determine the effects of H_1 and H_2 independently. The results are presented in Figure 4-7. According to this figure, a larger H_2 and a smaller H_1 is the best possible combination, and this general

conclusion should be considered in decanter design and control for other units with different configurations or capacities. In other words, a sufficient aqueous phase residence time in the decanter (large H_2) ensures no MIBK loss along with the aqueous phase outlet stream, and a smaller MIBK-rich phase holdup quantity (small H_1) reduces the holdup loss. It should be noted that this conclusion is based on an ideal condition specified in the simulation case, while in a real case, there are still some restrictions dictated by connection size, controller response time, space for instruments, liquid level calming, and turbulence control that might override this conclusion.

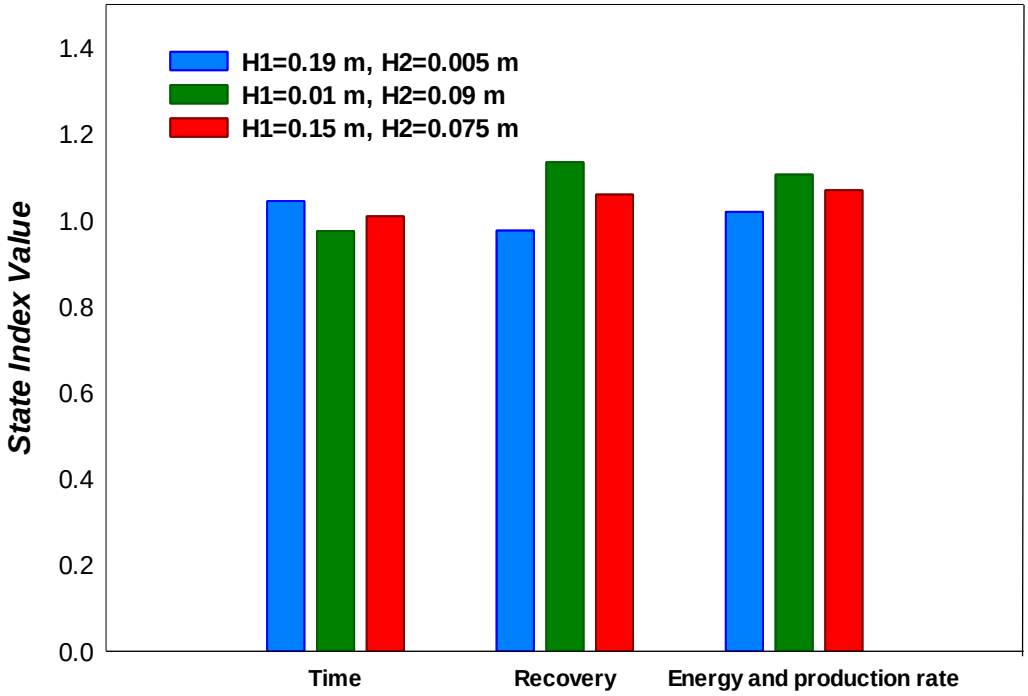

Figure 4-7. Comparison of state indexes in Mode II with different liquid levels in decanter

4.3.4. Inverted batch distillation (Mode III)

Operation with an inverted batch distillation configuration is simulated at different feeding times (flow rates) with the same amount of feed (15 kg). Considering the decanter evaluation in Mode II, decanter liquid levels of $H_1 = 0.15\,m$ and $H_2 = 0.075\,m$ are set in Mode III. Feeding time in the range of 0 to 66 minutes is studied. The state indexes obtained for all the scenarios evaluated are presented in Figure 4-8. The case with feeding time 0 represents the case with feed initially charged in the pot (Mode II). By applying Mode III and extending the feeding time up to 30 minutes, the unit experiences no significant change in the

state indexes. A slight improvement in recovery can be observed by extending the feeding time beyond 30 minutes. Also, the SEC, SPF, and process time improves by extending the feeding time from 30 to 54 minutes. The maximum index values, in all terms, are achieved at a feeding time of 54 minutes. A key observation here is that the total process time is 57 minutes, indicating that the feeding rate and separation rate are synchronized and both terminate almost simultaneously, as if the unit were operating in continuous mode. Further extending the feeding time increases the process time due to reaching the desired mixture purity (99.8 wt.% MIBK) before charging the entire feed quantity to the unit. Hence, the stop criteria must be revised to prevent premature convergence, allowing the operation to continue until the entire feed has been introduced into the column. Consequently, a higher purity of MIBK ($x_r > 0.998$) will be finally obtained in the still, and the total operation time will be equal to the feeding time. In other words, the batch distillation capacity (separation rate) in such cases is over the feeding rate, so the product will be over-purified, and the operation time will be controlled by feeding time. This condition can be analogized to a continuous distillation unit operating with a feed flow rate below its production capacity. Although recovery is not significantly affected by extending feeding time, the production rate and specific energy costs undergo undesirable changes. Based on these observations, it can be stated that a well-designed and properly controlled inverted batch distillation column offers a superior separation performance, but its performance strongly relies on the feeding rate and proper process planning so that it may lead to higher energy costs, lower production rates, longer process time, and even failure of the control system in case of incorrect operation scheduling/timing. Regardless of control and monitoring details, Figure 4-8 illustrates that Mode III, with an adjusted feeding time of 35 to 60 minutes, outperforms Mode II.

To explain the superior performance of Mode III, with a feeding time of 54 minutes, over that of Mode II, the profiles of the liquid and vapor flow rates entering the column are recorded, as can be seen in Figure 4-9. It is generally known that in Mode II (and Mode I), the entire feed content must be heated up to the bubble point in order to generate vapor, which takes a considerable time compared to the total operation time. Consistent with this, Figure 4-9 illustrates that there is no vapor and liquid flow within the column in a considerable fraction of the process duration for Mode II. By using an inverted batch unit (Mode III), there is no need to heat up the entire feed amount, but the amount partially charged into the unit is heated up and vaporized in a relatively short time. According to Figure 4-9, the feed

received in the pot in Mode III starts boiling immediately due to its small quantity, but the boiling declines as more fresh feed enters and causes condensation of the generated vapor. Boiling continues in a balance with the inlet liquid feed flow rate, resulting in the plot remaining nearly flat until a distinct time (approximately 12 minutes). Beyond this time, the inlet feed flow rate declines, and boiling intensifies, which indicates that the boiling rate outbalances the feed stream. On the other hand, in Mode II, the liquid feed content is heated continuously, and there is no boiling until about 13 minutes, which is approximately when the mixture reaches the bubble point. The intense boiling in Mode II can be observed after about 27 minutes. Comparing Mode II and Mode III, there is about a 15-minute time difference between the intense boiling time. This early vaporization is a potential key advantage of the gradual feeding approach, as it can accelerate the start-up step compared to a conventional batch distillation. This advantage is expected to be more significant in a process with a large feed content, in which the heat-up step takes a relatively long time to initiate vaporization. It is worth mentioning that the vapor rate profile in Mode III depends on the feeding rate, assuming a constant reboiler duty. As a result, in case of applying a high feeding rate (feeding time below 30 minutes), the boiling condition will resemble that of Mode II, and the indexes will match those of Mode II, as shown in Figure 4-8.

Observing the liquid flow profile of Mode III, the feed flow under the gravity feeding scenario enters the column at a high flow rate, and the flow rate decreases linearly with the decline of the feed tank liquid level. The decanter reaches the adjusted levels at about 40 minutes, and subsequently, the reflux stream is added to the liquid flow entering the column. In Mode II, since the feed is entirely charged into the pot, there is no liquid in the column before initiating the reflux stream at about 38 minutes. Considering the earlier vaporization in Mode III compared to Mode II, the reflux stream of Mode III was expected to form in a shorter time compared to Mode II, but it takes place later. This can be explained by the vapor-liquid contact and the resulting mass transfer in the column, which causes partial condensation of the rising vapor (internal reflux), so the reflux drum fills with a delay compared to Mode II.

Based on these observations, the superior performance of the inverted configuration (Mode III) over the conventional configuration (Mode II) can be attributed to two key mechanisms: (1) the earlier vaporization of the feed, which implies a shorter start-up and earlier production and (2) presence of a descending liquid flow from the beginning of operation, which drives the mass transfer

(stripping) within the column. The former expresses the impact of gradual feeding, and the latter expresses the impact of feeding location.

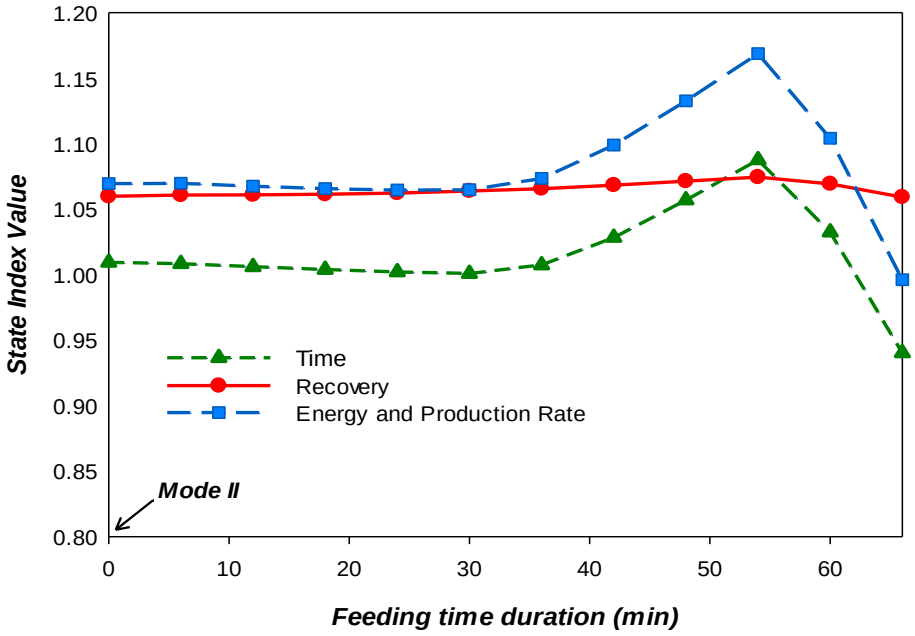

Figure 4-8. Effect of feeding time duration on distillation performance using Mode III (Inverted batch distillation)

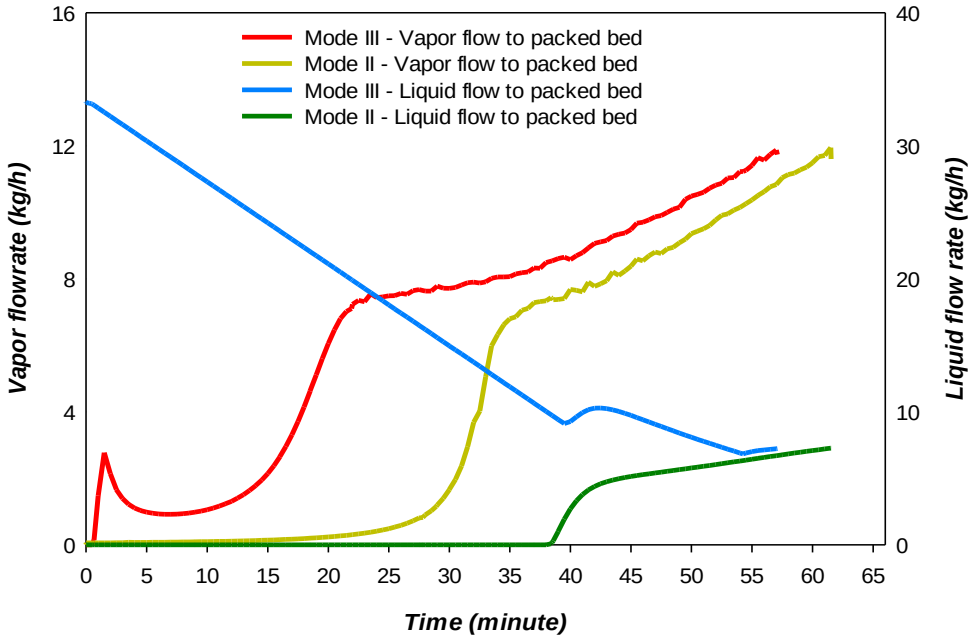

Figure 4-9. Vapor and liquid flow rate into the packing section for Mode III (feeding time: 54 min.) and Mode II.

4.4. Conclusion

Batch distillation of a heteroazeotropic binary mixture is studied employing three different unit configurations: Mode I represents a conventional unit, Mode II is a unit equipped with a decanter, and Mode III is an inverted batch distillation unit equipped with a decanter.

Evaluating the conventional distillation unit, Mode I shows that the total reflux step for starting up the operation is not necessary for the studied process and skipping it can offer even better unit performance. Also, the reflux ratio of $RR = 1$ ($RF = 0.5$) provides the maximum SPF and SEC, making it the optimal reflux ratio based on the "sequential batches" perspective. The feed quantity is also recognized as an effective factor, and a larger quantity of feed results in lower SEC and higher SPF, which is due to the lower ratio of holdup to feed quantity.

On the other hand, Mode II demonstrates superior performance compared to Mode I across the entire range of operations, which highlights the impact of a decanter on distillation performance. It was found that a decanter with a relatively high separation efficiency ($RF_1 = 0.875$ and $RF_2 = 0.125$) offers the most efficient distillation. In contrast, a perfect decanter ($RF_1 = 1$ and $RF_2 = 0$) may result in a lower production rate and higher energy cost since it relies on a relatively larger liquid holdup that causes a greater holdup loss. Therefore, optimizing decanter performance in Mode II shall involve balancing operational losses with holdup losses. Applying Mode II for MIBK-water separation offered up to 6% improvement in fractional recovery and up to 7% improvement in SEC and SPF compared to Mode I. It is also realized that, overall, a smaller organic phase holdup combined with a larger aqueous phase holdup in the decanter benefits the process in all aspects. The results showed that employing a high feeding rate in Mode III results in no significant change compared to Mode II, while extending the feeding time over a specific value benefits the process in all aspects. Moreover, there is an optimal feeding time that maximizes the state indices; extending the feeding time beyond this point adversely affects the state indexes. In the present study, the optimal feeding time for processing 15 kg of MIBK-water mixture is 54 minutes. In this case, the entire operation takes only 57 minutes, suggesting that the unit performance approximates continuous distillation, with separation and feeding ending almost simultaneously. In this study, the inverted batch distillation unit (Mode III) demonstrated approximately a 7% improvement in fractional recovery, a 9% reduction in process time, and around a 17% enhancement in SPF and SEC

compared to Mode I. The improvement in the operation performance is attributed to (1) the gradual feeding, which results in an earlier boiling/vaporization and shorter heat-up step, and (2) top feeding, which provides the vapor-liquid contact and stripping within the column immediately by starting the evaporation.

Outlook on the future: The inverted batch distillation, and generally the gradual feeding approach, is found as a practical approach to upgrade the batch distillation process. Also, an existing batch distillation unit can be transformed into a semi-batch distillation unit with minor changes in unit configuration and simple operational instructions. Moreover, due to the analogy to continuous distillation, it poses a great potential for further performance improvement by employing the techniques developed and applied for continuous distillation. Applying various feeding profiles and heat recovery strategies is planned as the next step to fully harness the potential of this approach. Additionally, the impact of feed location and gradual feeding in Mode III will be assessed to characterize this approach and advance its technical readiness for practical application. Regarding the decanter performance, employing an empirical model for phase separation prediction can also be an effective approach to achieve higher accuracy in simulation and design.

4.5. References

[1] S.E. Gad, Methyl Isobutyl Ketone, in: P. Wexler (Ed.), Encyclopedia of Toxicology (Second Edition), Second Edition, Elsevier, New York, 2005: pp. 79–81. https://doi.org/https://doi.org/10.1016/B0-12-369400-0/00615-3.

[2] S.D. Jackson, A.S. Canning, E. Mcleod, G.M. Parker, 89 - Strong Base Catalysts for Fine Chemical Synthesis: Relating Reaction Energetics to Base Strength, in: K. Eguchi, M. Machida, I. Yamanaka (Eds.), Science and Technology in Catalysis 2006, Elsevier, 2007: pp. 401–404. https://doi.org/https://doi.org/10.1016/B978-0-444-53202-2.50089-0.

[3] D.B. Kaymak, Design and control of an alternative intensified process configuration for separation of butanol-butyl acetate-methyl isobutyl ketone system, Chemical Engineering and Processing - Process Intensification 159 (2021) 108233. https://doi.org/https://doi.org/10.1016/j.cep.2020.108233.

[4] C. Barker, European MIBK spot prices continue to rise on feedstocks, Tightness, (2017). https://www.icis.com/explore/resources/news/2017/02/14/10078953/e uropean-

mibk-spot-prices-continue-to-rise-on-feedstocks-tightness/ (accessed February 6, 2024).

[5] F. Denes, P. Lang, G. Modla, X. Joulia, New double column system for heteroazeotropic batch distillation, Comput Chem Eng 33 (2009) 1631–1643. https://doi.org/https://doi.org/10.1016/j.compchemeng.2009.01.011.

[6] W.L. Luyben, Control of the Heterogeneous Azeotropic n-Butanol/Water Distillation System, Energy & Fuels 22 (2008) 4249–4258. https://doi.org/10.1021/ef8004064.

[7] S.S. Parhi, G.P. Rangaiah, A.K. Jana, A novel vapor recompressed batch extractive distillation: Design and retrofitting, Sep Purif Technol 260 (2021). https://doi.org/10.1016/j.seppur.2020.118225.

[8] H. Zhang, S. Wang, J. Tang, N. Li, Y. Li, P. Cui, Y. Wang, S. Zheng, Z. Zhu, Y. Ma, Multi-objective optimization and control strategy for extractive distillation with dividing-wall column/pervaporation for separation of ternary azeotropes based on mechanism analysis, Energy 229 (2021). https://doi.org/10.1016/j.energy.2021.120774.

[9] F. Zhao, Z. Xu, J. Zhao, J. Wang, M. Hu, X. Li, Z. Zhu, P. Cui, Y. Wang, Y. Ma, Process design and multi-objective optimization for separation of ternary mixtures with double azeotropes via integrated quasi-continuous pressure-swing batch distillation, Sep Purif Technol 276 (2021). https://doi.org/10.1016/j.seppur.2021.119288.

[10] G. Miao, K. Zhuo, G. Li, J. Xiao, An advanced optimization strategy for enhancing the performance of a hybrid pressure-swing distillation process in effective binary-azeotrope separation, Sep Purif Technol 282 (2022). https://doi.org/10.1016/j.seppur.2021.120130.

[11] L. Hegely, P. Lang, Optimisation of the higher pressure of pressure-swing distillation of a maximum azeotropic mixture, Energy 271 (2023). https://doi.org/10.1016/j.energy.2023.126939.

[12] Z. Zhang, Y. Wang, M. Zhang, C. Guang, M. Li, J. Gao, Energy-saving investigation of pressure-swing distillation strengthening configurations for benzene/isobutanol binary azeotrope, Sep Purif Technol 296 (2022). https://doi.org/10.1016/j.seppur.2022.121381.

[13] M. Ferchichi, L. Hegely, P. Lang, Economic and environmental evaluation of heat pump-assisted pressure-swing distillation of maximum-boiling azeotropic

mixture water-ethylenediamine, Energy 239 (2022). https://doi.org/10.1016/j.energy.2021.122608.

[14] A. Yu, Q. Ye, J. Li, Y. Wang, Q. Rui, Energy-saving improvement of heat integration and heat pump for separating multi-azeotropes mixture via novel pressure swing distillation, Chem Eng Sci 282 (2023). https://doi.org/10.1016/j.ces.2023.119239.

[15] D.Y. Aqar, I.M. Mujtaba, Economic feasibility of an integrated semi-batch reactive distillation operation for the production of methyl decanoate, Sep Purif Technol 257 (2021). https://doi.org/10.1016/j.seppur.2020.117871.

[16] D.Y. Aqar, A.S. Abbas, R. Patel, I.M. Mujtaba, Optimisation of semi-batch reactive distillation column for the synthesis of methyl palmitate, Sep Purif Technol 270 (2021). https://doi.org/10.1016/j.seppur.2021.118776.

[17] C. Zhang, Y. Liu, Z. Gao, L. Huang, J. Xiong, Process design, simulation and experimental studies of heteroazeotropic batch distillation for phenol dehydration, Chemical Engineering Research and Design 195 (2023) 682–690. https://doi.org/10.1016/j.cherd.2023.05.062.

[18] T. Ooms, S. Vreysen, G. Van Baelen, V. Gerbaud, I. Rodriguez-Donis, Separation of ethyl acetate–isooctane mixture by heteroazeotropic batch distillation, Chemical Engineering Research and Design 92 (2014) 995–1004. https://doi.org/https://doi.org/10.1016/j.cherd.2013.10.010.

[19] H. Gao, F. Zhao, L. Zhu, F. Yang, Y. Wang, D. Li, Dehydration of a Dilute Acetic Acid-Water Mixture via Batch Heteroazeotropic Distillation, Chem Eng Technol 44 (2021) 477–487. https://doi.org/10.1002/ceat.202000367.

[20] G. De Guido, C. Monticelli, E. Spatolisano, L.A. Pellegrini, Separation of the Mixture 2-Propanol + Water by Heterogeneous Azeotropic Distillation with Isooctane as an Entrainer, Energies (Basel) 14 (2021). https://doi.org/10.3390/en14175471.

[21] S. Skouras, V. Kiva, S. Skogestad, Feasible separations and entrainer selection rules for heteroazeotropic batch distillation, Chem Eng Sci 60 (2005) 2895–2909. https://doi.org/https://doi.org/10.1016/j.ces.2004.11.056.

[22] P. Lang, G. Modla, Generalised method for the determination of heterogeneous batch distillation regions, Chem Eng Sci 61 (2006) 4262–4270. https://doi.org/https://doi.org/10.1016/j.ces.2006.02.004.

[23] A. Yang, Z.Y. Kong, J. Sunarso, Design and optimisation of novel hybrid side-stream reactive-extractive distillation for recovery of isopropyl alcohol and ethyl acetate from wastewater, Chemical Engineering Journal 451 (2023) 138563. https://doi.org/https://doi.org/10.1016/j.cej.2022.138563.

[24] K. Jayant, C. Gupta, S. Seethamraju, S.M. Mahajani, Entrainer assisted production of high purity 2-phenyl ethyl acetate by reactive distillation, Sep Purif Technol 331 (2024) 125650. https://doi.org/https://doi.org/10.1016/j.seppur.2023.125650.

[25] U. Diwekar, Batch Distillation: Simulation, Optimal Design, and Control, Second Edition, CRC Press, 2011. https://books.google.es/books?id=jH06DwAAQBAJ.

[26] E. Sorensen, Chapter 5 - Design and Operation of Batch Distillation, in: A. Górak, E. Sorensen (Eds.), Distillation, Academic Press, Boston, 2014: pp. 187–224. https://doi.org/https://doi.org/10.1016/B978-0-12-386547-2.00005-3.

[27] H. Yu, Q. Ye, H. Xu, X. Dai, X. Suo, R. Li, Comparison of alternative distillation processes for the maximum-boiling ethylenediamine dehydration system, Chemical Engineering and Processing: Process Intensification 97 (2015) 84–105. https://doi.org/10.1016/j.cep.2015.09.008.

[28] B. Nemeth, L. Hegely, P. Lang, Investigating the processing capacity of batch distillation by applying a second, smaller column, Sep Purif Technol 280 (2022). https://doi.org/10.1016/j.seppur.2021.119883.

[29] K.-J. Kim, U. Diwekar, Batch distillation, in: Batch Processes, CRC Press, 2005: pp. 119–162.

[30] H.A. Kooijman, E. Sorensen, Recent advances and future perspectives on more sustainable and energy efficient distillation processes, Chemical Engineering Research and Design 188 (2022) 473–482. https://doi.org/10.1016/j.cherd.2022.10.005.

[31] M.I. Parma-García, J.A. Díaz-López, A. Nieto-Márquez, Separation of a water/MIBK mixture by batch heteroazeotropic distillation: A self-entrained case, Chemical Engineering and Processing - Process Intensification 171 (2022). https://doi.org/10.1016/j.cep.2021.108761.

[32] S. Niazi, J. Antonio Díaz-López, A. Nieto-Márquez, Process design and simulation of methyl isobutyl ketone (MIBK) dehydration by batch distillation: A

study on unit configuration and operational policies, Sep Purif Technol (2024) 127942. https://doi.org/10.1016/j.seppur.2024.127942.

[33] V. Diky, R.D. Chirico, A.F. Kazakov, C.D. Muzny, M. Frenkel, ThermoData Engine (TDE): software implementation of the dynamic data evaluation concept. 3. Binary mixtures, J Chem Inf Model 49 (2009) 503–517. https://doi.org/10.1021/ci800345e.

[34] E.E. Ludwig, Applied Process Design for Chemical and Petrochemical Plants, Gulf Professional Publishing, 1997.

[35] J. Stichlmair, J.L. Bravo, J.R. Fair, General model for prediction of pressure drop and capacity of countercurrent gas/liquid packed columns, 1989.

[36] B. Nemeth, L. Hegely, P. Lang, Comparison of batch heteroazeotropic distillation operational strategies for the dehydration of isopropanol, Chemical Engineering Research and Design 146 (2019) 486–498. https://doi.org/10.1016/j.cherd.2019.04.033.

[37] I. Rodríguez Donis, V. Gerbaud, X. Joulia, Heterogeneous entrainer selection for the separation of azeotropic and close boiling temperature mixtures by heterogeneous batch distillation, Ind Eng Chem Res 40 (2001) 4935–4950. https://doi.org/10.1021/ie0010363.

[38] S. Skouras, V. Kiva, S. Skogestad, Feasible separations and entrainer selection rules for heteroazeotropic batch distillation, Chem Eng Sci 60 (2005) 2895–2909. https://doi.org/10.1016/j.ces.2004.11.056.

[39] S. Skouras, S. Skogestad, V. Kiva, Analysis and control of heteroazeotropic batch distillation, AIChE Journal 51 (2005) 1144–1157. https://doi.org/10.1002/aic.10376.

[40] W.D. Monnery, W.Y. Svrcek, Successfully specify three-phase separators, Chem Eng Prog 90 (1994) 29.

[41] D.W. Green, R.H. Perry, Liquid-Liquid Extraction and Other Liquid-Liquid Operations and Equipment, McGraw Hill Professional, 2007.

[42] Y.B. Li, T.S. He, Z.M. Hu, Y.Q. Zhang, Q. Luo, W.F. Pu, J.Z. Zhao, Study on the mathematical model for predicting settling of water-in-oil emulsion, J Pet Sci Eng 206 (2021). https://doi.org/10.1016/j.petrol.2021.109070.

[43] C.S. Robinson, E.R. Gilliland, Find distillation stages graphically, Chem. Eng 65 (1985) 129.

[44] H.Z. Kister, J.R. Haas, D.R. Hart, D.R. Gill, Distillation design, McGraw-Hill New York, 1992.

[45] E. Sørensen, S. Skogestad, Comparison of regular and inverted batch distillation, Chem Eng Sci 22 (1996) 4949–4962.

[46] C. Bernot, M.F. Doherty, M.F. Malone, Feasibility and separation sequencing in multicomponent batch distillation, Chem Eng Sci 46 (1991) 1311–1326.

[47] D. George Akpan, Performance of Internals in Three-Phase Tank Separators, 2013. https://ntnuopen.ntnu.no/ntnu-xmlui/handle/11250/240273 (accessed June 26, 2024).

5. Heat integration and process improvement of a batch distillation unit using a gradual feeding strategy: a case study on MIBK-water separation

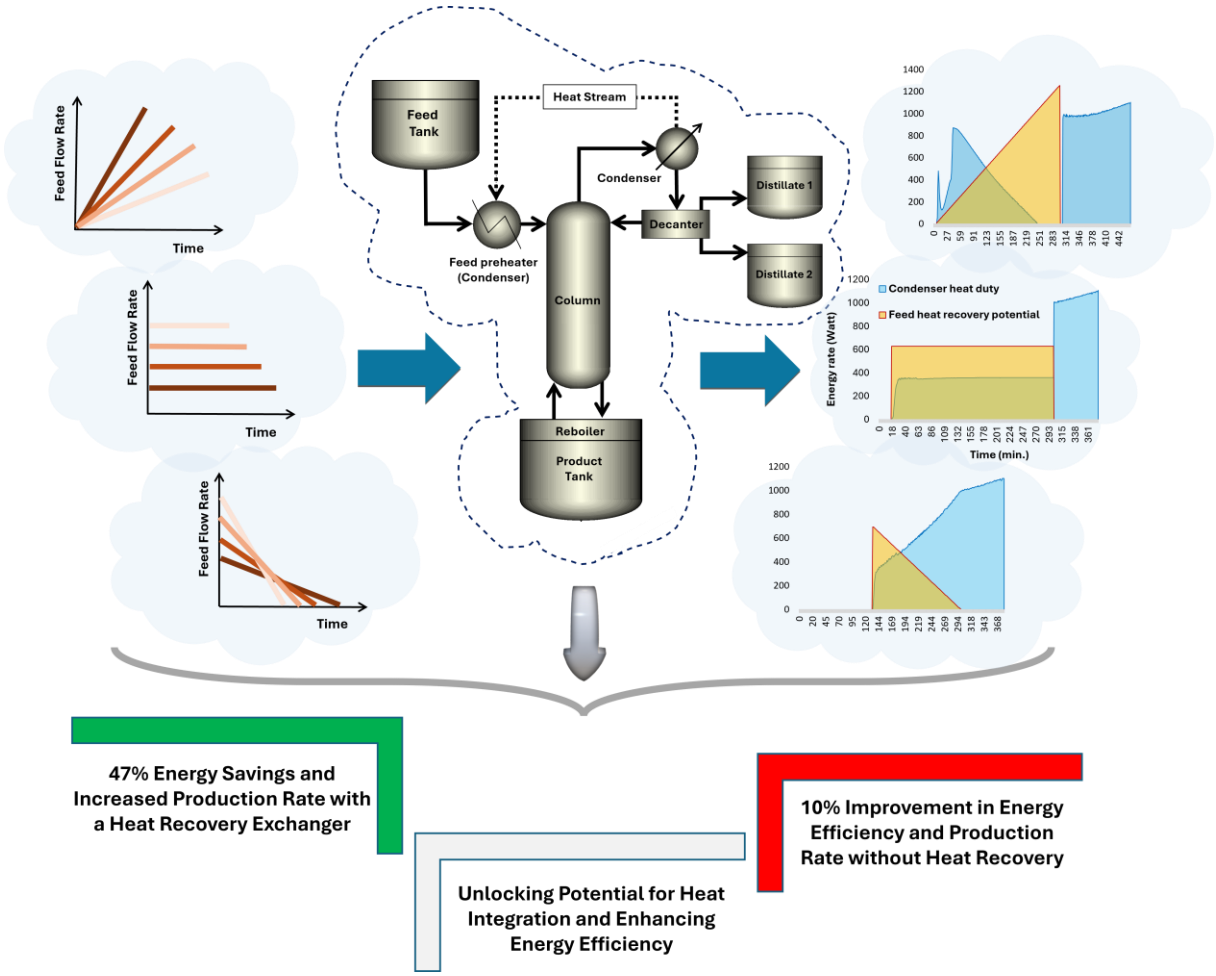

Abstract

This work focuses on upgrading a batch distillation unit in terms of energy efficiency and production capacity. Dehydration of methyl isobutyl ketone (MIBK) is performed as a case study. Since the MIBK-water mixture forms a heteroazeotrope, a decanter is applied to facilitate the separation process. The unit performance is evaluated in terms of specific product flow (SPF) and specific energy cost (SEC). Studying the impact of feed quantity in the range of 20 to 80 kg showed that due to the almost equal holdup loss, a larger batch feed quantity results in higher energy efficiency and production performance. Gradual feeding policy with different feeding strategies and locations (i.e., top feeding and bottom feeding) is also assessed in detail and compared with the conventional batch distillation process. Also, three feeding rate profiles (increasing, fixed, and decreasing) with varying feeding durations are evaluated in order to reach the optimal feeding time and profile. Overall, gradual feeding is found to be an efficient approach to upgrade the unit operation in terms of energy efficiency and production rate. Top feeding (also known as batch stripping or inverted batch distillation) has proved to be a more efficient policy for MIBK-water separation over bottom feeding. In addition, the decreasing feed flow rate scenario offers a more efficient operation compared to other feed rate profiles. Accordingly, employing the top feeding policy with a decreasing feed rate profile can lead to a 10% improvement in production rate and energy cost over a conventional batch distillation unit equipped with a decanter. Moreover, based on the gradual feeding approach, a novel and easy-to-apply strategy for heat integration and recovery in the batch distillation process is proposed, and its potential is assessed for different feeding scenarios. The proposed strategy is also found to be significantly effective in process intensification and acceleration. Applying this strategy to a batch distillation unit with top feeding at a fixed feed rate offers over 47% improvement in energy efficiency and production rate compared to a conventional batch distillation unit equipped with a decanter.

Keywords: Batch Distillation, Energy Efficiency, Heat Integration, Heat Recovery, MIBK-water, Heteroazeotropic Distillation.

5.1. Introduction

Methyl Iso-Butyl Ketone (MIBK) is a versatile solvent with a broad range of industrial applications. Its outstanding dissolution properties, biodegradability, and limited water solubility make it valuable in numerous chemical processes and in the industrial production of pharmaceuticals, paints, rubber, pesticides, cleaning solvents, etc. [1,2]. Specifically, it is used as a solvent in the paint industry, where it ends up mixed with water after use. There are also some other cases in which MIBK is polluted by a small fraction of water and needs to be recovered [3,4]. The low solubility of water in MIBK (about 2% by weight at room temperature and atmospheric pressure) allows for the mechanical removal of the major fraction of water. The remaining binary mixture forms a heteroazeotrope, similar to the water-tert-butanol (2-methyl-2-propanol) binary mixture [5] that needs to be removed by a suitable unit operation such as heteroazeotropic distillation, in continuous or batch mode. A batch distillation unit (BDU) is a suitable candidate for separation of MIBK-water mixture, especially in small production capacities and low budget for initial investment. The advantages of batch over continuous distillation can be listed as low capital cost, applicability in small scales, product traceability, possibility to cope with different separation tasks, offering a wide range of products using the same unit, availability of various configurations, and ability to handle high solid content [6–8]. Batch distillation is extensively used for purification goals or solvent recovery in the production of pharmaceuticals, polymers, fine and high-value market chemicals, and biochemical products [9,10].

Production rate and energy efficiency of a BDU, employed for separation of a heteroazeotropic mixture, can be upgraded by integrating a mechanical liquid-liquid separator into the unit. Zhang et al. [11] proposed using heteroazeotropic batch distillation for phenol dehydration as an alternative to direct distillation, providing higher product quality and approximately 20–25% energy savings. Adding a decanter to the BDU applied for MIBK dehydration has demonstrated successful operation, along with improvements in energy efficiency and production rate. To characterize the employed BDU and optimize the unit performance, effects of start-up policy, reflux ratio, decanting quality, column height, condenser temperature, and feed quantity have been studied previously. After development and characterization of an efficient unit operation based on batch distillation, a particular gradual feeding policy on unit performance was assessed, showing its positive impacts on the unit performance, including a higher production rate and

lower energy consumption [12–14]. In pursuit of our goal to develop an efficient unit operation for MIBK dehydration, developing a feasible and easy-to-apply heat integration approach to improve the energy and separation efficiency of the BDU is aimed in this study.

There are different approaches developed for heat integration and process intensification of a BDU, among which heat pumps have gained more attention recently. As representative examples, Nair and Raykar [15] used a two-stage vapor recompression (VRC) heat pump to enhance the separation of a ternary mixture of hexanol, octanol, and decanol, observing a 52% energy saving and a 12.2% total annual cost reduction. Radhika et al. [16] incorporated a double-stage VRC heat pump into a BDU to integrate heat and separate the ternary mixture. Their proposed integrated configurations resulted in a 41.7% lower energy consumption compared with a conventional BDU. Gandu et al. [17] proposed a heat pump-assisted batch distillation unit for separation of a ternary mixture aiming for reduced cost and carbon emissions. A multi-stage VRC algorithm is introduced as an alternative for the single-stage VRC approach due to its challenges with high vapor compression ratio (>3.5). They found that the feed composition determines each approach's cost-effectiveness, with the highest reported total annual cost reduction in their work being about 10%. Kazemi et al. [18] proposed using the bottom flashing heat pumps as an alternative to VRC heat pumps. They reported a total annual cost saving of 19%, using a flashing heat pump and lower annual costs in the range of 4.2-10.9% compared to the equivalent process with vapor recompression heat pumps. Modla and Lang [19] conducted a study on integrating different heat pump systems in batch distillation units, concerning the economic feasibility of heat integration and payback periods. According to their evaluation, direct application of VRC was not economically feasible, as the minimum payback period was over 10 years, while they managed to reduce it to about seven years by adding a heat exchanger. A conclusion extracted from these studies is that, while heat pumps for heat integration in a BDU offer significant improvements in energy efficiency, they face key challenges, including high capital costs, long payback periods, and complexity in design, control, and operation [20–22].

Alternatively, external energy integration by feed stream heating/flashing stands as a simple and practical approach in continuous distillation [23,24]; however, it is not feasible in batch distillation due to the absence of a feed stream. Building on the proven potential of gradual feeding to enhance unit performance in a previous study [14], this study advances the development by evaluating various feeding

strategies, including feeding locations and feed rate profiles, to identify the optimal operating policy in terms of energy cost and production capacity. Also, emerging a feed stream in the batch distillation unit unlocks the potential for heat recovery, as this feed stream can be easily heated by serving as a coolant in the condenser. Evaluating the potential of heat recovery for upgrading the batch distillation unit demonstrates a remarkable breakthrough in the unit's energy efficiency and production capacity.

5.2. Methodology and study plan

5.2.1. Simulation procedure

The simulations are conducted using the commercial package Aspen Plus V.14®, applying UNIQUAC model and the BatchSep module. The MIBK-water system exhibits significant deviations from ideality, particularly due to polarity differences between the two components and hydrogen bonding interactions. Given the moderate operating pressure (<10 bar) and the absence of electrolytes, the UNIQUAC model was selected to simulate the MIBK-water system due to its proven capability to handle highly non-ideal and polar liquid mixtures. While the UNIQUAC accuracy strongly depends on high-quality binary parameters (BIP), the validated parameters available in the Aspen Plus database ensure accurate simulation. Figure 5-1a shows the phase diagram of the MIBK-water mixture predicted by UNIQUAC together with experimental values provided by NIST Thermo Data Engine (TDE) database [25] indicating the high accuracy of this package in predicting the MIBK-water mixture behaviour. Further details on the binary mixture of MIBK-water and the methods applied for simulation are available in our previous studies [12–14]. The goal is to dehydrate a 98 wt.% MIBK solution, commonly found as a residue of paint industries, to achieve a minimum purity of 99.8 wt.% as standard purity of MIBK for reusing it as solvent.

As Figure 5-1b indicates, a conventional batch distillation unit consists of (1) a still/pot that contains the feed and embeds the reboiler, (2) the column including mass transfer media (trays or packed beds), and (3) a condenser. Some other accessories, such as a reflux drum, a decanter, a feed tank, and distillate collection tanks, might also be added to the unit, depending on the operation policy. The general geometrical features of the batch distillation unit are presented in Table 5-1, and the operating conditions defined in the simulation are presented in Table 5-2. The feed temperature is 25 ℃, and considering the still capacity, the feed

quantity can vary in the range of 20 to 80 kg. The condenser temperature is set to 85 ℃ providing a total condenser condition, and operation is conducted in atmospheric pressure. Reboiler duty (heating rate) is set to ensure processing the pot total feed capacity in less than 8 h, and the column dimensions are adjusted to handle the liquid and vapor provided by condenser and reboiler condition. The packing type is selected due to the availability in small size, and its size is selected to be small enough compared to the column diameter in order to prevent maldistribution of gas and liquid as well as providing high mass transfer efficiency due to high specific surface area.

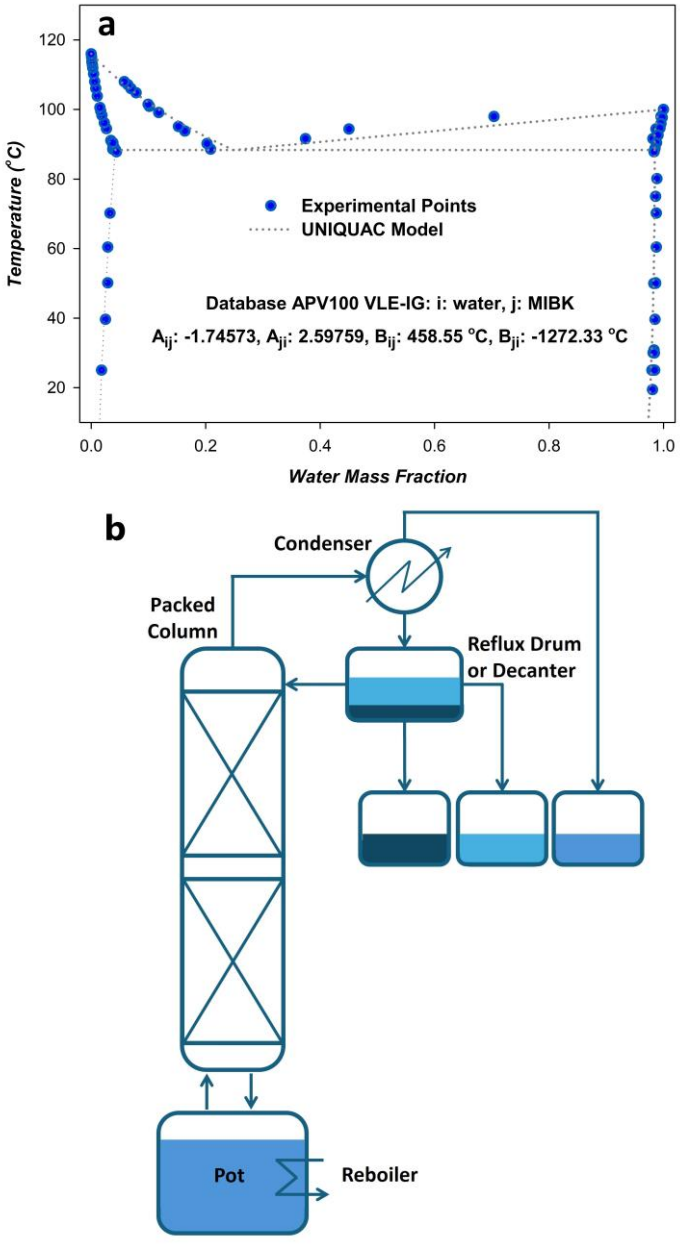

Figure 5-1. (a) Phase equilibrium diagram of MIBK-water system at 1 atm and temperature range: 0 - 116 ℃ [25] (b) Schematic view of the batch distillation unit.

Table 5-1. Geometrical and technical characteristics of simulated batch distillation unit.

Parameter	Symbol	Value/Description	Units
Applied Module	$-$	*BatchSep*	$[-]$
Still volume	V_s	*120*	$[l]$
Diameter at condenser inlet	ϕ_c	*0.1*	$[m]$
No. of distillate collectors	$-$	*3*	$[-]$
Column diameter	ϕ_s	*0.1*	$[m]$
Packing type	$-$	*Metal Raschig ring*	$[-]$
Packing size	ϕ_p	*1/2*	$[inch]$
Height of the equivalent theoretical plate	*HETP*	*1*	$[m]$
Packing Bed Height	H_p	*2*	$[m]$
Dry Packing factor	F_p	*984*	$[m^{-1}]$
Packing porosity	ε	*0.85*	$[-]$
Specific area of packing	α	*400*	$[m^2/m^3]$
Foaming (system) factor	f_f	*1*	$[-]$
Decanter diameter	ϕ_d	*0.1*	$[m]$
Decanter height	H_d	*0.4*	$[m]$

* Characteristic data for metal Raschig ring 1/2" can be found in [26].

Table 5-2. Operating conditions and general process characteristics of simulated batch distillation process.

Parameter	Symbol	Value	Units
Feed quantity	r_0	*20-80*	$[kg]$
Feed temperature	$T_f = T_{f1}$	*25*	[℃]
Product quantity (Recovered mass)	r	$-$	$[kg]$
Operating pressure (Condenser pressure)	$P = P_c$	*1*	$[atm]$
Initial MIBK mass fraction (Feed)	x_{r0}	*0.98*	$[-]$
Required MIBK mass fraction (Product)	x_r	*0.998*	$[-]$
Reboiler duty	W	*1200*	$[Watt]$
Condenser type	$-$	*Total*	$[-]$
Condenser outlet temperature	T_c	*85*	[℃]
Decanter separation efficiency	η_d	*1*	$[-]$
Organic phase (MIBK-rich) level in decanter	H_1	*0.2*	$[m]$
Aqueous phase level in decanter	H_2	*0.1*	$[m]$
Organic phase (MIBK-rich) return fraction	RF_1	*1*	$[-]$
Aqueous phase return fraction	RF_2	*0*	$[-]$

Due to the dynamic nature of the batch distillation process, all details regarding the fluids' holdup volume and flow regime within the unit are highly influential on simulation accuracy. Also, the pressure profile is a decisive factor for a precise simulation since it affects the equilibrium and, subsequently, the process evolution. Moreover, for cases involving small feed quantities, such as in batch distillation, hydraulic considerations become more critical due to the relatively high ratio of holdup volume to feed rate. Accordingly, the hydraulic calculations, including the pressure drop and flooding, are conducted using the Eckert model [27] to achieve an accurate prediction of the process.

The simulation is performed based on equilibrium stages, which is a reasonable assumption considering the small diameter of the column and packing size. As indicated in Figure 5-1a, three equilibrium phases, *vapor-liquid-liquid (VLL),* are defined and introduced to the simulation case, applying the UNIQUAC model.

A decanter is added to the unit downstream of the condenser as it is found to be an effective element in improving the heteroazeotropic batch distillation performance. Based on the simple decanter control approach described in a previous study [14], the liquid levels of $H_1 = 0.2\,m$ and $H_2 = 0.1\,m$ are set in the decanter to provide a perfect decanter condition. The term "return fraction," defined as the fraction of a condensed liquid phase returning to the column (along with the reflux stream), is applied to characterize the decanter performance. The relationship between return fraction, RF, and the well-known term reflux ratio, RR, is as follows:

$$RR = \frac{R}{D} \tag{1}$$

$$RF = \frac{R}{D+R} = \frac{RR}{1+RR} \tag{2}$$

where D and R are the mass flow rates of distillate and reflux streams, respectively. The return fraction value is bounded in the range $0-1$ in contrast with the reflux ratio that varies in the range $0\sim\infty$, which makes it easier to understand and relate to the decanter separation performance (e.g., decanting efficiency of 90% implies on $RF_1 = 0.9$ and $RF_2 = 0.1$).

The operation is defined by a constant reflux ratio for each phase, and simulation covers the operation in all steps of feeding, heating up, and production until achieving the desired purity of 99.8 $wt.$ % in the pot, defined as the simulation stop criteria. Based on the previous studies, the operation is simulated under the single-step operation (SSO) strategy, in which operation under total reflux condition as a

start-up step is skipped, and the top outlet streams (distillate) are open from the beginning of the operation. The desired product, mainly comprised of MIBK, is collected in the pot, and the aqueous phase containing a slight amount of MIBK leaves the unit as the top product and is collected in a distillate collector. The initial condition of the simulated unit is as an empty unit, and the final condition is set to discharge the holdups of the column, condenser, and decanter to the distillate collectors. The potential top product mixture is divided into three streams: (1) MIBK-rich phase liquid, (2) aqueous phase collection, and (3) vapor phase collecting. In order to simulate the operation from feeding and heat-up steps, nitrogen gas is introduced to the model as "pad gas" to initially fill the column and containers.

The *state variables* applied to evaluate the operation performance of batch distillation include process time (t), fractional recovery (η), specific product flow (SPF), and specific energy cost (SEC) as defined by the following relationships [12,28]:

$$\eta = \left[\frac{r.x_r}{r_0.x_{r0}}\right] = \left[\frac{kg_{MIBK\ obtained}}{kg_{MIBK\ fed}}\right] \quad (3)$$

$$SPF = \left[\frac{r.x_r}{t}\right] = \left[\frac{kg_{MIBK\ obtained}}{h_{operation}}\right] \quad (4)$$

$$SEC = \left[\frac{W}{SPF}\right] = \left[\frac{kJ/h_{operation}}{kg_{MIBK\ obtained}/h_{operation}}\right] = \left[\frac{kJ}{kg_{MIBK\ obtained}}\right] \quad (5)$$

5.2.2. Unit configurations and operation policies

Different parameters such as unit configuration, operation policy, accessory elements, and control strategy significantly affect the batch distillation performance. Three configurations are studied in the present work, as illustrated in Figure 5-2. The configuration, referred to as Mode I, is a conventional batch distillation unit equipped with a decanter. Mode II represents a unit with top feeding, commonly known as an inverted batch distillation unit, and Mode III is a unit with gradual feeding to the pot. The following sections provide a detailed description of the unit configurations and the operation scenarios. Different parameters, including feed quantity, feed stream position, and feed flow rate/feeding time, are studied. The detail of each assessment is presented in the following sections.

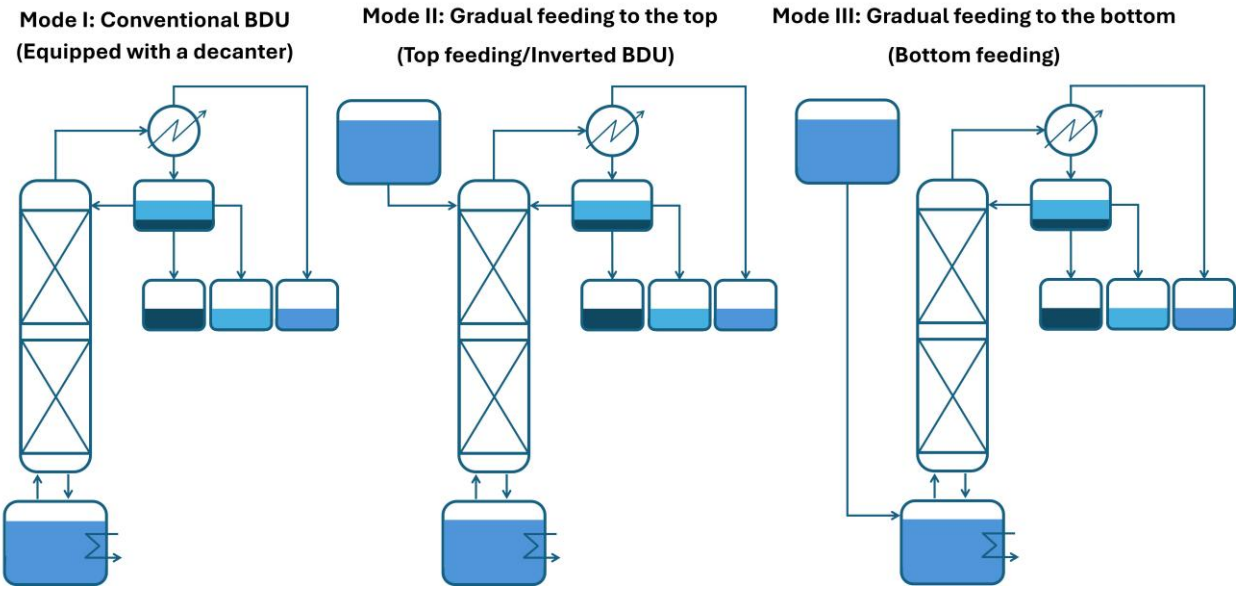

Figure 5-2. Three studied batch distillation configurations.

5.2.3. Effect of feed quantity - Mode I

As explained in section 5.2.1, the operation can be done with different feed amounts in the range of 20 to 80 kg. This limit depends on the still capacity and heating facilities of the unit. The holdup content in the column, condenser and decanter discharges at the end of operation, called "holdup loss", and its amount is almost constant, regardless of the feed quantity. Accordingly, processing a larger feed quantity at once is expected to lower the MIBK loss which consequently leads to a lower energy cost and a higher production rate. The feed quantity range of 20 - 80 kg is assessed in this part of the study to measure the impacts of feed quantity, and the relevant results are presented in section 5.3.1.

5.2.4. Top feeding (Inverted batch distillation) - Mode II

Typically, batch distillation units are initially fed in the pot, where the feed is heated during the operation. The configuration introduced as Mode II, is also known as inverted batch distillation or batch stripper [6,29,30], while the conventional batch distillation unit is known as a batch rectifier. This conveys the idea that Mode II can be applied to mixtures in which a small fraction of light components wants to be removed from heavy components, as in the MIBK-water mixture [31]. This configuration is also suggested for separation of mixtures with a minimum boiling azeotrope [32] and in cases for which the batch rectifier is not feasible [8]. The inverted batch distillation unit, modified by adding a decanter,

has been previously applied for MIBK-water separation and proved to be an efficient method for upgrading the unit performance in terms of energy efficiency and production rate [14].

The feed tank in Mode II is located above the column and contains the feed mixture at 25 ℃, which discharges to the column over the packing bed. The "feeding step" is defined and introduced to the model as the first step of the operation time schedule, in which the operation starts with the simultaneous commencement of feeding and pot heating. The feeding step finishes once the feed content is entirely discharged into the column. In the next steps, the feed stream is cut off, but the heating in the pot continues until the desired purity in the pot is achieved. The feed rate profile is specified by feeding time and the feeding scenario. Three different feeding scenarios are employed for Mode II (and Mode III), as described below:

1- Decreasing feed rate profile (gravity feeding): This scenario keeps the unit as simple as possible with no need for a fluid driver on the feed stream. It is assumed to discharge the feed mixture into the pot by opening the feed container discharge valve. The feed profile in this scenario depends on the liquid level within the feed tank, and it is assumed to decline linearly during the time until the feed tank is drained completely. For a specified feeding time of t_f, the initial and final feed flow rate will be equal to:

$$F_0 = \frac{2r_0}{t_f} \tag{6}$$

$$F_t = 0 \tag{7}$$

where r_0 is the total feed quantity, and F_0 is the feed stream flow rate at the moment of opening the valve, located on the feed tank outlet nozzle. A ramping-down profile is adjusted for the feed flow rate, which varies from F_0 to $F_t = 0$ along the feeding step duration, t_f.

2- Fixed feed rate profile: This scenario is potentially easier for operation and evaluation, but it probably needs a fluid driver and a feed flowrate control system, which impose an extra cost. Accordingly, it should be studied and well justified before applying. The feed profile in this scenario is fixed, and for a specified feeding time of t_f, the initial and final feed flow rates will be equal to:

$$F_0 = F_t = \frac{r_0}{t_f} \tag{8}$$

3- Increasing feed rate profile: This scenario also needs a fluid driver and a controller to increase the feed flow rate gradually. For a specified feeding time of t_f, the initial and final feed flow rates will be equal to:

$$F_0 = 0 \tag{9}$$

$$F_t = \frac{2r_0}{t_f} \tag{10}$$

where r_0 is the total feed quantity and F_0 is the feed stream flow rate right before opening the valve located on the feed tank outlet nozzle. A ramping-up profile is adjusted for the feed flow rate, which varies from $F_0 = 0$ to F_t along the feeding step duration, t_f.

Applying these three feed profiles with various feeding times in Mode II, the production rate and energy index is specified, and the results are presented in section 5.3.2.

5.2.5. Bottom feeding (Gradual feeding) - Mode III

Applying an inverted batch distillation unit has been proven to be an efficient approach to upgrading the studied batch distillation process [14]. Two main factors are identified as contributing to the unit's performance improvement: (1) top feeding, which leads to the contact between the descending liquid and the rising vapor, and (2) gradual feeding, which leads to an earlier feed boiling. The contribution of each factor to performance improvement needs to be determined to provide deeper insight into the operation. Accordingly, gradual feeding to the bottom of the column (below the packing bed) is also evaluated. This configuration represents a case in which the feed container and reboiler are separated, while in a conventional batch distillation unit, these elements are combined and located at the bottom of the column. Similar to the top feeding strategy assessment (section 5.2.4), three different feed profiles with various feeding times are applied and evaluated in Mode III. The results obtained for operation under this strategy and the comparison of Mode II and Mode III are presented in section 5.3.2.

5.2.6. Heat integration in a gradually fed BDU - Mode II

As explained in the section. 5.1, the primary challenge for heat recovery in a batch distillation unit is the higher temperature of the pot or reboiler compared to the top vapor stream. This temperature difference precludes the effective use of

conventional heat recovery methods or makes them economically infeasible due to high implementation costs. On the other hand, applying the gradual feeding operation policy transforms the batch process into a semi-continuous operation, in which the inlet stream with a remarkably lower temperature than the condenser has a great potential to receive the energy stream exiting the condenser. This opportunity enables us to employ the heat recovery techniques commonly implemented for continuous distillation. The first and simplest technique for heat recovery/integration is to employ a heat exchanger contacting the feed and the top vapor. Although this technique may be complex for theoretical evaluation or prediction, initial analysis and energy balance checks suggest that it can potentially (1) reduce condenser utility consumption and (2) intensify the process and accelerate the operation rate by preheating the feed, which implies higher input energy to the unit. The results and more details on heat recovery are provided in section 5.3.3.

5.3. Results and Discussion

Batch operations might be performed and analysed under two different perspectives of *single batch* and *sequential batches.* The former applies for the cases with only one time operation and the latter is applicable for the cases in which the process repeats frequently and subsequently provides a higher production capacity in the course of time. Depending on the frequency of operation and the subsequent applied perspective, different state variables should be employed to assess the operation. The evaluation of a batch unit operation in this study is done based in *sequential batches* perspective. Based on this perspective, the suitable criteria for performance evaluation are the SEC and SPF. Also, some state indexes are defined, enabling us to present the results concisely and more illustratively. These state indexes applied to present the fractional recovery, η, specific energy cost, SEC, and specific product flow, SPF, are calculated as follows [13,14]:

Recovery Index $$\eta_i = \left[\frac{\eta}{\eta_d}\right] \quad (11)$$

Production rate index: $$P_i = \left[\frac{SPF}{SPF_d}\right] \quad (12)$$

Energy cost index $$E_i = \left[\frac{SEC_d}{SEC}\right] \quad (13)$$

The letter 'd' represents the reference case, which is the case with a feed quantity of $r_0 = 80\ kg$ processed in Mode I. The state variables obtained from this case are presented in Table 5-3, and the associated state indexes are equal to 1. The higher value of state indexes implies a more favourable operation, and the values larger than 1 show the superior performance of an operation over the reference case. On the other hand, the indexes below 1 indicate a relatively unfavourable case compared to the reference case. It is worth mentioning that due to the relationship between the SPF and SEC in this study ($SEC \times SPF = W = Const.$) the relevant indexes (Eq. 12 & 13) are identical, so applying only one index is sufficient for both.

Table 5-3. State variables obtained in the reference case (Mode I with feed quantity of r_0=80 kg)

State variable	Symbol	Value	Units
Process time	t_d	402	$[minute]$
MIBK Recovery	η_d	98.86	[%]
Specific Energy Cost	SEC_d	369.2	$[kJ/kg]$
Specific Production Flow	SPF_d	11.70	$[kg/h]$

5.3.1. Effects of feed quantity - Mode I

As explained in section 5.2.3 and considering the pot volume, different feed quantities in the range 20 to 80 kg are evaluated. Figure 5-3 indicates the state indexes obtained in each case. As this graph shows, increasing the feed quantity leads to a higher recovery index as well as a higher production rate and energy index, so increasing the feed mass from 20 to 80 kg results in over 4% improvement in all state indexes. This can be explained by the smaller fraction of "holdup loss" in operations with larger feed quantities compared to multiple operations with smaller feed amount. Accordingly, the feed quantity of 80 kg is employed in the rest of this study.

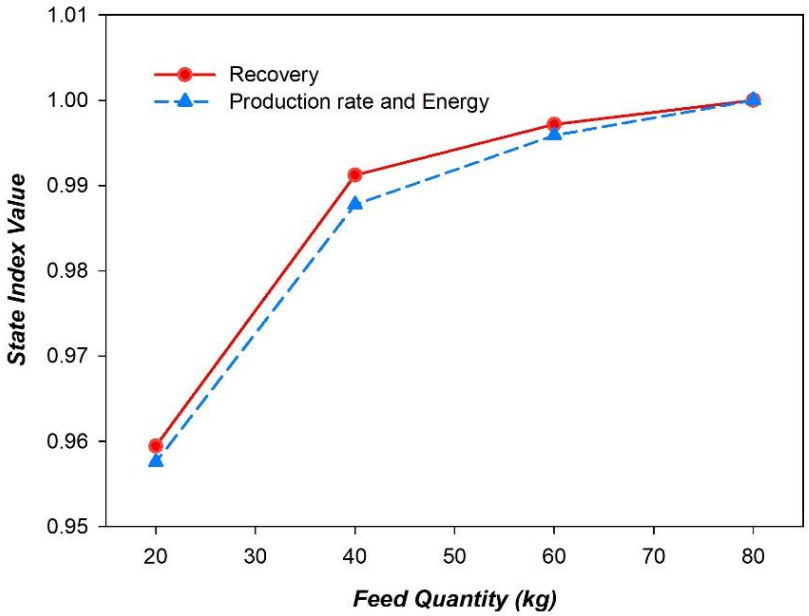

Figure 5-3. Effects of feed quantity on state indexes.

5.3.2. Gradual feeding strategy - Mode II and Mode III

Based on the operation time obtained in Mode I for processing an 80 kg feed mixture (402 min.), the feeding time in the range of 0 to 390 minutes is selected for gradual feeding assessment. Different feeding times are applied to three feeding scenarios: decreasing feed rate, fixed feed rate, and increasing feed rate to assess the impact of the feeding schedule (time and profile) on the unit performance and state variables. The values of production rate and energy index obtained at different feeding schedules are shown in Figure 5-4. The point $t_f = 0$ on the x-axis corresponds to the operation in Mode I, in which the feed is already charged in the pot. As this figure shows, the short feeding times (below 120 minutes) in Mode II and Mode III change the state index (production rate and energy index) very slightly, and it is almost equivalent to Mode I. By extending the feeding time, the differences become more significant, and each feeding schedule shows a unique behaviour. Overall, Mode II (top feeding) offers a more efficient operation in all cases compared to Mode III (bottom feeding) for the same feeding schedule. The results obtained for three feeding profiles are explained below:

1- The increasing feed rate profile causes adverse changes in the state index for both Mode II and Mode III, so it is not a potentially suitable feed profile.

2- The fixed feed profile in Mode III (bottom feeding) results in adverse changes in state index, and its effect becomes more significant with extending the feeding time, while the same feeding profile in Mode II (top feeding) results in a higher

state index. The maximum state index of 1.06 is obtained at a feeding time of 300 minutes, and extending the feeding time beyond this point leads to a decline in the production rate and energy index.

3- The decreasing feed rate profile in Mode III (bottom feeding) does not change the process significantly, and the results are almost the same as Mode I, while it favours the state index in Mode II (top feeding) by extending the feeding time up to 360 minutes, at which the maximum state index is obtained. At this point, the total operation time is 365 minutes, which means the operation takes only 5 minutes longer than the feeding, and it is very close to a continuous operation. The state index of 1.10 shows a 10% improvement in energy efficiency and production rate at this point. Beyond this point, the mixture reaches the desired purity before the end of the feeding stage, so the feeding time determines the total operation time.

In the previous work [14], two main mechanisms were identified as influencing separation performance in a gradual feeding scenario in Mode II: (1) the earlier boiling of the feed, implying a shorter start-up and quicker onset of production, and (2) the presence of a descending liquid flow in top-feeding configuration, which drives the mass transfer (stripping) within the column. The former highlights the impact of gradual feeding, while the latter emphasizes the effect of feeding location (top/bottom). Accordingly, superior performance of the top feeding scenario (Mode II) over the bottom feeding scenario can be explained by the impact of vapor-liquid contact provided through introducing a downward liquid feed stream to the column, which favours the intended stripping process (MIBK dehydration) in contact with the rising vapor flow provided shortly after the operation begins. Further details on the governing mechanism and explanations for these observations are provided in section 5.3.3.

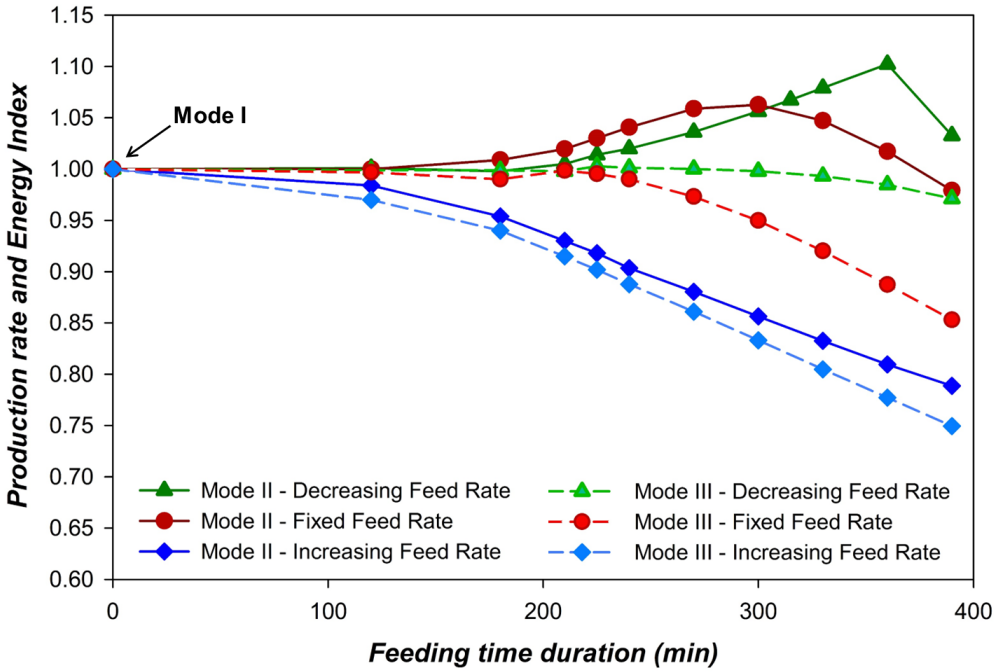

Figure 5-4. Effect of feeding time duration on distillation performance in Mode II (top feeding) and Mode III (bottom feeding)

5.3.3. Heat Recovery - Mode II and Mode III

As explained in section 5.3.2, top feeding (Mode II) is potentially a more effective approach compared to conventional feeding policy (Mode I) under a proper feeding profile, while bottom feeding (Mode III) is almost equal to or less efficient than Mode I. Regardless of these differences, both of the so-called "gradual feeding" scenarios (Mode II and Mode III) enable us to easily apply any well-developed heat recovery approach on a batch distillation unit and upgrade its energy efficiency.

Figure 5-5 illustrates a simple configuration that enables the recovery of heat from the top vapor stream to the feed stream. In this configuration, two condensers (HEX I and HEX-II) are employed. In the first one (HEX-I), which can also be referred to as a heat recovery exchanger or a feed preheater, the feed stream serves as a coolant. Due to the limits in the dynamic batch distillation module (BatchSep) provided by Aspen Plus, the proposed heat recovery configuration cannot be defined in simulations, but a fraction of the heat stream leaving the distillation column condenser is transferred to the inlet feed stream by adding a heater block to the flowsheet. Hence, the following assumptions are made to simplify the assessment and keep the solution consistent with the real case:

1- The feed stream (F-MII) can be heated up to 85℃ (below the bubble point at the azeotropic composition) and boiling in the feed stream does not take place. There is certainly potential for boiling in some cases, which may intensify the process beyond the predictions in this study. However, it is preferable to underestimate the potential of the proposed approach rather than overestimate it.
2- The condenser outlet temperature (HEX-II) is fixed to 85 ℃. Accordingly, considering the condenser as a preheater with a hot stream outlet temperature of 85 ℃, heating a cold stream to 85℃ is not a critical task, and it can be done by employing a simple and small heat exchanger, which also ensures the viability and low capital cost of the proposed solution.
3- Reboiler duty and condenser outlet temperature (HEX-II) are equal to the previously studied cases (Table 5-2). Heat recovery serves as a process intensification approach, requiring minor modifications and simple control systems in the unit.
4- Based on assumptions 2 and 3, the heat transfer/recovery to the feed begins a few seconds after initiating the condensation in the condenser. The heat recovery gradually increases the feed temperature to 85 ℃ by 10 minutes, and it remains fixed until the end of the feeding step.

According to these assumptions, the estimation of heat recovery potential in this study is conservative and it is possibly higher in real cases compared to the results provided in this study. Before addressing heat recovery, a primary evaluation is conducted on the potential of heat recovery and subsequent operation enhancement through theoretical discussion. To this end, the condenser heat duty profile during the process is compared to the inlet feed heat absorption potential, that is calculated as the maximum enthalpy change that can undergo when changing its temperature from T_{f1} and T_{f2}, which are the feed temperature upstream and downstream of the heat recovery exchanger, equal to 25 ℃ and 85 ℃, respectively. Accordingly, the instant heat recovery to the feed stream, dQ, is determined as follows:

$$dQ = FC_p\left(T_{f2} - T_{f1}\right)dt \tag{14}$$

where, F is the feed mass flow rate, C_p is the feed mixture specific heat capacity and t is the process time duration. Integrating this relationship over the process time results in the potential capacity of heat recovery by feed stream, Q.

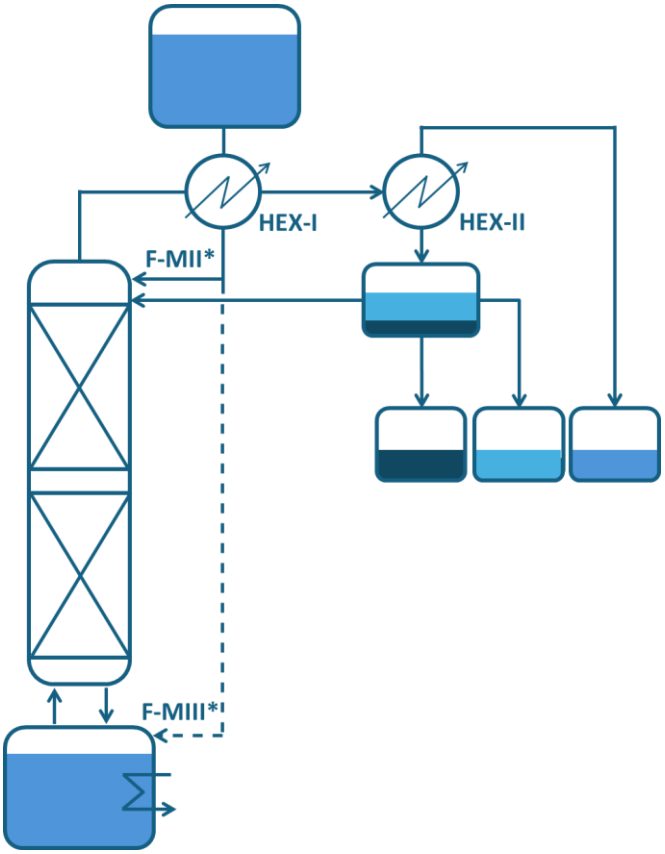

Figure 5-5. Proposed configuration for heat recovery from top vapor to the feed stream in a batch distillation unit operating under gradual feeding scenario (Mode II / Mode III).
* Feed streams, F-MII and F-MIII, correspond to Mode II and Mode III, respectively.

Figure 5-6 presents the temporal variation of condenser heat duty and the estimated heat recovery potential of the feed stream for Mode II and Mode III at the same feeding time (300 minutes). As this figure shows, the condensation starting time depends on the feed rate profile (increasing, decreasing, or fixed rate) and the feeding location (top or bottom). The condenser heat duty and the feed heat recovery potential follow the same trend in Mode II and Mode III, and there are only minor differences between the two configurations. On the other hand, different feed profiles lead to distinctly different unit behaviours, highlighting the significant impact of the feed rate profile. These observations align with Figure 5-4 and the discussions in section 5.3.2. According to Figure 5-6, the condenser heat duty and the heat recovery potential, which are equal to zero before a specific time, start rising as soon as the vapor reaches the condenser. The condenser heat duty profile reflects the dynamic behaviour of vaporization in the reboiler and condensation in the condenser.

Comparing different feeding locations (Mode III vs. Mode II), condensation begins sooner in Mode III (bottom feeding) than in Mode II (top feeding). Also, the condenser duty increases gradually in Mode III while it rises sharply in Mode II. This ramping trend gains importance in the feed stream temperature rising time since the heat transfer to the feed cannot exceed the condenser heat duty. In the present study, a 10-minute period for raising the feed stream temperature has been adjusted based on this limitation (assumption no. 4, section 5.3.3). Comparing different feeding profiles (increasing, decreasing, or fixed feed rate) shows that boiling and condensation start sooner for an increasing feed flowrate, followed by the fixed feed flowrate and the decreasing feed flowrate, respectively.

Despite the earlier boiling and condensation in Mode III, which implies a shorter start-up and earlier production, it results in a longer operation time compared to Mode II (see section 5.3.2). Also, despite the shorter start-up period by applying an increasing feed rate profile (in both Mode III and Mode II), it results in a longer operation time (section 5.3.2) and the lowest state indexes compared to other feed rate profiles (even lower than Mode I). The undesirable results obtained from a top feeding configuration (Mode III) with an increasing feed rate profile indicate that the suitable feeding location and early boiling/condensation initiation (shorter start-up period) do not necessarily guarantee a desired operation. This suggests that there is a third factor influencing the operation: the stability of operation and quality of liquid-vapor contact within the column. This stability is defined by uninterrupted vapor and liquid streams with well-balanced flow rates, ensuring neither dominates each other nor disrupts the process. Maintaining these conditions creates a favourable hydraulic environment, preventing issues such as flooding, dry stages, choking, or suppressed boiling in the pot. In other words, consistent vapor and liquid streams with properly balanced flow rates is the key to efficient operation and desirable results. Accordingly, the unfavourable performance of Mode II (top feeding) with an increasing feed rate can be attributed to interrupted boiling and condensation, as illustrated in Figure 5-6. The results for the three feeding profiles are outlined below:

- For the increasing feed rate profile, boiling and condensation take place soon after starting the operation, which is due to the small content of the mixture within the unit. As explained, having a shorter start-up period in this case does not lead to a desirable result, and it offers the lowest state indexes compared to other studied operation policies. As shown in Figure 5-6, the condenser heat duty starts growing sharply and then declines drastically in the first few

minutes of operation. The initial sharp rise can be attributed to the small content of feed mixture vaporized immediately by reboiler, and the sharp decline is due to entering a growing rate of low-temperature liquid feed, which cools down the unit content and dampens the boiling. By further heating in the pot, the boiling intensifies again, leading to a second rise in condenser heat duty, which continues for about 15 minutes but diminishes again down to 0, which persists until the end of the feeding stage. This is also due to introducing a greater amount of low-temperature liquid feed into the unit, which lowers the pot content temperature and halts boiling. The growing rate of liquid and the unstable vapor rate yield in a poorly balanced flow rate of liquid and vapor, an improper vapor-liquid contact within the column (implying a poor hydraulic condition), and ultimately leads to pausing the vapor generation by quenching the pot content. Also, the production is halted in a large fraction of the feeding period, and the operation after this period does not leverage any downward liquid flow in the column, which is similar to operation in Mode I. Accordingly, the production stage takes place initially for a short period, then it halts until the end of the feeding period, and it continues with the same principles as in Mode I. Overall, this condition resembles an interrupted operation in Mode I, and it explains why an increasing feed rate profile results in state indexes lower than Mode I. Since the interruption is basically due to entering low-temperature liquid, applying heat recovery and increasing the feed stream temperature may potentially prevent the interruption in process and accelerate the operation. A higher condenser duty compared to the feed stream heat recovery capacity at the start of the production step ensures the heat recovery potential, while after a particular time, the heat rate required to increase the feed temperature to 85 °C (based on assumption no. 1 in section 3.2) exceeds the condenser duty, which is not consistent with the heat recovery principle. This can be predicted by observing the rising profile of the feed stream heat recovery potential in Figure 5-6. In addition, the increasing feed rate, along with the boosted liquid and vapor rate induced by heat recovery, can further complicate the hydraulic conditions, escalate the risk of extreme scenarios such as flooding, and complicate the process control.

- For the fixed feed rate, the boiling and condensation start time is shorter than the decreasing feed profile and longer than the increasing feed profile. The feed heat recovery potential and the condenser duty remain constant until the end of the feeding stage. Immediately after the feed stream is cut off, a drastic rise in condenser heat duty can be observed. This happens because the liquid feed

entering the unit mitigates the boiling during the feeding phase, which lowers the vapor reaching the condenser and, subsequently, the heat duty of the condenser. These values rise sharply by cutting off the feed stream. These observations indicate that while the gradual feeding at a fixed flow rate improves the production rate and energy cost (at least in Mode II), it defers a large fraction of condenser thermal load to the end of the operation. Since this amount of heat load does not coincide with the feeding stage, it may seem out of reach for recovery by feed stream. Nevertheless, the heat recovery will intensify the process, reduce the process time, and escalate the condenser heat duty. Accordingly, an intensified process would take a shorter time after the feeding stage, and the peak heat duty at the end of the operation will be shifted to the left, where it can be recovered by feed stream. Based on this explanation, a fixed-flow feed stream has a high potential for heat recovery.

- For the decreasing feed rate profile, the heat recovery capacity of the feed stream declines linearly until it reaches $dQ = 0$ by finishing the feeding stage. Due to the relatively long delay in starting the boiling and condensation and the higher flow rate of the feed stream at first, a large fraction of feed enters the column before observing any boiling or condensation, so it loses the potential of feed for heat recovery, and considering the limit of 85 ℃ for feed temperature and excluding the boiling in the feed stream, the remained feed content has a low potential for heat recovery. Hence, despite the superior performance of the unit under a decreasing feed profile, this feeding profile is probably not the ideal case for heat integration.

Given that feed preheating (introducing a higher temperature feed) and condenser heat duty are interdependent and changes in one directly impact the other, heat recovery is expected to elevate the condenser duty and influence the overall operation trend. In other words, a preheated feed stream (higher temperature feed) intensifies the boiling rate in the pot, which in turn leads to an increased condenser duty. Accordingly, transferring heat from the condenser outlet to the inlet feed stream initiates a complex cascade of effects.

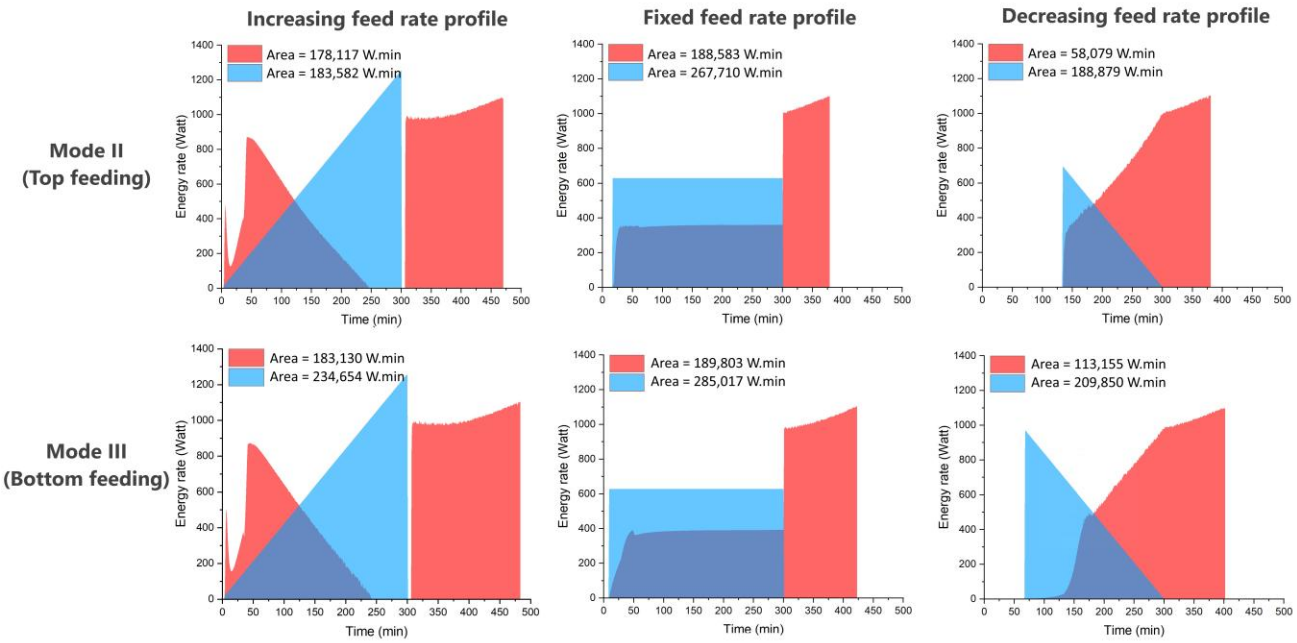

Figure 5-6. Condenser heat duty and feed stream heat recovery potential in Mode II and Mode III under different feed profiles

As explained, Figure 5-6 is applied to partially explain the observations in section 5.3.2 and assess the feasibility of heat recovery in each scenario by comparing the heat duty of the condenser and the heat absorption potential of the feed stream. Due to the higher duty of the condenser compared to the estimated potential of feed stream heat recovery capacity, higher feed temperature and partial vaporization of feed are also possibly achievable in some cases (e.g., in decreasing feed rate profile).

Since the performance of Mode II (top feeding) is considerably higher than Mode III in this study, the heat recovery scenario is only applied to Mode II to achieve the maximum potential of introduced solutions for upgrading the batch distillation operation. Also, according to the insights gained from Figure 5-6, a fixed-rate feed stream shows a great potential for heat recovery and a decreasing feed rate profile provides the highest state indexes. Accordingly, these two feed profiles are applied in Mode II for the further steps in heat recovery evaluations.

Figure 5-7 demonstrates the energy and production rate index for Mode II (top feeding) with and without heat recovery implementation. Two feeding profiles of decreasing feed rate and fixed feed rate are evaluated. According to this graph, the fixed feed flow rate is a more efficient option for heat recovery as it can improve

the production rate and energy index by 47%, while employing the decreasing feed rate profile, the maximum achievable improvement is about 22%.

The range of 210 to 330 minutes for decreasing feed profile is selected because, with the feeding times shorter than 210 minutes, the boiling/condensation starts shortly before or after feeding termination, so transferring the condenser heat outlet to the feed stream feed is impossible. Additionally, if the feeding time exceeds 330 minutes, the desired purity will be achieved before the end of the feeding stage; thereby, the feeding time will be the controlling factor, which adversely impacts the production rate and the energy index. On the other hand, the range of 210 to 330 minutes for a fixed feed rate is selected because, with the feeding times shorter than 210 minutes, the required heat duty for heating up the feed to 85 ℃ exceeds the condenser heat duty during the operation, so it is not consistent with the principles of heat recovery and the assumptions of this study. Extending the time beyond 330 minutes does not enhance the process further, as the graph shows a decline as the feeding time increases.

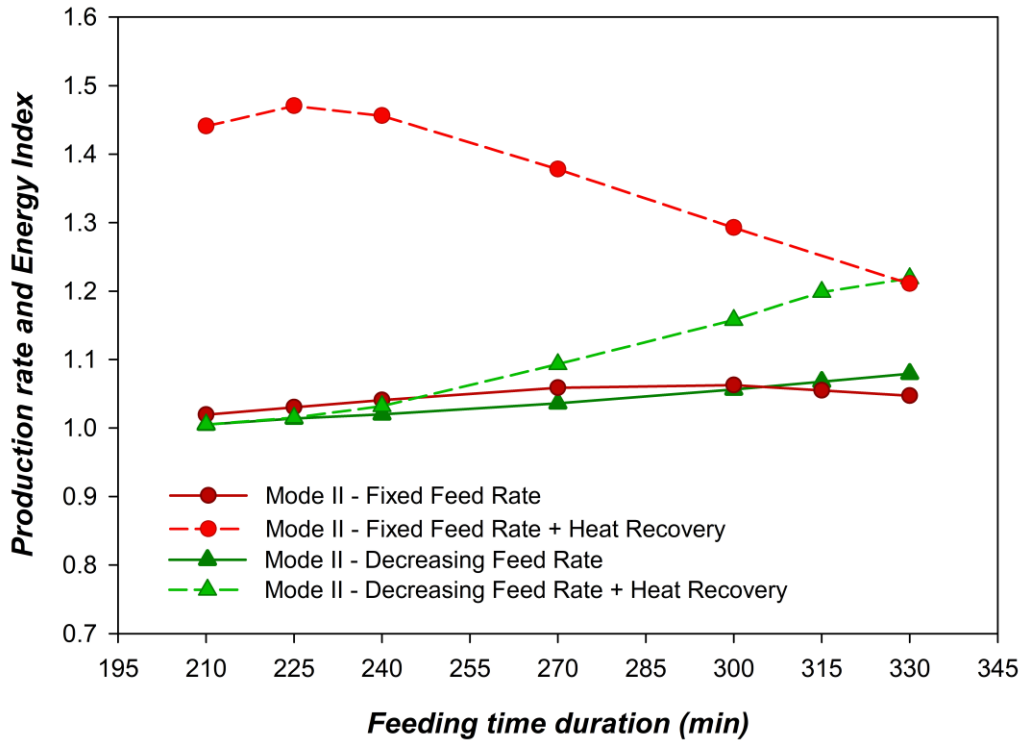

Figure 5-7. Effect of heat recovery on Mode II (top feeding) with decreasing feed rate and fixed feed rate profiles

5.4. Outlook on the future

By harnessing gradual feeding as an effective approach to improve batch distillation energy efficiency, different options become available for heat recovery. In addition to the proposed configuration in Figure 5-5, some other configurations can potentially be applied under a gradual feeding scenario, such as the one shown in Figure 5-8a. In this configuration, instead of installing a heat exchanger for contacting the top vapor and the feed stream, the top vapor passes through a coil embedded inside the feed tank. Also, as shown in Figure 5-8b, a specially designed heat exchanger with more than one coolant stream [33] can be applied instead of two condensers proposed in Figure 5-5, or a heat pump can be applied to recover energy as much as possible [20]. These ideas or any other potential solution must be assessed in detail in further studies. Also, the heat energy profiles showed that an increasing feed flow rate profile leads to a shorter heat-up step. In this case, boiling initiates earlier, making heat recovery possible from the very first minutes of operation. On the other hand, a fixed feed rate has more potential for overall heat recovery, and it facilitates operation control. Hence, a combination of these approaches is probably ideal. In this scenario, the feed stream enters the unit with a ramping-up flow rate and, after a specific time, continues at a fixed rate until the end of the operation. These scenarios can be studied in further studies, along with other heat recovery approaches already developed for continuous distillation.

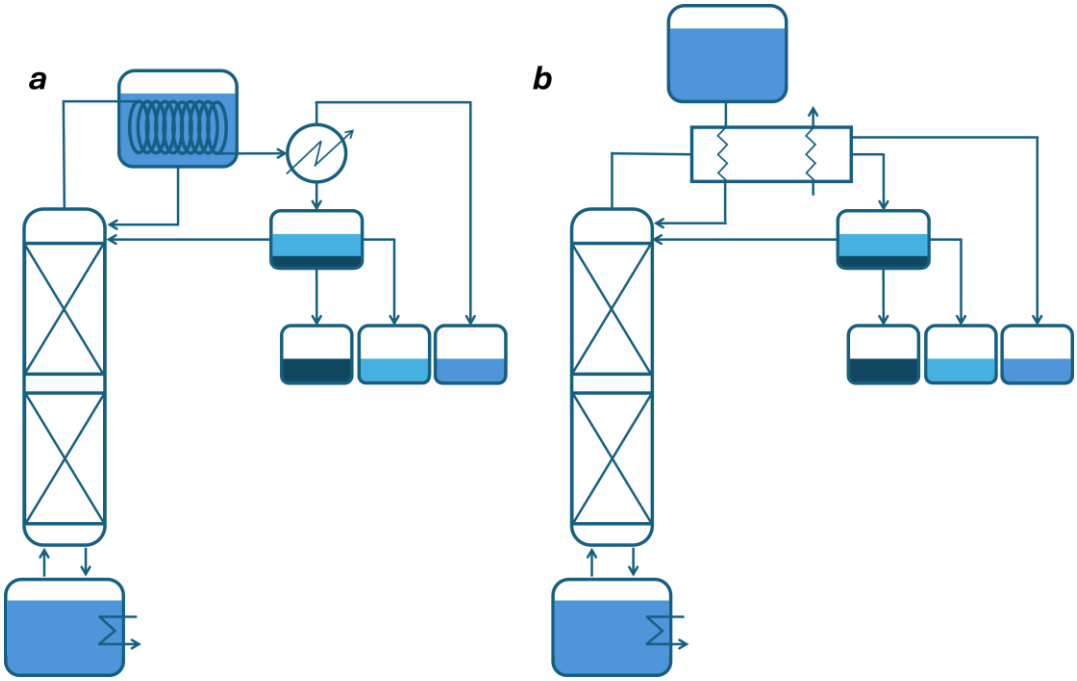

Figure 5-8. Simple alternative configurations proposed for heat recovery from top vapor to the feed

5.5. Conclusion

Batch distillation is applied for the dehydration of MIBK, which forms a heteroazeotrope with water. Three different unit configurations are evaluated in terms of production rate and energy efficiency. The main conclusions of the study on the conventional unit equipped with a decanter, Mode I, are outlined as follows:

- Evaluating the process by Mode I for different feed quantities in the range 20 to 80 kg shows that the larger feed quantity results in better unit performance, so the production rate and energy cost for 80 kg feed are around 4% better than the case with 20 kg feed. This is explained by almost constant "holdup loss" regardless of the feed quantity, which leads to a lower fraction of loss to feed in cases with a larger feed quantity.

The evaluation of batch distillation unit with gradual feeding, Mode II (top feeding), and Mode III (bottom feeding), and comparing them to Mode I revealed that:

- The top feeding approach (Mode II) is found to be a more efficient approach compared to Mode III for separation of MIBK-water binary system by offering a higher production rate and energy index in almost all studied cases.
- All feed rate profiles provide very slight differences from Mode I for feeding time below 120 minutes (high feeding rate), and the differences become more tangible with the longer feeding times.
- The decreasing feed rate profile in Mode II offers up to 10% enhancement in state index, while in Mode III it results in very slight changes.
- The fixed feed rate in Mode II can provide up to 7% improvement in state index, while in Mode III results in adverse changes.
- The increasing feed rate profile in both Mode II and Mode III results in an equal or lower state index than Mode I, and its impact aggravates with extending the feeding time.
- Three main factors are identified as contributing to the effectiveness of the gradual feeding approach: (1) boiling commencement time, (2) feeding location, and (3) the quality and quantity of vapor-liquid contact within the column. The feed flow rate and profile determine these three factors in cases with constant reboiler duty.

Based on these results, the gradual feeding approach can serve as an effective method for upgrading a batch distillation unit by employing a proper feeding

schedule (time and rate profile) and location. On the other hand, the temperature difference between the feed stream and the top vapor exiting the column in a gradual feeding scenario (Mode II or Mode III) provides a significant opportunity for heat recovery/process intensification. Leveraging this opportunity, the condenser outlet heat energy is transferred to the feed stream, heating it to 85 ℃. The results for heat recovery potential assessment are outlined as follows:

- In case of implementing heat recovery, a fixed feed flow rate offers superior performance over a decreasing feed rate.
- The proposed heat recovery approach in Mode II with a fixed feed rate offers up to 47% improvement in energy efficiency and production rate compared to Mode I, while the maximum achieved improvement with a decreasing feed rate profile is 22%.

These findings indicate that the gradual feeding policy can transform the technical and economic framework in many applications of batch distillation via unlocking the heat recovery viability.

5.6. References

[1] S.E. Gad, Methyl Isobutyl Ketone, in: P. Wexler (Ed.), Encyclopedia of Toxicology (Second Edition), Second Edition, Elsevier, New York, 2005: pp. 79–81. https://doi.org/https://doi.org/10.1016/B0-12-369400-0/00615-3.

[2] S.D. Jackson, A.S. Canning, E. Mcleod, G.M. Parker, 89 - Strong Base Catalysts for Fine Chemical Synthesis: Relating Reaction Energetics to Base Strength, in: K. Eguchi, M. Machida, I. Yamanaka (Eds.), Science and Technology in Catalysis 2006, Elsevier, 2007: pp. 401–404. https://doi.org/https://doi.org/10.1016/B978-0-444-53202-2.50089-0.

[3] D.B. Kaymak, Design and control of an alternative intensified process configuration for separation of butanol-butyl acetate-methyl isobutyl ketone system, Chemical Engineering and Processing - Process Intensification 159 (2021) 108233. https://doi.org/https://doi.org/10.1016/j.cep.2020.108233.

[4] C. Barker, European MIBK spot prices continue to rise on feedstocks, Tightness, (2017). https://www.icis.com/explore/resources/news/2017/02/14/10078953/e uropean-mibk-spot-prices-continue-to-rise-on-feedstocks-tightness/ (accessed February 6, 2024).

[5] B.S. Bhatnagar, J. Sonje, E. Shalaev, S.W.H. Martin, D.L. Teagarden, R. Suryanarayanan, A refined phase diagram of the tert-butanol–water system and implications on lyophilization process optimization of pharmaceuticals, Physical Chemistry Chemical Physics 22 (2020) 1583–1590.

[6] E. Sorensen, Chapter 5 - Design and Operation of Batch Distillation, in: A. Górak, E. Sorensen (Eds.), Distillation, Academic Press, Boston, 2014: pp. 187–224. https://doi.org/https://doi.org/10.1016/B978-0-12-386547-2.00005-3.

[7] U. Diwekar, Batch Distillation: Simulation, Optimal Design, and Control, Second Edition, CRC Press, 2011. https://books.google.es/books?id=jH06DwAAQBAJ.

[8] K.-J. Kim, U. Diwekar, Batch distillation, in: Batch Processes, CRC Press, 2005: pp. 119–162.

[9] H. Yu, Q. Ye, H. Xu, X. Dai, X. Suo, R. Li, Comparison of alternative distillation processes for the maximum-boiling ethylenediamine dehydration system, Chemical Engineering and Processing: Process Intensification 97 (2015) 84–105. https://doi.org/10.1016/j.cep.2015.09.008.

[10] B. Nemeth, L. Hegely, P. Lang, Investigating the processing capacity of batch distillation by applying a second, smaller column, Sep Purif Technol 280 (2022). https://doi.org/10.1016/j.seppur.2021.119883.

[11] C. Zhang, Y. Liu, Z. Gao, L. Huang, J. Xiong, Process design, simulation and experimental studies of heteroazeotropic batch distillation for phenol dehydration, Chemical Engineering Research and Design 195 (2023) 682–690. https://doi.org/10.1016/j.cherd.2023.05.062.

[12] M.I. Parma-García, J.A. Díaz-López, A. Nieto-Márquez, Separation of a water/MIBK mixture by batch heteroazeotropic distillation: A self-entrained case, Chemical Engineering and Processing - Process Intensification 171 (2022). https://doi.org/10.1016/j.cep.2021.108761.

[13] S. Niazi, J. Antonio Díaz-López, A. Nieto-Márquez, Process design and simulation of methyl isobutyl ketone (MIBK) dehydration by batch distillation: A study on unit configuration and operational policies, Sep Purif Technol (2024) 127942. https://doi.org/10.1016/j.seppur.2024.127942.

[14] S. Niazi, J.A. Díaz-López, A. Nieto-Márquez, Improvement of energy efficiency and production performance in a heteroazeotropic batch distillation unit:

A study on decanter control and feeding strategy, Sep Purif Technol 357 (2025) 130132.

[15] R.R. Nair, A. Raykar, Performance investigation of vapour recompressed batch distillation for separating ternary wide boiling constituents, Resource-Efficient Technologies 3 (2017) 452–458.

[16] G. Radhika, A.K. Burolia, P.K. Raghu Raja, S.R. Ambati, D.S. Patle, U.B.B. Gara, Energy saving in batch distillation for separation of ternary zeotropic mixture integrated with vapor recompression scheme: dynamics and control, Chemical Product and Process Modeling 16 (2021) 101–115.

[17] R. Gandu, A.K. Burolia, S.R. Ambati, U.B.B. Gara, Reducing total annual cost and CO2 emissions in batch distillation for separating ternary wide boiling mixtures using vapor recompression heat pump, Chemical Product and Process Modeling 18 (2023) 177–194.

[18] A. Kazemi, A. Mehrabani-Zeinabad, M. Beheshti, Novel heat pump assisted distillation configurations for energy and economic savings and their application on propylene/propane and I-butane/N-butane separation systems, Chem Eng Sci 295 (2024) 120139.

[19] G. Modla, P. Lang, Heat pump systems with mechanical compression for batch distillation, Energy 62 (2013) 403–417. https://doi.org/10.1016/j.energy.2013.09.036.

[20] A.A. Kiss, C.A.I. Ferreira, Heat pumps in chemical process industry, CRC Press, 2016.

[21] M.M. Vibhute, S.S. Jogwar, Optimal operation and tracking control of vapor-recompressed batch distillation, AIChE Journal 66 (2020). https://doi.org/10.1002/aic.17049.

[22] G. Modla, P. Lang, Heat pump systems with mechanical compression for batch distillation, Energy 62 (2013) 403–417.

[23] H.A. Kooijman, E. Sorensen, Recent advances and future perspectives on more sustainable and energy efficient distillation processes, Chemical Engineering Research and Design 188 (2022) 473–482. https://doi.org/10.1016/j.cherd.2022.10.005.

[24] M. Ledezma-Martínez, M. Jobson, R. Smith, Simulation–optimization-based design of crude oil distillation systems with preflash units, Ind Eng Chem Res 57 (2018) 9821–9830.

[25] V. Diky, R.D. Chirico, A.F. Kazakov, C.D. Muzny, M. Frenkel, ThermoData Engine (TDE): software implementation of the dynamic data evaluation concept. 3. Binary mixtures, J Chem Inf Model 49 (2009) 503–517. https://doi.org/10.1021/ci800345e.

[26] E.E. Ludwig, Applied Process Design for Chemical and Petrochemical Plants, Gulf Professional Publishing, 1997.

[27] J. Stichlmair, J.L. Bravo, J.R. Fair, General model for prediction of pressure drop and capacity of countercurrent gas/liquid packed columns, 1989.

[28] B. Nemeth, L. Hegely, P. Lang, Comparison of batch heteroazeotropic distillation operational strategies for the dehydration of isopropanol, Chemical Engineering Research and Design 146 (2019) 486–498. https://doi.org/10.1016/j.cherd.2019.04.033.

[29] C.S. Robinson, E.R. Gilliland, Find distillation stages graphically, Chem. Eng 65 (1985) 129.

[30] H.Z. Kister, J.R. Haas, D.R. Hart, D.R. Gill, Distillation design, McGraw-Hill New York, 1992.

[31] E. Sørensen, S. Skogestad, Comparison of regular and inverted batch distillation, Chem Eng Sci 22 (1996) 4949–4962.

[32] C. Bernot, M.F. Doherty, M.F. Malone, Feasibility and separation sequencing in multicomponent batch distillation, Chem Eng Sci 46 (1991) 1311–1326.

[33] M. Rahimi, S. Niazi, H. Faramarzi, M. Nazari, A. Parvareh, B. Jadidi, A.A. Alsairafi, Experimental and numerical study on a novel heat exchanger with spiral shell and U-junction tubes, Journal of Enhanced Heat Transfer 28 (2021).

6. Aspen Plus model of PEM electrolysis system for hydrogen production

Abstract

A model of a proton exchange membrane electrolyzer (PEMEL) is developed for semi-dynamic simulation purposes adaptable to typical available renewable power profiles. For unit-scale simulation, Aspen Plus is employed due to its robust capabilities in modeling a wide range of unit operations and its integrated tools for establishing detailed mass and energy balances across all process blocks involved in the electrolysis system. Since there is no built-in model for the PEMEL stack in this software, an Aspen Custom Modeler (ACM) model is developed and integrated into the Aspen Plus environment. The ACM model is based on empirical and semi-empirical correlations provided in the literature, and it comprises thermodynamic and electrochemical modeling to predict the open-circuit voltage, overpotentials, and ultimately the polarization curve. It also includes mass and energy balances within the stack. Moreover, Faraday efficiency is introduced as a function of current density. Other components of the unit are simulated using standard Aspen Plus models. The results show that the model is in close agreement with the experimental findings in the literature, making it an accurate tool for simulation of a PEM electrolyzer unit. Running the model at different operating pressures shows that lower operating pressure improves the electrolysis system's performance. Also, increasing the temperature from 40 to 80 °C results in about 13.7% lower cell voltage at a current density of 2 A/cm² (from 2.24 to 1.93). Accordingly, two different operation scenarios of (1) fixed circulating water flow rate and (2) fixed operating temperature are proposed for operation of a PEMEL unit, and the model is adapted to enable both options in simulation, aiming at a comparative study. Theoretically, while the fixed temperature operation scenario is the commonly practiced control approach, the fixed water flow rate scenario, capable of sustaining the temperature in the allowed range, offers various benefits such as simpler control system requirements, smaller heat exchanger size, higher voltage efficiency, and voiding any excess stress by variation of water flow rate in the electrolyzer cells. The provided PEMEL model and the proposed scenario are potentially adaptable to variable input power profiles, and they can be employed to carry out techno-economic evaluation of a hydrogen production unit coupled with renewable energy sources or to be integrated with downstream unit operations such as green ammonia or green methanol plants.

Keywords: Hydrogen production, Aspen Plus Model, Aspen Custom Modeler, PEM Electrolyzer, System simulation, Electrolysis Process optimization

6.1. Introduction

The energy sector remains the predominant contributor to greenhouse gas emissions within the European Union, accounting for over 75% of total emissions [1]. Recognizing this, the European Commission has set an ambitious target to increase the share of renewable energy in the EU's overall energy mix to at least 42.5% by 2030, with aspirations to reach 45% [2]. Electrification, particularly in sectors like heating and cooling, is identified as a key strategy to achieve these goals, enhancing energy efficiency and reducing reliance on fossil fuels [3].

Power-to-X technology, which utilizes renewable energy to produce various end products (referred to as e-products), is considered a promising approach for large-scale and long-term energy storage [4,5]. Hydrogen (H_2) serves as a crucial product or intermediate energy vector in the majority of Power-to-X pathways and can be generated through the electrolysis of water [6]. The environmental impact of this process is minimal, with associated emissions primarily stemming from the upstream production of renewable electricity and the manufacturing of the electrolyzer system [7,8]. Among the various electrolyzer technologies available, Proton Exchange Membrane Electrolyzer (PEMEL) stands out due to its unique features, including high current density, compact structure, flexibility, quick dynamics, fast response, and adaptability to variable energy resources [9,10]. These features, along with its technical readiness level, make it an extremely promising technology in the development of green hydrogen production, and it is expected to serve as a core element in the global shift toward carbon-neutral energy systems. This explains the recent impulse in the development of PEM electrolyzers, which were initially developed in the 1960s. Furthermore, an enhancement of efficiency from 55-60% up to 68% is predicted by 2030, which will hopefully decrease the costs of deployment [6]. Currently, integrating photovoltaic (PV) and wind turbine (WT) energy systems with PEM water electrolyzers seems to be a promising strategy to support the transition to a low-carbon economy by lowering the levelized cost of hydrogen with minimum grid dependency [11,12]. Meanwhile, this approach introduces new challenges that need to be addressed to ensure efficient, safe, and reliable operation to support the commercialization of this solution [13–15]. Simulation and modelling play a crucial role in advancing the design and optimization of hydrogen technologies by providing detailed insights into the fundamental processes and subsequently enabling faster analysis, performance prediction, and innovation. These tools can span a broad spectrum, from detailed component-level to complex multi-system level in

dynamic, semi-dynamic, or static frameworks [16]. The efforts focused on modelling in hydrogen technology, particularly in the electrolysis process, are expected to provide standardized and validated modules, applications of which extend beyond simulation of the isolated units [17]. Electrolysis operation is a multiphysics process dealing with various phenomena, including fluidics, energy transfer, thermodynamics, electrochemistry, and reaction. Accordingly, it is necessary to include different fundamental aspects of the process for modelling the electrolyzer and conduct a realistic simulation. On the other hand, while there are rigorous models to simulate the electrolyzer with high accuracy in dynamic mode or multi-dimensions, some other models are focused on an isolated part of the system (sub-system studies) [18–21]. Moreover, coupling different technologies such as PV panels or wind turbines to the electrolysis units on a large commercial scale would lead to more complications, making the rigorous dynamic and multidimensional models excessively time-consuming and impractical. Accordingly, there is a strong demand for a robust model that can adapt to variable power sources while maintaining sufficient accuracy and computational efficiency, thereby addressing both the precision and practicality requirements of a system-scale PEMEL model [22,23].

In this study, a PEMEL model is developed based on empirical and semi-empirical correlations derived from thermodynamics and electrochemistry to represent the electrical behavior of the electrolysis process through the polarization curve. Additionally, mass and energy balances are established at the system level to enable accurate simulation and realistic prediction, thereby allowing the evaluation of various process design and operational scenarios.

6.2. Theoretical background

6.2.1. PEM electrolyzer principles

PEM electrolyzers operate according to the same fundamental principle as other water electrolysis systems: they use electrical energy to drive the electrochemical decomposition of water into hydrogen and oxygen gases. A PEM electrolyzer consists of three main parts: (1) the polymer electrolyte membrane (proton exchange membrane), which is sandwiched between two electrodes, (2) the anode, and (3) the cathode, known as the membrane electrode assembly (MEA).

Figure 6-1a presents a schematic illustration of a typical PEM water electrolyzer; the electrochemical reactions at each electrode and the key stack components of a PEM electrolyzer are shown in Figure 6-1b. Each electrode section consists of a catalyst layer, a porous transport layer (PTL), also known as gas diffusion layer (GDL), a bipolar plate containing the flow channels and a current collector for connecting to the external power source for electron flow [24,25] The global reaction of a PEM electrolyzer is as follows:

$$H_2O \rightarrow H_2 + ½O_2 \quad (1)$$

In proton exchange membrane (PEM) electrolyzers, deionized water is fed into the flow channels of the bipolar plate on the anode side, where it undergoes the oxygen evolution reaction (OER) under the influence of the applied electric current, splitting into protons, electrons, and molecular oxygen [26]:

$$H_2O \rightarrow 2H^+ + ½O_2 + 2e^- \quad (2)$$

The protons (hydrogen ions) migrate through the polymer electrolyte membrane (PEM) toward the cathode, where they are reduced by electrons transferred to the cathode through a power source to produce molecular hydrogen via the hydrogen evolution reaction (HER) [26]:

$$2H^+ + 2e^- \rightarrow H_2 \quad (3)$$

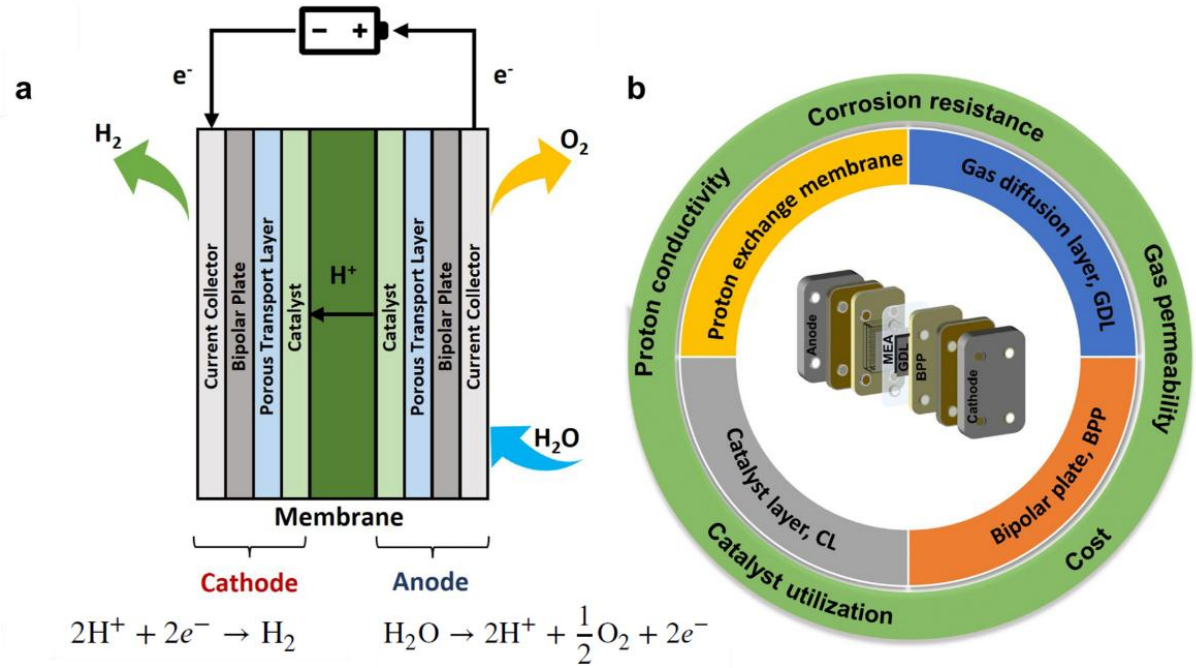

Figure 6-1. (a) Cross-sectional view of PEMEL cell and (b) key structural components and operational parameters [27,28].

6.2.2. PEMEL unit

A PEM stack is an assembly of individual cells, each containing electrodes and membranes and details, as shown in Figure 6-1. In addition to the stack, the electrolysis system includes a component essential for safe and efficient operation. Figure 6-2 illustrates a schematic of an integrated PEM electrolysis system consisting of water (1) supply tanks that store deionized water, which is fed into the system using (2) circulation pumps to maintain consistent flow through the anode side of the stack, (3) gas–liquid separators employed to separate the produced hydrogen and oxygen from residual water, (4) cooling systems, often involving cooling heat exchangers, to manage the heat generated during electrolysis and maintain optimal operating temperature (typically 40–80 °C), (5) instruments and control units including pressure sensors, thermometers, flowmeters, and (6) power electronics such as DC power supplies or rectifiers that deliver regulated voltage to the stack. There might be optional components considered in the electrolysis unit, such as dryers or purification units to ensure high gas purity, compressors to elevate the pressure of the generated gases depending on system design and end use, and storage tanks for safely collecting the produced hydrogen and oxygen.

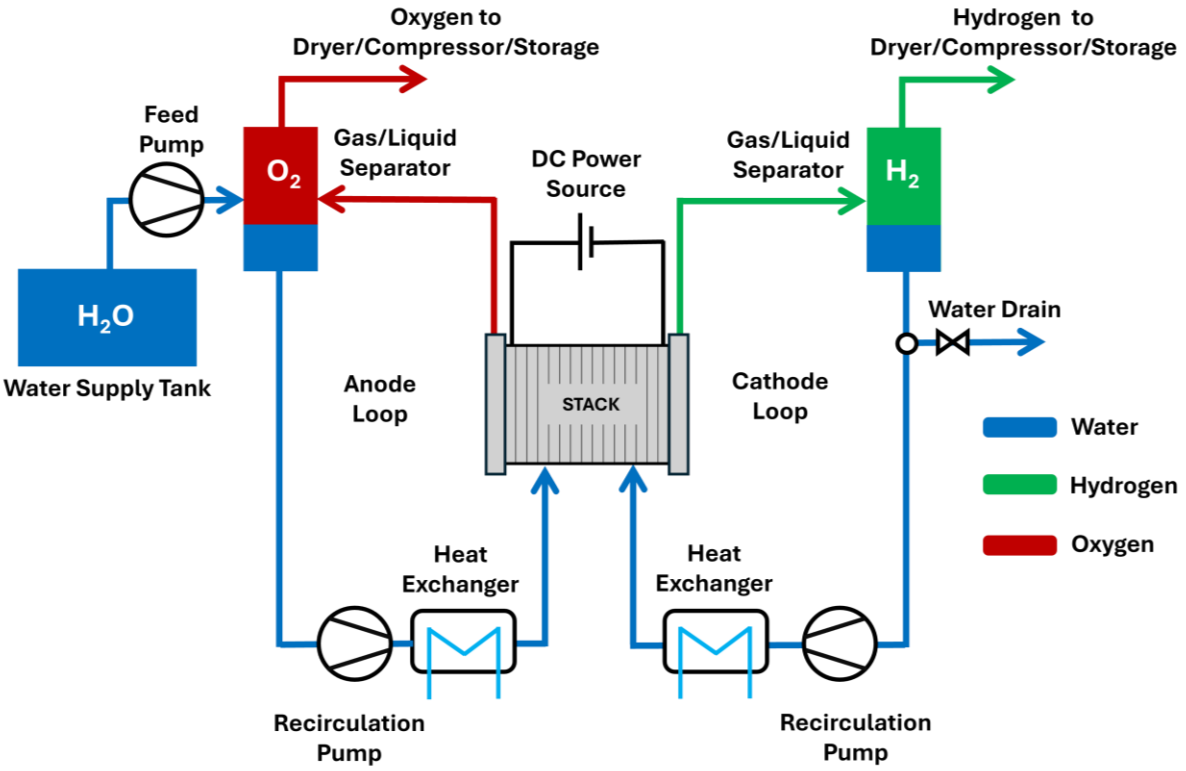

Figure 6-2. Schematic of PEM electrolysis unit [29].

In addition to serving as the reactant for electrolysis and the feedstock for hydrogen production, water performs multiple functions within the unit: it carries the generated oxygen out of the system, regulates the stack temperature, and hydrates the electrodes and membrane to prevent damage.

Although two water circuits are shown in Figure 6-2, water predominantly circulates on the anode side. The secondary water loop at the cathode can be eliminated in the case of an efficient design that ensures adequate humidification of the cathode and membrane. However, in this study, both water loops are employed to manage membrane and cathode hydration and to supply water for potential reverse water transport from the cathode to the anode, particularly at low power input levels, where the higher pressure in the cathode compartment outweighs the electro-osmotic water transport driving force from the anode to the cathode (explained in section 6.2.8.3).

6.2.3. PEMEL polarization curve

The operating principle of the PEM electrolysis cell follows the familiar relationship of the power equation in an electrical circuit, $W = IV$) which appears as ($W_{cell} = I_{cell} . V_{cell}$) for one electrolysis cell, where W_{cell} is the cell electric power input, V_{cell} is the voltage across the electrolysis cell, and I_{cell} *is* the current passing the cell. The current fundamentally defined as the number of electrons per unit of time, can be related to the molar rate of hydrogen production (2 electrons per hydrogen molecule). However, there are several nonidealities and nuances in the PEM devices that must be accounted for. The correlations applied to define the PEM stack model are presented in the following discussion.

Since the electrolysis cells in a stack are installed in series, the total power input to the electrolyzer stack, W_{stack}, will be correlated to the stack current, I_{stack}, and the stack voltage, V_{stack}, as below:

$$W_{stack} = V_{stack}. I_{stack} = V_{cell} . N_{cells}. i_{cell}. A_{cell} \quad (4)$$

where, i_{cell} is the current density, A_{cell} is the cell area, V_{cell} is a single cell voltage and N_{cell} is the number of electrolysis cells embedded in series within the stack.

Based on the correlation above, and considering the stack and the power source as a current circuit, there will be a particular cell voltage per a specific power/current input at a constant operating condition. Accordingly, electrolyzer performance can

be presented via the cell voltage corresponding to a specific current density in the cell, and the cell voltage can be defined as a function of power/current. This relationship is conventionally represented by the polarization curve, which illustrates the cell voltage as a function of current density. The polarization curve serves as a comprehensive diagnostic tool that reflects the overall electrochemical behavior of the electrolyzer. A schematic of the polarization curve is provided in Figure 6-3 with the horizontal axis of current density and vertical axis of cell voltage/potential. A major part of the research and development works on electrolyzers is contributed to achieving a polarization curve with lower voltage, as shown in this figure. According to this figure, the research can be focused on cell diagnostics to find the potential cell bottlenecks leading to malfunctions and high cell voltage or concentrated on electrode design, including the catalyst selection or hydraulic design for proper handling of the fluid flow and the stack/unit scale design for proper operation and control.

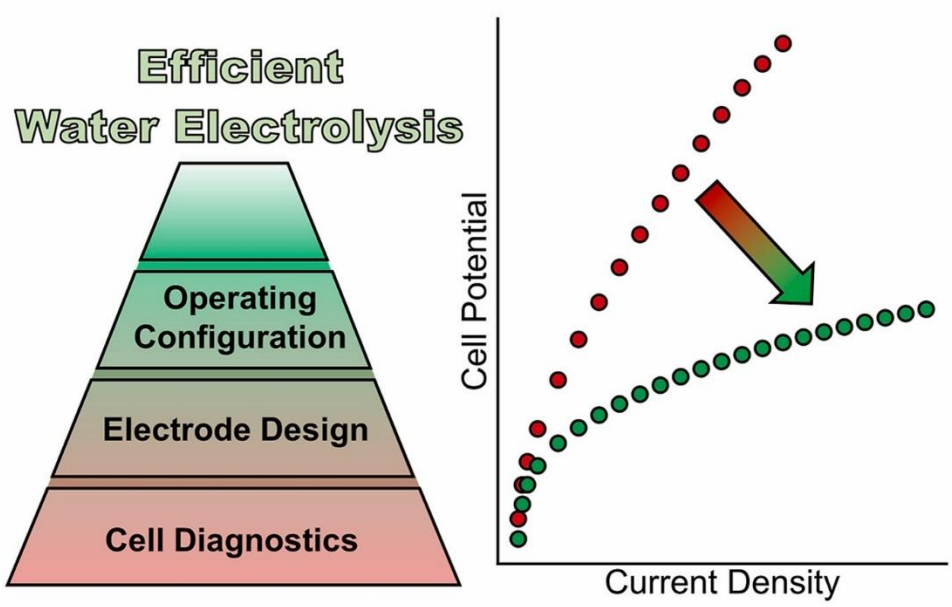

Figure 6-3. Schematic of electrolyzer polarization curve with favourable development works [30].

6.2.4. PEMEL modelling

Due to the high potential of PEM electrolyzers for integration with variable renewable energy (VRE) sources, developing a theoretical model that incorporates the physical, chemical, electrical, thermal, and fluidic aspects of the system is essential for accurately predicting performance under various energy transition scenarios. Furthermore, a reliable model validated against experimental data and

capable of adapting to different operating conditions provides deeper insight into the operational behavior and efficiency of PEM electrolyzers.

PEM electrolyzers are mainly modelled in steady-state mode with fixed power input and particular operating conditions [16]. In this approach, obtaining the polarization curve, including the open-circuit voltage and various electrochemical losses, is crucial. The resulting polarization curve can directly describe the operation when coupled with other parameters such as Faraday efficiency. This approach is completely reliable for fixed operating conditions, avoids excess computational cost, and is useful for diagnosing operational issues such as degradation or fouling in the electrolyzer cells.

Dynamic modelling has also been applied by various researchers, and it has been observed that the transition time after a step change in power input is very short and the average deviation of cell voltage from the polarization curve, implying the difference between dynamic and steady-state modes, during these transitions is typically below 10% and only lasts for a few seconds, and the total system transition time also lasts less than 2 minutes [28,31,32].

In real-world scenarios, changes in power input rarely occur as discrete steps; they are more commonly in the form of ramps, and the deviation of a steady-state model from transitions in the form of a ramp is less pronounced than with step changes. Moreover, these ramping rates are typically reported on a per-minute basis, and high-resolution data over long-time durations are not available. On the other hand, running an accurate dynamic model and capturing such transitions requires high-resolution input data (i.e., power values at sub-minute intervals), which is typically not accessible. For the reasons outlined below, a steady-state modelling approach is adopted in this study to balance simulation accuracy with computational efficiency:

1. The available power input data are segregated and transforming them into a continuous profile would require an additional stage of data processing.
2. Given the inherently fast dynamic response of PEM water electrolyzers (typically under 1–2 minutes) and the use of power profiles with 1-hour resolution, the difference between dynamic and steady-state modelling becomes insignificant. Capturing sub-minute phenomena would require even smaller time steps, which dramatically increases computational demands, making it impractical for long-term simulations over months or years.

3. The inherent fluctuations (upward ramps and downward ramps) in VRE power profiles tend to neutralize each other over time, reducing the net impact of transient effects.
4. Accurately modelling other dynamic parameters, such as water flow, temperature, and pressure, adds significant complexity and computational burden.
5. This study focuses on macro-scale, long-term system behavior (over a year), where appropriate simplifications are necessary to manage computational costs effectively.

The following sections describe the models employed and the procedure to develop the models of the PEMEL in Aspen Custom Modeler (ACM) and Python adaptable to a VRE profile.

6.2.5. PEMEL model assumptions and considerations

The model is supposed to represent the performance of the electrolyzer, focused on hydrogen production, and it is structured by subsystems for its components: the anode, the cathode, and the membrane. The model is developed based on electrochemical principles, energy balance, and mass transfer equations. To ensure a balance between computational efficiency and model accuracy, certain simplifications and assumptions are applied to the PEM model development procedure [33]. The following list outlines the general assumptions adopted for modelling:

- A uniform temperature is assumed across the electrodes and membrane.
- The model is formulated as one-dimensional, implying uniform distribution of current density and reactant concentrations throughout the electrolyzer components. While this approach inherently neglects spatial gradients and time-dependent behavior, it is a simplified method suitable for large time-scale studies and applicable to discrete power input profiles, enabling a semi-dynamic simulation of the hydrogen production process.
- Gas diffusion (crossover) through the membrane is not included in the model, and subsequently the generated oxygen and hydrogen gases are assumed to be pure. Meanwhile, the impact of hydrogen loss is considered through Faraday efficiency.

- The parameters, such as partial pressure, temperature, etc., are obtained from the Aspen properties package. In the case of Python modelling, the methods are described separately.
- The electrolyzer operation is subject to on/off cycles when the power input is equal to 5% of the rated power, since the Faraday efficiency is too low and there is a risk of hydrogen crossover exceeding 4% (lower explosion limit) [34].

6.2.6. Electrochemical and thermodynamic modelling

For a particular temperature and pressure, the energy required to drive the water electrolysis reaction can be expressed by the enthalpy change, ΔH, of the process. For this reaction to take place, a portion of this energy must be supplied electrically and is associated with the change in Gibbs free energy change, ΔG, representing the minimum electrical work necessary for the reaction to proceed. The remaining portion is provided as thermal energy, Q, which corresponds to the product of the operating temperature and the entropy change, $T\Delta S$. The Gibbs-Helmholtz equation presents the relationship among these thermodynamic quantities as follows:

$$\Delta G(T,P) = \Delta H(T,P) - Q(T,P) = \Delta H(T,P) - T\Delta S(T,P) \quad (5)$$

Two voltages are defined based on the thermodynamics of the water electrolysis, including open circuit (or reversible) voltage, V_{oc}, which is associated with the Gibbs free energy of reaction, and thermoneutral voltage, V_{tn}, which is associated with the enthalpy change of the process. These two voltages are explained in the following sections.

6.2.6.1. Open circuit voltage (reversible potential)

The open circuit voltage, V_{oc} (also referred to as reversible cell potential, E_{rev}, and Nernst voltage) represents the minimum theoretical voltage necessary to drive the electrolysis reaction under standard conditions, in the absence of any losses. It is directly related to the Gibbs free energy change of the reaction, ΔG, as expressed below:

$$V_{oc}(T,P) = \frac{\Delta G(T,P)}{nF} \quad (6)$$

where $n = 2$ is the number of electrons involved in the overall reaction, and F (= $96485.33 \frac{C}{mol}$) is the Faraday constant, representing the electric charge carried by one mole of electrons.

Open circuit voltage is practically determined when there is no current flow in the PEM electrolyzer. The open-circuit voltage can be calculated by the Nernst equation by considering the operating temperature, pressure, the activity of the reactant, and the partial pressure of products [35–37]. Assuming that products are ideal gases, these equations take the following form:

$$V_{oc}(T,P) = V_{oc}(T,P_{ref}) + \frac{RT}{nF}\ln\left(\frac{P_{H2}\,P_{O2}^{0.5}}{\gamma_{H2O}}\right) \quad (7)$$

$$V_{oc}(T,P) = \frac{\Delta G(T,P_{ref})}{2F} + \frac{RT}{nF}\ln\left(\frac{P_{H2}\,P_{O2}^{0.5}}{\gamma_{H2O}}\right) \quad (8)$$

where V_{rev} is the reversible voltage, R (= 8.314 $\frac{J}{mol.K}$) is the universal gas constant, T_{stack} is the temperature of the electrolyzer, P_{H2} and P_{O2} are the partial pressure of hydrogen and oxygen, respectively, and ($\gamma_{H2O} = 1$) is activity of water fed to the stack in the liquid state.

In this correlation $V_{oc}(T,P_{ref})$ accounts for the impact of temperature changes and $\frac{RT}{2F}\ln\left(\frac{P_{H2}\,P_{O2}^{0.5}}{\gamma_{H2O}}\right)$ accounts for the impact of pressure change on open circuit voltage.

Typically, V_{oc} is in the range 1.2–1.25 V in the range 25–80°C for water electrolysis, and Its value can be calculated using the following equations at reference pressure [38,39]:

$$V_{oc}(T,P_{ref}) = 1.229 - 0.9 \times 10^{-3}(T - 298.15) \quad (9)$$

$$V_{oc}(T,P_{ref}) = 1.5184 - 1.5421 \times 10^{-3}T + 9.523 \times 10^{-5}T\ln T + 9.84 \times 10^{-8}T^2 \quad (10)$$

Under standard conditions (typically defined as $P = 1\,atm$, $T = 298.15\,K$), the Gibbs free energy change for the water electrolysis reaction is $\Delta G(T_{ref},P_{ref}) = 236.483 \frac{\text{kj}}{\text{mol}}$ [40] and the corresponding reversible cell voltage, denoted as $V_{oc}\,(T_{ref},P_{ref})$ is commonly referred to as the ideal voltage, V_{id}:

$$V_{oc}\,(T_{ref},P_{ref}) = V_{id} = \left(\frac{\Delta G(T_{ref},P_{ref})}{nF}\right) = \frac{236.483}{2 \times 96485} = 1.229\,V$$

Accordingly, the following correlation can be used to estimate the V_{oc} at different temperatures The electrolysis process in respect to the open circuit voltage can be interpreted as below:

- If $V_{cell} < V_{oc}$: No electrochemical reaction occurs.
- If $V_{cell} = V_{oc}$: The system is at equilibrium, and no net current flows.
- If $V_{cell} > V_{oc}$: A net current is generated, and water electrolysis proceeds.

6.2.6.2. Thermoneutral voltage

The thermoneutral voltage, V_{tn}, in an electrolyzer, is the theoretical cell voltage that drives an isothermal electrolysis process (no net heat exchange occurs during water electrolysis). In other words, it's the voltage at which the electrical energy input exactly matches the total enthalpy change of the reaction, so the process neither absorbs nor releases heat. In an analogy to open circuit voltage, which was correlated to Gibbs free energy, $V_{oc} = \frac{\Delta G}{nF}$, thermoneutral voltage is correlated to theoretical enthalpy change, ΔH, as below [41]:

$$V_{tn} = \frac{\Delta H}{nF} = \frac{\Delta G}{nF} + \frac{T\Delta S}{nF} = V_{oc} + \frac{T\Delta S}{nF} \tag{11}$$

Theoretical enthalpy change, ΔH, represents the energy required for building/breaking up a bond for a chemical reaction, while the entropy change, ΔG, is the change of Gibbs free energy, and the entropy change, ΔS, is a measure of the irreversibility for a thermodynamic system. Accordingly, thermoneutral voltage includes the irreversibility of the process.

Under standard state ($P = 1\ atm, T = 298.15\ K$) for water electrolysis reaction, $\Delta H\left(T_{ref}, P_{ref}\right) = 285.4$ kJ /mol and the V_{tn} will be:

$$V_{tn} = \left(\frac{\Delta H\left(T_{ref}, P_{ref}\right)}{nF}\right) = \frac{285.4}{2 \times 96485} = 1.481\ V \tag{12}$$

Accordingly, as expected, the thermoneutral voltage (~1.481 V), is higher than the reversible voltage (~1.229 V). However, the voltage in PEM electrolyzers often exceeds the thermoneutral voltage due to overpotentials, and the process becomes exothermic. Accordingly, heat management becomes critical for system efficiency and durability, especially at higher current density and power input levels.

The electrolysis process in respect to the thermoneutral voltage can be interpreted as below:

- If $V_{oc} < V_{cell} < V_{tn}$: Reaction absorbs heat (Endothermic)
- If $V_{cell} = V_{tn}$: No net heat exchange (Isothermal)
- If $V_{cell} > V_{tn}$: Reaction releases heat (Exothermic)

6.2.6.3. Cell voltage and polarization curve modelling

In order to drive the electrolysis reaction, the electrolyzer cell voltage shall be higher than the open circuit voltage because of the inherent irreversibility of the electrolysis reaction explained by the Gibbs-Helmholtz equation. Accordingly, in order to obtain a particular reaction rate (or current density) in the electrolysis cell, the applied electrical power needs to overcome open-circuit voltage and some over-voltages. Accordingly, the cell voltage corresponding to the demanded current (or current density), V_{cell} , can be determined as sum of open circuit voltage, V_{oc}, and several nonidealities (overpotentials, ΔV_i) as below [36,37]:

$$V_{cell} = V_{oc}(T, P) + \sum \Delta V_i\,(T, P, I_{cell}) \tag{13}$$

$$V_{cell} = V_{oc} + \Delta V_{act} + \Delta V_{ohm} + \Delta V_{diff} \tag{14}$$

where ΔV_{act}, ΔV_{ohm}, ΔV_{diff} are called activation overpotential, ohmic overpotential, and diffusion overpotential (also known as concentration or mass transport overpotential), respectively. Accordingly, for determining the cell voltage across different current density values and plotting the polarization curve for an electrolyzer, the contributions of various overvoltages is necessary. Figure 6-4 schematically shows the contribution of overpotentials in the polarization curve.

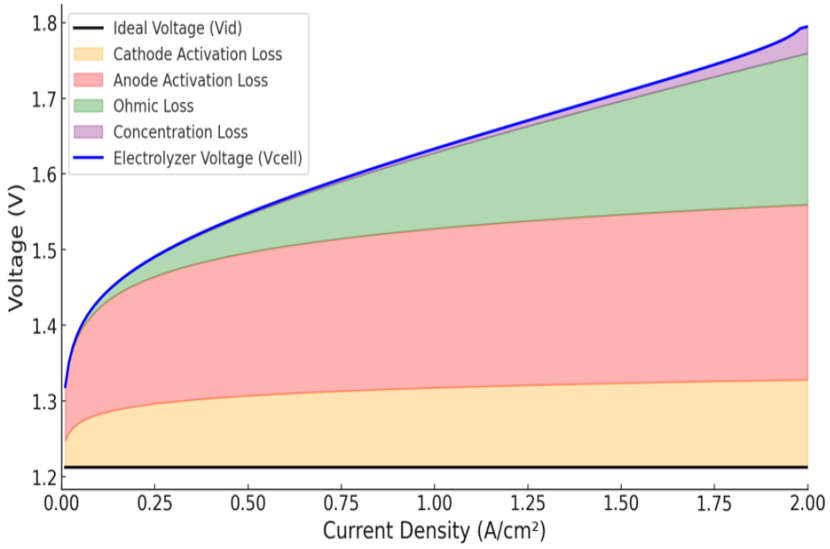

Figure 6-4. PEM electrolyzer polarization curve formed of open circuit voltage and various overpotentials

In general, at low current densities, the polarization curve presents a sharp logarithmic rise that highlights activation losses caused by sluggish electrode kinetics, particularly at the oxygen evolution reaction (OER) site. In the intermediate region, a linear voltage rise is observed due to ohmic losses primarily associated with ionic resistance in the membrane and electronic resistance in the cell components. At high current densities, the curve steepens again due to mass transport limitations, as the reactants become depleted or products accumulate at the reaction interface. Figure 6-5 shows the polarization curve of the electrolyzer cell divided into three zones based on the controlling overpotential mechanisms. Hence, analysing the shape and slope of the polarization curve enables the identification of performance-limiting mechanisms, comparison between cell designs or materials, and optimization of operating parameters. It remains one of the most essential tools in both experimental characterization and model validation of PEM electrolyzers. Generally, open-circuit voltage represents the minimum theoretical voltage, determined solely by thermodynamic properties, required to drive the water-splitting reaction under equilibrium conditions and is defined as the potential difference between the two electrodes when no external current is flowing through the circuit. The deviation of the actual cell voltage from the reversible voltage, resulting from the inherent irreversibility of the electrochemical process, is referred to as the overpotential. This overpotential can originate from various sources, including activation losses, ohmic resistance, and mass transport limitations. Different overpotentials contributing to the cell voltage are explained in the following sections.

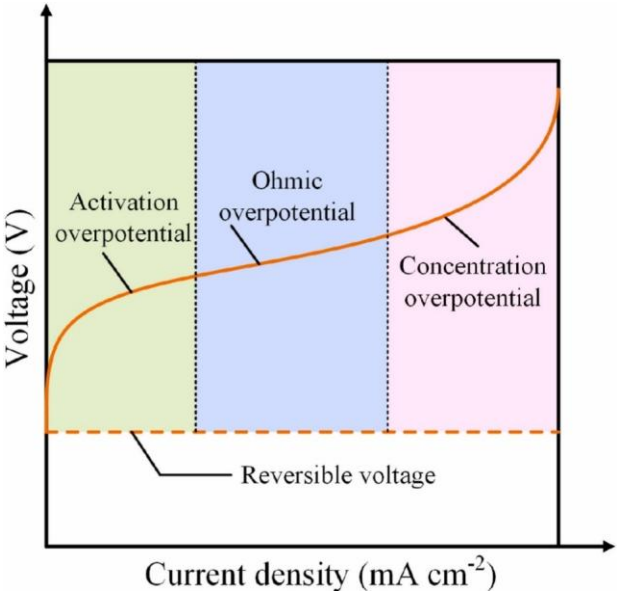

Figure 6-5. Polarization curve divided into three zones based on the prominent overpotential mechanisms [42].

6.2.6.4. Activation overvoltage

Activation overvoltage is the additional voltage required to overcome the kinetic barriers of the electrochemical reactions at the electrodes, enabling the hydrogen evolution reaction (HER) and oxygen evolution reaction (OER) to proceed at a measurable rate. In other words, it is the energy required (beyond the reversible voltage) to initiate and sustain the electrode reactions due to sluggish kinetics. The activation overpotential can be calculated using the Butler-Volmer equation, which relates electrode current density to electrode potential [43]:

$$i = i_0 \left[e^{\frac{\alpha_a n F \Delta V_{act}}{RT}} - e^{\frac{\alpha_c n F \Delta V_{act}}{RT}} \right] \quad (15)$$

where i and i_0 are the electrode current density and exchange current density, respectively. α_c and α_a are the cathodic and anodic charge transfer coefficients, respectively.

Note: A smaller magnitude of the transfer charge coefficients in an electrode implies a faster reaction in that electrode. $\alpha_a = \alpha_c = 0.5$ imply a symmetrical transition state and it is a common approximation. According to the literature, the charge transfer coefficients of anode α_a vary between 0-1 and the charge transfer coefficients for cathode, α_c, varies between 0-2 [44,45]. The α_c and α_a are specified in this study as fitting parameters to match the prepared model with experimental data (Explained in section 6.3.1).

By applying the Butler-Volmer equation, activation overpotential, comprised of anodic (OER) activation overpotential, $\Delta V_{act,a}$, and cathodic (HER) activation overpotential, $\Delta V_{act,c}$, can be calculated [16]:

$$\Delta V_{act} = \Delta V_{act,a} + \Delta V_{act,c} \quad (16)$$

$$\Delta V_{act,a} = \frac{RT}{2\alpha_a F} \, sinh^{-1}\left(\frac{i}{2i_{0,a}}\right) \quad (17)$$

$$\Delta V_{act,c} = \frac{RT}{2\alpha_c F} \, sinh^{-1}\left(\frac{i}{2i_{0,c}}\right) \quad (18)$$

For a simpler calculation, the Tafel approximation can also be used [46]:

$$\Delta V_{act,a} = \frac{RT}{2\alpha_a F} \ln\left(\frac{i}{i_{0,a}}\right) \quad (19)$$

$$\Delta V_{act,c} = \frac{RT}{2\alpha_c F} \ln\left(\frac{i}{i_{0,c}}\right) \quad (20)$$

where $i_{0,c}$ and $i_{0,a}$ are the exchange current densities, representing the exchange rates between the reactants and products in the equilibrium. In other words, it represents how difficult it is for electrons to be transferred between the electrode and the reactant species (Higher i_0 represents easier reaction and lower activation overpotential, and it can be considered as electrochemical activity of an electrode).These parameters have a substantial impact on the activation overpotential and depend on different factors such as porosity and material of the electrodes, concentration, distribution, and size of the catalyst particles, and the operating temperature. Accordingly, activation overpotential can be mitigated via using modified catalysts, optimized operating temperatures, and increasing the active reaction sites (electrode surface) via increasing the electrode roughness [42].

The exchange current density of the IrO_2-based anode, $i_{0,a}$, is in the range 10^{-12}-10^{-9} and the exchange current density of Pt-based cathode, $i_{0,c}$, is in the range 10^{-4}-10^{-3} [44,47]

In this study, due to the importance of temperature in operation and aiming to account for the temperature impact on the electrolyzer performance, the following correlations are applied to calculate the $i_{0,c}$ and $i_{0,a}$ values [43]:

$$i_{0,a} = i_{0,a}^{ref} . e^{\frac{E_a}{R}\left(\frac{1}{T}-\frac{1}{T_{ref}}\right)} \quad (21)$$

$$i_{0,c} = i_{0,c}^{ref} . e^{\frac{E_c}{R}\left(\frac{1}{T}-\frac{1}{T_{ref}}\right)} \quad (22)$$

where $i_{0,c}^{ref}$ and $i_{0,a}^{ref}$ are the reference exchange current density of electrodes at a reference temperature, T_{ref} (K). Due to the complexity of predicting their values, they are often considered fitting parameters in the models [48,49]. The reference value of current exchange densities i_0^{ref} in this study are considered as below [46]:

$$i_{0,a}^{ref} = 2 \times 10^{-6}\ A/cm^2 \ (\text{at } T_{ref} = 353.15\ K) \quad (23)$$

$$i_{0,c}^{ref} = 1 \times 10^{-1}\ A/cm^2 \ (\text{at } T_{ref} = 353.15\ K) \quad (24)$$

Also, E_a and E_c are the kinetic activation energy for electrode reactions, which are specified according to the available data in the literature as below:

$E_c = 16000\ J/mole$ for Pt/C catalyst [50]

$E_a = 50000\ J/mole$ for IrO_2 catalyst [51]

Note: In the range with small current density, $(i \leq i_0)$ the reaction is close to equilibrium, meaning that the forward (oxidation) and reverse (reduction)

reactions occur at nearly equal rates. In this range, activation overpotential is close to zero, and the Tafel approximation cannot reliably predict the activation overpotential (it may result in negative values at low current density levels). In addition, experimental data is rarely available in the low-current range due to low sensitivity of potentiostats and high noise-to-signal ratio for experimental current measurements.

6.2.6.5. Ohmic overpotential

Ohmic overvoltage is the voltage required to overcome resistance in the circuit. It includes the electrical loss due the movement of electrons through the PEM electrolyzer components, R_{el}, the ionic loss due to the movement of protons through the membrane, R_{mem}, and the imperfect contact of different electrolyzer components, $R_{contact}$. Ohmic overvoltage can be calculated using Ohm's law [43,52]:

$$\Delta V_{ohm} = (R_{el} + R_{mem} + R_{contact}) \,.\, i.A \tag{25}$$

where A is the electrode area, and i is the electrical current. According to this equation, the ohmic overpotential is linearly proportional to the electrical current, and it increases with increasing the current density. The electrical resistance can be expressed as the sum of bulk material resistance for the anode and cathode as below:

$$R_{el} = \left(\frac{t_a\,\rho_a}{A}\right) + \left(\frac{t_c\,\rho_c}{A}\right) \tag{26}$$

where t_a and t_c represent the electron path length in the electrodes, which is equal to the electrode thickness (including the catalyst layer, porous transport layer and in some cases the bipolar plates), $\rho_a = \rho_c = 7.5\, m\Omega.cm$ [37] are the material resistivity of anode and cathode, and A is the conductor cross-sectional area, which is often equal to the cell area A_{cell}. It should be noted that the electronic resistance magnitude is often negligible compared to membrane and contact resistance.

The membrane resistance, which is significantly larger than electrode resistance, can be calculated using the following correlation [53]:

$$R_{membrane} = \frac{t_{mem}}{\sigma_{mem} A} \tag{27}$$

where σ_{mem} is the membrane conductivity ($s.m^{-1}$) (the inverse of resistance), and it is calculated using the following correlation [53]:

$$\sigma_{mem} = (0.005139\lambda_m - 0.00326)\exp\left(1268\ \left(\frac{1}{303} - \frac{1}{T}\right)\right) \quad (28)$$

This correlation is obtained based on measuring the conductivity of the Nafion 117 membrane at 30 °C and observing the linear dependency of σ_{mem} on λ_m.

The contact resistance directly depends on the quality of physical contact between the electrolyzer components, and it can vary widely (in the range $5\ m\Omega \cdot cm^2$ to $50\ m\Omega \cdot cm^2$) depending on factors such as surface roughness, clamping pressure, material compatibility, and aging [46,54,55]. Also, the bubble coverage resistance is not provided in numbers or models. Accordingly, these two resistances are lumped together and incorporated as a correction factor of 1.2 in the correlation for ohmic resistance:

$$\Delta V_{ohm} = 1.2 \times (R_{el} + R_{mem}).i.A \quad (29)$$

6.2.6.6. Diffusion overvoltage

Diffusion overvoltage (or mass transfer loss) represents the mass transport limitations. When the concentration of products (H_2 and O_2 gases) increases, the reaction rate decreases due to mass transport limitations [31,37]. The diffusion overvoltage is not significant for low and moderate current densities with appropriate gas flow passes, and it is orders of magnitude smaller than the other overvoltage, and it could be neglected below a specific current density [52], while at high current densities, it can sharply increase, affecting the total cell voltage. Some features, such as a thicker and denser catalyst layer and a more hydrophilic surface aimed to make water transport easier in the anode section, may cause tortuosity and prevent oxygen gas escape. Also, the main water input to the cell is fed to the anodic section, which makes the flow management more critical. Accordingly, oxygen gas can cause significant overpotential at high current density, which corresponds to the high gas production rate. Hence, the diffusion overvoltage is mainly rooted in the anodic compartment [43]. The diffusion overpotential can be evaluated using the following correlation [56]:

$$E_{\text{diff}} = i\left(\beta_1 \cdot \frac{i}{i_{\text{lim}}}\right)^{\beta_2} \quad (30)$$

where i_{lim} is the limiting current density, $\beta_2 = 2$ and β_1 is a function of temperature as below:

$$\beta_1 = (8.66 \times 10^{-5}\, T - 0.068)\gamma - 1.6 \times 10^{-4} T + 0.54 \qquad if\ \gamma > 2$$
$$\beta_1 = (7.16 \times 10^{-4}\, T - 0.622)\gamma - 1.45 \times 10^{-3} T + 1.68 \qquad if\ \gamma \leq 2 \tag{31}$$

where T is the operating temperature of the electrolyzer, and γ is a function of pressure:

$$\gamma = 8.41366809 \times 10^{-5} P^{O2} + 8.41366809 \times 10^{-5} P^{sat} \tag{32}$$

where P^{O2} and P^{sat} are partial pressure of oxygen and saturation pressure of water at operating temperature of the PEM electrolyzer. It should be noted that in commercial PEM electrolyzers the diffusion overvoltage and limitations arising from it are barely observed in industrial units because the working current densities are much lower than the limiting current density. Despite the values reported in literature in the range $1\ to\ 2\ A.cm^{-2}$[44,56,57] in this study assumed to be $i_L = 6\ A.cm^{-2}$ [37].

6.2.7. Electrolyzer efficiency and specific energy consumption

As explained in section 6.2.6.2, the electrolysis process is associated with irreversibility and losses in various forms. Accordingly, the input power transforms to product (chemical energy) or thermal energy (heat), and each one of these two can be divided into useful and lost categories. Figure 6-6 shows the energy flow in an electrolyzer stack. Hence, the quality of an electrolyzer performance is evaluated based on the composition of such a graph, and to measure the quality of the process, defining the electrolyzer efficiency is necessary.

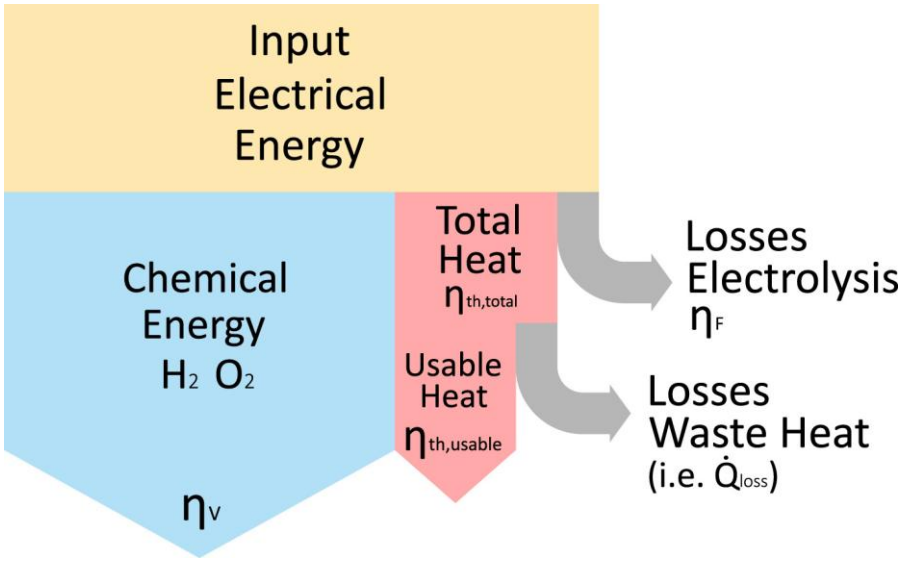

Figure 6-6. Sankey diagram of energy stream in an electrolyzer stack [58].

Efficiency of a system is basically defined as the ratio of usable outputs to the inputs. Dealing with electrolyzers, different efficiencies can be defined. The main efficiencies utilized for evaluating electrolyzer performance are the Faraday efficiency (η_F), voltage efficiency (η_V), and electrolyzer efficiency (η_{el}), which are linked by the following expression [31]:

$$\eta_{el} = \eta_F . \eta_V \tag{33}$$

6.2.7.1. Voltage efficiency

The ratio of thermoneutral voltage to the cell voltage in an electrolyzer is called voltage efficiency or DC efficiency. While Faraday efficiency considers the impact of gas diffusion on electrolyzer performance, voltage efficiency represents the polarization losses, including mass transfer loss, ohmic loss, activation loss, and heat losses. Hence, Faraday efficiency is normally higher than voltage efficiency in a normal operation. Voltage efficiency can be calculated as below [59]:

$$\eta_V = \frac{V_{tn}}{V_{cell}} \tag{34}$$

6.2.7.2. Faraday efficiency:

Faraday efficiency, also known as coulombic efficiency and current efficiency, represents the current losses due to the gas diffusion (crossover) [53,54]. Faraday efficiency is often expressed as the ratio of the real hydrogen production rate, $\dot{N}_{H2}^{gen}$, to the theoretical hydrogen production rate, $\dot{N}_{H2,th}^{gen}$ [60]. For a single electrolysis cell Faraday efficiency will be:

$$\eta_F = \frac{\dot{N}_{H2}^{gen}}{\dot{N}_{H2,th}^{gen}} = \frac{\dot{N}_{H2}^{gen}}{I_{cell}/nF} \tag{35}$$

While Faraday efficiency is usually assumed to be equal to or higher than 99% [24,46], it decreases significantly at low current densities [61,62]. Faraday efficiency is a function of membrane properties such as thickness and type and operating conditions such as pressure, temperature, and current density, and it determines the real hydrogen and oxygen production rates and directly affects the electrolyzer energy efficiency, η_{el} . The production rates of an electrolyzer stack can be calculated as below [36,63]:

$$\dot{N}_{H2}^{gen} = \eta_F . \frac{I_{cell} . N_{cell}}{nF} \tag{36}$$

$$\dot{N}_{O2}^{gen} = \eta_F . \frac{I_{cell} . N_{cell}}{2nF} \quad (37)$$

Faraday efficiency of an electrolyzer can be modelled by an empirical expression, and some models are already proposed for alkaline electrolyzers [64,65]. While Faraday efficiency has a great impact on the electrolyzer performance, it has received less attention compared to electrochemical domain modelling, and there are only two researchers directly addressing Faraday efficiency of PEM electrolyzers. Tijani and Rahim [24] investigated the influence of operating temperature, pressure, and membrane thickness on the Faraday efficiency of a PEM electrolyzer. They concluded that membrane thickness and gas pressure affect Faraday efficiency, particularly at low current densities, while temperature has a very slight and negligible impact in the case of PEM water electrolyzers. However, they did not propose a model for calculating Faraday efficiency. The only study that provides an empirical model for this purpose is the work of Yodwong et al. [66], which includes the effect of operating pressure up to 10 bar. Furthermore, Faraday efficiency has been reported to decrease at high pressures due to increased crossover currents, as noted in the literature [59,62,67]. Since that time, no additional studies have been published on the modelling of Faraday efficiency specifically for PEM electrolyzers. Considering the fundamental structural differences, the models developed for alkaline electrolyzers are not applicable to PEM electrolyzers. Hence, further research is needed to better understand the effects of operating conditions and structural factors such as membrane thickness on Faraday efficiency.

Since this study is under constant operating pressure, the impact of temperature on Faraday efficiency is negligible, and a fixed cell structure is employed for the modelling, a fixed Faraday efficiency function is assumed according to the following function [52]:

$$\eta_F = \frac{i - i_{loss}}{i} = 1 - \frac{i_{loss}}{i} \quad (38)$$

where i is the current density, and i_{loss} is "crossover current loss" due to gas cross over. The quantity of i_{loss} is a function of operating conditions such as temperature, pressure, etc., and its dependency on operating conditions can be determined by fitting this equation with experimental data. Figure 6-7 shows the Faraday efficiency against current density for various quantities of i_{loss}.

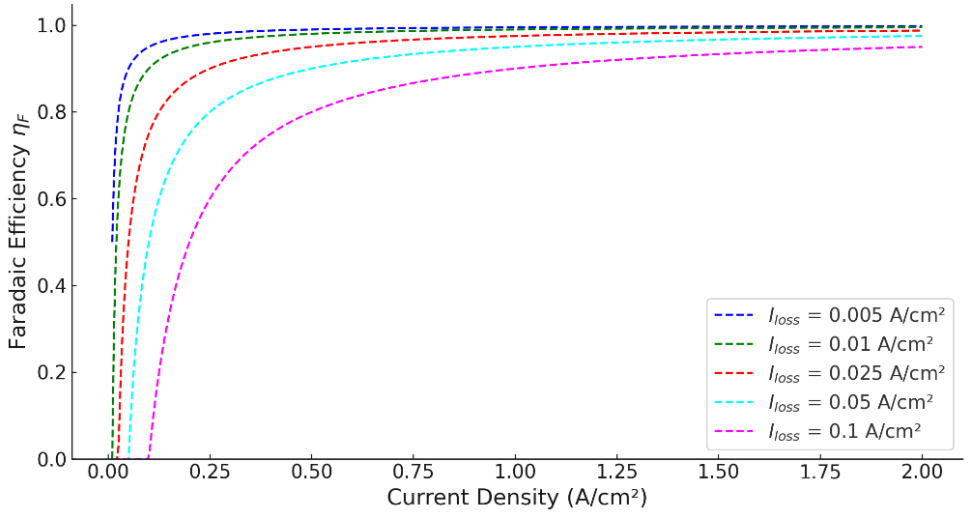

Figure 6-7. General faraday efficiency function plotted against current density for various values of i_{loss}.

Since i_{loss} depends on various factors such as membrane properties, stack assembly, operating conditions, etc., and available data in the literature is limited, the Faraday efficiency curve with constant i_{loss} $(= 0.025\ A.cm^{-2})$ is assumed for the studied PEM stack, as shown in Figure 6-8 .

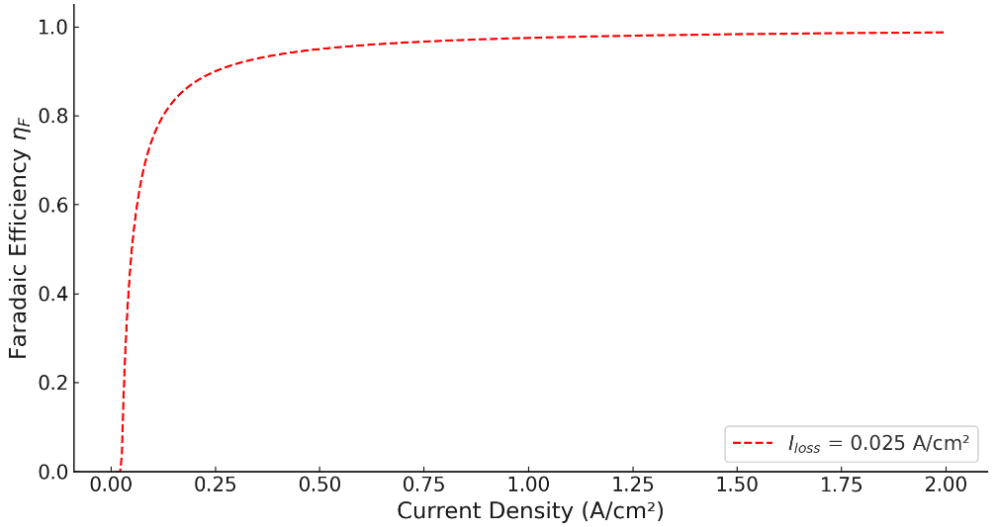

Figure 6-8. The Faraday efficiency function assumed for the studied PEM stack.

6.2.7.3. Electrolyzer energy efficiency:

Electrolyzer energy efficiency, also referred to as stack efficiency, expresses how effectively an electrolyzer stack converts electrical energy into chemical energy (excluding the auxiliary systems or possibly applied AC/DC converters). It is defined as the amount of energy obtainable by produced hydrogen per amount of energy consumed for hydrogen production. Accordingly, it can be calculated as the

ratio of the energy content of produced hydrogen to the electrical energy input of the electrolyzer [68].

Two concepts of higher heating value of hydrogen, HHV ($= 285.83\ kJ/mol$) or lower heating value, LHV ($= 241.83\ kJ/mol$) are commonly utilized to report the electrolyzer efficiency [68,69]. The HHV is defined as he total energy released in hydrogen combustion, including the latent heat of water vapor condensation (assumes water produced from hydrogen combustion condenses to liquid at the end of the process), while LHV is defined as the energy released in hydrogen combustion excluding the heat recovered from water vapor condensation (assumes water stays as vapor after combustion). The electrolyzer efficiency can be reported as the ratio *of* LHV or HHV to the electrical power consumed for hydrogen production:

$$\eta_{el}^{HHV} = \frac{HHV}{(W_{stack}/\dot{N}_{H_2,prod})} = \frac{HHV}{V_{cell}.n.F} \tag{39}$$

$$\eta_{el}^{LHV} = \frac{LHV}{(W_{stack}/\dot{N}_{H_2,prod})} = \frac{LHV}{V_{cell}.n.F} \tag{40}$$

where $W_{stack} = V_{stack}.I_{stack}$ is the electrical power input for molar hydrogen production rate of $\dot{N}_{H_2,prod}$.

For a PEM electrolyzer, η_{el}^{LHV} (normally in the range of 55-75%) is lower than η_{el}^{HHV} (normally in the range of 65-85%) for the PEMWE.

$$HHV - LHV = latent\ heat\ of\ water\ (\sim 44 \frac{kJ}{mol}) \tag{41}$$

The LHV and HHV values per kg of hydrogen are equal to ($LHV = 33.3\ kWh/kg$) and ($HHV = 39.4\ kWh/kg$).

6.2.7.4. System Efficiency

An electrolysis unit needs auxiliary components, including water circulation, purification, deionization, cooling, control system, possible gas compression, and hydrogen drying operation. The power required for the auxiliary components or balance of plant (BoP) should be involved in the unit performance evaluation. To this end, an actual system-level efficiency, called “system efficiency” is defined as follows:

$$\eta_{system}^{HHV} = \frac{HHV}{Total\ power\ (stack\ +\ aux)} = \frac{HHV}{(W_{stack}/\dot{N}_{H_2,prod}) + (W_{aux}/\dot{N}_{H_2,prod})} \tag{42}$$

$$\eta_{system}^{LHV} = \frac{LHV}{Total\ power\ (stack\ +\ aux)} = \frac{LHV}{(W_{stack}/\dot{N}_{H_2,prod}) + (W_{aux}/\dot{N}_{H_2,prod})} \quad (43)$$

where W_{aux} is the power consumed for auxiliary components. The system efficiency is lower than the stack efficiency (DC efficiency) due to additional power loads involved in the power consumption. The auxiliary power is generally considered as a small percentage of the rated power, in the range of 0.22 to 2% [57,70]. In this study, it is assumed to be 1% of the electrolyzer rated power for hot standby and normal operation. The hot standby is considered a preparatory mode, not an operational (Faraday-active) mode for hydrogen production.

Different efficiency concepts and their relative behaviors across the input power load range up to the rated (nominal) load of a PEM electrolyzer unit are illustrated in Figure 6-9. According to this figure, Faraday efficiency is very low at low power levels, and it increases rapidly with increasing the input power. For the power levels corresponding to the cell voltage in the range ($V_{oc} < V_{cell} < V_{tn}$), the voltage efficiency can be over 100% (this range is not operational in industrial units), while it linearly decreases with increasing the input power to the rated level.

The stack/electrolyzer efficiency as product of the Faraday efficiency and voltage efficiency increases with increasing the input power, along with increasing the Faraday efficiency, and after reaching a peak value (about 50-60%) decreases linearly along with the decline in voltage efficiency. Accordingly, at low power ranges, Faraday efficiency is the dominant parameter, affecting the stack efficiency, while at higher power levels, Faraday efficiency is close to 1, and voltage efficiency dominantly affects the stack efficiency.

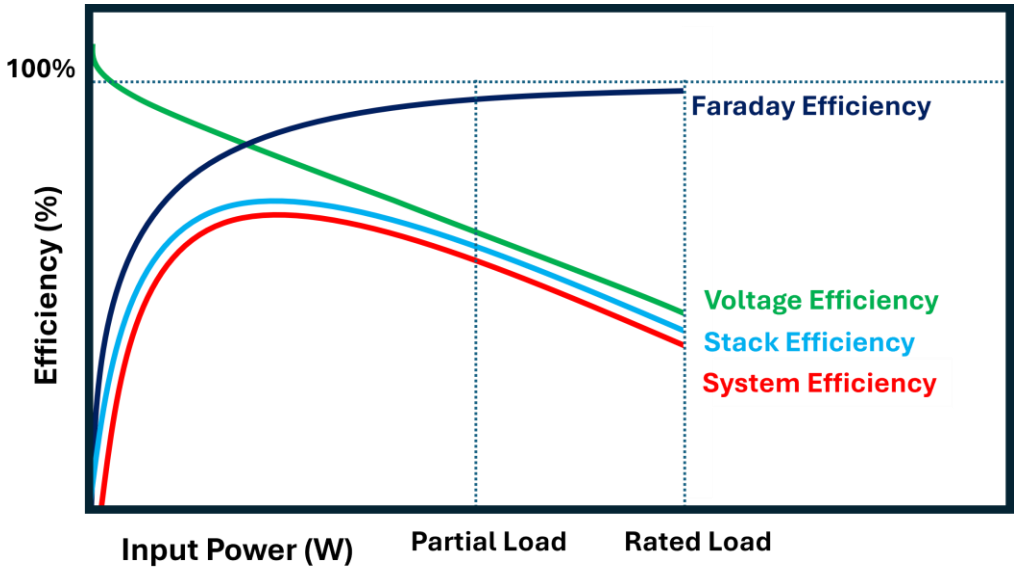

Figure 6-9. Electrolyzer efficiency in stack and system scales against input power load

The electrochemical model and the various efficiency concepts are incorporated together to predict the polarization curve and hydrogen production rate and assess the process efficiency at different scales.

While a model incorporating the polarization curve, Faraday efficiency, and system efficiency can assist in estimating hydrogen production, developing an integrated model that includes mass and energy balances within the electrolyzer stack is essential for understanding the synergies among thermodynamics, electrochemistry, and heat and mass transfer. Such a model enables the identification of optimization opportunities at the unit scale and exploring novel operation and control scenarios.

6.2.8. Mass balance modelling

The mass balance model is a mathematical framework applied for describing the transport of the chemical species within the PEM water electrolyzer cell. Incorporating mass balance submodels for each component of the electrolyzer, including anode, cathode, and membrane, is crucial for accurately predicting hydrogen and oxygen generation, power demand, and water consumption. The mass balance model is formulated neglecting a storage term, as it requires detailed geometrical features of the flow channels. Also, the gas diffusion across the membrane (gas crossover) is neglected in this study, implying that the gas products are pure, while the impact of gas crossovers is included through Faraday efficiency.

6.2.8.1. Anode mass balance sub-model

In the modelled PEM electrolyzer, water is introduced at the anode, where it undergoes electrochemical splitting into hydrogen and oxygen. Due to neglecting the gas crossover, the species existing in anode compartment are water and oxygen. The mass balance for oxygen is set by considering the generation rate and the corresponding outflow from the anode. Given that the model operates under steady-state conditions and gas crossover effects are neglected, the analysis is simplified to focus solely on generation and outlet flow rates of oxygen within the anode side:

$$\dot{N}_{O2}^{gen} = \dot{N}_{O2}^{out,a} \tag{44}$$

where the oxygen generated in the stack, $\dot{N}_{O2,gen}$, is given by Faraday's law:

$$\dot{N}_{O2}^{gen} = \frac{I_{useful}.N_{cells}}{Z_{O2}\,F} = \frac{i_{useful}\,.A_{cell}.N_{cells}}{4F} \tag{45}$$

where N_{cells} is the number of cells in the stack, A_{cell} is the cell area, Z_{o2} is the stoichiometric coefficient of oxygen in the electrolysis reaction, I_{useful} is the effective current passing the cell and i_{useful} is the net current density determined by Faraday efficiency as below:

$$i_{useful} = \eta_F.i_{cell} \tag{46}$$

where i_{cell} is the theoretical current density corresponding to the polarization curve, and η_F is Faraday efficiency.

The flow balance for the water within the anode takes into account the liquid water inlet flow, $\dot{N}_{H2O}^{in,a}$, the water consumption through electrolysis process, $\dot{N}_{H2O}^{cons,a}$, and water transfer through the membrane, $\dot{N}_{H2O}^{mem}$, as below:

$$\dot{N}_{H2O}^{in,a} - \dot{N}_{H2O}^{cons,a} - \dot{N}_{H2O}^{mem} = \dot{N}_{H2O}^{out,a} \tag{47}$$

$$\dot{N}_{H2O}^{in,a} - \dot{N}_{H2O}^{cons,a} - \dot{N}_{H2O}^{eo} - \dot{N}_{H2O}^{diff} + \dot{N}_{H2O}^{\Delta P} = \dot{N}_{H2O}^{out,a} \tag{48}$$

In this study water consumption is calculated directly from material balance, while in some references water consumption, $\dot{N}_{H2O}^{cons,a}$, is estimated as 25% over the theoretical hydrogen production rate as below [43]:

$$\dot{N}_{H2O}^{cons,a} = 1.25\,\frac{I_{useful}.N_{cells}}{2F} = 1.25\frac{i_{useful}.A_{cell}.N_{cells}}{2F} \tag{49}$$

6.2.8.2. Cathode mass balance sub-model

Given no gas crossover in the prepared model, water and hydrogen presenting within the cathode side of the PEM electrolyzer. The flow balance analysis for the water over the cathode includes the water inlet from the membrane, $\dot{N}_{H2O}^{mem}$, the water outlet, $\dot{N}_{H2}^{out,c}$, and the inlet water flow, $\dot{N}_{H2O}^{out,c}$, in case of applying an inlet water stream to the cathode compartment :

$$\dot{N}_{H2O}^{in,c} + \dot{N}_{H2O}^{mem} = \dot{N}_{H2O}^{out,c} \tag{50}$$

$$\dot{N}_{H2O}^{in,c} + \dot{N}_{H2O}^{eo} + \dot{N}_{H2O}^{diff} - \dot{N}_{H2O}^{\Delta P} = \dot{N}_{H2O}^{out,c} \tag{51}$$

On the other hand, since the simulation is in the steady-state condition and gas crossovers are neglected in this study, the analysis for hydrogen flow balance is expressed as:

$$\dot{N}_{H2}^{gen} = \dot{N}_{H2}^{out,c} \tag{52}$$

where $\dot{N}_{H2}^{out,c}$ is the outcoming hydrogen, and $\dot{N}_{H2}^{gen,c}$ accounts for hydrogen generated, which depends on the electrochemical behaviour of the electrolyzer cells, given by Faraday's law as below:

$$\dot{N}_{H2}^{gen,c} = \frac{I_{useful}\, N_{cells}}{2F} = \frac{i_{useful}\, A_{cell}\, N_{cells}}{2F} \tag{53}$$

This correlation is known as "electrolysis reaction extent" and is applied to determine the hydrogen and oxygen production and water consumption.

6.2.8.3. Membrane mass balance sub-model

As explained before, Faraday efficiency is mainly affected by gas crossover, while voltage efficiency is mainly affected by activation, ohmic, and mass transfer losses. Accordingly, the membrane affects both Faraday and voltage efficiency, and subsequently the electrolyzer efficiency. Thus, the membrane features, including the material, thickness, water content, permeability, and porosity, should be carefully adjusted for an efficient electrolyzer. Since the gas crossover is neglected in this study, only water transfer in the membrane is included in the model.

Although the membrane is designed to allow only proton permeation, it is not completely impermeable to water. Water permeation through the PEM membrane , $\dot{N}_{H2O}^{mem}$, occurs due to three mechanisms, which are anode-to-cathode diffusion, $\dot{N}_{H2O}^{diff}$, cathode-to-anode migration due to the hydraulic pressure, $\dot{N}_{H2O}^{\Delta P}$, and the anode-to-cathode electro-osmosis drag, $\dot{N}_{H2O}^{eo}$ [71]. In some references, the term $\dot{N}_{H2O}^{\Delta P}$ is neglected as it is not a major term in normal operation with constant pressure condition and current densities close to the electrolyzer capacity [72]. The water flow balance (the net water transport from anode to cathode) can be expressed as follows:

$$\dot{N}_{H2O}^{mem} = \dot{N}_{H2O}^{eo} + \dot{N}_{H2O}^{diff} - \dot{N}_{H2O}^{\Delta P} \tag{54}$$

1- The water flow rate dragged from anode to cathode by electro-osmotic forces, $\dot{N}_{H2O}^{eo}$, can be calculated as below [72,73]:

$$\dot{N}_{H2O}^{eo} = \frac{n_d\, i_{useful}\, A_{cell}\, N_{cells}}{F} = n_d \frac{I_{stack}}{F} \tag{55}$$

where the electro-osmotic drag coefficient, n_d, can be assumed constant or calculated as a function of the membrane hydration [36,74].

$$n_d = 0.0029\,\lambda_m^2 + 0.05\lambda_m - 3.4 \times 10^{-19} \quad (56)$$

where λ_m is the water content through the membrane and is equal to the arithmetic mean of the water contents of the anode, λ_a, and the cathode, λ_c [74,75], normally set as input variables that subsequently define the membrane water content.

In case of using a Nafion® membrane, the water content, λ_m values in the range of 7 to 22 are reported (= 7dry enough; = 14 good hydration; = 22 bathed) [53,76]. In a PEM electrolyzer with a Nafion 117 membrane, it can be assumed that the entire membrane is fully hydrated. Accordingly, the water content, λ_m, in the range of 14 to 22 is assumed as a function of temperature so that the water content of λ_m =14 assumed at 30 ℃ increases linearly with temperature up to λ_m=22 at 80 ℃ [31,77]:

$$\lambda_m = 14 + 0.16\,(T_{op} - 303.15) \quad (57)$$

2- In PEM electrolysis, water is normally pumped into the anode channel at high concentration, which leads to a small quantity permeating through the membrane towards the cathode channel due to the concentration gradient between the electrodes. The diffusivity-driven water flow rate due to the difference in concentration between anode and cathode is given by Fick's diffusion law [63,73]:

$$\dot{N}_{H2O}^{diff} = \frac{D_{H2o,eff}\,(C_{H2o,a} - C_{H2o,c})A_{cell}\,N_{cell}}{t_{mem}} \quad (58)$$

where $D_{H2o,eff}$ is the effective water diffusivity, t_{mem} is the membrane thickness, $C_{H2O,c}$ and $C_{H2O,a}$ are the concentrations of water on the surface of the membrane at the interface of the cathode and the anode, respectively. These concentrations can be expressed as:

$$C_{\mathrm{H_2O}\,a} = \frac{\rho_{\mathrm{mem}}}{M_{\mathrm{mem}}} \cdot \lambda_a \quad (59)$$

$$C_{\mathrm{H_2O}\,c} = \frac{\rho_{\mathrm{mem}}}{M_{\mathrm{mem}}} \cdot \lambda_c \quad (60)$$

where ρ_{mem} and M_{mem} are the density and the equivalent dry weight of the membrane, respectively. Both are physical properties of the material used in the manufacture of the PEM membrane, which is considered a key component in PEMEL. Nafion®, among perfluorinated polymers, is the most widely used electrolyte in PEMEL due to its chemical and electrochemical stability, as well as high proton conductivity [78]:

Finally, the effective water diffusivity, $D_{H2o,eff}$, is a function of the membrane porosity and diffusivity, ε, and diffusivity of water, D_{H2O}, [37,73]:

$$D_{H2O,eff} = D_{H2O} . \varepsilon^{1.5} \tag{61}$$

where the diffusion coefficient of water, D_{H2O}, is a function of temperature, T_{op}, and water content of the membrane,λ_m and it can be calculated as below [53,78]:

$$D_{H2O} = D_{\lambda_m} . exp\left(2416 \left(\frac{1}{T_{amb}} - \frac{1}{T_{op}}\right)\right) \tag{62}$$

where,

$$\begin{aligned} D_{\lambda_m} &= 10^{-10} \ \ for \ \ \lambda_m < 2 \\ D_{\lambda_m} &= 10^{-10} . \left(1 + 2(\lambda_m - 2)\right) \ \ for \ \ 2 \leq \lambda_m < 3 \\ D_{\lambda_m} &= 10^{-10} . \left(3 - 1.67(\lambda_m - 3)\right) \ \ for \ \ 3 \leq \lambda_m < 4.5 \\ D_{\lambda_m} &= 1.25 \times 10^{-10} \ \ for \ \ \lambda_m \geq 4.5 \end{aligned} \tag{63}$$

Since in this study λ_m is in the range 14 to 22, D_{H2O} will be:

$$D_{H2O} = 1.25 \times 10^{-10} \exp\left(2416 \left(\frac{1}{T_{amb}} - \frac{1}{T_{op}}\right)\right) \tag{64}$$

The diffusivity-driven water transport, $\dot{N}_{H2O}^{diff}$, is very small because the difference in water concentration across the membrane $\left(C_{H2o,a} - C_{H2o,c}\right)$ is practically negligible. In the ACM, the water concentrations are computed with a flash on the anode and cathode sides.

3- The cathode side often operates at a higher pressure than the anode and this pressure difference at the two sides of the membrane causes water transfer from cathode to anode. This pressure difference is to ensure safety, hydrogen purity, membrane durability, and compression efficiency. The pressure-driven crossflow (flow back from cathode to anode), $\dot{N}_{H2O}^{\Delta P}$, offsets the electro-osmotic water transfer from anode to cathode. This phenomenon can be assessed using Darcy's law, which takes into account the membrane's permeability [71,79]:

$$\dot{N}_{H2O}^{\Delta P} = \frac{A_{cell} K_m \rho_{H2O} * \left(P_{cat} - P_{an}\right)}{\mu_{H2O} \, t_{mem}} \tag{65}$$

where μ_{H2O} and ρ_{H2O} are the water viscosity and density, respectively, computed with Aspen properties package. Also, $K_m = 1.58 \times 10^{-18} \, m^2$ [20] represents the membrane permeability to water.

Similar to water transfer in the membrane, gas crossover takes place in two directions so that hydrogen and oxygen generated in the cathode and anode, respectively, transfer to the other side through membrane.

Permeation of hydrogen to the anode, $\dot{N}_{H2}^{mem}$,,caused by electro-osmosis drag effect, $\dot{N}_{H2O}^{eo}$, pressure gradient, $\dot{N}_{H2}^{\Delta P}$, and the concentration difference between the PEM electrodes, $\dot{N}_{H2}^{diff}$ [24,71]:

$$\dot{N}_{H2}^{mem} = \dot{N}_{H2}^{diff} + \dot{N}_{H2}^{\Delta P} - \dot{N}_{H2O}^{eo} \tag{66}$$

Also, permeation of oxygen to the anode is similarly caused electro-osmosis drag effect, $\dot{N}_{O2}^{eo}$, and the concentration difference between the PEM electrodes, $\dot{N}_{O2}^{diff}$: [24,71]:

$$\dot{N}_{O2}^{mem} = \dot{N}_{O2}^{diff} + \dot{N}_{O2}^{eo} \tag{67}$$

The gas crossover phenomenon can lead to impurity issues and pose safety hazards, particularly in the production of low current density. To mitigate the risks, it is necessary to monitor and control the gas crossover in electrolysis unit design, operation, and control to produce a controlled gas purity [16]. However, this study is aimed at hydrogen production so that the gas crossover is excluded for simplifying the model; meanwhile, the impact of gas crossover on hydrogen production is accounted for via Faraday efficiency.

6.2.9. Energy balance sub-model

According to the assumption mentioned in section 6.2.5, all material streams leaving the cathode and anode sides are at the same operating temperature, T_{op}. The stack is assumed to operate adiabatically apart from a minor loss of heat due to free convection of ambient air. As the simulation is in a steady state and there is no cooler or heater in the electrolysis system, the energy balance on the stack includes the electrical power input W_{stack}, inlet stream enthalpy, Q_{in}, outlet streams enthalpy, Q_{out}, and heat loss to the environment , Q_{loss}, as below:

$$Q_{in} + W_{stack} = Q_{out} + Q_{loss} \tag{68}$$

$$Q_{in,a} + Q_{in,c} + W_{stack} = Q_{out,a} + Q_{out,c} + Q_{loss} \tag{69}$$

where to the stack, $Q_{in,a}$ and $Q_{in,c}$ are the enthalpy of the streams entering the anode and cathode, respectively. Also, $Q_{out,a}$ and $Q_{out,c}$ are the enthalpy of the streams exiting the anode and cathode, respectively.

The assumed heat loss, Q_{loss}, to the ambient air is calculated as below:

$$Q_{loss} = h.A_{ext}\,(T_s - T_{amb}) \tag{70}$$

To generalize the exterior area, A_{ext}, it has been scaled to the cell area and number of cells using the following geometry:

$$A_{ext} = 0.22\,.A_{cell}.N_{cells} \tag{71}$$

and T_s represents the exterior surface temp, assumed to be 10 ℃ below the operating temperature of the stack.

$$T_s = T_{op} - 10 \tag{72}$$

Also, the heat transfer coefficient, h, is estimated with the following rule of thumb [80]:

$$h = 1.37\left(\frac{T_s - T_{amb}}{L}\right)^{1.4} \tag{73}$$

where L is the characteristic length of the stack determined as below [81]:

$$L = A_{cell}{}^{\frac{1}{2}} \tag{74}$$

It should be noted that in operations including voltages higher than thermoneutral temperature, there will be a heat generation causing increment of stack temperature:

$$Q_{gen} = I_{stack}.(V - V_{tn}) \tag{75}$$

Figure 6-10 shows a simplified diagram of the calculation process for the integrated subsystems of the electrolyzer.

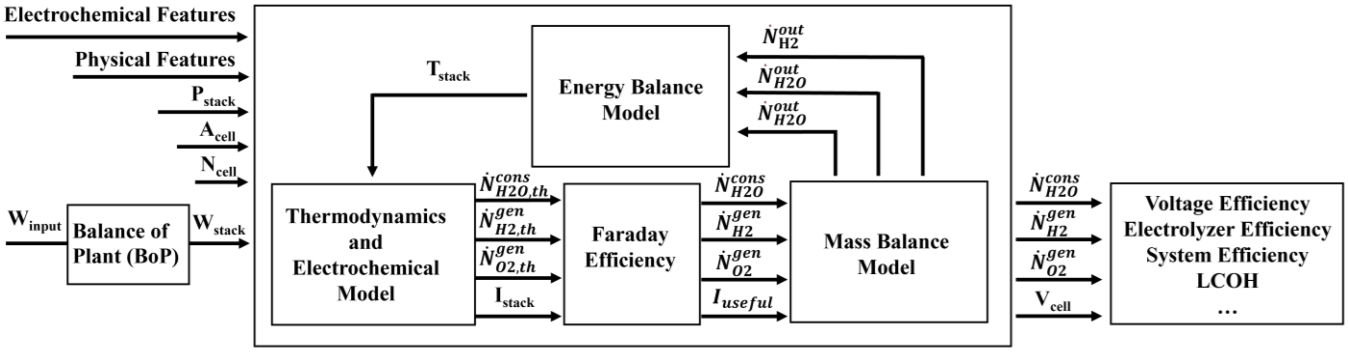

Figure 6-10. Integrated submodels applied for PEM electrolyzer modelling

6.2.10. Effects of operating condition

Since the electrolyzer performance is fundamentally dependent on transport phenomena, operating conditions, including temperature and pressure, determine the process effectiveness [42,82]. Figure 6-11 shows the dependency of cell voltage (polarization curve) on operating pressure and temperature. According to this figure, in general, higher temperature results in low cell voltage, while higher pressure results in higher cell voltage. On the other hand, a higher operating pressure may cause excessive gas crossover, and high temperature is limited by membrane mechanical features and electrolyzer lifetime [83]. Hence, an optimized operation in terms of operating pressure and temperature is necessary to ensure an efficient operation. The details of both parameters are explained in the following subsections.

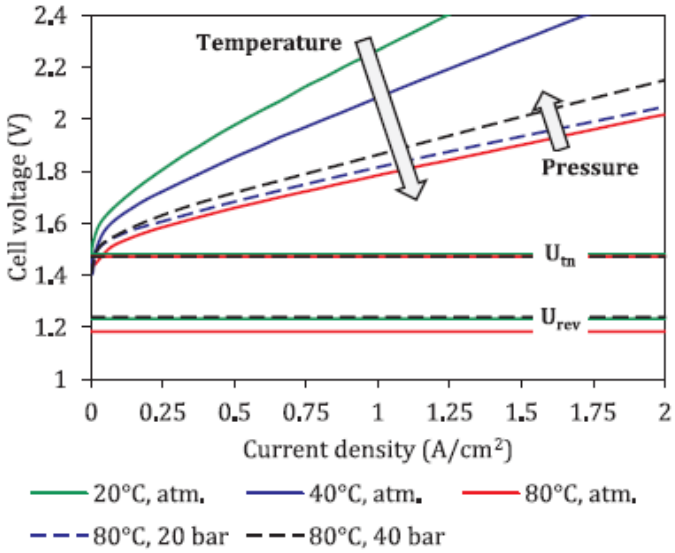

Figure 6-11. Influence of temperature and pressure on the polarization curve of a PEM electrolyzer [84].

It should be noted that operating pressure is normally fixed for an electrolyzer, and changing it leads to complications in process, design, and stack durability, so that operating pressure is not a controlled parameter but a fixed design parameter. On the other hand, operating temperature is basically a dynamic parameter controlled by circulating water flow rate or, in smaller units, using an external heater/cooler. Accordingly, in an electrolysis operation under variable renewable energy (VRE) sources, it has to be controlled for operational stability and mechanical unit protection, especially the delicate parts such as membrane. Moreover, since operating temperature affects the unit performance, operating it

can be harnessed for a more flexible and efficient electrolysis unit and reduce the capital and operational expenditures.

6.2.10.1. Effects of pressure

In many PEM electrolyzers, the cathode pressure is intentionally maintained higher than the anode pressure. The main reasons are preventing oxygen crossover (safety), improving hydrogen purity, and reducing the hydrogen compression cost for storage, transport, or use. On the other hand, as shown in Figure 6-11, higher pressure results in lower voltage efficiency. Higher cathode pressure (differential pressure) affects the open circuit voltage and increases it according to the Nernst equation. Pressure can also affect the diffusion overpotential and decrease it slightly [85]. In addition, the hydrogen permeation through the membrane (from cathode to anode) increases linearly with pressure, and for operations at higher pressure, it should be maintained below the safety threshold, particularly in low current densities [86]. Higher hydrogen permeation is associated with lower Faraday efficiency. Hence, higher operating pressure results in a lower electrolyzer efficiency value. Accordingly, an elevated operating pressure shall be justified by compression cost, including the compression and drying energy cost (operating cost) [85]. The impact of pressure on faraday efficiency, voltage efficiency and electrolyzer efficiency is shown in Figure 6-12

A 10% increment of operating pressure can cause about a 2% increment of the hydrogen-to-oxygen (HTO) factor, while its impact on cell voltage is negligible [87]. In another study it was found that increasing the hydrogen outlet pressure from 30 to 200 bar at 60°C adds 55 mV to the cell voltage, mainly due to the Nernst voltage variation that is equivalent to a voltage efficiency decrement from 75% to 61%. This pressure change led to decreasing the Faraday efficiency from 100% to 90% and electrolyzer efficiency declining from 75% to 66% [85].

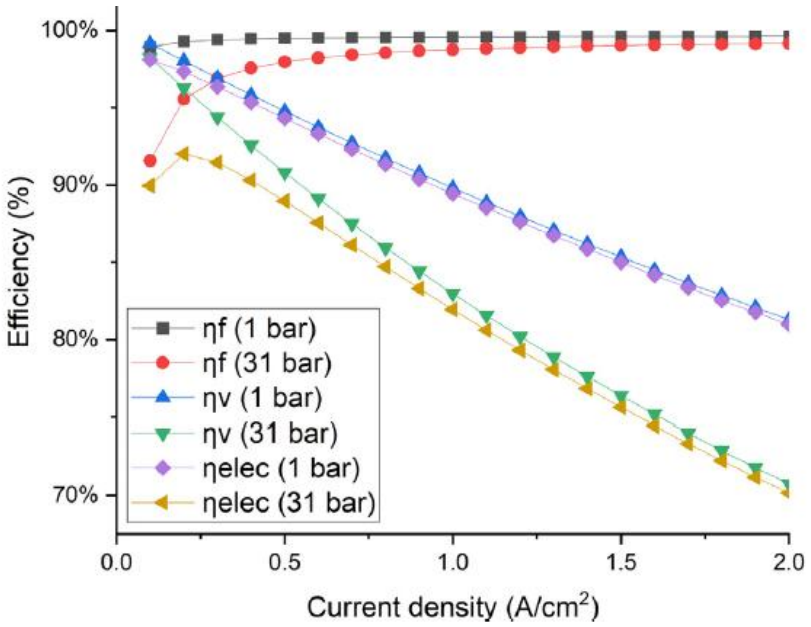

Figure 6-12. Effects of pressure on electrolyzer efficiency [28].

6.2.10.2. Effect of Temperature

As mentioned, higher operating temperature results in a lower cell potential (polarization curve) due to the impacts of temperature on transport phenomena and conductivity of the electrolyzer components [88].

Higher temperature obviously affects the thermodynamic voltage (open circuit voltage and decrease according to the Nernst Equation [89]. Higher operating temperature results in a higher exchange current density and consequently a lower activation overpotential; meanwhile, it can also increase the Tafel slope and cause an increase in the activation overpotential so that there will be a different balance for each PEM electrolyzer depending on the temperature range and the reaction kinetics [90]. Also, higher temperature leads to a lower ohmic resistance due to improved membrane conductivity, which leads to a lower ohmic overpotential according to the Arrhenius equation [53]. Diffusion overpotential also decreases with temperature, according to Zhang et al. [56]. On the other hand, Faraday efficiency can also be affected by temperature [86] while it is reported to be very minor and negligible [24]. The impact of temperature on PEM electrolyzer efficiency is shown in Figure 6-13. As this figure shows, the electrolyzer efficiency increases with increasing the operating temperature.

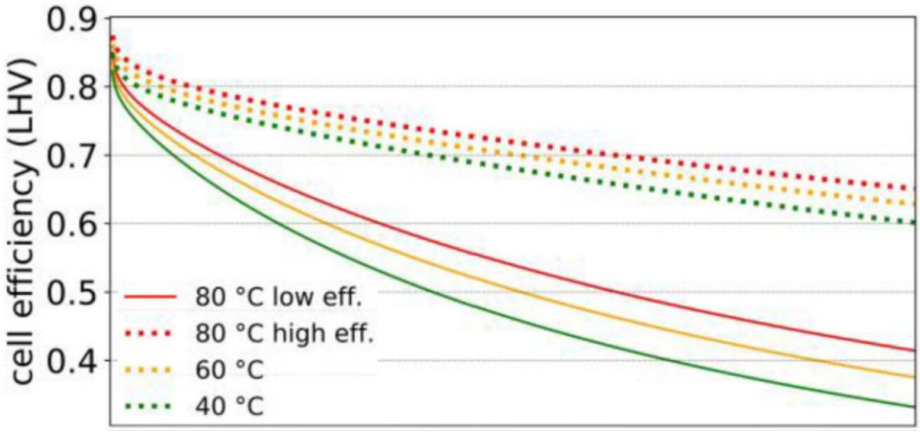

Figure 6-13. Dependency of PEM electrolyzer efficiency on operating temperature for different membrane thicknesses [91].

6.2.11. PEMEL modelling in Aspen Plus

As Aspen Plus lacks a built-in unit operation for modelling a PEMEL stack, a custom user-defined stack model is developed in Aspen Custom Modeler (ACM) and later integrated within the overall unit operation flowsheet in Aspen Plus for simulations at any specified condition or purpose [92].

Figure 6-14 shows the ACM software, and the icon designed for the PEM electrolyzer stack, including the power port and stream as well as material ports and streams for water, oxygen, and hydrogen. This model is developed based on the preceding subsections and incorporates the governing correlations of the PEM electrolyzer to describe various phenomena, including energy and mass balances and electrochemical behaviour within the electrolyzer stack. This model can be applied in various simulation scenarios, either coupled with other units or as an independent unit, for detailed studies on electrolysis unit design and operation.

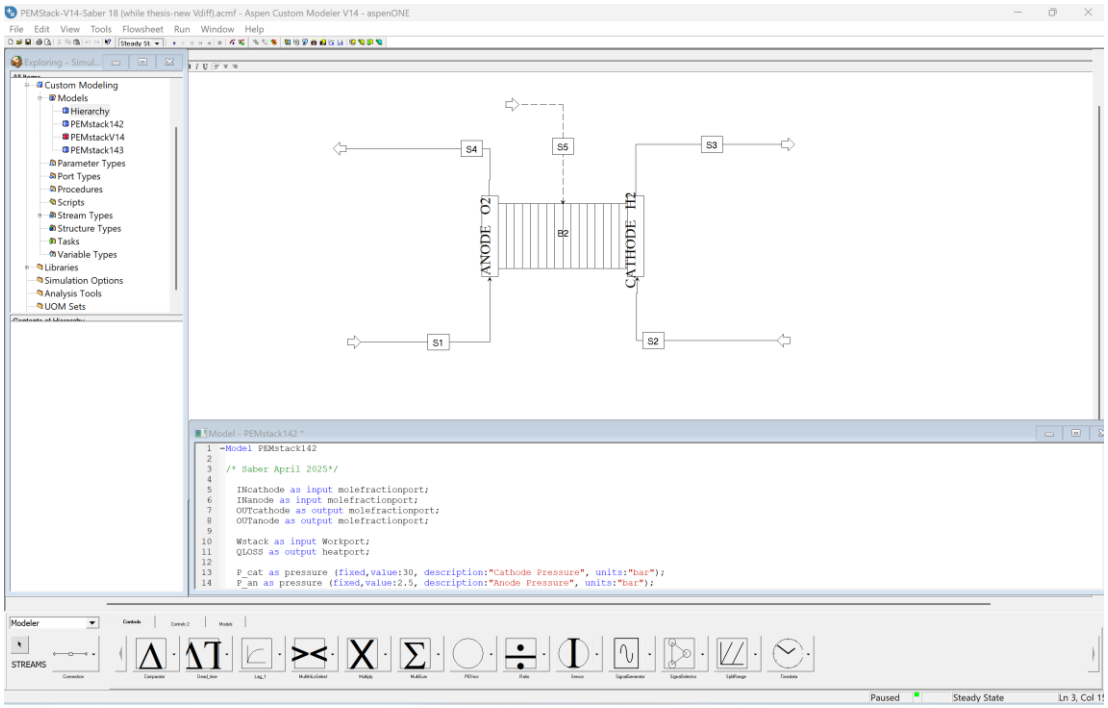

Figure 6-14. PEM electrolyzer model prepared in Aspen Custom Modeler (ACM), including the PEM electrolyzer block, power stream and material streams.

After transferring the electrolyzer block to the Aspen Plus environment, the electrolyzer unit is completed as shown in Figure 6-15. The unit is comprised of separate circuits for the anode and cathode sides. Water is fed into both sides, where it is cooled and directed into the electrolyzer stack (the cathode water loop can be eliminated in a real case in case of applying strategies to hydrate the cathode and membrane at low current levels). The resulting gas-liquid mixtures are sent to separators to extract O_2 and H_2 gases from the two-phase product, which are exiting the unit afterwards. To maintain system stability, make-up water is adjusted by calculator blocks and added through makeup streams. The heat losses are accounted for via an energy stream connected to the electrolyzer block.

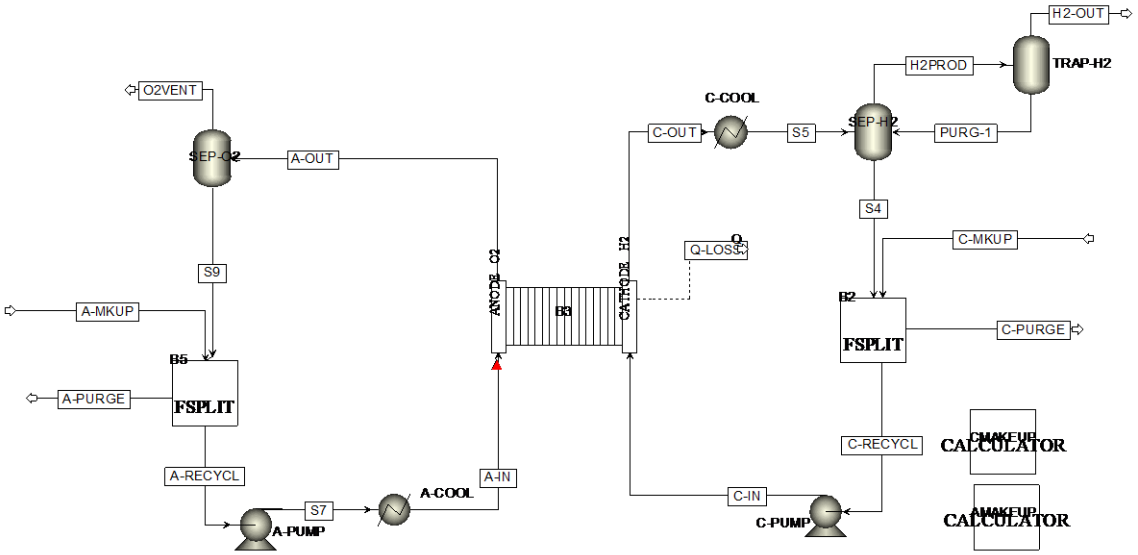

Figure 6-15. PEM electrolyzer flowsheet developed din Aspen Plus.

Water circulation predominantly occurs on the anode side, while a limited cathode-side flow helps maintain membrane hydration, especially at low current densities (low power input), at which water crossover in the membrane can occur in reverse direction from cathode to anode due to dominance of cathode-anode pressure difference and insufficient electro-osmotic water drag from anode to cathode. Hence, water is circulated on both sides of the electrolyzer for the simulation purpose and covering the full operational range with no limit. Also, the calculator blocks are applied to manage the water imbalances and maintain the input water flow rates to the stack via setting the make-up water for each steady-state simulation case. This approach may not represent realistic transient effects or pressure-driven asymmetries, but it is acceptable for simulation purposes. On the other hand, the circulating water flow rate should be adjusted to keep the temperature in a particular allowable range.

Given that each quantity of power input generates a specific quantity of heat, which affects the operating temperature, to keep the electrolyzer temperature fixed, a variable input water flow rate is required; otherwise, the temperature would vary with input power variation. On the other hand, controlling an electrolyzer unit working with variable input power is a complicated task, and it may lead to instability and failure of the unit operation. This is one reason to avoid a dynamic model in Aspen Plus, and instead a steady-state model is developed (other reasons are explained in section 6.2.4). Nevertheless, by applying a steady-state modelling strategy with water circulation loops adjusted by controller blocks,

Aspen Plus offers limited tools, which only allow a fixed water circulation flow rate rather than enabling a variable water flow rate adjustment.

Accordingly, in order to adjust the water flow rate required for each power level, the water loops are broken, and the makeup blocks are removed. This new configuration enabled us to set the stack inlet water flow rate to the operating temperature. Accordingly, the water flow rate would be set according to the required operating temperature. It should be noted that the fixed water flow rate can also be applied to monitor the variation of operating temperature with variation of input power. This approach is a simplified semi-dynamic simulation, enabling the Aspen model for variable input power profile. Figure 6-16 shows the final electrolysis unit modelled in Aspen Plus. The model is validated with the experimental data, and a parametric study is done to assess the impact of pressure and temperature on the electrolyzer performance.

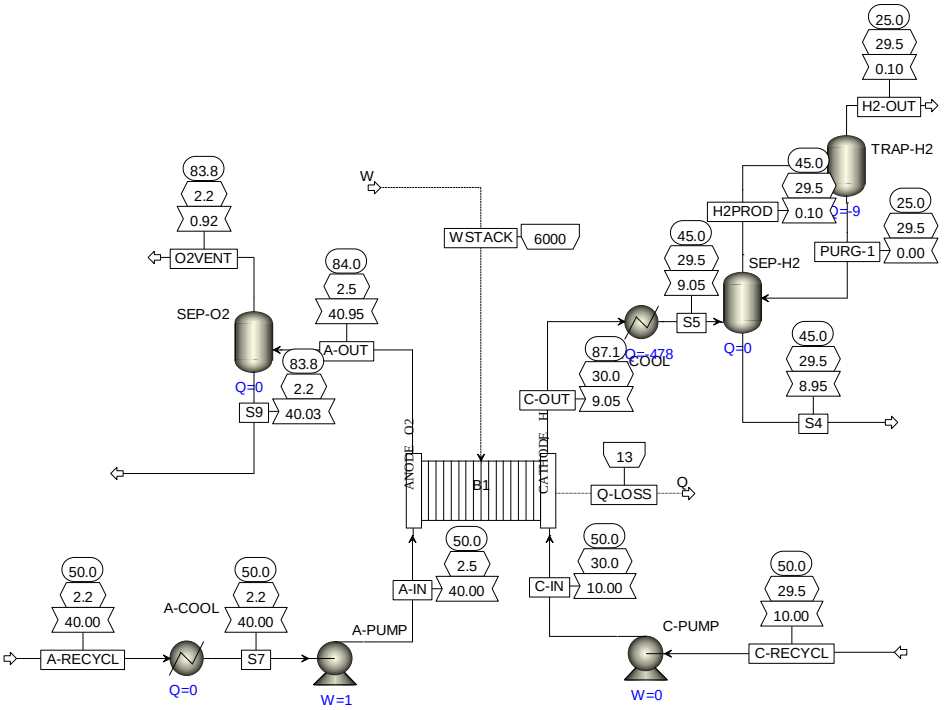

Figure 6-16. Water electrolysis unit with flexible water inlet flow rate adaptable variable input power in semi-dynamic mode.

6.3. Results and discussion

6.3.1. Model Validation

An electrolyzer consisting of a standard industrial-type membrane-electrode assembly (MEA) is used as a benchmark for validation and specifying the charge transfer coefficients [93]. The experimental reference case is a single-cell PEMEL composed of a Nafion 177 membrane, PtIr cathodes, and the MEA sandwiched

between standard GDLs compatible with H_2/O_2 operation. The test is conducted at 80 °C and an operating pressure of $P_{cat} = 13.6\ atm.$ and $P_{an} = 1\ atm.$ The values of reference exchange current densities ($i_{0,cat} = 0.1\ A/cm^2$, $i_{0,an} = 2 \times 10^{-6}\ A/cm^2$) are specified based on the study of Tijani et al. [46] and the values of charge transfer coefficients are specified by fitting the polarization curve with the available experimental results, as explained in section 6.2.6.4. Accordingly, the values of $\alpha_{an} \approx 0.3250$ and $\alpha_{cat} \approx 0.3187$ are obtained, resulting in the minimum squared error between the experimental curve and the model. Figure 6-17a shows the experimental results and modelling prediction employing these values for charge transfer coefficients. According to this figure, the model matches the experimental data perfectly at the same operating condition as the experimental study, ensuring the high accuracy of the developed model. Figure 6-17b also shows the polarization curve breakdown into its constituent overpotentials and the open-circuit voltage.

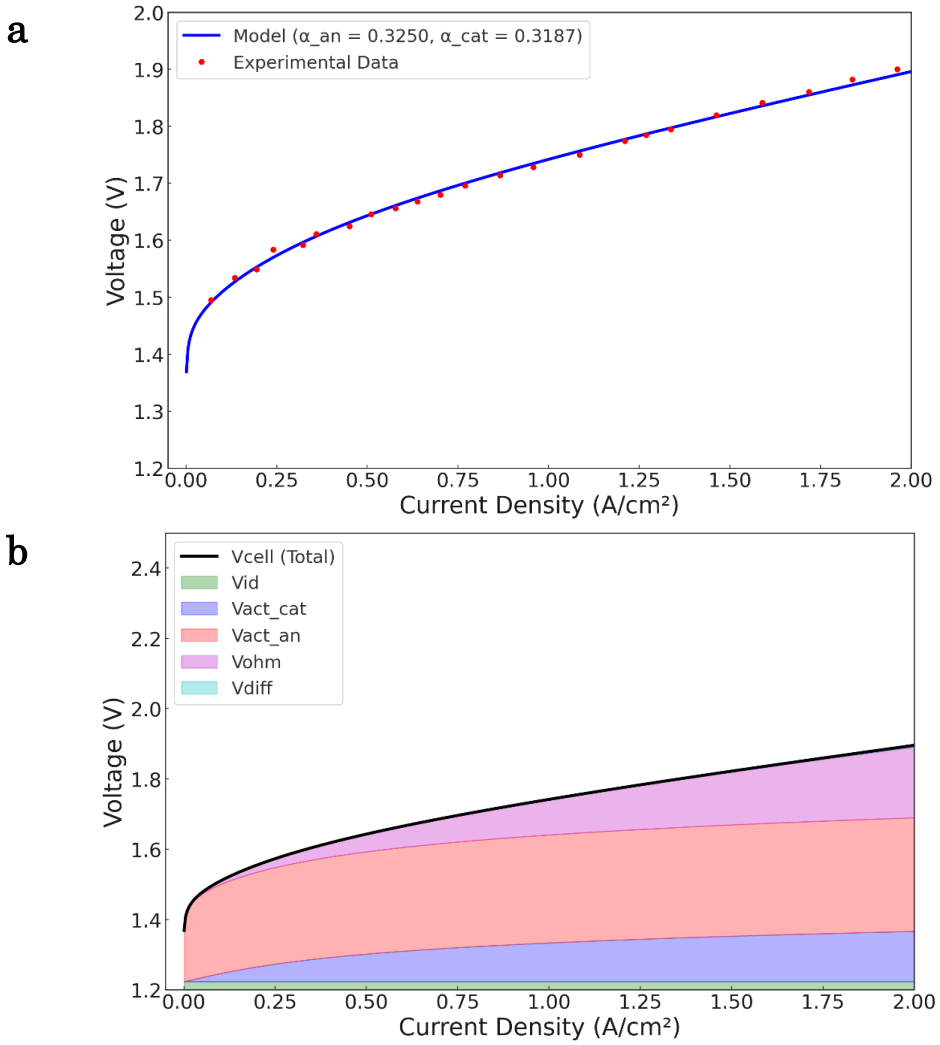

Figure 6-17. (a) Polarization curve obtained from modelling compared to the experimental results and (b) Polarization curve overpotential breakdown.

The model developed in this study is intended for simulating an industrial scale electrolyzer under various operating conditions, including $P_{cat} = 2.5\ bar\ and\ P_{an} = 30\ bar$ which is a common operating condition for electrolyzers available in the market. Accordingly, the simulation is repeated with different operating conditions. Figure 6-18 shows the polarization curve for both operating pressures. Conforming to the theoretical discussion in section 6.2.10.1, increasing the pressure increases the cell voltage slightly. This graph shows that the prepared model enables the operator to capture the impacts of pressure variation, and it can be used for any specific operating pressure and easily calibrated to match a particular PEM electrolyzer fabricated by any manufacturer.

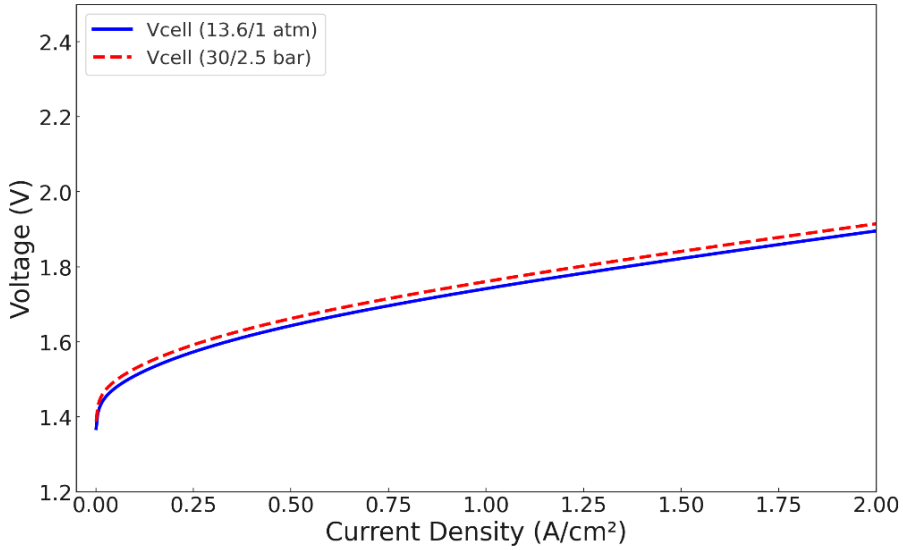

Figure 6-18. Effect of operating pressure on PEM electrolyzer polarization curve

6.3.2. Effects of temperature on the PEMEL cell voltage

As discussed in section 6.2.10.2, temperature is an important factor in PEM electrolyzer operation. Different overpotentials, open circuit voltage, and cell voltage are separately calculated and plotted against current density in Figure 6-19 in the range of 30 to 90°C. According to these graphs, increasing the operating temperature decreases open circuit voltage and all overpotentials, leading to lower cell voltage. In general, the impact of temperature on the high current density zone is more prominent, implying that a high-temperature condition can be a more efficient strategy for a high-power input condition.

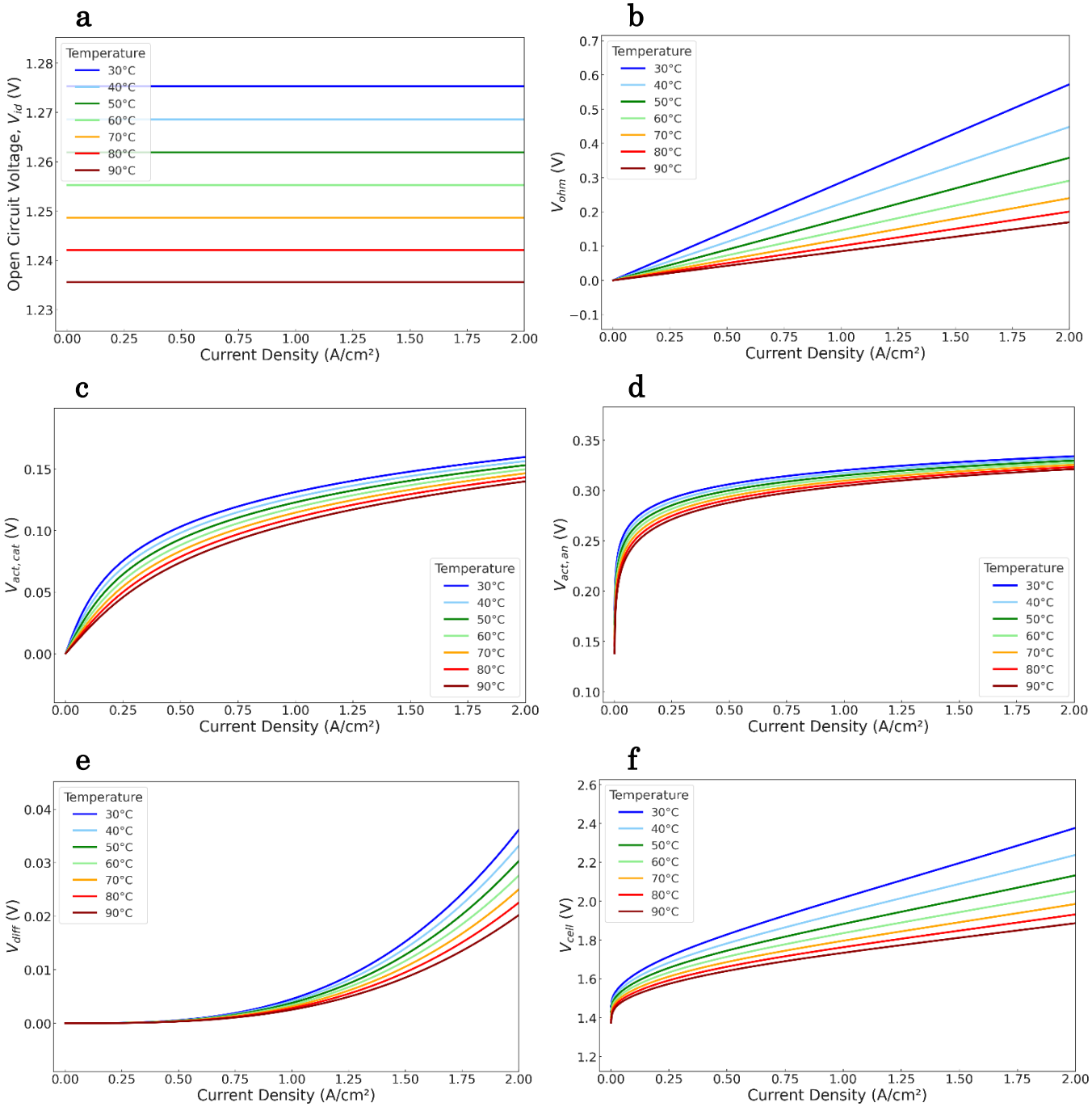

Figure 6-19. Variation of (a) open circuit potential, (b) ohmic overpotential, (c) cathode activation overpotential, (d) anode activation overpotential, (e) diffusion overpotential and (f) cell voltage of the simulated PEM electrolyzer cell with temperature

6.3.3. Effects of temperature on the partial contributions of overpotentials

Figure 6-20 shows the overpotential breakdown in the polarization curve of the PEM electrolyzer at different temperatures from 30 to 90 °C. According to these figures, the major difference among polarization curves of different operating

temperatures is due to the variation of ohmic overpotential. As these figures show, the contribution of ohmic overpotential decreases with temperature, which shows the strong dependency of ohmic overpotential on operating temperature compared to other overpotentials.

a

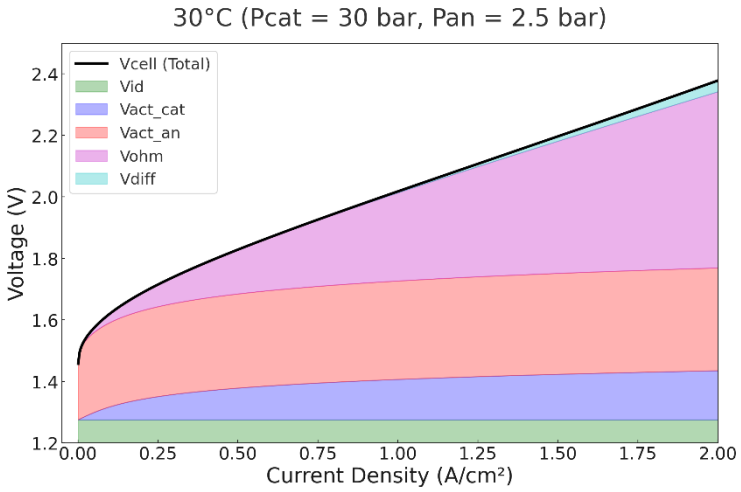

b

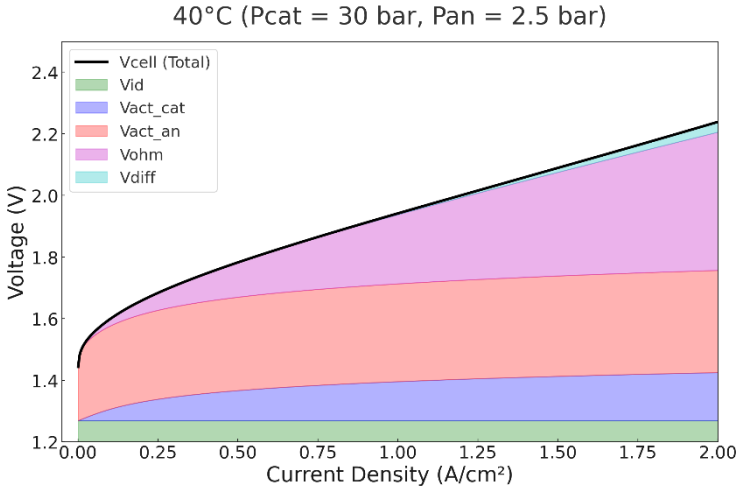

c

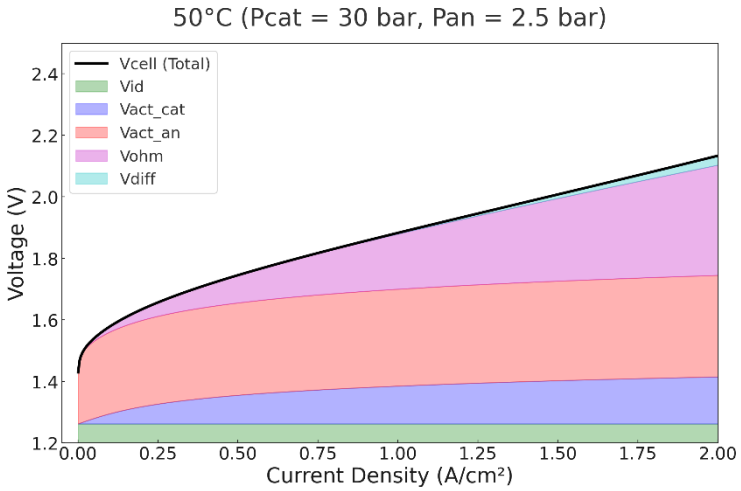

d

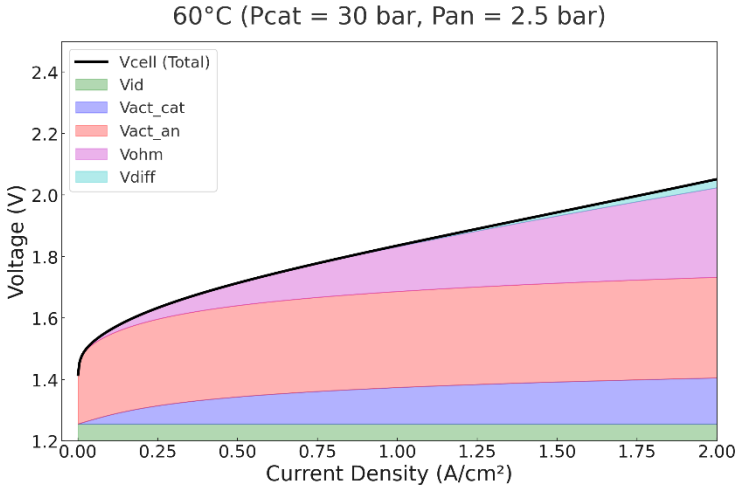
60°C (Pcat = 30 bar, Pan = 2.5 bar)
Vcell (Total)
Vid
Vact_cat
Vact_an
Vohm
Vdiff
Voltage (V)
Current Density (A/cm²)

e

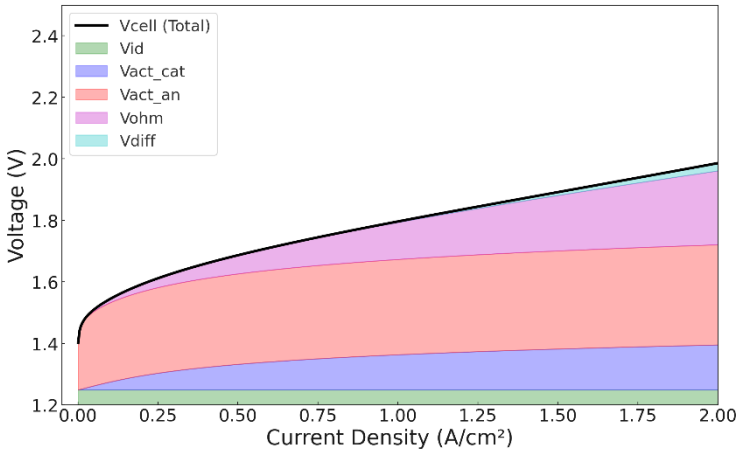
70°C (Pcat = 30 bar, Pan = 2.5 bar)
Vcell (Total)
Vid
Vact_cat
Vact_an
Vohm
Vdiff
Voltage (V)
Current Density (A/cm²)

f

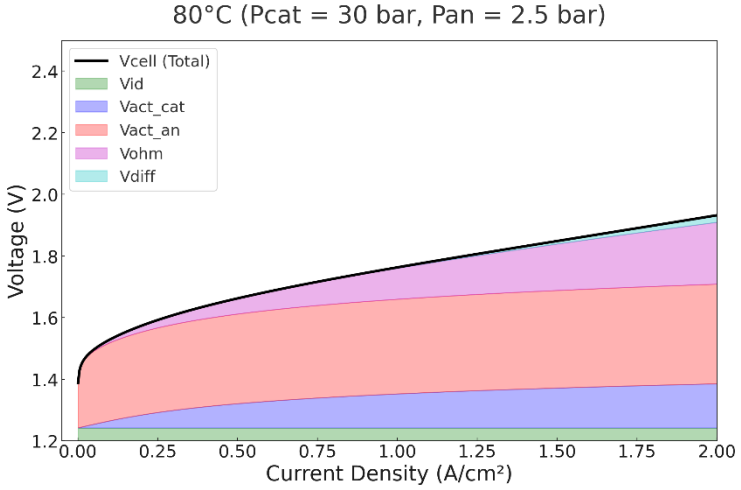
80°C (Pcat = 30 bar, Pan = 2.5 bar)
Vcell (Total)
Vid
Vact_cat
Vact_an
Vohm
Vdiff
Voltage (V)
Current Density (A/cm²)

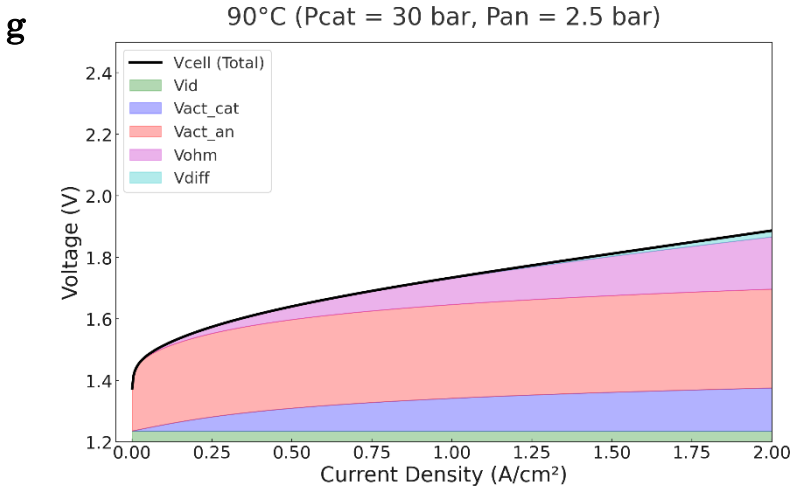

Figure 6-20. Overpotential breakdown of the PEM electrolyzer at different operating temperatures in range 30-90 °C and fixed pressure $P_{cat} = 2.5\ bar$ & $P_{an} = 30\ bar$.

6.4. Conclusions

In this study an Aspen Plus model of a PEM electrolysis plant is proposed, aiming at evaluating the performance of a complete system, including the electrolyzer stack and auxiliary parts. The model is adjusted to be adaptable to variable power input profiles and different operating conditions.

To this end, a custom model of the PEM electrolysis stack is developed as a subroutine using Aspen Custom Modeler. The empirical and semi-empirical correlations accounting for the variation of operating conditions are selected to make the model versatile to adapt to varying conditions with minimum operator interference and avoid excess adjustments. The model is then integrated into the Aspen Plus model.

To ensure the accuracy and validity of the model, the unknown coefficients, including the charge transfer coefficient and exchange current density, are specified through optimization, matching the model polarization curve to the experimental one with minimum RMS value. So, the PEM electrolysis model aligns with industrial units, replicating electrochemical and transport phenomena with reasonable accuracy.

Applying different operating pressures shows that the model predicts the dependency of polarization behavior on operating pressure correctly and increasing the pressure as an input in the model results in a higher cell voltage. Also, the model shows that the increment of operating temperature can improve the stack performance by reducing the cell voltage, increasing the operating

temperature from 40 to 80 °C results in about 13.7% lower cell voltage at a current density of 2 A/cm² (from 2.24 to 1.93). In general, the impact of temperature on the high current density zone is more prominent, implying that a high-temperature condition can be a more efficient strategy for high-power input conditions. On the other hand, since the water circulation is the main tool for temperature control of the electrolyzer (in addition to sustaining the electrochemical reactions), two different operation scenarios are proposed for running a PEMEL unit: (1) fixed circulating water flow rate and (2) fixed operating temperature are proposed for operation of a PEMEL unit, and the model is adapted to enable both options in simulation, aiming at a comparative study. Theoretically, while the fixed temperature operation scenario is the commonly practiced control approach, the fixed water flow rate scenario, capable of sustaining the temperature in the allowed range, offers various benefits such as simpler control system requirements, smaller heat exchanger size, higher voltage efficiency, and voiding any excess stress by variation of water flow rate in the electrolyzer cells. The provided PEMEL model and the proposed scenario are potentially adaptable to variable input power profiles, and they can be employed to carry out techno-economic evaluation of a hydrogen production unit coupled with renewable energy sources or to be integrated with downstream unit operations such as green ammonia or green methanol plants.

6.5. References

[1] | Greenhouse Gas (GHG) Emissions | Climate Watch, (n.d.). https://www.climatewatchdata.org/ghg-emissions (accessed June 7, 2025).

[2] Renewable energy targets - European Commission, (n.d.). https://energy.ec.europa.eu/topics/renewable-energy/renewable-energy-directive-targets-and-rules/renewable-energy-targets_en (accessed June 7, 2025).

[3] Ninth report on the state of the energy union - European Commission, (n.d.). https://energy.ec.europa.eu/strategy/energy-union/ninth-report-state-energy-union_en (accessed June 7, 2025).

[4] S. Mucci, A. Mitsos, D. Bongartz, Power-to-X processes based on PEM water electrolyzers: A review of process integration and flexible operation, Comput Chem Eng 175 (2023). https://doi.org/10.1016/j.compchemeng.2023.108260.

[5] World energy transitions outlook 2023 : 1.5°C pathway, International Renewable Energy Agency IRENA, 2023.
[6] The Future of Hydrogen – Analysis - IEA, (n.d.). https://www.iea.org/reports/the-future-of-hydrogen (accessed June 6, 2025).
[7] X.C. Schmidt Rivera, E. Topriska, M. Kolokotroni, A. Azapagic, Environmental sustainability of renewable hydrogen in comparison with conventional cooking fuels, J Clean Prod 196 (2018) 863–879. https://doi.org/10.1016/J.JCLEPRO.2018.06.033.
[8] N. Tenhumberg, K. Büker, Ecological and Economic Evaluation of Hydrogen Production by Different Water Electrolysis Technologies, Chem Ing Tech 92 (2020) 1586–1595.
https://doi.org/10.1002/CITE.202000090;WGROUP:STRING:PUBLICATION.
[9] Z. Kang, S. Yu, G. Yang, Y. Li, G. Bender, B.S. Pivovar, J.B. Green, F.Y. Zhang, Performance improvement of proton exchange membrane electrolyzer cells by introducing in-plane transport enhancement layers, Electrochim Acta 316 (2019) 43–51. https://doi.org/10.1016/J.ELECTACTA.2019.05.096.
[10] M.N.I. Salehmin, T. Husaini, J. Goh, A.B. Sulong, High-pressure PEM water electrolyser: A review on challenges and mitigation strategies towards green and low-cost hydrogen production, Energy Convers Manag 268 (2022) 115985. https://doi.org/10.1016/J.ENCONMAN.2022.115985.
[11] GREEN HYDROGEN COST REDUCTION SCALING UP ELECTROLYSERS TO MEET THE 1.5°C CLIMATE GOAL H 2 O 2, 2020. www.irena.org/publications.
[12] E.& I.Strategy. Department for Business, UK Hydrogen Strategy 2023, (2023) 122. https://www.gov.uk/government/publications/uk-hydrogen-strategy (accessed June 7, 2025).
[13] M.A.S.. Masoum, E.F.. Fuchs, Power quality in power systems and electrical machines, (2015).
[14] H. Zhang, T. Yuan, Optimization and economic evaluation of a PEM electrolysis system considering its degradation in variable-power operations, Appl Energy 324 (2022) 119760. https://doi.org/10.1016/J.APENERGY.2022.119760.
[15] S.S. Mohammadshahi, F.A. Boulaire, J. Love, S.A. Gorji, I.D.R. Mackinnon, A flexible analytical model for operational investigation of solar hydrogen plants, Int J Hydrogen Energy 47 (2022) 782–808. https://doi.org/10.1016/J.IJHYDENE.2021.10.072.
[16] A. Benmehel, S. Chabab, A.L. Do Nascimento Rocha, M. Chepy, T. Kousksou, PEM water electrolyzer modeling: Issues and reflections, Energy

Conversion and Management: X 24 (2024). https://doi.org/10.1016/j.ecmx.2024.100738.
[17] Strategic Research and Innovation Agenda Final Draft, 2020. https://hydrogeneurope.eu/wp-content/uploads/2021/11/20201027-SRIA-CHE-final-draft.pdf (accessed June 7, 2025).
[18] T. Franz, G. Papakonstantinou, K. Sundmacher, Transient hydrogen crossover in dynamically operated PEM water electrolysis cells - A model-based analysis, J Power Sources 559 (2023) 232582. https://doi.org/10.1016/J.JPOWSOUR.2022.232582.
[19] Á. Hernández-Gómez, V. Ramirez, D. Guilbert, B. Saldivar, Cell voltage static-dynamic modeling of a PEM electrolyzer based on adaptive parameters: Development and experimental validation, Renew Energy 163 (2021) 1508–1522. https://doi.org/10.1016/J.RENENE.2020.09.106.
[20] Z. Ma, L. Witteman, J.A. Wrubel, G. Bender, A comprehensive modeling method for proton exchange membrane electrolyzer development, Int J Hydrogen Energy 46 (2021) 17627–17643. https://doi.org/10.1016/J.IJHYDENE.2021.02.170.
[21] J. Gong, C. Sun, H. Shi, W. Tan, Response behaviour of proton exchange membrane water electrolysis to hydrogen production under dynamic conditions, Int J Hydrogen Energy 48 (2023) 30642–30652. https://doi.org/10.1016/J.IJHYDENE.2023.04.223.
[22] F. Gutiérrez-Martín, J.A. Díaz-López, A. Caravaca, A.J. Dos Santos-García, Modeling and simulation of integrated solar PV - hydrogen systems, Int J Hydrogen Energy 52 (2024) 995–1006. https://doi.org/10.1016/j.ijhydene.2023.05.179.
[23] S. Asiaban, D. Bozalakov, L. Vandevelde, Development of a dynamic mathematical model of PEM electrolyser for integration into large-scale power systems, Energy Conversion and Management: X 23 (2024) 100610. https://doi.org/10.1016/J.ECMX.2024.100610.
[24] A.S. Tijani, A.H.A. Rahim, Numerical Modeling the Effect of Operating Variables on Faraday Efficiency in PEM Electrolyzer, Procedia Technology 26 (2016) 419–427. https://doi.org/10.1016/J.PROTCY.2016.08.054.
[25] S. Shiva Kumar, V. Himabindu, Hydrogen production by PEM water electrolysis – A review, Mater Sci Energy Technol 2 (2019) 442–454. https://doi.org/10.1016/j.mset.2019.03.002.
[26] M. Carmo, D.L. Fritz, J. Mergel, D. Stolten, A comprehensive review on PEM water electrolysis, Int J Hydrogen Energy 38 (2013) 4901–4934. https://doi.org/10.1016/J.IJHYDENE.2013.01.151.

[27] X. Li, Y. Yao, Y. Tian, J. Jia, W. Ma, X. Yan, J. Liang, Recent advances in key components of proton exchange membrane water electrolysers, Mater Chem Front 8 (2024) 2493–2510. https://doi.org/10.1039/d4qm00086b.

[28] H. Sayed-Ahmed, I. Toldy, A. Santasalo-Aarnio, Dynamic operation of proton exchange membrane electrolyzers—Critical review, Renewable and Sustainable Energy Reviews 189 (2024). https://doi.org/10.1016/j.rser.2023.113883.

[29] J. Brauns, T. Turek, Alkaline Water Electrolysis Powered by Renewable Energy: A Review, Processes 2020, Vol. 8, Page 248 8 (2020) 248. https://doi.org/10.3390/PR8020248.

[30] A.W. Tricker, J.K. Lee, J.R. Shin, N. Danilovic, A.Z. Weber, X. Peng, Design and operating principles for high-performing anion exchange membrane water electrolyzers, J Power Sources 567 (2023). https://doi.org/10.1016/j.jpowsour.2023.232967.

[31] Á. Hernández-Gómez, V. Ramirez, D. Guilbert, Investigation of PEM electrolyzer modeling: Electrical domain, efficiency, and specific energy consumption, Int J Hydrogen Energy 45 (2020) 14625–14639. https://doi.org/10.1016/J.IJHYDENE.2020.03.195.

[32] D. Guilbert, G. Vitale, Experimental Validation of an Equivalent Dynamic Electrical Model for a Proton Exchange Membrane Electrolyzer, Proceedings - 2018 IEEE International Conference on Environment and Electrical Engineering and 2018 IEEE Industrial and Commercial Power Systems Europe, EEEIC/I and CPS Europe 2018 (2018). https://doi.org/10.1109/EEEIC.2018.8494523.

[33] K.K.T. Thanapalan, J.G. Williams, G.P. Liu, D. Rees, MODELLING OF A PEM FUEL CELL SYSTEM, IFAC Proceedings Volumes 41 (2008) 4636–4641. https://doi.org/10.3182/20080706-5-KR-1001.00780.

[34] J.C. Maya, F. Chejne, C.A. Gómez, J. Montoya, H. Chaquea, B. Pecha, Analysys of the performance a PEM-type electrolyzer in variable energy supply conditions, Chemical Engineering Research and Design 196 (2023) 526–541. https://doi.org/10.1016/J.CHERD.2023.07.002.

[35] A. Awasthi, K. Scott, S. Basu, Dynamic modeling and simulation of a proton exchange membrane electrolyzer for hydrogen production, Int J Hydrogen Energy 36 (2011) 14779–14786. https://doi.org/10.1016/J.IJHYDENE.2011.03.045.

[36] H. Görgün, Dynamic modelling of a proton exchange membrane (PEM) electrolyzer, Int J Hydrogen Energy 31 (2006) 29–38. https://doi.org/10.1016/J.IJHYDENE.2005.04.001.

[37] P. Colbertaldo, S.L. Gómez Aláez, S. Campanari, Zero-dimensional dynamic modeling of PEM electrolyzers, Energy Procedia 142 (2017) 1468–1473. https://doi.org/10.1016/J.EGYPRO.2017.12.594.

[38] R.L. LeRoy, C.T. Bowen, D.J. LeRoy, The Thermodynamics of Aqueous Water Electrolysis, J Electrochem Soc 127 (1980) 1954–1962. https://doi.org/10.1149/1.2130044/XML.

[39] L. Xing, J. Xuan, P.K. Das, Fuel cell fundamentals, in: Fuel Cells for Transportation: Fundamental Principles and Applications, Elsevier, 2023: pp. 29–72. https://doi.org/10.1016/B978-0-323-99485-9.00006-X.

[40] D. Bessarabov, H. Wang, H. Li, N. Zhao, PEM electrolysis for hydrogen production: Principles and applications, PEM Electrolysis for Hydrogen Production: Principles and Applications (2016) 1–382. https://doi.org/10.1201/B19096/PEM-ELECTROLYSIS-HYDROGEN-PRODUCTION-HUI-LI-HAIJIANG-WANG-DMITRI-BESSARABOV-NANA-ZHAO/RIGHTS-AND-PERMISSIONS.

[41] B. Han, S.M. Steen, J. Mo, F.Y. Zhang, Electrochemical performance modeling of a proton exchange membrane electrolyzer cell for hydrogen energy, Int J Hydrogen Energy 40 (2015) 7006–7016. https://doi.org/10.1016/J.IJHYDENE.2015.03.164.

[42] H. Lv, J. Chen, W. Zhou, X. Shen, C. Zhang, Mechanism analyses and optimization strategies for performance improvement in low-temperature water electrolysis systems via the perspective of mass transfer: A review, Renewable and Sustainable Energy Reviews 183 (2023). https://doi.org/10.1016/j.rser.2023.113394.

[43] R. García-Valverde, N. Espinosa, A. Urbina, Simple PEM water electrolyser model and experimental validation, Int J Hydrogen Energy 37 (2012) 1927–1938. https://doi.org/10.1016/J.IJHYDENE.2011.09.027.

[44] R. Escobar-Yonoff, D. Maestre-Cambronel, S. Charry, A. Rincón-Montenegro, I. Portnoy, Performance assessment and economic perspectives of integrated PEM fuel cell and PEM electrolyzer for electric power generation, Heliyon 7 (2021) e06506. https://doi.org/10.1016/J.HELIYON.2021.E06506/ASSET/E8068186-231A-48FF-859A-E07A0506DEA9/MAIN.ASSETS/GR19.JPG.

[45] M.G. Santarelli, M.F. Torchio, P. Cochis, Parameters estimation of a PEM fuel cell polarization curve and analysis of their behavior with temperature, J Power Sources 159 (2006) 824–835. https://doi.org/10.1016/J.JPOWSOUR.2005.11.099.

[46] A.S. Tijani, N.A. Binti Kamarudin, F.A. Binti Mazlan, Investigation of the effect of charge transfer coefficient (CTC) on the operating voltage of polymer electrolyte membrane (PEM) electrolyzer, Int J Hydrogen Energy 43 (2018) 9119–9132. https://doi.org/10.1016/J.IJHYDENE.2018.03.111.

[47] N.M. Marković, B.N. Grgur, P.N. Ross, Temperature-dependent hydrogen electrochemistry on platinum low-index single-crystal surfaces in acid solutions, Journal of Physical Chemistry B 101 (1997) 5405–5413. https://doi.org/10.1021/JP970930D/ASSET/IMAGES/LARGE/JP970930DF00008.JPEG.

[48] J. Milewski, G. Guandalini, S. Campanari, Modeling an alkaline electrolysis cell through reduced-order and loss-estimate approaches, J Power Sources 269 (2014) 203–211. https://doi.org/10.1016/J.JPOWSOUR.2014.06.138.

[49] J. Qi, Y. Zhai, J. St-Pierre, Effect of contaminant mixtures in air on proton exchange membrane fuel cell performance, J Power Sources 413 (2019) 86–97. https://doi.org/10.1016/J.JPOWSOUR.2018.12.023.

[50] J. Durst, C. Simon, F. Hasché, H.A. Gasteiger, Hydrogen Oxidation and Evolution Reaction Kinetics on Carbon Supported Pt, Ir, Rh, and Pd Electrocatalysts in Acidic Media, J Electrochem Soc 162 (2015) F190–F203. https://doi.org/10.1149/2.0981501JES/XML.

[51] M. Suermann, T.J. Schmidt, F.N. Büchi, Comparing the kinetic activation energy of the oxygen evolution and reduction reactions, Electrochim Acta 281 (2018) 466–471. https://doi.org/10.1016/J.ELECTACTA.2018.05.150.

[52] T. Yigit, O.F. Selamet, Mathematical modeling and dynamic Simulink simulation of high-pressure PEM electrolyzer system, Int J Hydrogen Energy 41 (2016) 13901–13914. https://doi.org/10.1016/j.ijhydene.2016.06.022.

[53] T.E. Springer, T.A. Zawodzinski, S. Gottesfeld, Polymer Electrolyte Fuel Cell Model, J Electrochem Soc 138 (1991) 2334–2342. https://doi.org/10.1149/1.2085971/XML.

[54] L. Bornemann, J. Lange, M. Kaltschmitt, Optimizing temperature and pressure in PEM electrolyzers: A model-based approach to enhanced efficiency in integrated energy systems, (2025). https://doi.org/10.5281/zenodo.1.

[55] F. Scheepers, M. Stähler, A. Stähler, E. Rauls, M. Müller, M. Carmo, W. Lehnert, Temperature optimization for improving polymer electrolyte membrane-water electrolysis system efficiency, Appl Energy 283 (2021). https://doi.org/10.1016/j.apenergy.2020.116270.

[56] H. Zhang, S. Su, G. Lin, J. Chen, Efficiency Calculation and Configuration Design of a PEM Electrolyzer System for Hydrogen Production, Int J Electrochem Sci 7 (2012) 4143–4157. https://doi.org/10.1016/S1452-3981(23)19527-7.

[57] P. Fragiacomo, M. Genovese, Modeling and energy demand analysis of a scalable green hydrogen production system, Int J Hydrogen Energy 44 (2019) 30237–30255. https://doi.org/10.1016/j.ijhydene.2019.09.186.

[58] M. Pfennig, B. Schiffer, T. Clees, Thermodynamical and electrochemical model of a PEM electrolyzer plant in the megawatt range with a literature analysis of the fitting parameters, Int J Hydrogen Energy (2024). https://doi.org/10.1016/j.ijhydene.2024.04.335.

[59] M. Schalenbach, M. Carmo, D.L. Fritz, J. Mergel, D. Stolten, Pressurized PEM water electrolysis: Efficiency and gas crossover, Int J Hydrogen Energy 38 (2013) 14921–14933. https://doi.org/10.1016/j.ijhydene.2013.09.013.

[60] E. Amores, J. Rodríguez, J. Oviedo, A. De Lucas-Consuegra, Development of an operation strategy for hydrogen production using solar PV energy based on fluid dynamic aspects, Open Engineering 7 (2017) 141–152. https://doi.org/10.1515/ENG-2017-0020/ASSET/GRAPHIC/J_ENG-2017-0020_FIG_013.PNG.

[61] G. Tjarks, A. Gibelhaus, F. Lanzerath, M. Müller, A. Bardow, D. Stolten, Energetically-optimal PEM electrolyzer pressure in power-to-gas plants, Appl Energy 218 (2018) 192–198. https://doi.org/10.1016/J.APENERGY.2018.02.155.

[62] F. Scheepers, M. Stähler, A. Stähler, E. Rauls, M. Müller, M. Carmo, W. Lehnert, Improving the Efficiency of PEM Electrolyzers through Membrane-Specific Pressure Optimization, Energies 2020, Vol. 13, Page 612 13 (2020) 612. https://doi.org/10.3390/EN13030612.

[63] F. Marangio, M. Santarelli, M. Calì, Theoretical model and experimental analysis of a high pressure PEM water electrolyser for hydrogen production, Int J Hydrogen Energy 34 (2009) 1143–1158. https://doi.org/10.1016/J.IJHYDENE.2008.11.083.

[64] O. Ulleberg, Stand-alone power systems for the future: Optimal design, operation and control of solar-hydrogen energy systems, (1998).

[65] W. Hug, H. Bussmann, A. Brinner, Intermittent operation and operation modeling of an alkaline electrolyzer, Int J Hydrogen Energy 18 (1993) 973–977. https://doi.org/10.1016/0360-3199(93)90078-O.

[66] B. Yodwong, D. Guilbert, M. Phattanasak, W. Kaewmanee, M. Hinaje, G. Vitale, Faraday's Efficiency Modeling of a Proton Exchange Membrane

Electrolyzer Based on Experimental Data, Energies 2020, Vol. 13, Page 4792 13 (2020) 4792. https://doi.org/10.3390/EN13184792.

[67] V. Liso, G. Savoia, S.S. Araya, G. Cinti, S.K. Kær, Modelling and Experimental Analysis of a Polymer Electrolyte Membrane Water Electrolysis Cell at Different Operating Temperatures, Energies 2018, Vol. 11, Page 3273 11 (2018) 3273. https://doi.org/10.3390/EN11123273.

[68] A. Ursúa, L.M. Gandía, P. Sanchis, Hydrogen production from water electrolysis: Current status and future trends, Proceedings of the IEEE 100 (2012) 410–426. https://doi.org/10.1109/JPROC.2011.2156750.

[69] A. Ursúa, L. Marroyo, E. Gubía, L.M. Gandía, P.M. Diéguez, P. Sanchis, Influence of the power supply on the energy efficiency of an alkaline water electrolyser, Int J Hydrogen Energy 34 (2009) 3221–3233. https://doi.org/10.1016/J.IJHYDENE.2009.02.017.

[70] R. Dufo-López, J.M. Lujano-Rojas, J.L. Bernal-Agustín, Optimisation of size and control strategy in utility-scale green hydrogen production systems, Int J Hydrogen Energy 50 (2024) 292–309. https://doi.org/10.1016/j.ijhydene.2023.08.273.

[71] E. Afshari, S. Khodabakhsh, N. Jahantigh, S. Toghyani, Performance assessment of gas crossover phenomenon and water transport mechanism in high pressure PEM electrolyzer, Int J Hydrogen Energy 46 (2021) 11029–11040. https://doi.org/10.1016/J.IJHYDENE.2020.10.180.

[72] Z. Abdin, C.J. Webb, E.M.A. Gray, Modelling and simulation of an alkaline electrolyser cell, Energy 138 (2017) 316–331. https://doi.org/10.1016/J.ENERGY.2017.07.053.

[73] P. Medina, M. Santarelli, Analysis of water transport in a high pressure PEM electrolyzer, Int J Hydrogen Energy 35 (2010) 5173–5186. https://doi.org/10.1016/J.IJHYDENE.2010.02.130.

[74] S. Dutta, S. Shimpalee, J.W. Van Zee, Numerical prediction of mass-exchange between cathode and anode channels in a PEM fuel cell, Int J Heat Mass Transf 44 (2001) 2029–2042. https://doi.org/10.1016/S0017-9310(00)00257-X.

[75] H. Matsushima, T. Nishida, Y. Konishi, Y. Fukunaka, Y. Ito, K. Kuribayashi, Water electrolysis under microgravity: Part 1. Experimental technique, Electrochim Acta 48 (2003) 4119–4125. https://doi.org/10.1016/S0013-4686(03)00579-6.

[76] M.E. Lebbal, S. Lecœuche, Identification and monitoring of a PEM electrolyser based on dynamical modelling, Int J Hydrogen Energy 34 (2009) 5992–5999. https://doi.org/10.1016/J.IJHYDENE.2009.02.003.

[77] T.A. Zawodzinski, M. Neeman, L.O. Sillerud, S. Gottesfeld, Determination of water diffusion coefficients in perfluorosulfonate ionomeric membranes, Journal of Physical Chemistry 95 (1991) 6040–6044. https://doi.org/10.1021/J100168A060.
[78] D.J. Kim, M.J. Jo, S.Y. Nam, A review of polymer–nanocomposite electrolyte membranes for fuel cell application, Journal of Industrial and Engineering Chemistry 21 (2015) 36–52. https://doi.org/10.1016/J.JIEC.2014.04.030.
[79] F. Moradi Nafchi, E. Afshari, E. Baniasadi, N. Javani, A parametric study of polymer membrane electrolyser performance, energy and exergy analyses, Int J Hydrogen Energy 44 (2019) 18662–18670. https://doi.org/10.1016/J.IJHYDENE.2018.11.081.
[80] M.R.. Lindeburg, Chemical engineering reference manual : for the PE exam, (2013).
[81] V. Botsis, Development of a Stationary and a Preliminary Dynamic Model for Proton Exchange Membrane (PEM) Electrolyzer, (2019). https://www.academia.edu/38874989/Development_of_a_Stationary_and_a_Preliminary_Dynamic_Model_for_Proton_Exchange_Membrane_PEM_Electrolyzer (accessed June 7, 2025).
[82] Ö.F. Selamet, M.C. Acar, M.D. Mat, Y. Kaplan, Effects of operating parameters on the performance of a high-pressure proton exchange membrane electrolyzer, Int J Energy Res 37 (2013) 457–467. https://doi.org/10.1002/ER.2942.
[83] A. Laconti, H. Liu, C. Mittelsteadt, R. McDonald, Polymer Electrolyte Membrane Degradation Mechanisms in Fuel Cells - Findings Over the Past 30 Years and Comparison with Electrolyzers, ECS Trans 1 (2006) 199–219. https://doi.org/10.1149/1.2214554/XML.
[84] A. Buttler, H. Spliethoff, Current status of water electrolysis for energy storage, grid balancing and sector coupling via power-to-gas and power-to-liquids: A review, Renewable and Sustainable Energy Reviews 82 (2018) 2440–2454. https://doi.org/10.1016/j.rser.2017.09.003.
[85] R. Hancke, T. Holm, Ø. Ulleberg, The case for high-pressure PEM water electrolysis, Energy Convers Manag 261 (2022). https://doi.org/10.1016/j.enconman.2022.115642.
[86] H. Ito, N. Kawaguchi, S. Someya, T. Munakata, Pressurized operation of anion exchange membrane water electrolysis, Electrochim Acta 297 (2019) 188–196. https://doi.org/10.1016/J.ELECTACTA.2018.11.077.
[87] M. Sánchez, E. Amores, L. Rodríguez, C. Clemente-Jul, Semi-empirical model and experimental validation for the performance evaluation of a 15 kW

alkaline water electrolyzer, Int J Hydrogen Energy 43 (2018) 20332–20345. https://doi.org/10.1016/J.IJHYDENE.2018.09.029.
[88] M. Sánchez-Molina, E. Amores, N. Rojas, M. Kunowsky, Additive manufacturing of bipolar plates for hydrogen production in proton exchange membrane water electrolysis cells, Int J Hydrogen Energy 46 (2021) 38983–38991. https://doi.org/10.1016/J.IJHYDENE.2021.09.152.
[89] R.L. Leroy, C.T. Bowen, D.J. Leroy, R.L. Leroy, C.T. Bowen, D.J. Leroy, The Thermodynamics of Aqueous Water Electrolysis, JElS 127 (1980) 1954. https://doi.org/10.1149/1.2130044.
[90] F.B.P. Ryan O'Hayre, Suk-Won Cha, Whitney Colella, Fuel Cell Fundamentals, 3rd Edition, (2016) 600. https://www.wiley.com/en-us/Fuel+Cell+Fundamentals%2C+3rd+Edition-p-9781119113805 (accessed June 7, 2025).
[91] G. Zwaschka, L. Thiel, R. Leskau, Temperature optimization of PEM water electrolyzers for minimum hydrogen prices, Int J Hydrogen Energy 138 (2025) 58–63. https://doi.org/10.1016/j.ijhydene.2025.05.146.
[92] Aspen Custom Modeler | Quick and Easy | AspenTech, (n.d.). https://www.aspentech.com/en/products/engineering/aspen-custom-modeler (accessed June 7, 2025).
[93] M.K. Debe, S.M. Hendricks, G.D. Vernstrom, M. Meyers, M. Brostrom, M. Stephens, Q. Chan, J. Willey, M. Hamden, C.K. Mittelsteadt, C.B. Capuano, K.E. Ayers, E.B. Anderson, Initial Performance and Durability of Ultra-Low Loaded NSTF Electrodes for PEM Electrolyzers, J Electrochem Soc 159 (2012) K165–K176. https://doi.org/10.1149/2.065206JES/XML.

7. Conclusion and outlook on future

7.1. Heteroazeotropic batch distillation for MIBK-water separation

This comprehensive investigation on heteroazeotropic batch distillation for MIBK-water separation has demonstrated significant potential for process intensification through strategic modification of the unit configuration and optimization of operation.

The first part of this study, focused on evaluating three batch distillation configurations for MIBK-water heteroazeotropic separation demonstrates that strategic process modifications can significantly enhance separation performance. The key Findings from three studies BDU configurations, taking Mode I as the benchmark for design enhancement, are as below:

Mode II (Batch Distillation with Decanter):

- Most effective configuration achieving near-complete recovery ($\eta \approx 0.995$) with perfect decanter.
- Provides 5-9% recovery improvement and 8-11% better energy/production rate vs. conventional operation.
- Critical design parameters: $RF_1 \geq 0.75$ and $RF_2 \leq 0.4$ (recovery focus) or $RF_1 \geq 0.5$ and $RF_2 \leq 0.55$ (production focus).
- Decanter design must prioritize MIBK-rich phase retention over aqueous phase control.
- Any organic phase loss linearly impacts all performance metrics.
- Aqueous phase reflux below 40% has minimal adverse effects.

Mode III (Refluxless Operation):

- Fastest operation with 6-10% time reduction compared to other modes.
- About 16-25% lower recovery compared to Mode I and Mode II.
- Only justified when processing speed is prioritized over product recovery.

Design Considerations:

- Two theoretical stages provide optimal column efficiency with diminishing returns beyond this point.
- Condenser temperature effects are configuration-dependent: adverse for Mode I, beneficial for Mode II.

- Without equilibrium stages, desired purification requires either lower condenser temperature or refluxless operation.

Industrial Implementation Recommendation:

- Decanter integration (Mode II) with optimized return fractions provides the most balanced approach for achieving high recovery, production rate, and energy efficiency in heteroazeotropic batch distillation operations.

The second part of this study, focused on evaluating three batch distillation configurations for MIBK-water heteroazeotropic separation demonstrates that the proposed feeding strategies and decanter optimization can achieve substantial performance improvements over conventional operations. The key findings from the three configuration studies are as below:

Mode I (Conventional Unit):

- Total reflux startup step is unnecessary and can be eliminated for better performance.
- Optimal reflux ratio RR=1 (RF=0.5) provides maximum SPF and SEC from sequential batches perspective.
- Larger feed quantities result in lower SEC and higher SPF due to reduced holdup-to-feed ratio.
- Feed quantity emerges as a critical performance factor.

Mode II (Unit with Decanter):

- Superior performance across entire operational range compared to Mode I.
- Optimal decanter efficiency at RF_1=0.875 and RF_2=0.125 rather than perfect separation.
- Perfect decanter (RF_1=1, RF_2=0) causes lower production rate and higher energy cost due to holdup losses.
- Provides up to 6% improvement in fractional recovery and 7% improvement in SEC and SPF vs. Mode I.
- Smaller organic phase holdup combined with larger aqueous phase holdup optimizes process performance.
- Decanter optimization requires balancing operational losses with holdup losses.

Mode III (Inverted Batch Distillation with Decanter):

- High feeding rates show no significant advantage over Mode II
- Optimal feeding time identified as 54 minutes for 15 kg MIBK-water mixture.
- Total operation time of only 57 minutes approximates continuous distillation performance.
- Demonstrates 7% improvement in fractional recovery, 9% reduction in process time, and 17% enhancement in SPF and SEC vs. Mode I.
- Performance improvement attributed to: (1) gradual feeding enabling earlier boiling and shorter heat-up, and (2) top feeding providing immediate vapor-liquid contact and stripping.

Process Enhancement Mechanisms:

- Gradual feeding approach enables practical upgrading of existing batch distillation units.
- Feeding time optimization is critical and extending it beyond optimal point adversely affects performance.
- Inverted batch distillation approximates continuous operation when feeding and separation end simultaneously.

The third part of this study, focused on evaluating three batch distillation configurations for MIBK-water heteroazeotropic separation demonstrates that gradual feeding strategies combined with heat recovery can achieve transformational improvements in energy efficiency and production rate. The key findings from the three configuration studies are as below:

Mode I (Conventional Unit with Decanter):

- Feed quantity optimization shows 4% better production rate and energy cost for 80 kg vs. 20 kg feed.
- Performance improvement is attributed to constant holdup loss resulting in lower loss-to-feed fraction for larger quantities.
- Establishes baseline for comparing gradual feeding strategies.

Mode II (Top Feeding/Gradual Feeding):

- Consistently more efficient than bottom feeding (Mode III) across almost all studied cases.
- Decreasing feed rate profile provides up to 10% enhancement in performance index.

- Fixed feed rate achieves up to 7% improvement in performance index.
- Superior performance maintained across different feeding durations and rate profiles.

Mode III (Bottom Feeding/Gradual Feeding):

- Less effective than top feeding approach for MIBK-water separation.
- Decreasing feed rate profile results in only slight performance changes.
- Fixed feed rate causes adverse performance changes.
- Generally less efficient than Mode II configuration.

Feed Rate Profile Analysis:

- High feeding rates (feeding time <120 minutes) show minimal differences from conventional operation.
- Performance differences become significant with longer feeding times.
- Increasing feed rate profiles result in equal or lower performance than Mode I in both feeding modes.
- Performance deterioration worsens with extended feeding times for increasing rate profiles.

Success Factors for Gradual Feeding:

- Three main contributing factors identified: (1) boiling start time, (2) feeding location, and (3) vapor-liquid contact quality and quantity
- Feed flow rate and profile determine these factors under constant reboiler duty conditions
- Proper feeding schedule (time and rate profile) and location critical for optimization

Heat Recovery and Process Intensification:

- Gradual feeding policy transforms the technical and economic framework of batch distillation

- Temperature difference between feed stream and top vapor creates significant heat recovery opportunity and strategic feeding approaches unlock the heat recovery viability in batch distillation unit.
- Heat recovery implementation transfers condenser outlet energy to heat feed stream to 85°C.

- Fixed feed flow rate superior to decreasing feed rate for heat recovery applications.
- Mode II with fixed feed rate and heat recovery achieves up to 47% improvement in energy efficiency and production rate vs. Mode I.
- Maximum improvement with decreasing feed rate profile limited to 22%.

7.1.1. Outlook on the future

The investigation has proved a well-designed decanter and gradual feeding as transformative approaches for batch distillation energy efficiency improvement, opening multiple pathways for advanced heat recovery and process intensification. Future research should focus on several key areas to fully realize this potential.

Other heat recovery configurations can be assessed, including embedded coil systems where top vapor passes through coils within the feed tank, multi-stream heat exchangers replacing dual condenser systems, and heat pump integration for maximum energy utilization. The development of hybrid feeding strategies combining ramping-up flow rates for early boiling initiation with fixed rates for superior overall heat recovery represents an ideal approach that leverages complementary advantages while facilitating operation control.

The demonstrated similarities between inverted batch distillation and continuous processes create opportunities for applying established continuous distillation enhancement techniques to batch operations. Empirical modelling development for phase separation prediction will improve simulation accuracy and enable optimal decanter design under varying conditions. The ability to transform existing units into semi-batch operations with minor modifications presents significant industrial implementation opportunities, requiring standardized retrofitting procedures and control strategies.

Future studies should extend these methodologies to other heteroazeotropic systems, conduct pilot-scale demonstrations, and perform comprehensive techno-economic evaluations including capital costs, operating savings, and environmental impact assessments. The convergence of these research directions positions batch distillation technology for significant transformation, achieving continuous process-level efficiency while maintaining operational flexibility essential for specialty chemical production.

7.2. Aspen Plus model for PEM electrolyzer

A semi-dynamic PEMEL model has been successfully developed and integrated into the Aspen Plus environment using Aspen Custom Modeler, enabling accurate simulation of complete electrolysis systems adaptable to variable renewable power profiles. The model incorporates empirical and semi-empirical correlations for thermodynamic and electrochemical modelling, achieving close agreement with experimental literature data through optimized charge transfer coefficients and exchange current densities. Key performance findings demonstrate that lower operating pressures improve system performance, while temperature increases from 40 to 80°C reduce cell voltage by 13.7% at 2 A/cm² current density, with high-temperature operation proving particularly efficient for high-power input conditions.

Two operational scenarios were developed and compared: fixed circulating water flow rate versus fixed operating temperature. While fixed temperature represents the commonly practiced approach, the fixed water flow rate scenario offers significant advantages including simpler control requirements, smaller heat exchanger sizing, higher voltage efficiency, and reduced mechanical stress from flow rate variations. The validated model framework enables techno-economic evaluation of hydrogen production units coupled with renewable energy sources and facilitates integration with downstream processes such as green ammonia and green methanol production.

7.2.1. Outlook on the future

Future research directions will be focused on integrating the model with dynamic renewable energy profiles and finding the optimal operation control strategy under fluctuating power conditions and conducting comprehensive techno-economic analyses for various industrial applications. The model's adaptability to variable input power profiles positions it as a foundation for investigating hybrid renewable energy systems, energy storage integration, and process optimization for large-scale hydrogen production facilities. Further development should include validation through pilot-scale demonstrations and coupling the model with other processes such as green ammonia or green methanol plants.

License

Some chapters of this thesis include content previously published by the author in the journal Separation and Purification Technology (Elsevier), under a Creative Commons Attribution-NonCommercial-NoDerivatives 4.0 International (CC BY-NC-ND 4.0) license. Under the terms of this license, the content is reproduced without modification, with due credit, and exclusively for academic and non-commercial purposes. The full references of the original articles are:

1- S. Niazi, J. A. Díaz-López, A. Nieto-Márquez. "Heat integration and process improvement of a batch distillation unit using a gradual feeding strategy: A case study on MIBK-water separation." Separation and Purification Technology (2025): 131956.
2- S. Niazi, J. A. Díaz-López, A. Nieto-Márquez. "Improvement of energy efficiency and production performance in a heteroazeotropic batch distillation unit: A study on decanter control and feeding strategy." Separation and Purification Technology 357 (2025): 130132.
3- S. Niazi, J. A. Díaz-López, A. Nieto-Márquez. "Process design and simulation of Methyl Isobutyl Ketone (MIBK) dehydration by batch distillation: A study on unit configuration and operational policies." Separation and Purification Technology (2024): 127942.

This thesis is not for commercial purposes and is presented exclusively as an academic requirement for obtaining a PhD.